UNIVERSITY OF CALIFORNIA, MERCED

An interwoven transcriptional network controls chlamydospore formation in the human fungal pathogen *Candida albicans*

A dissertation submitted in partial fulfillment of the requirements for the degree of

Doctor of Philosophy

in

Quantitative and Systems Biology

by

Priyanka Shirish Bapat

Committee in Charge
Professor Andy LiWang, Chair
Professor Aaron D Hernday
Professor Marcos E Garcia-Ojeda
Professor Clarissa J Nobile, Advisor

2021

Chapter 3 Bapat, Singh, Nobile 2021

Chapter 4 Bapat, Nobile 2021

The dissertation of Priyanka S Bapat titled "An interwoven transcriptional network controls chlamydospore formation in the human fungal pathogen *Candida albicans*" is approved, and is acceptable ion quality ad form for publication on microfilm and electronically:

Advisor

_____

Date Dr. Clarissa J Nobile, Ph.D.

Chair

_____

Date Dr. Andy LiWang, Ph.D.

_____

Date Dr. Aaron D Hernday, Ph.D.

_____

Date Dr. Marcos E García- Ojeda, Ph.D.

University of California, Merced
2021

Table of contents

List of tables……...vii
List of figures……viii
Acknowledgements……xi
Curriculum Vitae……..xii
Abstract of dissertation……...…...xv

CHAPTER 1 Introduction to *Candida* species and *Candida* chlamydospores……...1
1.1 Introduction to *Candida* chlamydospores……..…...2
1.2 Genetic regulation of chlamydospores…….……...6
1.2.1 Transcription factors regulating chlamydospore formation…….....6
1.2.2 Other genes involved in chlamydospore formation……....7
1.2.3 Transcriptomic analyses of chlamydosporulation……...9
1.2.4 Proteomic analyses of chlamydosporulation……...9
1.3 References……10

CHAPTER 2 An interwoven transcriptional network controls chlamydospore formation in *Candida albicans* ……..……16
2.1 Abstract……16
2.2 Introduction……..17
2.3 Materials and Methods……18
2.3.1 Strains and media …...……..18
2.3.2 Transcription factor deletion library screen for chlamydospore formation……..18
2.3.3 Strain construction……19
2.3.3.1 GFP tagging the identified transcription factor regulators……19
2.3.3.2 Target gene knockout and gene complementation strains……19
2.3.4 RNA sequencing……...19
2.3.4.1 Cell harvesting for RNA extraction …….....19
2.3.4.2 Library generation and RNA 3'tag sequencing…….20
2.3.4.3 RNA-seq data analysis……...20
2.3.4.4 Functional Enrichment analysis…….20
2.3.5 Chromatin Immunoprecipitation followed by sequencing……....21
2.3.5.1 Cell Harvesting, DNA extraction and library preparation …….21
2.3.5.2 ChIP-seq data analysis with TF motif binding sequence identification…….21
2.3.6 Identification of functionally relevant candidate target genes in the chlamydospore regulatory network……...……..22
2.3.7 Conservation of the chlamydospore regulatory network …….22
2.4 Results……..22
2.4.1 Identification and phenotypic characterization of transcription factor regulator mutants or chlamydospore formation in *C. albicans*…….……22
2.4.2 Transcriptional relationships among core chlamydospore regulators……25
2.4.2.1 Genome wide differential gene expression patterns chlamydospore regulators……25
2.4.2.2 Functional enrichment analysis of the target genes……28

2.4.2.3 Chromatin Immunoprecipitation followed by sequencing on the core TF regulators…….....28
2.4.2.4 Chlamydospore regulatory network of *C. albicans*……..……...29
2.4.2.5 Core TF regulatory circuit……..……33
2.4.2.6 De novo motif binding for core chlamydospore regulators……....36
2.4.3 Identifying functionally relevant targets for chlamydospore regulatory network…..36
2.5 Discussion……..……...……...…40
2.5.1 Core chlamydospore regulators…….....40
2.5.2 Interwoven chlamydospore regulatory network and circuit complexity……41
2.5.3 Conservation of chlamydospore regulatory network……42
2.6 Supplementary materials……..44
2.7 References……51

CHAPTER 3 Visible light combined with photosensitizing compounds are effective against *Candida albicans* biofilms…….....…….58
3.1 Abstract……..……..……58
3.2 Introduction……..58
3.3 Materials and Methods……62
3.3.1 Strains and media used……..62
3.3.2 LED light sources and photosensitizers……62
3.3.3 Biofilm assays…….…..62
3.3.4 Determination of Colony Forming Units……...……63
3.3.5 Viability staining of biofilm cells……..63
3.3.6 Assessment of cellular morphologies of biofilm cells……..64
3.4 Results……..64
3.4.1 Effects of red, green, and blue lights on *C. albicans* biofilm formation……...64
3.4.2 Effects of red, green and blue lights with photosensitizer compounds on *C. albicans* biofilm formation……...……66
3.5 Discussion……72
3.6 Supplementary materials……..75
3.7 References……84

CHAPTER 4 Photodynamic therapy is effective against *Candida auris* biofilms…..91
4.1 Abstract……91
4.2 Introduction……..91
4.3 Materials and Methods……95
4.3.1 Strains and media……..95
4.3.2 Light sources and photosensitizing compounds……...95
4.3.3 Biofilm assays……...96
4.3.4 Determination of colony forming units (CFUs) from *Candida* biofilms……..96
4.3.5 Viability staining of *C. auris* biofilms……..97
4.4 Results……..97
4.4.1 Effects of red, green, and blue visible lights on *C. auris* biofilms…….....97
4.4.2 Effects of red, green and blue visible lights in combination with exogenous photosensitizing compounds on *C. auris* biofilm……...98

4.5 Discussion……..105
4.6 Supplementary materials……108
4.7 References……..134

List of Tables

Table 1.1 List of transcription factors known to be involved in chlamydospore formation….....9
Table 1.2 List of other genes known to be involved in chlamydospore formation…….9
Table 2.1 Summary of ChIP-binding events detected in the upstream regulatory regions of core TF regulators…….…….…….29
Table 2.2 Summary of genes shared between RNA-seq and ChIP-seq datasets.....32
Table S2.1 List of target gene transcription factors and kinases of chlamydospore regulatory network……50-51
Table S4.1 Reported MICs for the *C. auris* strains used in the study…..……..134

List of Figures

Figure 1.1 C. albicans chlamydospores……..….4
Figure 2.1 Screening and characterization of chlamydospore defective transcription factor regulator mutants……...……...24-25
Figure 2.2 Functional enrichment analyses of chlamydospore formers and chlamydospore non-formers…….……...27
Figure 2.3 The chlamydospore regulatory network of *C. albicans*……...30-31
Figure 2.4 Chlamydospore regulatory transcription factor circuit……....34
Figure 2.5 Chromatin Immunoprecipitation mapping and motif dentification of core chlamydospore regulators……35-36
Figure 2.6 Functionally relevant targets of chlamydospore regulatory network…….38-39
Figure 2.7 Conservation of chlamydospore regulatory network……..….43
Figure S2.1 Colony morphology and cellular phenotypes of chlamydospore defective transcription factor core regulators on rice extract tween 80 agar medium……44
Figure S2.2 Colony morphology and cellular phenotypes of chlamydospore defective transcription factor core regulators on potato carrot bile agar medium…….....45
Figure S2.3 Colony and cellular phenotypes for chlamydospore formation by *C. albicans* clinical isolates on CMA tween 80 agar medium……..…46
Figure S2.4 Commonly upregulated and downregulated genes for chlamydospore formers and chlamydospore non-formers…….....47
Figure S2.5 The color-coded chlamydospore regulatory network of *C. albicans* with emphasis on number of ChIP binding events detected for each gene……..48
Figure S2.6 Chlamydospore formation by the complemented strains…….....49
*Figure 3.*1 The *C. albicans* biofilm life cycle and the biofilm assays used in this study to assess the antibiofilm properties of visible lights and photosensitizing compounds…....59
Figure 3.2. Effects of red, green and blue visible lights on *C. albicans* biofilms……..…65
Figure 3.3. Effects of red visible light in combination with the photosensitizing compounds new methylene blue, toluidine blue O, and rose bengal on *C. albicans* biofilms……..67
Figure 3.4. Effects of green visible light in combination with the photosensitizing compounds new methylene blue, toluidine blue O, and rose bengal on *C. albicans* biofilms……..69
Figure 3.5. Effects of blue visible light in combination with the photosensitizing compounds new methylene blue, toluidine blue O, and rose bengal on *C. albicans* biofilms……..……71
Figure S3.1. Chemical structures of the photosensitizing compounds used in these studies……75
Figure S3.2. Effects of red visible light in combination with the photosensitizing compounds new methylene blue, toluidine blue O, and rose bengal on biofilms formed by additional *C. albicans* strains……75
Figure S3.3. Effects of green visible light in combination with the photosensitizing compounds new methylene blue, toluidine blue O, and rose bengal on biofilms formed by additional *C. albicans* strains……76

Figure S3.4. Effects of blue visible light in combination with the photosensitizing compounds new methylene blue, toluidine blue O, and rose bengal on biofilms formed by additional *C. albicans* strains……..……..77
Figure S3.5. Effects of red visible light in combination with the photosensitizing compound rose bengal on cell viability of cells resuspended from biofilms in the developmental inhibition biofilm assay…….…….……78
Figure S3.6. Effects of green visible light in combination with the photosensitizing compound new methylene blue on cell viability of cells resuspended from biofilms in the developmental inhibition biofilm assay……...……..79
Figure S3.7. Effects of blue visible light in combination with the photosensitizing compound new methylene blue on cell viability of cells resuspended from biofilms in the developmental inhibition biofilm assay…….……80
Figure S3.8. Effects of blue visible light in combination with the photosensitizing compound new methylene blue on cell viability of cells resuspended from biofilms in the disruption biofilm assay…….……..……..81
Figure S3.9. Effects of red visible light in combination with the photosensitizing compound rose bengal on cell viability of biofilms in the developmental inhibition biofilm assay…….……..81
Figure S3.10. Effects of green visible light on cell viability of biofilms in the developmental inhibition biofilm assay….……81
Figure S3.11. Effects of blue visible light on cell viability of biofilms in the developmental inhibition biofilm assay…….…….……82
Figure S3.12. Effects of blue visible light on cell viability of biofilms in the disruption biofilm assay……..82
Figure S3.13. Assessment of cellular morphology of biofilm cells……..83
Figure 4.1. The *C. auris* biofilm life cycle and the three biofilm assays used in this study to assess the antibiofilm properties of visible lights with and without photosensitizing compounds…….93
Figure 4.2. Effects of red, green, and blue visible lights on *C. auris* biofilms…….98
Figure 4.3. Effect of red visible light in combination with photosensitizing compounds on *C. auris* biofilms……..……100
Figure 4.4. Effect of green visible light in combination with photosensitizing compounds on *C. auris* biofilms……...……..102
Figure 4.5. Effect of blue visible light in combination with photosensitizing compounds on *C. auris* biofilms…….……..……104
Figure S4.1. Effects of red, green, and blue visible lights on biofilms formed by an additional *C. auris* clinical isolate…….…….……..108
Figure S4.2. Effect of red visible light in combination with photosensitizing compounds on biofilms formed by an additional *C. auris* clinical isolate…….……..…….109
Figure S4.3 Effect of green visible light in combination with photosensitizing compounds on biofilms formed by an additional *C. auris* clinical isolate……..……..……111
Figure S4.4 Effect of blue visible light in combination with photosensitizing compounds on biofilms formed by an additional *C. auris* clinical isolate……..……..…113
Figure S4.5. Effect of red visible light in combination with photosensitizing compounds on cell viability of *C. auris* biofilms in the developmental inhibition biofilm assay…..115

Figure S4.6. Effect of red visible light in combination with photosensitizing compounds on cell viability of *C. auris* biofilms in the disruption biofilm assay……..…117
Figure S4.7. Effect of green visible light in combination with photosensitizing compounds on cell viability of *C. auris* biofilms in the developmental inhibition biofilm assay…….....119
Figure S4.8. Effect of blue visible light in combination with photosensitizing compounds on cell viability of *C. auris* biofilms in the developmental inhibition biofilm assay…..121
Figure S4.9. Effect of blue visible light in combination with photosensitizing compounds on cell viability of *C. auris* biofilms in the disruption biofilm assay…….….123
Figure S4.10. Effect of red visible light in combination with photosensitizing compounds on cell viability of cells resuspended from C. *auris* biofilms in the developmental inhibition biofilm assay……...…….125
Figure S4.11. Effect of red visible light in combination with photosensitizing compounds on cell viability of cells resuspended from C. *auris* biofilms in the disruption biofilm assay…….127
Figure S4.12. Effect of green visible light in combination with photosensitizing compounds on cell viability of cells resuspended from C. *auris* biofilms in the developmental inhibition biofilm assay……...…129
Figure S4.13. Effect of blue visible light in combination with photosensitizing compounds on cell viability of cells resuspended from C. *auris* biofilms in the developmental inhibition biofilm assay…….…..131
Figure S4.14. Effect of blue visible light in combination with photosensitizing compounds on cell viability of cells resuspended from C. *auris* biofilms in the developmental inhibition biofilm assay……..…..133

Acknowledgments

This dissertation work would not have been possible without the contributions of many individuals. I would like to first express my heartfelt appreciation and gratitude for my advisor Professor Clarissa J Nobile, who welcomed me into her lab, supported me in every way, and properly guided me throughout the entirety of my graduate studies. Prof Nobile gave me the freedom and resources to explore my ideas, always provided guidance on research techniques, and was enthusiastic towards my growth as a scientist. I look forward to future collaborations and friendship with her.

I would like to acknowledge my dissertation committee members, who have given me essential feedback every step of the way. First, I would like to thank my committee chair, Professor Andy LiWang, who has been very supportive, helpful and has guided me throughout this journey. I would like to thank Professor Aaron Hernday who helped me to think critically, had excellent suggestions for improving my presentation and public speaking skills through our joint lab meetings. Next, I want to thank Professor Marcos Garcia-Ojeda for his constant support and interest in my work; having taught with Prof Garcia-Ojeda on multiple occasions, I admire his willingness to make the lives of all his students better. Together, my committee members were always supportive of me and made me into a well-rounded scientist and I am very grateful to them.

The biggest personal thanks of my graduate life, I owe to my husband Nirav, for your unending support and thoughtfulness; this journey would not have been possible without you. To my parents, you were my first team and taught me about unconditional love, if it were not for you both, my journey to the US would not have been possible. Ma, I miss you, and feel your love and blessings always with me. I am also super grateful to my in-laws for always being so accepting, so understanding and for motivating and supporting me. So, to my families, a big thank you.

Finally, for your constant support and willingness to help, I thank the UC Merced graduate division and QSB, in particular Joy Sanchez Bell and Jan Zarate. Additionally, I also want to thank the Office of International Affairs, in particular Becky Mirza and Lacey Long Vajer, for being so helpful with the immigration aspects of my journey. I also acknowledge my all colleagues, and past and present lab mates for being supportive. In particular, to my lab family, I am deeply thankful to Ashley, Melanie, Deepika, Diana, Craig, Akshay and Megha for your constant friendship and support that made this tough journey bearable. So, cheers to us! And also, cheers to Mr. Coffee, my reliable friend!

Curriculum Vitae

EDUCATION

PhD Candidate January 2016- August 2021
Quantitative and Systems Biology
University of California, Merced, USA

Master of Science 2010- 2012
Department of Biochemistry and Biotechnology
University of Missouri-St. Louis, USA

Master of Science- Awarded with Distinction 2007- 2009
Department of Biotechnology
University of Mumbai, India

Bachelor of Science 2004-2007
Department of Biotechnology
University of Mumbai, India

PROFESSIONAL APPOINTMENTS

Research Experience

Graduate Student Researcher Jan 2016- August 2021
Mentor: Dr. Clarissa J Nobile
Quantitative and Systems Biology
University of California, Merced, USA

Research Associate June 2012- August 2013
Mentor: Dr. James Bashkin
Department of Biochemistry and Biotechnology
University of Missouri-St. Louis, USA

Graduate Research Assistant Feb 2011- May 2012
Mentor: Dr. James Bashkin
Department of Biochemistry and Biotechnology
University of Missouri-St. Louis, USA

***Student intern* (Industrial project)** May 2008-September 2008
Mentor: Dr. Archana Krishnan
Biogenomics Pvt. Ltd, Mumbai, India

Teaching Experience

Teaching Assistant January 2016- May 2018
Quantitative and Systems Biology, School of Natural Sciences
University of California, Merced, USA

Lecturer June 2009- July 2010
Department of Biotechnology
G.N. Khalsa College, University of Mumbai, India

PUBLICATIONS

Bapat PS, Gunasekaran D, Nobile CJ. "An interwoven transcriptional regulatory network controls chlamydospore formation in *Candida albicans*" (Manuscript in preparation).

Bapat PS, Nobile CJ. "Chlamydospore formation in *Candida* clade" (Manuscript in preparation).

Bapat PS, Nobile CJ **(2021)**. "Photodynamic therapy is effective against *C. auris* biofilms". (Submitted to *Frontiers in Cellular and Infection Microbiology*).

Seher T, Nguyen N, Ramos D, **Bapat P**, Nobile CJ, Sindi S, Hernday AD **(2021).** "AddTag, a two-step approach with supporting software package that facilitates CRISPR/Cas-mediated precision genome editing" (In Press *G3: Genes, Genomics and Genetics*).

Bapat P, Singh G, Nobile CJ **(2021).** "Visible lights combined with photosensitizing compounds are effective against *Candida albicans* biofilms". *Microorganisms,* 9, 500.

Sircaik S, Román E, **Bapat P**, Lee KK, Andes DR, Gow NAR, Nobile CJ, Pla J and Panwar SL **(2021)**. "The protein kinase Ire1 impacts pathogenicity of *Candida albicans* by regulating homeostatic adaptation to endoplasmic reticulum stress" *Cellular Microbiology*, e13307.

Gulati M, Lohse M, Ennis C, Gonzalez R, Perry A, **Bapat P**, Arevalo A, Rodriguez D, Nobile CJ **(2018)**. "*In Vitro* Culturing and Screening of *Candida albicans* Biofilms". *Current Protocols in Microbiology*. Vol 50, Issue 1, e60.

Srivastava A, Sircaik S, Husain F, Thomas E, Ror S, Rastogi S, Alim D, **Bapat P**, Andes D, Nobile CJ and Panwar SL **(2017).** "The 7-transmembrane receptor protein Rta3 plays dual roles in biofilm formation and maintenance of plasma membrane phosphatidylcholine asymmetry in *Candida albicans". Cellular Microbiology*.19: e12767.

HONORS and AWARDS

QSB USAP fellowship (University of California, Merced) Summer 2019
Graduate Student Marshal (University of Missouri- St. Louis) May 2012

PRESENTATIONS and TALKS

Bapat P, Gunasekaran D, Nobile CJ. Discovering the chlamydospore regulatory network in *Candida albicans.* Poster presented at *Candida* and Candidiasis meeting, March 2021.

Bapat P. Discovering the regulatory network controlling a unique morphology in the pathogenic fungus *Candida albicans*. Molecular Cell Biology seminar, University of California, Merced. Nov 2019

Bapat P, Nobile CJ. Discovering the chlamydospore regulatory network in *Candida albicans.* Poster presented at University of California, Berkeley, Microbiology Symposium. March 2019.

Bapat P, Nobile CJ. Discovering the chlamydospore regulatory network in *Candida albicans.* Poster presented at Bay Area Microbiology and Pathogenesis Symposium. University of California, San Francisco. March 2019.

Bapat P, Nobile CJ. Discovering the chlamydospore regulatory network and light sensing in *Candida albicans.* Poster presented at Northern California Branch Annual Society for Microbiology. Pleasanton, CA, March 2018.

Bapat P, Nobile CJ. Discovering the transcriptional network controlling chlamydospore formation and light sensing in *Candida albicans.* Poster presented at Bay Area Microbiology and Pathogenesis Symposium. University of California, San Francisco. March 2018.

Bapat P, Nobile CJ. Discovering the transcriptional network controlling chlamydospore formation and light sensing in *Candida albicans.* Poster presented at Bay Area Microbiology and Pathogenesis Symposium. University of California, San Francisco. March 2017.

Abstract of the Dissertation

An interwoven transcriptional network controls chlamydospore formation in the human fungal pathogen *Candida albicans*

By Priyanka S Bapat
Doctor of Philosophy, Quantitative and Systems Biology
University of California, Merced, 2021
Advisor: Dr. Clarissa J. Nobile

The primary project of my dissertation focused on studying the regulation of chlamydospores, a morphology formed by the common human fungal pathogen *Candida albicans. C. albicans* produces chlamydospores under stressful conditions, however, the biological functions of chlamydospores are still unknown. Since this important human fungal pathogen produces these enigmatic structures, I believe that chlamydospores must provide a selective advantage to *C. albicans*. I hypothesized that there must be underlying developmental and regulatory pathways dedicated to chlamydospore formation, and that identifying these pathways will be useful in understanding the biological functions of chlamydospores. Using forward genetics and genome-wide approaches including RNA-seq and ChIP-seq, I discovered that the *C. albicans* chlamydospore transcriptional regulatory network is highly interwoven comprised of nine core transcriptional regulators (i.e., transcription factors) controlling over 3,200 downstream target genes. Of these nine core regulators, I have found that six core transcription factor deletion mutant strains fail to form chlamydospores, while three core transcription factor deletion mutant strains form higher numbers of chlamydospores relative to the wildtype strain. Analysis of the chlamydospore regulatory network suggests roles for SNARE vesicular transport and fatty acid degradation pathways along with roles for enzymes involved in cell wall biosynthesis pathways. Preliminary network conservation analyses based on orthologous relationships of proteins within the chlamydospore network revealed that the network is comprised largely of "old" proteins (65%) interspersed with some "young" proteins (35%), indicative of the network being fairly well conserved. Further analysis of this regulatory network will be useful in identifying the biological functions of chlamydospores and will also give us insight into the regulation of *C. albicans* morphological transitions more generally.

Another project of my dissertation focused on studying non-drug therapeutic strategies to target biofilm formation in *C. albicans* and *Candida auris*. *C. albicans* and *C. auris* form robust and drug resistant biofilms and treatment of biofilm infections caused by these species is challenging. I focused on exploring red, green and blue visible lights in combination with exogenous photosensitizing compounds as a non-drug therapeutic strategy against *C. albicans* and *C. auris* biofilm *in vitro*. I demonstrated that red, green and blue visible lights in combination with exogenous photosensitizing compounds are an effective non-drug therapeutic strategy against both *Candida* species biofilms. Blue light with and without photosensitizing compounds was the most effective treatment at inhibiting biofilm formation and also disrupting mature biofilms of both species, closely followed by red light in combination with photosensitizing compounds.

CHAPTER 1

Introduction to *Candida species* and *Candida* chlamydospores

Fungi are presently estimated to include ~3.8 million species, the majority of which are not known to cause disease in humans [1]. In fact, only ~300 fungal species (0.00008% of fungi) are known to cause disease in humans [1]. Of these human disease-causing fungal species, they cause infections ranging from superficial foot and nail infections (e.g., the dermatophytes) to cutaneous and systemic invasive infections (e.g., *Aspergillus, Candida, Pneumocystis and Cryptococcus* species), with the latter systemic infections representing >90% of all human deaths caused by fungal infections [2]. Fungi are broadly divided into 9 lineages, of which the phylum Ascomycota has been the most studied to date [3]. Ascomycota includes some of the most characterized and commonly used fungal model organisms like *Saccharomyces cerevisiae* and *Neurospora crassa*, among other disease-causing fungi [3].

Candida species belong to the *Saccharomycotina* lineage of the *Ascomycota* phylum, which reside on inanimate objects in the environment and as members of the normal microbiota of humans and other warm-blooded animals. *Candida* species are also the most commonly isolated human fungal pathogens from clinical settings [4,5]. Among the *Candid*a species, *Candida albicans* was identified over 2000 years ago, as an organism responsible for causing oral thrush [6]. *C. albicans* is a diploid and polymorphic species capable of causing superficial infections as well as invasive infections in humans [6,7]. *C. albicans* has been rarely isolated from environmental samples [8] and its main reservoir is thought to be humans [5] and other warm-blooded animals, where it typically resides as an asymptomatic commensal organism colonizing the mucocutaneous surfaces of the mouth, skin, and gastrointestinal and genitourinary tracts [9]. However, in the event of microbial dysbiosis, disruptions in the host immune defenses, and dietary changes, *C. albicans* can become a pathogen, especially in immunocompromised and critically ill individuals [10,11]. It is, therefore, considered to be an opportunistic pathogen of humans. For example, in individuals whose immune system is compromised after contracting human immunodeficiency virus (HIV), *C. albicans* can cause a wide range of secondary infections, ranging from oral thrush to deep-seated invasive candidiasis [9]. In addition, it is estimated to cost approximately one billion dollars annually to treat *C. albicans* infections in the US [12].

Candida auris, is a newly emerged fungal "superbug" that has recently been declared a global health threat because of its multidrug resistance and high transmission rates [13–15]. *C. auris* has developed molecular resistance mechanisms making it less susceptible to the three major classes of antifungal drugs used to treat invasive fungal infections in humans, with different clinical isolates reported to be resistant to one or more classes of antifungal drugs, and some isolates displaying pan resistance to all three of the major antifungal drug classes [16]. Both *C. albicans* and *C. auris* are known to form recalcitrant and drug resistant biofilms, communities of adherent microbial cells encased in an extracellular matrix. As *C. albicans* and *C. auris* clinical isolates have been shown to

be naturally resistant and/or tolerant to antifungal drugs or can develop resistance over time, the development of alternative non-drug therapeutic strategies is urgently needed. My discoveries on the use of visible lights in combination with photosensitizing compounds as a non-drug antifungal therapeutic strategy against biofilm infections caused by *C. albicans* and *C. auris* are discussed in Chapter 3 and Chapter 4, respectively, of this dissertation.

C. albicans possesses several virulence traits, such as the ability to undergo morphological transitions in response to environmental cues, which is known to play roles in the establishment and maintenance of *C. albicans* infections [17]. Multiple morphologies have been identified in *C. albicans* including the round budding yeast form, the mating competent opaque form, the ellipsoidal pseudohyphal form, the elongated hyphal form, and chlamydospores [18–20]. The ability to transition from the yeast form to hyphal form is known to play key roles in the infection process [21]. The chlamydospore form, which is a major focus of my research, is the least studied morphology to date and is discussed in Chapters 1 and 2 of this dissertation.

1.1. Introduction to *Candida* chlamydospores

Background and Introduction

Fungi are able to adapt to and exist in diverse and extreme environmental conditions [22]. Many fungi exist in different morphological states depending on their environmental conditions [23,24]. Some fungi are dimorphic, where they have been found to exist in at least two morphological states, such as the yeast form and hyphal form, depending on environmental cues (e.g., pH, CO_2 and temperature) [24,25]. The yeast form is spherical, while the hyphal form is elongated and lacks constrictions at the sites of septation [26]. Other than these two classic morphological forms, many fungal species are also known to produce spores, either sexual or asexual, usually as part of their reproductive cycle [27]. For many fungal species, such as *Fusarium* species found in the soil, asexual spores serve as a means for survival under harsh and highly unfavorable environmental conditions (e.g., nutrient depletion, extreme temperatures, dry conditions leading to desiccation and the presence of UV radiation) [28,29]. These asexual spores are quiescent, resistant structures that remain dormant until favorable conditions return, upon which they have the ability to germinate and produce viable fungal cells [27].

The human fungal commensal and opportunistic pathogen *C. albicans* possesses several virulence traits such as the production of secreted aspartyl proteases, the ability to form biofilms and the ability to grow in different cellular morphologies that are known to play roles in the establishment and maintenance of *C. albicans* infections [17]. These virulence traits synchronously operate in a coordinated fashion, involving multiple signal transduction pathways, to ultimately cause an infection in the host [30]. The ability to undergo morphological transitions and switch to a morphology best suited to thrive in a given environmental condition is one of the most important virulence traits of *C. albicans*. Environmental cues that can induce morphological transitions in *C. albicans* include, for example, changes in pH, temperature, serum levels, oxygen and nitrogen levels, and nutrient levels [31,32]. Multiple morphologies have been identified in *C. albicans* including the round budding yeast form, the mating competent opaque form, the grey form, the ellipsoidal pseudohyphal form, the elongated hyphal form, the commensal specific GUT form and chlamydospores [18–20]. The chlamydospore form is the least studied

morphology to date, even though we have known about this form for over a century. Chlamydospores are defined as non-deciduous, terminal or lateral asexual spores [33]. The name chlamydospores is derived from the word “chlamyds” meaning coating or mantle.

C. dubliniensis is the only other *Candida* species known to be able to form chlamydospores. *C. dubliniensis* was identified and classified in 1995, and prior to then was likely misidentified as *C. albicans* [34]. *C. albicans* and *C. dubliniensis* share many phenotypic traits including the ability to form hyphae and chlamydospores, however, *C. dubliniensis* is reported to be less likely to cause to cause bloodstream infections and more likely to cause superficial mucosal infections, such as oral candidiasis [35].

Chlamydospore production

Many fungal species ranging from *Phytophthora cinnamomic* [36], *Aspergillus parraciticus* [37], *Cryptococcus neoformans* [38], *dermatophytes* [39], *Fusarium* species [28], *Histoplasma farciminosum* [40], *Paracoccioides brasiliensis* [41], and *C. albicans* and *C. dubliniensis* [42] have been reported to form chlamydospores. The specialized functions imparted by chlamydospores have been characterized in certain species. For example, the chlamydospores produced by *P. cinnamomic* are known to provide desiccation resistance, and chlamydospores produced by *A. parraciticus* are known to mediate the production of the mycotoxin aflatoxin [37]. Here, we focus on chlamydospores produced by the two members of *Candida* clade, *C. albicans* and *C. dubliniensis*, whose biological functions are as of yet unknown.

A historical dive into chlamydospores

C. albicans chlamydospores were described for the very first time in 1877 by Paul Grawitz, a German pathologist [6]. Several years later, in 1890, respectively, Hugo Plaut, Gabriel Roux and Georges Linossier, shared the earliest drawings of *C. albicans* chlamydospores [15, 33]. Of the *Candida* clade, only *C. albicans* and *C. dubliniensis* are known to be able to form chlamydospores [42], and as such, chlamydospore formation is used as a diagnostic tool for distinguishing *C. albicans* or *C. dubliniensis* from other *Candida* as well as other fungal species in clinical samples [6]. Chlamydospores are characterized by their large size (7-12µm) relative to yeast cells (2-3µm), their spherical shape, their thick-walled outer layer, and their location at the terminal or lateral ends of hyphae (Figure 1.1) [19,44].

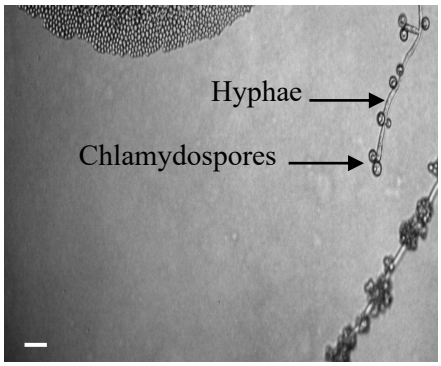

Figure 1.1 *C. albicans* chlamydospores. Chlamydospore formation by the *C. albicans* wildtype reference strain (SN250) grown under standard chlamydospore inducing conditions (cornmeal agar (CMA) plus Tween 80 medium, incubated at room temperature under oxygen limiting conditions in the dark for 8 days) and observed microscopically at 20X magnification. Scale bar represents 10μM.

The biological functions of chlamydospores are currently unknown [45,46]; however, some researchers hypothesize that chlamydospores exist as storage structures for lipids [45], carbohydrates and nucleic acids [47], or as resilient dormant structures that germinate under specific environmental conditions [48]. In support of the latter hypothesis, Citiulo *et.al* showed that chlamydospores were able to germinate into hyphae and yeast form cells under specific environmental conditions [49]. However, in this same study, chlamydospores were unable to withstand adverse environmental conditions, such as desiccation, and nutrient limitation, which are typical attributes of other fungal spores, and actually died faster compared to yeast form cells [49]. Thus, concrete evidence for the functions of chlamydospores is still nonexistent.

Growth conditions, structure, composition and germination

Candida chlamydospores have been rarely observed from *in vivo* tissue samples [50,51]. They are, however, readily observed *in vitro* under standard chlamydospore-inducing conditions, consisting of growth on complex nutrient media supplemented with detergents like Tween 80 at room temperature, under oxygen-limitation, and in the dark [46,52]. Commonly used media to induce chlamydospore formation is corn meal agar (CMA) with Tween 80 and rice meal extract (RE) with Tween 80 [53]. As *C. dubliniensis* was not identified as a different species until the year 1995, early studies in on *Candida* chlamydospores largely focused on empirically establishing the different media components and environmental conditions that could induce chlamydospore formation in *C. albicans*. The finding that the addition of detergent like Tween 80 to rice infusion agar improved chlamydospore formation was first described by Claire Taschdijan in 1953 [54]. Other media used for the induction of *Candida c*hlamydospores include potato carrot agar with bile salts [55], soil extract agar [56], RIOT medium [57] and cornmeal broth plus 5% milk [58]. As *C. albicans* and *C. dubliniensis* both share similar phenotypic traits including chlamydospore formation distinguishing between these two species in the clinic can be difficult. However, *C. albicans* and *C. dubliniensis* have different carbon assimilation

profiles as well as differences in their abilities to form chlamydospores on Staib agar and Pal's agar [59,60].

In the early 1970's, studies describing the composition and structure of *C. albicans* chlamydospores were published. Electron microscopy studies by Miller *et.al* and Daroczy *et.al* [61,62] described the structure of *C. albicans* chlamydospores, and a study by Jansons and Nickerson used chemical and staining methods to study their composition [63]. Together, these studies revealed that *C. albicans* chlamydospores are composed of a double layered cell wall, with a thinner outer layer largely composed of ß-1, 3 glucan and chitin, and a thicker inner layer composed of keratin [61–63]. Interestingly, the inner layer of the double cell wall of *C. dubliniensis* chlamydospores is composed of chitosan (deacetylated chitin) instead of keratin [64]. The thickness of the cell wall is known to increase with the age of the chlamydospore (mature chlamydospores have cell walls ~ 400nm in thickness). Chemical analyses and staining procedures revealed that the center of chlamydospores is rich in lipids, proteins, mitochondria, ribosomes and nucleic acids [45,47,63]. As both DNA and RNA have been found to be present inside chlamydospores, several researchers hypothesize that chlamydospores are active structures that can germinate once favorable conditions reappear. Interestingly, it has been shown that the lifespan and activity of chlamydospores is dependent on the age of the spore, with older chlamydospores (>2 weeks old) reported to be non-responsive to germination [49]. There have been conflicting reports about germination of chlamydospores. Some studies have shown that young chlamydospores (~2-3 days old) can germinate to form yeast form cells and pseudohyphal cells [48,49,65].

Candida chlamydospores: formation and isolation

In 2005, Martin *et.al* studied the temporal formation of *C. albicans* chlamydospores using time lapse fluorescence microscopy [66]. This study revealed that by day 3, an immature chlamydospore starts to form at the tip of a specialized cell called a suspensor cell at the terminal or lateral end of a hyphal cell. At this time, a septin ring forms at the neck of the suspensor cell and the immature chlamydospore. Nuclear division takes place inside the suspensor cell and one daughter nucleus migrates to the immature chlamydospore; a process distinct from other morphological transitions. For example, in order for yeast form cells to bud, nuclear division takes place across the mother-daughter neck junction, while for hyphal cell formation, the two nuclei travel to the daughter cell and one nucleus returns to the mother cell [44]. Once the nucleus migrates inside the immature chlamydospore, the maturation of the chlamydospore begins, and a thick cell wall and septin proteins surround the chlamydospore.

To study chlamydospores as separate entities, detached from the hyphal cell parent, some studies have focused on methods to isolate chlamydospores. It was found that by growing *C. albicans* in liquid chlamydospore inducing media, such as corn meal broth, a large number of chlamydospores can be included to form in bulk and these chlamydospores can then be isolated using enzymatic separation methods (e.g., zymolase or B-glucuronidase treatments) or using physical ultrasonic treatment, followed by sucrose density ultracentrifugation [45,49,67]. However, this isolation procedure has been shown to impact the structure of the isolated chlamydospores, likely due to the harsh enzymatic separation methods used.

1.2 Genetic regulation of chlamydospore formation

Transcription factors (TFs) are sequence specific DNA binding proteins that control the transcription of specific genes by binding to upstream intergenic regions (i.e., *cis* regulatory elements) that ultimately affect the spatial and temporal expression of downstream target genes. Known TFs reported to play roles in *C. albicans* chlamydospore formation are listed in Table 1.1. Other proteins known to play functional roles in *C. albicans* chlamydospore formation are listed in Table 1.2. These proteins have largely been studied in *C. albicans*, and while orthologous proteins have been identified in *C. dubliniensis*, their roles are still uncharacterized.

1.2.1. Transcription factors regulating chlamydospore formation

1. Efg1

Efg1, a bHLH transcription factor was the first TF reported to be involved in chlamydospore formation in *C. albicans*. Efg1 belongs to the APSES group of proteins, sharing a highly conserved 100bp region that is known to be involved in different morphological programs (e.g., Asm1 from *N. crassa*, Ptd1 and Sok2 from *S. cerevisiae*, StuA from *Aspergillus nidulans*) [68,69]. *C. albicans* Efg1 is known to be involved in multiple signaling pathways, including initiation of hyphal formation [70], white-opaque switching [71], and glycolytic metabolic pathways [68]. Efg1 is an important downstream target of the Ras-1 cAMP/PKA signaling pathway acting as an activator of filamentation under specific hyphal inducing conditions [70]. Under chlamydospore inducing conditions, however, Sonneborn *et al.* reported that the Δ/Δ*efg1* strain is hyperfilamentous, thus uncovering a role for Efg1 as a repressor of filamentation under chlamydospore inducing conditions [72]. Based on these findings, Efg1 can act as both an activator and as a repressor of filamentation depending on the environmental conditions [73]. In addition, under chlamydospore inducing conditions, the Δ/Δ*efg1* strain is defective in chlamydospore formation, establishing it as an important regulator of this process [73]. Efg1 is known to be phosphorylated by the protein kinase Tpk2, and this phosphorylation event is necessary for chlamydospore formation [73]. Additionally, other components of the Ras-1 cAMP/PKA pathway, including the RAS signal transduction GTPase Ras1, and the adenylyl cyclase Cyr1 are also required for chlamydospore formation (Δ/Δ*ras1* and Δ/Δ*cyr1* strains fail to produce chlamydospores) [74].

2. Nrg1

Nrg1 is a highly conserved zinc finger TF that is a general repressor of transcription in *C. albicans* that is known to act via Tup1-Ssn6. [72,75]. The Δ/Δ*nrg1* strain is known to be hyperfilamentous under nonfilament inducing conditions, thus elucidating a role for Nrg1 as a repressor of filamentation [75]. In terms of chlamydospore formation, the Δ/Δ*nrg1* strain is hypersporulative, forming a higher number of chlamydospores compared to the wildtype strain [74], indicating that Nrg1 is a repressor of chlamydospore formation in *C. albicans*. Of the *Candida* clade, only *C. dubliniensis* and *C. albicans* form chlamydospores. *C. dubliniensis* but not *C. albicans* has been shown to form chlamydospores when grown on Staib agar [59]. This phenotypic difference has been

attributed to differential expression of *NRG1* between the two species, in which *CdNRG1* is specifically downregulated to allow for chlamydospore formation on Staib agar, while *CaNRG1* is not [76]. More importantly, it has also been shown that deletion of *CaNRG1* allows for chlamydospore formation on Staib agar by *C. albicans* and that heterologous expression of *CaNRG1* in *C. dubliniensis* restricts chlamydospore formation on Staib agar [76].

3. Rme1

Recently, Rme1 was identified as a key regulator necessary for chlamydospore formation [77]. Hernández-Cervantes *et al.* performed genome wide binding studies to identify the downstream target genes of Rme1 under chlamydospore inducing conditions using potato carrot bile agar. Their findings demonstrated that under the conditions tested, Rme1 acts as a master regulator of chlamydospore formation in *C. albicans* [77]. The Rme1 ortholog in *S. cerevisiae* is well characterized and is known to be a repressor of meiosis [78].

4. Grf10

Grf10 is a homeobox transcription factor that has a 60bp conserved homeodomain [79]. In general, homeodomain containing transcription factors have been identified to be involved in morphological and developmental pathways in eukaryotes. In terms of *C. albicans*, Ghosh *et al.* reported that the Δ/Δ*grf10* strain rarely forms chlamydospores and exhibits filamentation defects under chlamydospore inducing conditions (CMA plus 1% Tween 80 at 25^0C for 3-5 days) [80].

5. Isw2 and Rim101

Nobile *et al.* conducted one of the first genetic screens to identify genes involved in chlamydospore formation by screening a library of 217 insertion mutant strains [46]. This study identified 2 TFs, Isw2 and Rim101, that were required for efficient chlamydospore formation in *C. albicans*; the Δ/Δ*isw2* strain failed to form chlamydospores, while the Δ/Δ*rim101* strain showed delayed chlamydospore formation [46].

6. Gcn4, Gln3, Gat1

In order to understand the nutritional control of *C. albicans* chlamydosporulation, Bottcher *et al.* tested different nutrient medium varying in sugar and nitrogen sources and found that the presence of a readily fermentable carbon source (glucose) and a nitrogen source (peptone) strongly inhibit chlamydospore formation [74]. TFs involved in nitrogen catabolite repression (Gln3 and Gat1) and amino acid biosynthesis (Gcn4), were found to be important for chlamydospore formation (Δ/Δ*gcn4* and Δ/Δ*gat1* strains failed to produce chlamydospores and a Δ/Δ*gln3* strain formed fewer chlamydospores than the wildtype strain) [74].

1.2.2 Other proteins involved in chlamydospore formation

1. The MAP kinase Hog1

The mitogen activated protein (MAP) kinase pathway is important for chlamydospore formation. Oxygen limitation is required for chlamydospore formation, and

one of the kinases in the MAPK pathway, Hog1, acts a general repressor of filamentation during oxygen limitation [81–83]. Alonso-Monge *et al.* studied the role of the MAP kinase Hog1 in chlamydospore formation, and found that Hog1 is essential for chlamydospore formation under chlamydospore inducing conditions [82].

2. The fatty acid desaturase Ole1

As cell membrane stability and fluidity play important roles in morphological transitions, Krishnamurthy *et al.* studied the importance of cell membrane oleic acid levels in morphogenesis. They found that oleic acids were essential for cell wall fluidity, hyphal formation, and morphological transitions in *C. albicans* [84]. They also found that the fatty acid desaturase Ole1 is essential for *C. albicans* chlamydospore formation [84]. Interestingly, addition of Tween 80 (an oleic acid ester surfactant) was shown to enhance chlamydospore formation [54], possibly via stabilization of the cell membrane.

3. The dityrosine synthase Dit2

In *S. cerevisiae,* the cytochrome P450 family monooxygenase enzyme Dit2 is important for dityrosine synthesis, which is necessary for formation of the outer spore wall. In *C. albicans*, Dit2 is required for N,N'-bisformyl dityrosine production and chlamydospore formation (a Δ/Δ*dit2* strain formed pseudohyphae but failed to produce chlamydospores) [85]. In contradiction to this earlier finding, however, a study by Bemena *et al*. found that dityrosine was not a component of the cell wall of *C. albicans* or *C. dubliniensis* chlamydospores [64]. Both studies induced chlamydospore formation using cornmeal agar plus Tween 80. The contradictory results between these two studies could be due to the fact that the former study assayed the presence of dityrosine in the chlamydospore cell wall using fluorescence microscopy under UV illumination, while the latter study used a dityrosine optimized filter set.

4. The dolichol phosphate mannose synthase Dpm

Dolichol phosphate mannose (Dpm) acts as a substrate donating mannose to enzymes of the endoplasmic reticulum. The enzyme that produces Dpm is Dpm synthase (consisting of 3 subunits: Dpm1, Dpm2, and Dpm3), whose activity is essential for cell viability and glycosylation. By expressing the 3 Dpm synthase subunits under doxycycline inducible promoters, and growing these strains under chlamydospore inducing conditions, Juchimuik *et al.* found that Dpm1 and Dpm3 are required for chlamydospore formation, but Dpm2 is not [86].

5. **Sch9, Suv3, Mds3 and Rim13**

Other proteins involved in chlamydospore formation that were identified by Nobile *et al*. were Sch9, Suv3, Mds3, and Rim13 [46]. Sch9 and Suv3 are well characterized in *S. cerevisiae*, where Sch9 is a protein kinase involved in stress signaling pathways and Suv3 is a mitochondrial ATP dependent RNA helicase. Rim13 and Mds3 are involved in pH sensing in *C. albicans.* The Δ/Δ*sch9* and Δ/Δ*suv3* strains failed to form chlamydospores, while the Δ/Δ*mds3* and Δ/Δ*rim13* strains were important for timely formation of chlamydospores [46].

Table 1.1: List of transcription factors (TFs) known to be involved in chlamydospore formation.

TF name	Known functions and or pathways	Reference
Efg1	Filamentation, white opaque switch	[73]
Nrg1	General repressor	[76]
Rme1	Chlamydospore formation	[77]
Grf10	Morphogenesis	[80]
Isw2	Chromatin remodelling	[45]
Rim101	pH dependent filamentation	[46]
Gat1	Nitrogen utilization	[74]
Gcn4	Amino acid assimilation	[74]
Gln3	Nitrogen starvation induced filamentation	[74]

Table 1.2: **List of other proteins known to be involved in chlamydospore formation.**

Protein name	Known functions and or pathways	Reference
Sch9	Protein kinase involved in growth control	[46]
Suv3	RNA helicase	[46]
Mds3	TOR signalling pathway, hyphal formation	[46]
Hog1	MAP kinase, stress signalling	[83]
Rim13	Protease of pH response pathway	[46]
Ole1	Fatty acid desaturase involved in oleic acid synthesis	[84]
Dit2	Monooxygenase of cytochrome 450 family	[85,87]
Dpm1 and Dpm3	Dolichol phosphate mannose synthase subunit 1	[86]
Ras1	Ras GTPase, important in signalling pathways	[74]
Cyr1	Adenylate cyclase, cAMP PKA signalling pathway	[74]
Csp1	Cell wall protein	[88]
Csp2	Cell wall protein	[88]

1.2.3 Transcriptomic analyses of chlamydosporulation

Palige *et al.* compared the global transcriptomic profiles of *C. albicans* and *C. dubliniensis* by RNA sequencing. This study identified two cell wall related proteins, Csp1 and Csp2, that were exclusively localized to the chlamydospore cell wall and were termed chlamydospore specific markers for *C. albicans* and *C. dubliniensis* [88]. In another study, Giosa *et al*. compared whole RNA transcriptomic assembly datasets under chlamydospore inducing conditions of the hyperchlamydosporulating *C. albicans* strain GE1 and a biovariant strain of *C. albicans*, called *Candida africana*, that does not form chlamydospores. This comparative study identified two novel transcriptionally active regions (nTARs), nTAR1 and nTAR2, that are highly transcriptionally active during chlamydospore formation [89].

1.2.4 Proteomic analyses of chlamydosporulation

Recently, proteomic analyses of *C. albicans* cells undergoing chlamydosporulation have been reported [90,91]. LC-MS/MS and SWATH-MS were used to identify proteomic profiles complementing the metabolic and gene expression changes occurring during chlamydosporulation (e.g., changes in cellular architecture, stress adaptation, and

cytoskeletal rearrangements). The *Candida* Genome database (CGD), Kyoto encyclopedia of genes and genomes (KEGG) pathways, *Saccharomyces* genome database (SGD) and UniProt were used to identify putative functions for the proteins identified. A total of 1177 proteins were identified of which 319 were shown to be significantly modulated (137 upregulated and 182 downregulated) during chlamydosporulation.

1.3 References

1. Hawksworth, D.L.; Lü Cking, R. Fungal Diversity Revisited: 2.2 to 3.8 Million Species 4. *Fungal branches Eukaryot. tree life* **2018**, 79–95.
2. Brown, G.D.; Denning, D.W.; Gow, N.A.R.; Levitz, S.M.; Netea, M.G.; White, T.C. Hidden killers: Human fungal infections. *Sci. Transl. Med.* 2012, *4*, 165rv13-165rv13.
3. Naranjo-Ortiz, M.A.; Gabaldón, T. Fungal evolution: diversity, taxonomy and phylogeny of the Fungi. *Biol. Rev.* **2019**, *94*, 2101–2137.
4. Sardi, J.C.O.; Scorzoni, L.; Bernardi, T.; Fusco-Almeida, A.M.; Mendes, M.J.S.; Correspondence, G.; Mendes Giannini, M.J.S. *Candida* species: current epidemiology, pathogenicity, biofilm formation, natural antifungal products and new therapeutic options. *J. Med. Microbiol.* **2013**, *62*, 10–24.
5. Pfaller, M.A.; Diekema, D.J. Epidemiology of Invasive Candidiasis: a Persistent Public Health Problem. *Clin. Microbiol. Rev.* **2007**, *20*, 133–163.
6. Barnett, J.A. A history of research on yeasts 12: medical yeasts part 1,*Candida albicans*. *Yeast* **2008**, *25*, 385–417.
7. Almon, L.; Stovall, W.D. Serologic Reactions of Cultures of *Monilia* and of Some Other Yeastlike Fungi. *J. Infect. Dis.* **1934**, *55*, 12–25.
8. Bensasson, D.; Dicks, J.; Ludwig, J.M.; Bond, C.J.; Elliston, A.; Roberts, I.N.; James, S.A. Diverse Lineages of*Candida albicans* Live on Old Oaks. *Genetics* **2019**, *211*, 277–288.
9. Nobile, C.J.; Johnson, A.D. *Candida albicans* biofilms and human disease. *Annu. Rev. Microbiol.* **2015**, *69*, 71–92.
10. da Silva Dantas, A.; Lee, K.K.; Raziunaite, I.; Schaefer, K.; Wagener, J.; Yadav, B.; Gow, N.A. Cell biology of *Candida albicans* –host interactions. *Curr. Opin. Microbiol.* **2016**, *34*, 111–118.
11. Desai, J. V. *Candida albicans* hyphae: From growth initiation to invasion. *J. Fungi* 2018, *4*.
12. Benedict, K.; Jackson, B.R.; Chiller, T.; Beer, K.D. Estimation of direct healthcare costs of fungal diseases in the United States. *Clin. Infect. Dis.* **2018**, *68*, 1791–7.
13. Satoh, K.; Makimura, K.; Hasumi, Y.; Nishiyama, Y.; Uchida, K.; Yamaguchi, H. *Candida auris* sp. nov., a novel ascomycetous yeast isolated from the external ear canal of an inpatient in a Japanese hospital. *Microbiol. Immunol.* **2009**, *53*, 41–44.
14. Sherry, L.; Ramage, G.; Kean, R.; Borman, A.; Johnson, E.M.; Richardson, M.D.; Rautemaa-Richardson, R. Biofilm-forming capability of highly virulent, multidrug-resistant *Candida auris*. *Emerg. Infect. Dis.* **2017**, *23*, 328–331.
15. Stone, J. .
16. Lockhart, S.R.; Etienne, K.A.; Vallabhaneni, S.; Farooqi, J.; Chowdhary, A.;

Govender, N.P.; Colombo, A.L.; Calvo, B.; Cuomo, C.A.; Desjardins, C.A.; et al. Simultaneous emergence of multidrug-resistant *Candida auris* on 3 continents confirmed by whole-genome sequencing and epidemiological analyses. *Clin. Infect. Dis.* **2017**, *64*, 134–140.

17. Ciurea, C.N.; Kosovski, I.B.; Mare, A.D.; Toma, F.; Pintea-Simon, I.A.; Man, A. *Candida* and Candidiasis—opportunism versus pathogenicity: A review of the virulence traits. *Microorganisms* 2020, *8*, 1–17.
18. Odds, F.C.; Kerridge, D. Morphogenesis in *Candida albicans*. *Crit. Rev. Microbiol.* **1985**, *12*, 45–93.
19. Noble, S.M.; Gianetti, B.A.; Witchley, J.N. *Candida albicans* cell-type switching and functional plasticity in the mammalian host. *Nat. Rev. Microbiol.* **2017**, *15*, 96–108.
20. Villa, S.; Hamideh, M.; Weinstock, A.; Qasim, M.N.; Hazbun, T.R.; Sellam, A.; Hernday, A.D.; Thangamani, S. Transcriptional control of hyphal morphogenesis in *Candida albicans*. *FEMS Yeast Res.* 2020, *20*, 5.
21. Kornitzer, D. Regulation of *Candida albicans* Hyphal Morphogenesis by Endogenous Signals. *J. fungi (Basel, Switzerland)* **2019**, *5*.
22. Yong-Sun Bahn, C.X.; , Alexander Idnurm, Julian C. Rutherford, Joseph Heitman, and M.E.C. Sensing the environment: lessons from fungi. *Nat. Rev. Microbiol.* **2007**, *5*, 57–69.
23. Garry T. Cole Basic Biology of Fungi - Medical Microbiology - NCBI Bookshelf. *Med. Microbiol.* **1996**.
24. McGinnis R Michael and Tyring K. Stephen Introduction to Mycology - Medical Microbiology - NCBI Bookshelf Available online: https://www.ncbi.nlm.nih.gov/books/NBK8125/ (accessed on Nov 21, 2020).
25. Gauthier, G.M. Fungal Dimorphism and Virulence: Molecular Mechanisms for Temperature Adaptation, Immune Evasion, and In Vivo Survival. *Hiwandi Mediat. Inflamm.* **2017**.
26. Momany, M.; Talbot, N.J. Septins focus cellular growth for host infection by pathogenic fungi. *Front. Cell Dev. Biol.* **2017**, *5*, 1–7.
27. Huang, M.; Hull, C.M. Sporulation: how to survive on planet Earth (and beyond). *Curr. Genet.* **2017**, *63*, 831–838.
28. Couteaudier, Y.; Alabouvette, C. Survival and inoculum potential of conidia and chlamydospores of *Fusarium oxysporum* f.sp. lini in soil. *Can. J. Microbiol.* **1990**, *36*, 551–556.
29. NASH, S. M., CHRISTOU, T., and SNYDER, W.C. Existence of *Fusarium solani* f.sp. phaseoli as chlamydospores in soil. *Phyto- Pathol.* **1961**, *51*, 308–312.
30. Dhillon, N.K.; Sharma, S.; Khuller, G.K. Signaling Through Protein Kinases and Transcriptional Regulators in *Candida albicans*. *Crit. Rev. Microbiol.* **2003**, *293*.
31. Ene, I. V.; Brunke, S.; Brown, A.J.P.; Hube, B. Metabolism in fungal pathogenesis. *Cold Spring Harb. Perspect. Med.* **2014**, *4*, 1–21.
32. Brown, A.J.P.; Budge, S.; Kaloriti, D.; Tillmann, A.; Jacobsen, M.D.; Yin, Z.; Ene, I. V; Bohovych, I.; Sandai, D.; Kastora, S.; et al. Stress adaptation in a pathogenic fungus. *J. Exp. Biol.* 2014, *217*, 144–155.
33. GC, A. A Dictionary of the Fungi. Kew, Surrey: Commonwealth Mycological

Institute. Available online: https://books.google.com/books?hl=en&lr=&id=IFD4_VFRDdUC&oi=fnd&pg=PR11&dq=Ainsworth+GC,+A+dictionary+of+the+Fungi+1961&ots=s-iTilpkd6&sig=Dx-re1WvYXOTw_hd5yIM33Yb2e0#v=onepage&q=Ainsworth GC%2C A dictionary of the Fungi 1961&f=false (accessed on Nov 21, 2020).

34. Sullivan, D.J.; We, J.; Bennettn, D.E.; Coleman, D.C. Molecular characterization of a novel species associated with oral candidosis in HIV-infected individuals. *MiCrObiology* **1995**, *141*, 1507–1521.
35. Sullivan, D.J.; Moran, G.P.; Coleman, D.C. *Candida dubliniensis*: Ten years on. *FEMS Microbiol. Lett.* **2005**, *253*, 9–17.
36. Mccarren, K.L.; Mccomb, J.A.; Shearer, B.L.; St, G.E.; Hardy, J. The role of chlamydospores of Phytophthora cinnamomi-a review. *Australas. Plant Pathol.* **2005**, *34*, 333–338.
37. Abou-Gabal, M.; Fagerland, J. Ultrastructure of the Chlamydospore Growth Phase of *Aspergillus parasiticus* Associated with Higher Production of Aflatoxins. *Mycoses* **2009**, *24*, 307–311.
38. Lin, X.; Heitman, J. Chlamydospore Formation during Hyphal Growth in *Cryptococcus neoformans*. *Eukaryot. Cell* **2005**, *4*, 1746–1754.
39. bei Dermatophyten Gy Simon, C.; Galgoczy, J.; Simon, G.; Galgóczy, J. Chlamydospores of Dermatophytes. *Mykosen* **1986**, *29*, 469–473.
40. Garrison, R.G.; Boyd, K.S. *Histoplasma farciminosum*: A light and electron microscopic study. *Sabouraudia J. Med. Vet. Mycol. 13*, 174–184.
41. Miyaji, M.; Sano, A.; Sharmin, S.; Kamei, K.; Nishimura, K. The Role of Chlamydospores of *Paracoccidioides brasiliensis*. *Jpn. J. Med. Mycol* **2003**, *44*, 133–138.
42. Staib, P.; Morschhäuser, J. *Chlamydospore formation in* Candida albicans *and* Candida dubliniensis *– an enigmatic developmental programme*; 2007; Vol. 50, pp. 1–12;.
43. James Arthur Barnett, L.B. Medical Yeasts. In *Yeast Research A Historical Overview*; ASM press, 2011; p. undefined-379.
44. Whiteway, M.; Bachewich, C. Morphogenesis in Candida albicans. *Annu. Rev. Microbiol.* **2007**, *61*, 529–553.
45. Navarathna, D.H.M.L.P.; Pathirana, R.U.; Lionakis, M.S.; Nickerson, K.W.; Roberts, D.D. *Candida albicans* ISW2 Regulates Chlamydospore Suspensor Cell Formation and Virulence In Vivo in a Mouse Model of Disseminated Candidiasis. *PLoS One* **2016**, *11*, e0164449.
46. Nobile, C.J.; Bruno, V.M.; Richard, M.L.; Davis, D.A.; Mitchell, A.P. Genetic control of chlamydospore formation in *Candida albicans*. *Microbiology* **2003**.
47. Vidotto, V.; Bruatto, M.; Accattatis, G.; Caramello, S.; Vidotto, V, Bruatto M, Accattatis G, C.S.; Vidotto, V.; Bruatto, M.; Accattatis, G.; Caramello, S. Observation on the nucleic acids in the chlamydospores of *Candida albicans*. *New Microbiol.* **1996**, *19*, 327–334.
48. Raudonis, B.M.; Smith, A.G. Germination of the chlamydospores of *Candida albicans*. *Mycopathologia* **1982**, *78*, 87–91.
49. Citiulo, F.; Moran, G.P.; Coleman, D.C.; Sullivan, D.J. Purification and

germination of *Candida albicans* and *Candida dubliniensis* chlamydospores cultured in liquid media. *FEMS Yeast Res.* **2009**, *9*, 1051–1060.
50. Cole, G.T.; Seshan, K.R.; Phaneuf, M.; Lynn, K.T. Chlamydospore-like cells of *Candida albicans* in the gastrointestinal tract of infected, immunocompromised mice. *Can. J. Microbiol.* **1991**, *37*, 637–646.
51. Chabasse, D.; Bouchara, J.P.; de Gentile, L.; Chennebault, J.M. Candida albicans chlamydospores observed in vivo in a patient with AIDS. *Ann. Biol. Clin. (Paris).* **1988**, *46*, 817–818.
52. Dujardin, L.; Walbaum, S.; Biguet, J. Chlamydosporulation in "*Candida albicans*". Course of the morphogenesis; influence of light and sowing density. *Ann. Microbiol. (Paris). 131A*, 141–149.
53. Walker, L.; Huppert, M.; Woods, A. Corn Meal-Tween Agar: An Improved Medium for the Identification of *Candida albicans*. *Am. J. Clin. Pathol.* **1960**, *33*, 190–194.
54. Taschdjian, C.L. Routine Identification of *Candida albicans*: Current methods and new medium. *Mycologia* **1957**, *49*, 332–338.
55. PAVLATOU M, M.U. Rapid identification of *Candida albicans* with PCB medium. . *J Trop Med Hyg* **1961**, *64*, 268–270.
56. Bakerspigel, A. Soil-extract agar for *Candida albicans*. *A. M. A. Arch. Dermatology Syphilol.* **1954**, *69*, 735–737.
57. Beheshti, F.; Smith, A.G.; Krause, G.W. Germ tube and chlamydospore formation by *Candida albicans* on a new medium. *J. Clin. Microbiol.* **1975**, *2*, 345–348.
58. Alicia, Z.-S.; Blanca, O.-S.; Garcia, H.M.; Castillo-Casanova, M.; Alexandro, B. Rapid Production of *Candida albicans* Chlamydospores in Liquid Media under Various Incubation Conditions. *Jpn. J. Med. Mycol* **2006**, *47*, 231–234.
59. Staib, P.; Morschhäuser, J. Liquid growth conditions for abundant chlamydospore formation in *Candida dubliniensis*. *Mycoses* **2005**.
60. Al Mosaid, A.; Sullivan, D.J.; Coleman, D.C. Differentiation of Candida dubliniensis from Candida albicans on Pal's agar. *J. Clin. Microbiol.* **2003**, *41*, 4787–4789.
61. Daróczy, J.; Galgóczy, J.; Simon, G. Scanning Electron Microscopy of *Candida albicans* Chlamydospores. *Mycoses* **1988**, *31*, 523–526.
62. Miller, S.E.; Spurlock, B.O.; Michaels, G.E. Electron microscopy of young *Candida albicans* chlamydospores. *J. Bacteriol.* **1974**, *119*, 992–999.
63. Jansons, V.K.; Nickerson, W.J. Chemical Composition of Chlamydospores of *Candida albicans*. *J. Bacteriol.* **1970**, *104*, 922–932.
64. Leo D. Bemena, Kyunghun Min, James B. Konopka, and A.M.N. A conserved machinery underlies the synthesis of a chitosan layer in the *Candida* chlamydospore cell wall. *bioRxiv* **2021**, https://doi.org/10.1101/2021.01.19.427374.
65. Bakerspigel A, B.S. A possible function of the chlamydospores of *Candida albicans*. *Mycopathol Mycol Appl* **1974**, *54*, 147–52.
66. Martin, S.W.; Douglas, L.M.; Konopka, J.B. Cell Cycle Dynamics and Quorum Sensing in *Candida albicans* Chlamydospores Are Distinct from Budding and Hyphal Growth. *Eukaryot. Cell* **2005**, *4*, 1191–1202.

67. Fabry, W.; Schmid, E.N.; Schraps, M.; Ansorg, R. Isolation and purification of chlamydospores of *Candida albicans*. *Med. Mycol.* **2003**, *41*, 53–58.
68. Doedt, T.; Krishnamurthy, S.; Bockmühl, D.P.; Tebarth, B.; Stempel, C.; Russell, C.L.; Brown, A.J.P.; Ernst, J.F. APSES proteins regulate morphogenesis and metabolism in *Candida albicans*. *Mol. Biol. Cell* **2004**, *15*, 3167–3180.
69. Bockmühl, D.P.; Ernst, J.F. A Potential Phosphorylation Site for an A-Type Kinase in the Efg1 Regulator Protein Contributes to Hyphal Morphogenesis of *Candida albicans*. *Genetics* **2001**, *157*, 1523–1530.
70. Volker R.Stoldt, Anja Sonneborn, C.E.L. and J.F.E.; Stoldt, V.R.; Sonneborn, A.; Leuker, C.E.; Ernst, J.F. Efg1p, an essential regulator of morphogenesis of the human pathogen *Candida albicans*, is a member of a conserved class of bHLH proteins regulating morphogenetic processes in fungi. *EMBO J* **1997**, *16*, 1982–1991.
71. Hernday, A.D.; Lohse, M.B.; Fordyce, P.M.; Nobile, C.J.; DeRisi, J.L.; Johnson, A.D. Structure of the transcriptional network controlling white-opaque switching in *Candida albicans*. *Mol. Microbiol.* **2013**, *90*, 22–35.
72. Basso, V.; Znaidi, S.; Bachellier-Bassi, S.; D'Enfert, C.; Znaidi, S.; Bachellier-Bassi, S. From Genes to Networks: The Regulatory Circuitry Controlling *Candida albicans* Morphogenesis. *Curr. Top. Microbiol. Immunol.* **2019**, *422*, 61–69.
73. Sonneborn, A.; Bockmühl, D.P.; Ernst, J.F. Chlamydospore formation in *Candida albicans* requires the Efg1p morphogenetic regulator. *Infect. Immun.* **1999**, *67*, 5514–5517.
74. Bettina, B.; Pollath Christine , Peter Staib, B.H.S.B. *Candida* species rewired hyphae developmental programs for chlamydospore formation. *Front. Microbiol.* **2016**, *7*, 1–17.
75. Braun, B.R.; Kadosh, D.; Johnson, A.D. NRG1, a repressor of filamentous growth in *Candida albicans* , is down-regulated during filament induction. *EMBO J.* **2001**, *20*, 4753–4761.
76. Staib, P.; Morschhäuser, J. Differential expression of the NRG1 repressor controls species-specific regulation of chlamydospore development in *Candida albicans* and *Candida dubliniensis*. *Mol. Microbiol.* **2005**, *55*, 637–652.
77. Hernández-Cervantes, A.; Znaidi, S.; van Wijlick, L.; Denega, I.; Basso, V.; Ropars, J.; Sertour, N.; Sullivan, D.; Moran, G.; Basmaciyan, L.; et al. A conserved regulator controls asexual sporulation in the fungal pathogen *Candida albicans*. *Nat. Commun.* **2020**, *11*, 6224.
78. Covitz, P.A.; Herskowitz, I.; Mitchell, A.P. The yeast RME1 gene encodes a putative zinc finger protein that is directly repressed by a1-alpha2. *Genes Dev.* **1991**, *5*, 1982–1989.
79. Bürglin, T.R. Homeodomain subtypes and functional diversity. *Subcell. Biochem.* **2011**, *52*, 95–122.
80. Ghosh, A.K.; Wangsanut, T.; Fonzi, W.A.; Rolfes, R.J. The GRF10 homeobox gene regulates filamentous growth in the human fungal pathogen *Candida albicans* . *FEMS Yeast Res.* **2015**, *15*.
81. Smith, D.A.; Nicholls, S.; Morgan, B.A.; Brown, A.J.P.P.; Quinn, J. A conserved stress-activated protein kinase regulates a core stress response in the human

pathogen *Candida albicans*. *Mol. Biol. Cell* **2004**, *15*, 4179–4190.
82. Alonso-Monge, R.; Navarro-García, F.; Román, E.; Negredo, A.I.; Eisman, B.; Nombela, C.; Pla, J. The Hog1 Mitogen-Activated Protein Kinase Is Essential in the Oxidative Stress Response and Chlamydospore Formation in *Candida albicans*. *Eukaryot. Cell* **2003**, *2*, 351–361.
83. Eisman, B.; Alonso-Monge, R.; Román, E.; Arana, D.; Nombela, C.; Pla, J. The Cek1 and Hog1 mitogen-activated protein kinases play complementary roles in cell wall biogenesis and chlamydospore formation in the fungal pathogen *Candida albicans*. *Eukaryot. Cell* **2006**, *5*, 347–358.
84. Krishnamurthy, S.; Plaine, A.; Albert, J.; Prasad, T.; Prasad, R.; Ernst, J.F. Dosage-dependent functions of fatty acid desaturase Ole1p in growth and morphogenesis of *Candida albicans*. *Microbiology* **2004**, *150*, 1991–2003.
85. Melo, N.R.; Moran, G.P.; Warrilow, A.G.S.; Dudley, E.; Smith, S.N.; Sullivan, D.J.; Lamb, D.C.; Kelly, D.E.; Coleman, D.C.; Kelly, S.L. CYP56 (Dit2p) in Candida albicans: Characterization and investigation of its role in growth and antifungal drug susceptibility. *Antimicrob. Agents Chemother.* **2008**, *52*, 3718–3724.
86. Juchimiuk, M.; Kruszewska, J.; Palamarczyk, G. Dolichol phosphate mannose synthase from the pathogenic yeast *Candida albicans* is a multimeric enzyme. *Biochim. Biophys. Acta 1850* **2015**, *1850*, 2265–2275.
87. Bemena, L.D.; Min, K.; Konopka, J.B.; Neiman, A.M. A Conserved Machinery Underlies the Synthesis of a Chitosan Layer in the *Candida* Chlamydospore Cell Wall. *mSphere* **2021**, *6*.
88. Palige, K.; Linde, J.; Martin, R.; Böttcher, B.; Citiulo, F.; Sullivan, D.J.; Weber, J.; Staib, C.; Rupp, S.; Hube, B.; et al. Global Transcriptome Sequencing Identifies Chlamydospore Specific Markers in *Candida albicans* and *Candida dublliniensis*. *PLoS One* **2013**, *8*.
89. Giosa, D.; Felice, M.R.; Lawrence, T.J.; Gulati, M.; Scordino, F.; Giuffrè, L.; Passo, C. Lo; D'Alessandro, E.; Criseo, G.; Ardell, D.H.; et al. Whole RNA-sequencing and transcriptome assembly of *Candida albicans*and *Candida africana* under chlamydospore-inducing conditions. *Genome Biol. Evol.* **2017**, *9*, 1971–1977.
90. Ingle, S.; Kazi, R.; Patil, R.; Zore, G. Proteome analysis of *Candida albicans* cells undergoing chlamydosporulation. *J. Proteins Proteomics* **2019**, *10*, 269–290.
91. Ingle, S.; Kodgire, S.; Shiradhone, A.; Patil, R.; Zore, G. Chlamydospore specific proteins of *Candida albicans*. *Data* **2017**, *2*, doi:10.3390.

CHAPTER 2

An interwoven transcriptional network controls chlamydospore formation in the human fungal pathogen *Candida albicans*

In preparation for submission; Authors: Bapat Priyanka S, Gunasekaran Deepika, Nobile Clarissa J.

2.1 Abstract

Fungi are known to survive in diverse environmental conditions. Many fungi are polymorphic and can switch between different morphologies best suited to thrive in a particular environment. A normal resident of healthy humans and warm-blooded animals, *Candida albicans* is a commensal fungus that is also among the most common opportunistic pathogens of humans. *C. albicans* forms large, spherical thick-walled morphological structures called chlamydospores, routinely observed terminally or laterally to hyphae under *in vitro* conditions. Chlamydospores have been rarely observed on *C. albicans* infected *in vivo* tissue samples and the biological functions of *C. albicans* chlamydospores are currently unknown. Our understanding of transcriptional regulation of chlamydospore formation in *C. albicans* is limited. In this study, we aimed to identify the transcriptional regulatory network controlling chlamydospore formation in *C. albicans* using forward genetics and genome wide approaches. We screened a library of 211 *C. albicans* transcription factor homozygous deletion mutants to assay for their abilities to form chlamydospores under standard chlamydospore-inducing growth conditions. We identified nine core regulators of chlamydospore formation from this screen. Six of these regulators (Sfl1, Rme1, Cup9, Aaf1, Efg1, and Ume6), when deleted fail to produce chlamydospores and three of these regulators (Nrg1, Zcf8, and Rfg1), when deleted produce high levels of chlamydospores relative to the wildtype strain. Using genome wide approaches (RNA-seq and ChIP-seq), we identified the complete *C. albicans* chlamydospore transcriptional network that is composed of these nine core regulators and over ~3200 downstream target genes. Functional enrichment analysis for metabolic pathways that are enriched in the RNA-seq data suggests roles for SNARE vesicular transport, fatty acid degradation, and cell wall biosynthesis pathways in chlamydospore formation. We also identified other transcription factors, such as Rob1 and Tye7, and kinases, such as Ssk2, as downstream targets regulated by the core regulators. Network analyses based on conserved orthologous relationships of select genes within the network revealed that the network is comprised of 65% “old” genes and 35% “young” genes, indicative of the network being fairly well conserved.

2.2 Introduction

Fungi are known to survive under diverse environmental conditions and to adapt quickly to environmental changes [1]. Many fungal species are polymorphic and can switch between different morphologies best suited to thrive in a particular environment [2–4]. *Candida albicans* is a an asymptomatic commensal organism of humans and other warm blooded animals that colonizes the mucocutaneous surfaces of the mouth, skin, and gastrointestinal and genitourinary tracts of most humans [5,6]. *C. albicans* can switch between different morphologies depending on the environmental conditions [7–10]. Some of the phenotypes and morphologies that have been identified for *C. albicans* include the round yeast form, the hyphal form, pseudohyphal form, and chlamydospores [11–13]. Chlamydospores are enigmatic structures that are formed by two closely related members of the *Candida* clade species: *C. albicans* and *C. dubliniensis* [14,15].

Chlamydospores are characterized by their relatively large size (7-12μm), spherical shape, thick-walls, and are observed to form on the terminal or lateral ends of hyphae under specific *in vitro* environmental conditions (complex nutrient media, room temperature, oxygen-limiting and dark conditions) [12,16–18]. Chlamydospores have been rarely observed *in vivo* [19,20]. *C. albicans* chlamydospores are composed of a double layered cell wall, with a thinner outer layer largely composed of ß-1, 3 glucan and chitin, and a thicker inner layer composed of keratin [21–23]. Chemical analyses and staining procedures revealed that the center of chlamydospores is rich in lipids, proteins, mitochondria, ribosomes and nucleic acids [23–25]. As both DNA and RNA have been found to be present inside chlamydospores, several researchers hypothesize that chlamydospores are active structures that can germinate once favorable conditions reappear. Interestingly, it has been shown that the lifespan and activity of chlamydospores is dependent on the age of the spore, with older chlamydospores (>2 weeks old) reported to be non-responsive to germination [26]. There have been conflicting reports about germination of chlamydospores. Some studies have shown that young chlamydospores (~2-3 days old) can germinate to form yeast form cells and pseudohyphal cells [26–28].

Little is known about how *C. albicans* chlamydospores are regulated. Transcription factors like Efg1, Nrg1, Rme1, Grf10, Rim101, Isw2, Gln3, Gat1, and Gcn4 [16,24,29–33] and enzymes like Hog1, Ole1, Sch9, and Suv3 [16,34,35] have been implicated in *C. albicans* chlamydosporulation. Δ/Δ*efg1,* Δ/Δ*rme1,* and Δ/Δ*grf10* transcription factor mutant strains are known to fail to produce chlamydospore under chlamydospore inducing conditions. The transcription factors Rim101 and Isw2 were found to be required for the timely development of chlamydospores and for suspensor cell formation, respectively. The Δ/Δ*nrg1* mutant strain was found to be hypersporulative, forming a higher number of chlamydospores relative to the wildtype (WT) strain. Nonetheless, the regulatory network controlling chlamydospore formation in *C. albicans* is currently unidentified. Understanding how chlamydospores are regulated may provide insight into their biological functions.

Here, we combine forward genetics and genome wide approaches, particularly RNA sequencing and chromatin immunoprecipitation followed by sequencing to comprehensively map the transcriptional regulatory network controlling chlamydospore formation in *C. albicans.* We identified a highly interwoven chlamydospore transcriptional

network consisting of nine core regulators controlling over ~3200 downstream target genes. We also identified genes encoding other transcription factors (e.g., *ROB1* and *TYE7*) and genes encoding kinases (e.g., *SSK2*) as downstream target genes regulated by one or more of the core regulators. Preliminary network analyses based on conserved orthologous relationships of select genes within the network revealed that the network is comprised of 65% "old" genes and 35% "young" genes.

2.3 Materials and Methods

2.3.1 Strains and media

The previously described *C. albicans* reference strain SN250 (His+Leu+Arg- background), a derivative of clinical isolate strain SC5314 was used throughout the study as the wildtype reference strain (WT) [36,37]. The previously described 211 *C. albicans* transcription factor (TF) deletion mutant library (His+Leu+Arg-) [38,39] was used to screen for chlamydospore formation (available at the Fungal Genetics Stock Center (http://www.fgsc.net/). *C. albicans* cells were recovered from -80ºC glycerol stocks for two days at 30ºC on yeast extract peptone dextrose (YPD) agar plates (1% yeast extract (Thermo Fisher Scientific, Catalog #211929), 2% Bacto peptone (Gibco, Catalog #211677), 2% dextrose (Fisher Scientific Catalog #D16-3), and 2% agar (Criterion, Catalog #89405-066)). Overnight cultures were grown for ~15h at 30˚C, shaking at 225rpm in YPD liquid medium (1% yeast extract (Thermo Fisher Scientific, Catalog #211929), 2% Bacto peptone (Gibco, Catalog #211677), and 2% dextrose (Fisher Scientific Catalog #D16-3)). Overnight cultures were grown for ~15h at 30ºC, shaking at 225rpm in YPD liquid (1% yeast extract, 2% Bacto peptone, and 2% dextrose). Other C. *albicans* clinical isolates used in this study are strain #0761 (AR0761) and #0762 (AR0762) (Centers for Disease Control and Prevention (CDC) AR Isolate Bank, Drug Resistance *Candida* species panel; https://wwwn.cdc.gov/ARIsolateBank/, and *C. albicans* strains P76067, P57055, P87, and P75010 [40].

2.3.2 Transcription factor deletion library screen for chlamydospore formation

Serial dilutions were made in PBS (Phosphate buffer saline) and incubated under standard chlamydospore inducing conditions on 17g/L cornmeal agar (CMA) (Hardy Diagnostics Catalog #C5491) plus 0.33% Tween 80 agar plates (Sigma Aldrich Catalog #P4780) unless otherwise indicated, under a sterile glass coverslip (Fisher Scientific # 12-541-B) using Dalmau inoculation technique and stored in the dark at room temperature for 8 days [16,41]. WT strain was incubated under non-chlamydospore inducing conditions which included growth on 17g/L cornmeal agar (CMA) (Hardy Diagnostics Catalog #C5491) plus 0.33% Tween 80 agar plates (Sigma Aldrich Catalog #P4780), under a sterile glass coverslip (Fisher Scientific # 12-541-B) using Dalmau inoculation technique and stored under white light conditions at room temperature for 8 days [16,41]. The plates were then examined via light microscopy at 20X magnification, counting 15 representative fields of view for chlamydospore formation for all strains. TF mutant strains that failed to form any chlamydospores were grouped together as chlamydospore non-former strains and TF mutants that produced higher chlamydospores compared to the WT strain were grouped together as chlamydospore high-former strains. Chlamydospore formation was also

assessed on 20g/L rice extract agar (RE) (Fisher Scientific Catalog # L11567) [42] and 24g/L potato carrot bile medium (PCB) (HiMedia Catalog # M696500G plus 1.5% bile salts Difco Catalog # DF0130-15-6) [31]. All core TF regulators were screened and confirmed at least five times on CMA plus Tween 80 medium and three times on RE Tween 80 medium and PCB medium; and the entire 211 TF deletion mutant library was tested at least two times on CMA Tween 80 medium.

2.3.3 Strain construction

2.3.3.1 GFP tagging of core transcription factors

GFP tagged strains were generated using a previously described method [43]. In brief, we used CRISPR-Cas9 to incorporate a GFP tag at the 3' end of the identified core TFs in the SN250 background. Briefly, gRNA was identified near the stop codon of the TF of interest, and GFP sequence was introduced from the plasmid pCE001. Upstream donor DNA was designed with a minimum 50bp homology upstream into the 5'end of TF of interest and a minimum 20bp in the start of the eGFPtag. The downstream donor DNA was constructed with 20bp homology at the end of the eGFPtag and 50bp homology to the downstream sequence of the TF. After the amplifying the A, B and C fragments and the donor DNA, transformations were performed for 15 min at 44°C, the cells were plated YPD+NAT_{200} medium (1% yeast extract (Thermo Fisher Scientific, Catalog #211929), 2% Bacto peptone (Gibco, Catalog #211677), 2% dextrose (Fisher Scientific Catalog #D16-3), and 2% agar (Criterion, Catalog #89405-066), 0.2g/L nourseothricin (GoldBio Catalog # N-500-2) and incubated for 2 days at room temperature. Colonies were patched on SD-Leu plates and positive colonies were patched on YPD and YPD+NAT_{400} (1% yeast extract (Thermo Fisher Scientific, Catalog #211929), 2% Bacto peptone (Gibco, Catalog #211677), 2% dextrose (Fisher Scientific Catalog #D16-3), 2% agar (Criterion, Catalog #89405-066) and 0.2g/L nourseothricin (GoldBio Catalog # N-500-2) [43]. The LeUP-OUT colonies were confirmed using colony PCR. The expression of GFP tag was confirmed under chlamydospore inducing conditions using fluorescence EVOS microscope under 60X oil immersion lens.

2.3.3.2 Target gene deletion and complementation strains

The downstream target genes were deleted using a previously described CRISPR-Cas9 method [43]. Briefly, the gRNA was identified in the open reading frame (ORF) of the gene of interest, and upstream and downstream donor DNA was generated with at least 100bp homology from the site of orf deletion. For addback gene complementation strains, gRNA was designed within the donor DNA of the deletion strain and the complementation upstream and downstream donor DNA was designed with at least 200bp homology in upstream and downstream regions. The chlamydospore forming ability of target gene deletion and complementation strains were tested using the standard chlamydospore inducing conditions described above.

2.3.4. RNA sequencing

2.3.4.1 Cell harvesting for RNA extraction

RNA extraction was performed from the WT strain and core TF deletion mutant strains grown under chlamydospore inducing conditions (five plates per strain) for 8 days.

On day 8, the cells directly underneath the coverslips and those cells attached to coverslips were collected in 10 mL PBS using sterile loops and centrifuged at 3,000 x g for 5 min at 4ºC. RNA extractions were performed as per the user manual instructions using the Ribopure-Yeast RNA kit (Ambion, Catalog #AM1926). Briefly, the harvested cells were lysed in lysis buffer on Omni Bead beater for 8 cycles (30s On, 2 min Off), > 90% cell lysis was checked under the light microscope and aqueous phase was applied to filter cartridges; following which sequential wash steps were carried out as per the user manual instructions. After the final DNase treatment, the extracted and purified RNA was assessed for purity and yield using Nanodrop ND-1000 and stored at -80ºC freezer until further use. Two biological replicates per strain were processed.

2.3.4.2. Library generation and RNA 3' tag sequencing

The RNA-seq library was prepared using Lexogen's quantseq 3' mRNA-Seq Library Prep Kit FWD as per Illumina user manual instructions [44]. Briefly, poly(A) RNA was reverse transcribed, and second strand synthesis was carried out. Finally, double stranded cDNA library was processed for library amplification using i7 index adaptors. Following purification, the RNA quality and yield was determined using Qubit 4.0. Two biological replicates per strain prepared and libraries were sequenced on Hi-seq 5000 sequencer at DNA technologies core, UC Davis.

2.3.4.3 RNA sequencing data analysis

The RNA-seq data was analyzed using Lexogen quantseq Bluebee data analysis platform. In brief, Bluebee pipeline 1 was used for trimming and removal of low-quality tails using bbmap suite and STAR aligner with modified ENCODE settings was used for alignment to SC5314 genome [45]. Htseq-count with kit specific options (FWD) was used for gene count reading. DESeq2 was used to identify the differentially expressed genes between different strains (2 biological replicates each). The downstream target genes were identified using Upset plots [46,47] and functional enrichment analysis was performed as mentioned.

2.3.4.4 Functional enrichment analysis

Functional enrichment analyses of the genes regulated by transcription factors and other gene sets were performed using the clusterProfiler package (version 3.14.3) in R. The functional categories of these gene sets were identified using Gene Ontology (GO) enrichment and KEGG metabolic pathway enrichment. GO term annotations were retrieved from CGD and enriched cellular components, molecular functions and biological processes were identified using Enrichr [48]. A GO term was considered as enriched if the FDR adjusted p-value was less than 0.05. Metabolic pathways were annotated using the KEGG database for *C. albicans* and enriched KEGG pathways were identified using enrichKEGG with the clusterProfiler package (using FDR p-value cutoff of 0.05). The enriched KEGG pathways were then visualized using Pathview [49].

2.3.5 Chromatin Immunoprecipitation followed by sequencing (ChIP-seq)

2.3.5.1 Cell harvesting, DNA extraction and library preparation

ChIP sequencing was performed as previously described [50,51]. Briefly, the untagged control and GFP tagged strains were grown under chlamydospore inducing conditions on CMA plus 0.33% Tween 80 (ten plates per strain) for 8 days. On day 8, the cells were harvested in 24 mL nuclease free water and crosslinked with 1% formaldehyde (Sigma Aldrich Catalog # F8775-4X25 mL) for 15 min on nutator and quenched using 2.M glycine (Sigma Aldrich catalog # G7126) for 5 min and stored at -80 until further use. The cells were lysed using bead beating for 8 cycles and checked for >90% cell lysis. The chromatin was sheared using Bioruptor sonicator (20 cycles, 30s on, 1min off). For every ChIP sample, 5 uL of Living Colors Full length GFP Polyclonal Antibody (Clontech # 632692) and Protein-A Sepharose 4B Fast Flow beads (Sigma P9424) were used for the immunoprecipitation step. Samples were purified following protease treatment and crosslinks were reversed by incubating the samples at 65^{o}C. The ChIP-DNA was quantified using Qubit 4.0. and sent to Novogene for ChIP library preparation using NEB Next Ultra II DNA Library Prep Kit followed by sequencing on Illumina NovoSeq platform PE150 sequencer. Two biological replicates per strain were tested.

2.3.5.2 ChIP-seq data analysis with TF motif binding sequence identification

The reads were sequenced using Illumina NovoSeq platform PE150 and the quality of the sequencing data was verified using FastQC (version 0.11.9) [52]. The adapters were trimmed using Trimmomatic (version 0.38) and high-quality bases were enriched by removing leading and trailing bases below the quality score of 3. The reads were scanned with a 4-base sliding window and trimmed when the average quality per base dropped below 15 [53]. Additionally, trimmed reads less than 80 base pairs in length were discarded. The trimmed reads were mapped to the reference genome of *C. albicans* SC5314 obtained from the Candida Genome Database (CGD) (assembly version 21) using Bowtie2 (version 2.3.4.3) [54,55]. Reads that aligned to more than one locus in the genome were randomly mapped to a locus. Peaks were then called using MACS2 (version 2.1.2) by combining biological replicates, with a false discover rate cutoff of 0.05 [56,57]. The binding motif for each transcription factor (TF) was obtained using MochiView [57] as mentioned in Nobile et. al. 2012 [51]. Briefly, a 250 bp region flanking the peak summit was retrieved for each peak. For each TF, half of the peaks were used for motif identification and the top five identified motifs were tested for enrichment in the remaining peaks. The motifs were identified using the motif finder function and the refined motifs ('from CULL refinement') were tested for enrichment in the remaining 50% of peaks using the motif enrichment table function. The motif most enriched in the test set was then considered as the representative motif for the TF. Binding peaks were visualized using MochiView and file conversion between file types was performed using SAMtools [57,58]. The transcriptional regulatory network was constructed by combining peaks called using MACS2 and differentially expressed genes in WT strain SN250 subjected to chlamydospore inducing conditions (using an adjusted p-value threshold of < 0.05 and a $\log_2$ fold change threshold of 0.58). The chlamydospore regulatory network was visualized using the networkD3 package in R.

2.3.6 Identification of functionally relevant candidate target genes in the chlamydospore regulatory network

Functionally relevant downstream target genes were identified and prioritized based on two criteria: (1) by the target genes that were the most differentially expressed based on the RNA-seq data of the nine core TF mutant strains, and (2) by the total number of core TF regulator binding events detected in the upstream regulatory regions of the target genes.

2.3.7 Conservation of the chlamydospore regulatory network

Preliminary analyses on the conservation of the chlamydospore regulatory network using the nine core TFs and 27 commonly bound target genes were determined for *C. albicans*, non-*albicans Candida* species (*C. dubliniensis, C. tropicalis, C. parapsilosis,* and *C. glabrata), Saccharomyces cerevisiae* and other known chlamydospore forming fungi *(Blastomyces dermatitidis, Paracoccidioides brasiliensis*, and *Cryptococcus neoformans*). The annotated protein coding sequences for the reference strains of these species were obtained from NCBI. Orthologous groups across these species were identified using OrthoFinder with default parameters; approximately 90% of all protein coding sequences were assigned to orthogroups by OrthoFinder [59,60]. In addition, OrthoFinder also inferred the phylogenetic relationships between the species using unrooted gene trees from orthogroups containing all species [61,62]. This species tree was visualized using Interactive Tree of Life (iTOL) and annotated with orthologous relationships of the core TFs and 27 commonly regulated genes between the species (orf19.5191, orf19.5735.3 and orf19.4712 were excluded from the set of commonly regulated genes, due to ambiguous annotations) [63]. In this study, we define 'young' genes as those that are present and conserved only in the CTG clade in the species analyzed [64,65], and, we define 'old' genes as those that are present and conserved in other fungal species distantly related to *C. albicans,* such as *C. neoformans* and *P. brasiliensis*.

2.4 Results

2.4.1 Identification and phenotypic characterization of transcription factor mutants for chlamydospore formation in *C. albicans*

Transcription factors are proteins that bind DNA in a sequence specific manner and that regulate the expression of their nearby target genes [38,51]. TFs are central to the regulation of biological processes in response to external cues while maintaining internal homeostasis. In order to determine the transcriptional regulatory network controlling *C. albicans* chlamydospore formation, we screened an existing library of 211 TF deletion mutants [38,39] to identify the TF mutants most severely affected in their abilities to form chlamydospores under standard chlamydospore inducing conditions (CMA Tween 80 medium at 8 days) compared to the reference strain SN250 [66]. The TF deletion mutant strain library screen results were grouped into chlamydospore indices based on the ability of the TF mutant strain to form chlamydospores compared to the WT strain (normalized to 1) (Figure 2.1A). CI-1 (0 chlamydospores, TF mutant failed to form chlamydospores), CI-2 (0.01-1), CI-3 (1 and above, higher number of chlamydospores produced than WT strain).

From this screen, we identified 10 mutant strains (Figure 2.1B-J) that were severely affected in their abilities to form chlamydospores. 7 mutant strains failed completely to form chlamydospores (CI-1); Δ/Δ*sfl1,* Δ/Δ*rme1,* Δ/Δ*cup9,* Δ/Δ*aaf1,* Δ/Δ*efg1,* Δ/Δ*ume6,* Δ/Δ*orf19.2131* and are collectively referred to as chlamydospore non-former strains for the purposes of this study. 3 mutant strains produced higher number of chlamydospores relative to the WT strain (CI-3); Δ/Δ*nrg1,* Δ/Δ*rfg1 and* Δ/Δ*zcf8* and are collectively referred to as chlamydospore high-former strains for the purposes of this study. As these 10 transcription factor mutant strains were most severely affected in their abilities to form chlamydospores, we considered them to be core regulators of chlamydospore formation. Furthermore, we tested these 10 strains on additional medium reported to induce chlamydospore formation (e.g., rice extract agar medium and potato carrot bile agar medium) [31,42,67]. We found that the Δ/Δ*orf19.2131* strain did not form chlamydospores on CMA Tween 80 medium, however it readily formed chlamydospores on rice extract agar medium (Figure S2.1) and was deemed to be a CMA Tween 80 specific regulator. Since this strain formed chlamydospores in a condition specific manner, we did not include it in our downstream analysis. Results for chlamydospore formation on PCB medium were similar to results on CMA Tween 80 medium and are shown in (Figure S2.2). The screen was carried out blindly and identification of previously identified regulators like Efg1, Nrg1 and Rme1 which were previously reported to be involved in chlamydospore formation served as an internal control for the screen [29–31]. Of these mutant strains, it is noteworthy to mention that Δ/Δ*efg1* and Δ/Δ*nrg1* are hyperfilamentous under the tested conditions, as previously reported [29,68]. The Δ/Δ*ume6* mutant strain is yeast locked and did not form hyphae or pseudohyphae under the conditions tested (Figure 2G). Other noteworthy phenotypes under these chlamydospore inducing conditions were transcription factor mutant strains Δ/Δ*brg1* and Δ/Δ*ndt80*B which failed to produce long hyphal filaments but formed chlamydospores. Transcription factor mutant strain Δ/Δ*isw2* which has been previously reported to be required for suspensor cell formation and for timely formation of chlamydospores, grouped in our CI-2 index along with the transcription factor strain Δ/Δ*rob1*, both forming very few chlamydospores relative to WT strain [16,24]. We also tested seven other *C. albicans* clinical isolates for chlamydospore formation on CMA Tween 80 medium and found that five clinical isolates form chlamydospores comparable to the WT strain, while two isolates did not form chlamydospores under the conditions tested (Figure S2.3).

A

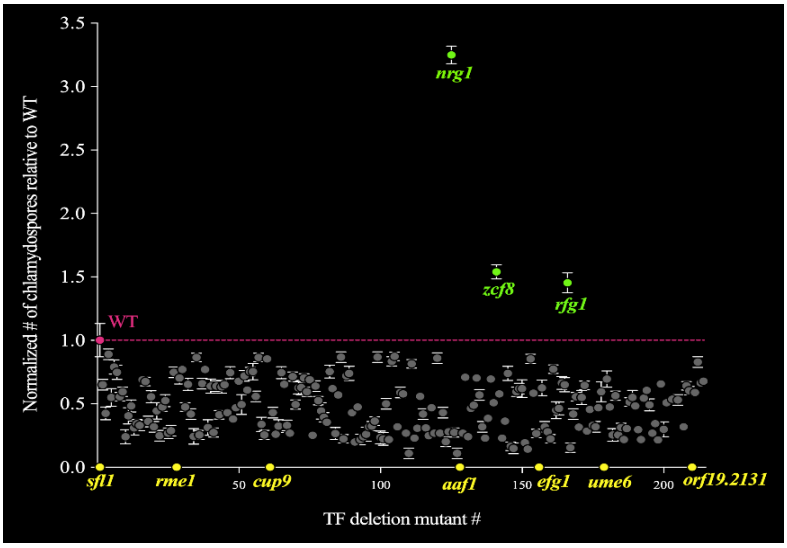
Normalized # of chlamydospores relative to WT
3.5
3.0
2.5
2.0
1.5
1.0
0.5
0.0
WT
nrg1
zcf8
rfg1
sfl1
rme1
50
cup9
100
aaf1
150
efg1
ume6
200
orf19.2131
TF deletion mutant #

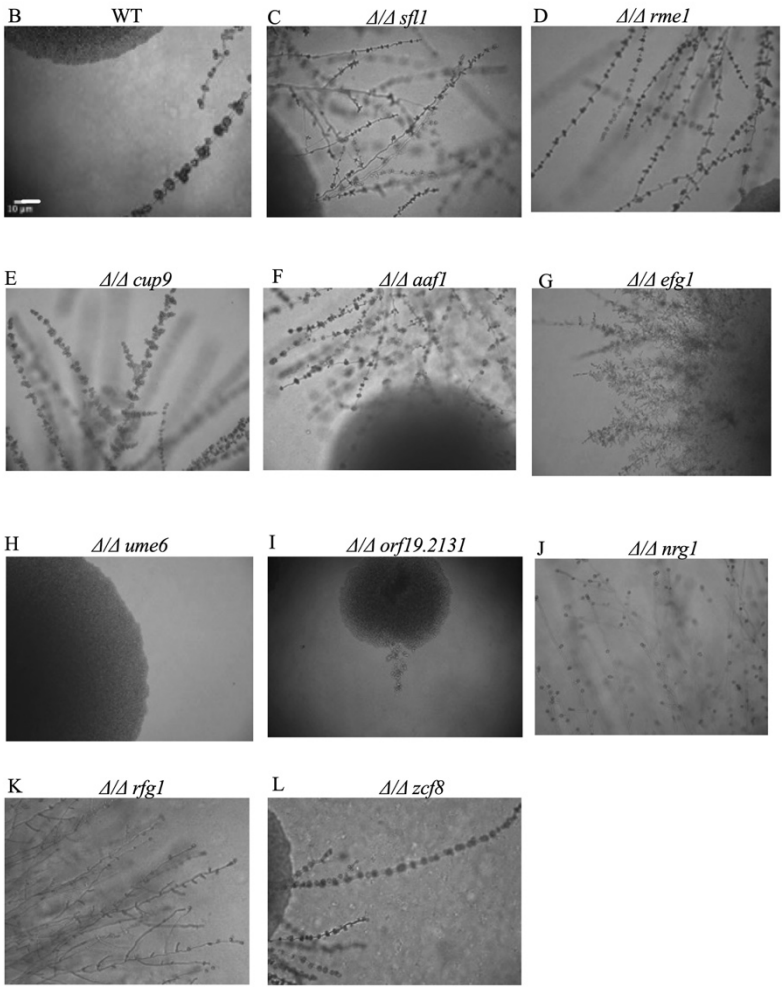
B WT
C Δ/Δ sfl1
D Δ/Δ rme1
E Δ/Δ cup9
F Δ/Δ aaf1
G Δ/Δ efg1
H Δ/Δ ume6
I Δ/Δ orf19.2131
J Δ/Δ nrg1
K Δ/Δ rfg1
L Δ/Δ zcf8

Figure 2.1 Screening and characterization of chlamydospore defective transcription factor mutants. (A) Scatter plot depicting the transcription factor deletion mutant strain library screen for chlamydospore formation. Wildtype reference strain (WT) and 211 transcription factor deletion mutant strains were grown under chlamydospore inducing conditions using CMA Tween 80 medium and incubated under sterile coverslips at room temperature in the dark for 8 days following which they were observed using a 20X objective under the light microscope. 15 representative fields of view were counted to determine the number of chlamydospores formed by a mutant strain relative to WT strain where WT strain was normalized to 1 (pink dashed line). Seven TF mutant strains failed to form chlamydospores (yellow) while three mutant strains formed more chlamydospores (green) relative to WT strain. Normalized average number of chlamydospores formed by each mutant strain relative to WT strain (n=2) are shown with standard deviation error bars. (B-L) Colony and cellular phenotypes of core chlamydospore transcription factor mutant strains under standard inducing conditions on CMA Tween 80 medium in the dark at room temperature under sterile coverslips for 8 days following which the plates were observed using a 20X objective with a brightfield microscope. Representative images are shown for (B) WT, (C) TF001 Δ/Δ*sfl1*, (D) TF028 Δ/Δ*rme1*, (E) TF061 Δ/Δ*cup9*, (F) TF128 Δ/Δ*aaf1*, (G) TF156 Δ/Δ*efg1*, (H) TF179 Δ/Δ*ume6*, (I) TF210 Δ/Δ*orf19.2131*, (J) TF125 Δ/Δ*nrg1*, (K) TF166 Δ/Δ*rfg1*, (L) TF141 Δ/Δ*zcf8*. Scale bar represents 10 μM.

2.4.2 Transcriptional relationships among core chlamydospore regulators

2.4.2.1 Genome wide differential gene expression patterns of chlamydospore regulators

To identify the differentially expressed genes in each of the nine core regulators, we performed RNA-seq on the WT strain and deletion mutant strains of the identified regulators under chlamydospore inducing conditions and also on the WT strain under non-chlamydospore inducing conditions. We used the 3'tagseq method for RNA-seq [69]. From the RNA-seq data, in comparison to the isogenic reference strain, we found that 838 genes were upregulated and 431 genes were downregulated in the Δ/Δ*sfl1* strain, 720 genes were upregulated and 833 genes were downregulated in the Δ/Δ*aaf1* strain, 819 genes were upregulated and 786 genes were downregulated in the Δ/Δ*efg1* strain, 699 genes were upregulated and 585 genes were downregulated in the Δ/Δ*ume6* strain, 900 genes were upregulated and 690 genes were downregulated in the Δ/Δ*nrg1* strain, 553 genes were upregulated and 729 genes were downregulated in the Δ/Δ*zcf8* strain, 951 genes were upregulated and 1093 genes were downregulated in the Δ/Δ*rme1* strain, 1025 genes were upregulated and 960 genes were downregulated in the Δ/Δ*cup9* strain, and 656 were upregulated and 774 genes were downregulated in the Δ/Δ*rfg1* strain (threshold of $\log_2>0.58$ and $\log_2< -0.58$, padj value of ≤ 0.05). Further, the number of common target genes regulated by multiple core TFs were identified and visualized using Upset plots [47] (Figure S2.A- S4D). From our RNA-seq data, the differential gene regulation of the core regulators to each other was also determined; we found that *SFL1* was downregulated in Δ/Δ*rme1,* Δ/Δ*cup9* and upregulated in Δ/Δ*nrg1*; *RME1* was downregulated in the Δ/Δ*sfl1,* Δ/Δ*cup9,* Δ/Δ*aaf1,* Δ/Δ*efg1,* Δ/Δ*ume6,* Δ/Δ*zcf8* strains and upregulated in the Δ/Δ*nrg1*

strain; *CUP9* was downregulated in the Δ/Δ*efg1* strain and upregulated in the Δ/Δ*nrg1* strain; *AAF1* was downregulated in the Δ/Δ*sfl1,* and Δ/Δ*efg1* strains and upregulated in the Δ/Δ*cup9* strain; *NRG1* was downregulated in the Δ/Δ*sfl1,* Δ/Δ*aaf1,* Δ/Δ*efg1*and Δ/Δ*ume6* strains; *EFG1* was upregulated in the Δ/Δ*nrg1* strain; *UME6* was upregulated in the Δ/Δ*nrg1, RFG1* was downregulated in the Δ/Δ*sfl1,* Δ/Δ*cup9,* Δ/Δ*aaf1,* Δ/Δ*efg1,* Δ/Δ*ume6,* Δ/Δ*zcf8,* Δ/Δ*nrg1,* and Δ/Δ*rme1* strains. Interestingly, *RFG1* was found to be downregulated in all six chlamydospore non-former strains and in the two other chlamydospore high-former strains and is notably mis-regulated in all the core regulators.

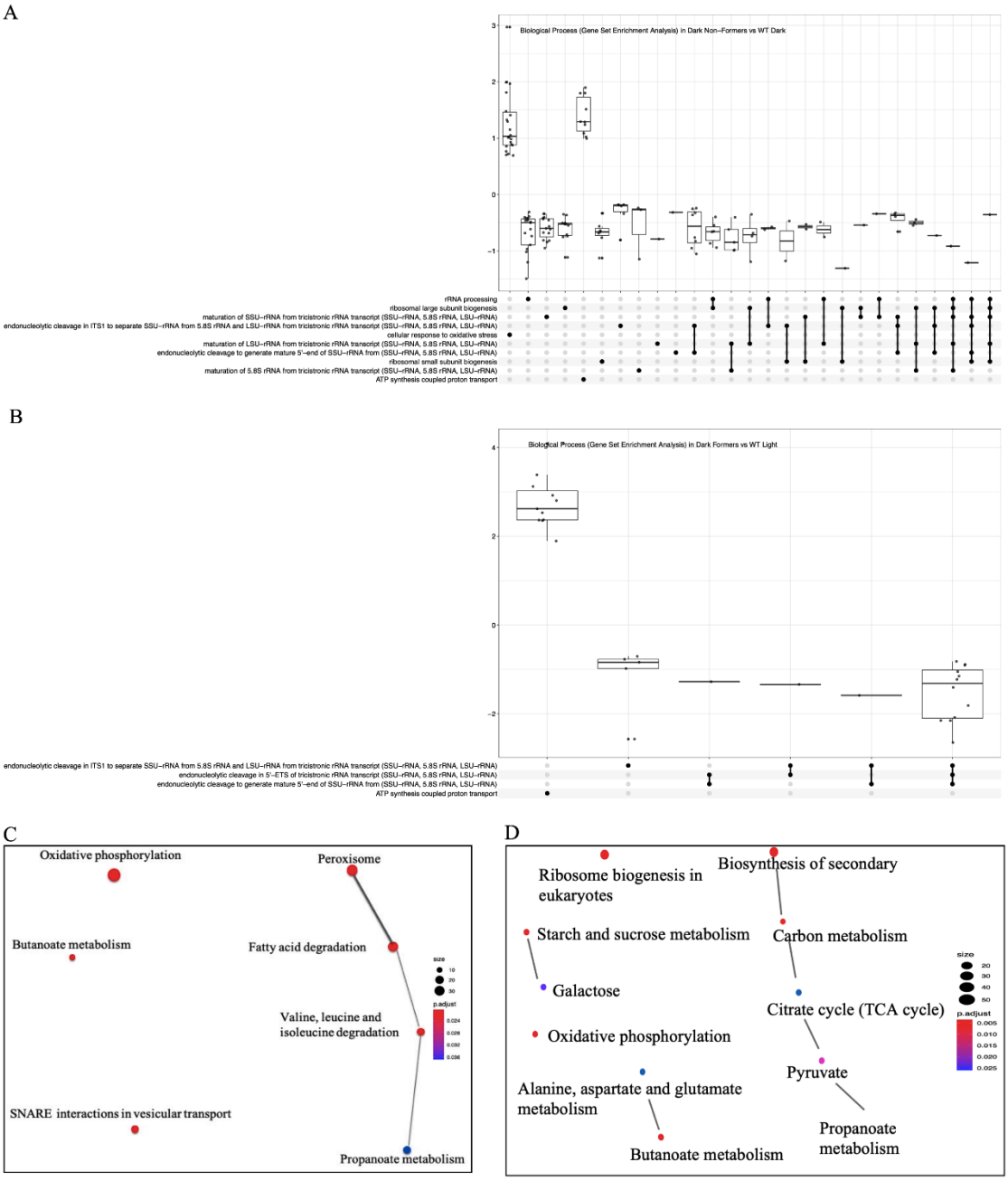

Figure 2.2 Functional enrichment analyses of chlamydospore high-former strains and chlamydospore non-former strains

Chlamydospore non-former strains, high-former strains and the WT strain were grown under standard chlamydospore inducing conditions on CMA Tween 80 medium under oxygen limiting conditions in the dark at room temperature for 8 days and RNA-sequencing was performed on the harvested cells following which functional enrichment analysis was performed (A) Upset plot for GSEA functional enrichment of biological processes for chlamydospore non-former strains vs the WT strain under chlamydospore inducing conditions using clusterProfiler GSEA (B) Upset plot for GSEA functional enrichment of

biological processes for chlamydospore high-former strains vs the WT strain under chlamydospore non-inducing conditions using clusterProfiler. (C) Network plot showing the KEGG pathway enrichment between chlamydospore high-former strains vs the chlamydospore non-former strains using enrichKEGG program. The sizes of the nodes range from 10 genes to 30 genes (padj ≤ 0.036). The thickness of the interconnecting lines shows the number of genes shared by the two pathways. (D) Network plot showing the KEGG pathway enrichment between chlamydospore non-former strains vs the WT strain under chlamydospore inducing conditions using enrichKEGG. The sizes of the nodes range from 10 genes to 50 genes (padj ≤ 0.025). The thickness of the interconnecting lines shows the number of genes shared by the two pathways.

For commonly regulated target genes for chlamydospore high-former strains, we found 27 genes commonly upregulated and 59 genes commonly downregulated (Figure S2.4A and S2.4B), while 12 genes were commonly downregulated in chlamydospore non-former strains (threshold of $\log_2$>0.58 and $\log_2$< -0.58, padj value of ≤0.05) (Figure S2.4C). We did not find any genes to be commonly upregulated in all chlamydospore non-former strains (set size of 10 genes minimum) (Figure S2.4D).

2.4.2.2 Functional enrichment analysis of the target genes

We performed Gene Set Enrichment Analyses (GSEA) on the RNA-sequencing data to identify the functionally enriched pathways in chlamydospore formation. We found many biological processes to be enriched including but not limited to rRNA cleavage pathways and ATP synthesis pathways for chlamydospore high-former strains (Δ/Δ*nrg1*, Δ/Δ*rfg1*, Δ/Δ*zcf8*) under chlamydospore inducing conditions vs the WT strain under chlamydospore non-inducing conditions (Figure 2.2A). We also found that for chlamydospore non-former strains vs WT strain under chlamydospore inducing conditions, the biological processes that were enriched included rRNA processing, cellular response to oxidative stress and ribosomal biogenesis (Figure 2.2B). The Kyoto encyclopedia of genes and Genomes (KEGG) ontology pathways of peroxisomal biogenesis, fatty acid degradation and interestingly SNARE vesicular transport are enriched for chlamydospore high-former strains vs chlamydospore non-former strains (Figure 2.2C), and lastly, KEGG pathways of oxidative phosphorylation, ribosomal biogenesis, amino acid and tricarboxylic acid (TCA) are enriched for chlamydospore non-former strains vs WT strain under chlamydospore inducing conditions (Figure 2.2D)

2.4.2.3 Chromatin Immunoprecipitation followed by sequencing on the core TF regulators

To identify and map direct TF binding events genome wide, we performed chromatin immunoprecipitation followed by sequencing (ChIP-seq) [50] on the nine GFP-tagged strains of the core TF regulators under chlamydospore inducing conditions. Based on the ChIP-seq data analysis, a list of all significantly bound target gene locations for each regulator were determined using MACS2 [56,70] and visualized using Mochiview [57]. We calculate the following number of upstream regulatory regions bound by each TF core regulator as summarized in Table 2.1.

Table 2.1: Summary of ChIP-seq binding events detected in the upstream regulatory regions of core TF regulators. The cells from GFP tagged versions of core TF regulators were harvested under standard chlamydospore inducing conditions of growth of CMA Tween 80 medium at room temperature under oxygen limitation in dark and ChIP-seq was performed. MACS2 [56] for binding and peak enrichment.

Core regulator	# of ChIP binding sites detected in each core regulator
Sfl1	100
Rme1	2411
Cup9	428
Aaf1	402
Efg1	540
Ume6	473
Nrg1	277
Rfg1	404
Zcf8	695

2.4.2.4 Chlamydospore regulatory network of *C. albicans*

If we convert the bound upstream regulatory regions to genes that are likely controlled by the core TFs, our analysis suggests that the chlamydospore regulatory network is composed of ~3200 genes. The chlamydospore regulatory network is shown in Figure 2.3A. Based on the ChIP-seq dataset, a high degree of overlap between target genes among the core TF regulators suggests that the chlamydospore network is considerably interwoven and that many genes are controlled by more than 1 regulator.

Next, we also generated a color-coded network primarily based on the total number of ChIP-seq binding events detected in the upstream regulatory regions of each target gene ranging from zero events detected as shown in blue and all nine-core regulator binding in the regulatory regions of target genes as shown in pink (Figure S2.5). We found that 30 upstream regulatory regions were bound by all nine core regulators (white circle), 82 upstream regulatory regions are bound by the three chlamydospore high-former strains and 7 upstream regulatory regions were bound by the six chlamydospore non-former strains (Figure 2.3B).

Next, by analyzing the overlap between our ChIP-seq and RNA-seq datasets, we find a strong correlation between transcription regulator binding and differential gene expression. For the correlation between the binding of a given single transcription factor core regulator and the RNA-seq data set for the differential gene expression in the core regulator deletion mutant, we find a range of 31%-55% (Table 2.2). This overlap suggests that binding of regulators is strongly associated with corresponding differential gene

expression under chlamydospore inducing conditions. We note that all nine chlamydospore regulators act both as activators and repressors of their target genes.

A

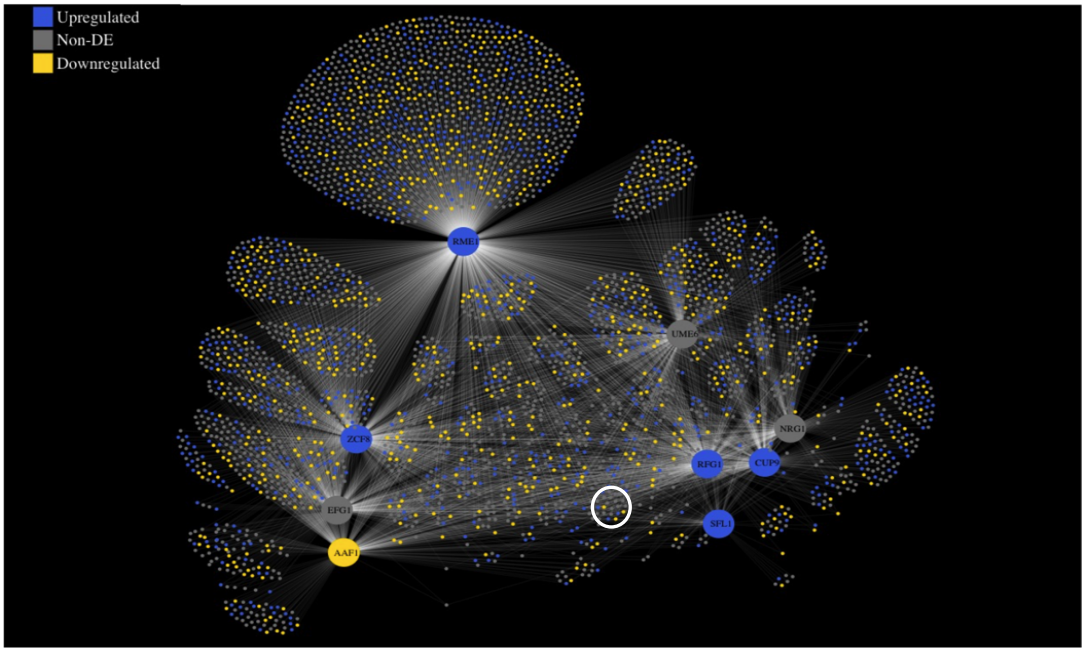

B

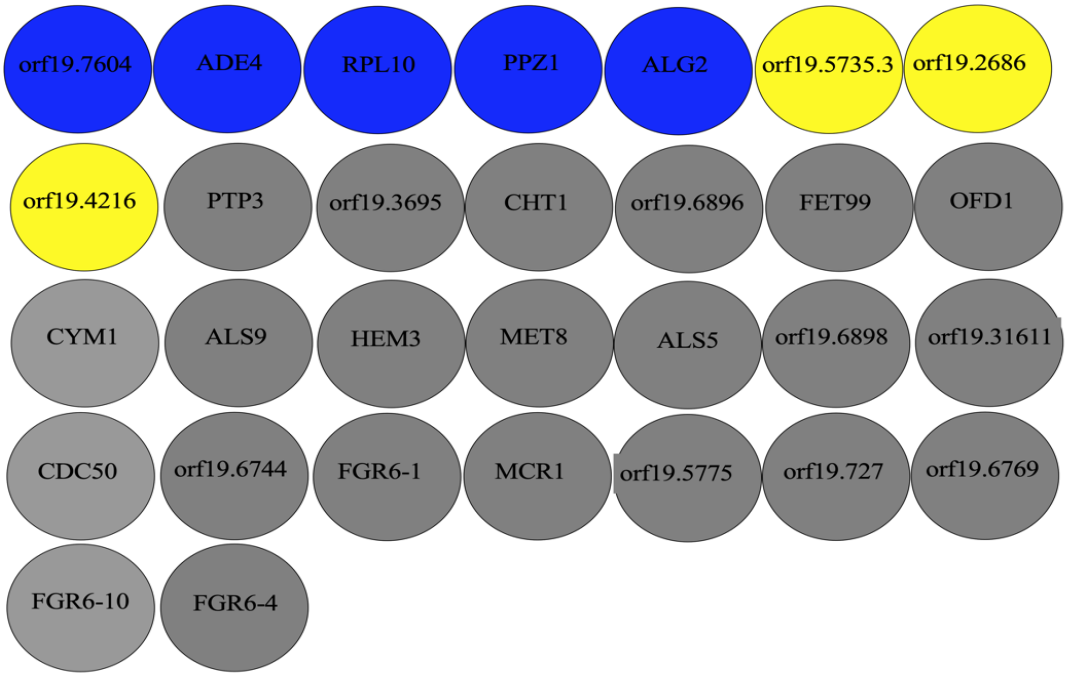

C

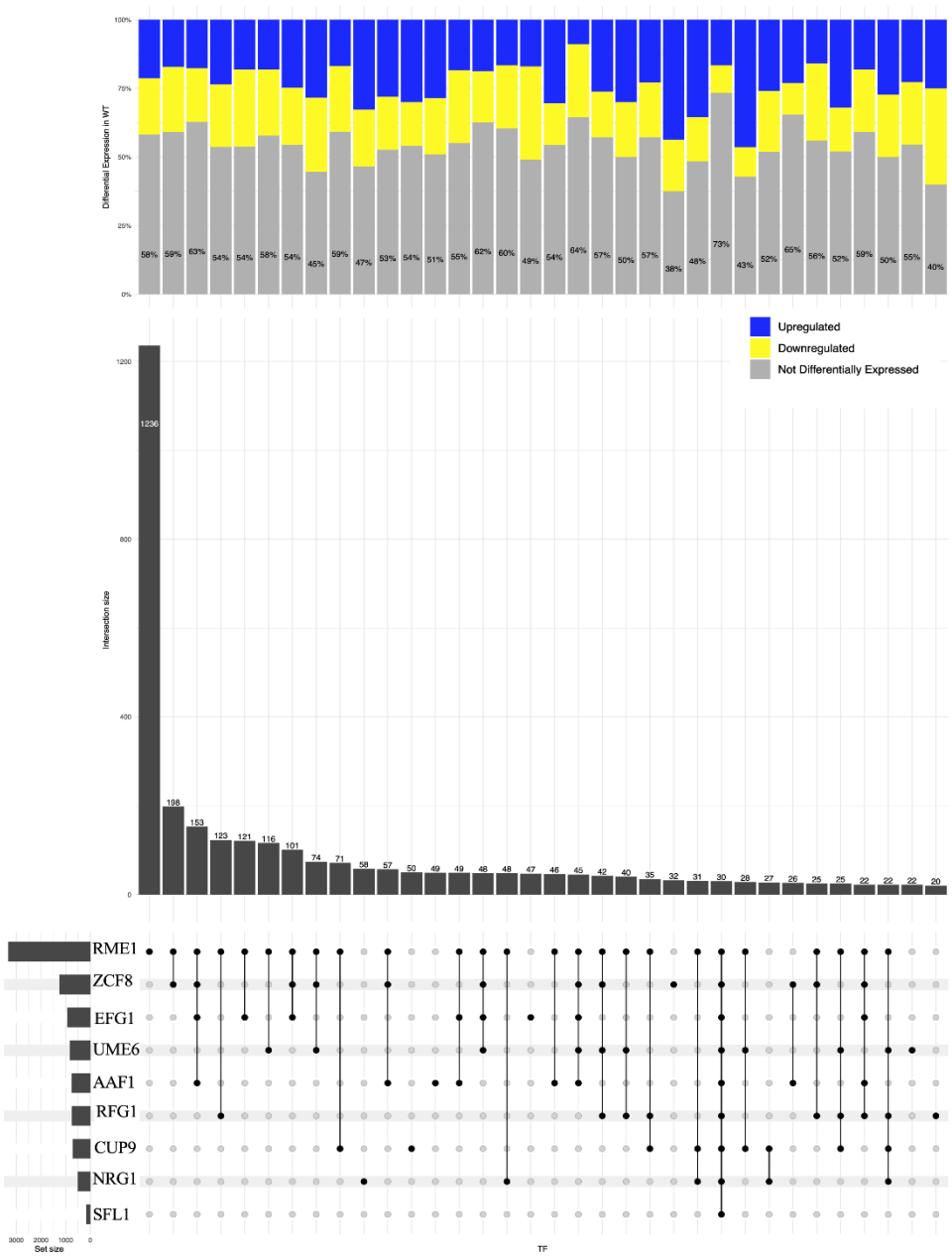

Figure 2.3 The chlamydospore regulatory network of *C. albicans*.
(A)The nine chlamydospore core regulators are represented by nine large circular hubs. Smaller circles represent target genes, which are connected by their respective regulators by lines, indicating a direct interaction as determined by genome wide ChIP-seq. Genes that are differentially regulated as determined by RNA-seq expression data (threshold $\log_2$ fold change of |0.58| cutoff) in the WT strain under chlamydospore inducing conditions vs non-chlamydospore inducing conditions formation as shown in blue for the upregulated genes, in yellow for downregulated genes and gray for the genes with no differential

expression detected. A white circle is drawn around the 30 target genes bound by all nine regulators. (B) The identity of the 30 target genes is indicated as colored circles (blue circles are genes that are upregulated, yellow circles are genes that are downregulated, and gray circles are genes with no change in WT strain under chlamydospore inducing conditions vs non-chlamydospore inducing conditions). Overall, 30 genes are bound by all nine regulators, 29 genes are bound by eight or more, 54 are bound by seven or more, 103 are bound by six or more, 212 are bound by five or more, 441 are bound by four or more, 575 are bound by three or more, 854 genes are bound by two or more of the chlamydospore core regulators. (C) The Upset plot showing the analysis for number of common connections shared by core TF regulators from chlamydospore regulatory network under chlamydospore inducing conditions. The bottom left panel are the names of the core TF regulators and bottom right side of the panel shows the number of connections shared between the nine core regulators. The top side of the figure shows the fraction of genes that are differentially regulated in WT strain under chlamydospore inducing conditions vs WT strain under non-chlamydospore inducing conditions (blue for upregulation, yellow for downregulation and grey for no change in the expression).

Table 2.2 Summary of genes shared between RNA-seq and ChIP-seq datasets. Summary table showing total number of ChIP-seq binding events detected for each core TF regulator, the percentage of genes shared between these binding events and differentially expressed genes gathered from RNA-seq dataset for the nine the core TF regulators under chlamydospore inducing conditions.

Core TF regulator	Total of ChIP binding sites	% of ChIP binding with differential gene expression in core TF mutant	# Of upregulated genes	# Of downregulated genes
Sfl1	100	36%	25	11
Rme1	2411	42%	484	536
Cup9	428	55%	96	142
Aaf1	402	43%	77	98
Efg1	540	42%	126	105
Ume6	473	31%	95	52
Nrg1	277	45%	86	39
Rfg1	404	45%	77	108
Zcf8	695	35%	111	134

Lastly, we also calculated the number of genes that were commonly connected by all nine core TF regulators, combinations of the core TF regulator connections and also the genes controlled by individual TF regulators (Figure 2.3C). We found that 30 genes are

commonly connected by nine core regulators, and of these 30 genes three genes (*ORF19.5191, ORF19.5735.3* and *ORF19.4712*) are reported to have ambiguous annotations, with 22 genes displaying no differential gene expression, five genes being upregulated, and three genes being downregulated in the WT strain under chlamydospore inducing conditions vs WT strain under non-chlamydospore inducing conditions (Figure 2.3C). We also note that transcription factor *RME1* regulates a subset of its genes on its own (1236 genes- nearly half of the genes bound by and regulated only by Rme1).

2.4.2.5 Core TF regulatory circuit

In order to generate the TF chlamydospore regulatory circuit for the nine core TFs with each other, we combined the RNA-seq and the ChIP-seq datasets (Figure 2.4). We found that Cup9 was the only core regulator that bound to its own upstream intergenic region, suggesting autoregulation. Additionally, the results also show that the nine core regulators identified control the expression of each other, where 4 regulators bind to the upstream intergenic region of *SFL1* (Figure 2.5A), 4 regulators bind to the upstream regulatory region of *RME1* (Figure 2.5B), 4 regulators bind to the upstream intergenic region of *CUP9* (Figure 2.5C), 2 regulators bind to the upstream intergenic region of *AAF1* (Figure 2.5D), 4 regulators bind in the upstream intergenic region of *EFG1* (Figure 2.5E), 1 regulator binds to the upstream regulatory region of *UME6* (Figure 2.5F), 4 regulators bind to the upstream intergenic region of *NRG1* (Figure 2.5G), and 4 regulators bind to the upstream intergenic region of *RFG1* (Figure 2.5H). For example, we observed a positive and negative feedback loop between Ume6 and Nrg1; and a feedforward loop between Nrg1, Rfg1 and Efg1 (Nrg1 activates Rfg1, and Nrg1 and Rfg1 inhibit Efg1).

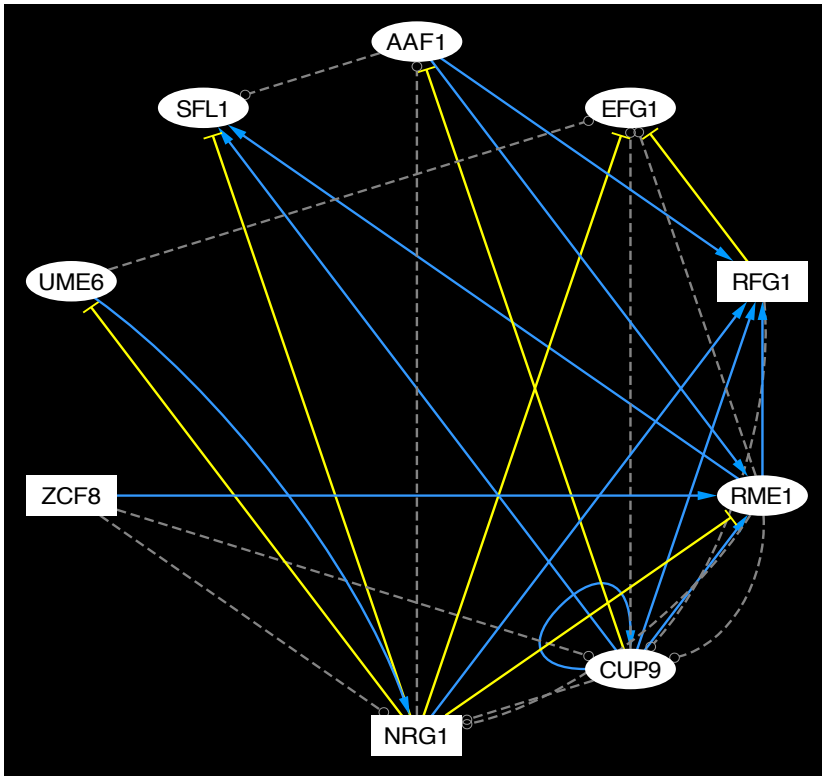

Figure 2.4 Chlamydospore regulatory circuit. The chlamydospore regulatory circuit based on ChIP-seq and RNA-seq datasets is shown. The rectangle boxes indicate TFs that when deleted are chlamydospore high-former strains and the six ellipses indicate TFs that when deleted are chlamydospore non-former strains. The directional lines indicate of binding interactions of the source TF in the upstream regulatory regions of the target TF as determined by ChIP-seq analysis. The color of the directional lines indicates the role of the source TF in the regulation of the target TF, based on RNA-seq expression of the TF in the deletion mutant of the source TF strain compared to the WT strain under chlamydospore inducing conditions. The directional blue arrows indicate activation of target TF by the source TF (i.e., downregulation of target gene in the source TF knockout), directional yellow inhibitory signs indicate repression (i.e., upregulation of target gene in TF knockout) and dashed gray lines with closed loops indicate no change in expression.

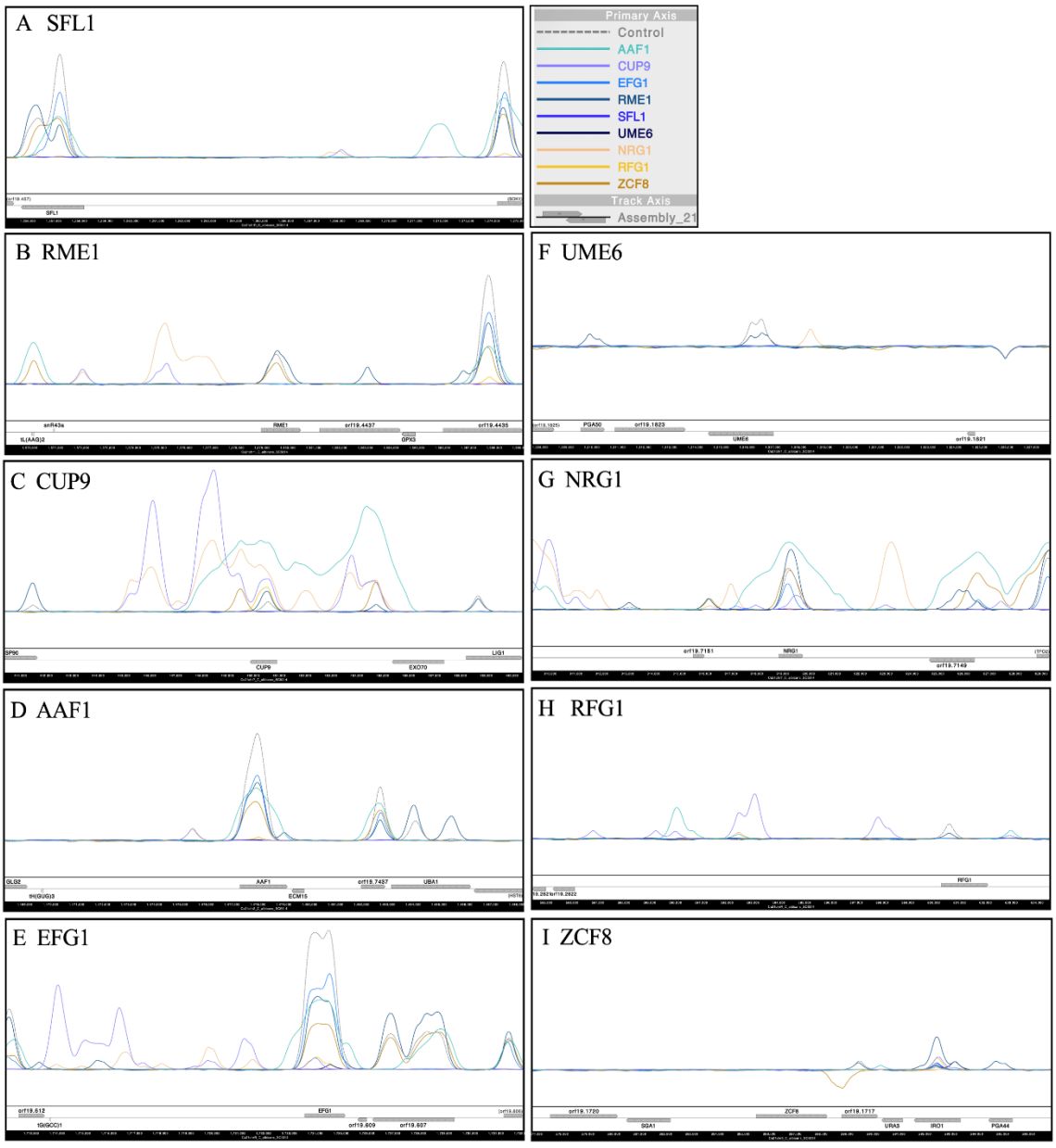
A SFL1
Primary Axis
Control
AAF1
CUP9
EFG1
RME1
SFL1
UME6
NRG1
RFG1
ZCF8
Track Axis
Assembly_21
B RME1
F UME6
C CUP9
G NRG1
D AAF1
H RFG1
E EFG1
I ZCF8
J
Sfl1
Rme1
Cup9
Aaf1
Efg1
Ume6
Nrg1
Rfg1
Zcf8

Figure 2.5 Chromatin immunoprecipitation mapping and motif identification of core chlamydospore regulators. (A-I) The binding of core regulators in the upstream regulatory regions of each TF are shown. Immunoprecipitation (IP) binding data for Sfl1-GFP (purple), Rme1-GFP (dark blue), Cup9-GFP (light purple), Aaf1-GFP (teal), Efg1-GFP (navy blue), Ume6-GFP (black), Nrg1-GFP (orange), Rfg1-GFP (yellow), Zcf8-GFP (brown) strains are shown. The ChIP-seq binding data was mapped and plotted onto the chromosomes containing (A) *SFL1*, (B) *RME1*, (C) *CUP9*, (D) *AAF1*, (E) *EFG1*, (F) *UME6*, (G) *NRG1*, (H) *RFG1* and (I) *ZCF8* using MochiView [57]. The upstream regulatory regions of these genes show significant peak enrichments for the binding of the indicated chlamydospore regulators. The X axis represents ORF chromosomal locations. (J) Using de novo motif finding based on our ChIP-seq, we identified significantly enriched core binding motifs for all nine core chlamydospore TFs. Motifs were identified and motif graphics were generated using MochiView [57].

2.4.2.6 De Novo Motif Finding for the core chlamydospore regulators

The non-randomly occurring cis-regulatory sequences "motifs" were identified based on several hundred significant binding events, these conserved binding motifs were determined for all nine chlamydospore regulators (Figure 2.5J). This motif generation was based solely on ChIP-seq data. The binding motifs for most of the core regulators have not been described in *C. albicans*, except for Efg1 using ChIP-ChIP experiments [51,71]. The Efg1 motif identified from our study (RGRGTGSCRS) is different from the one identified in earlier studies (RTGCATRW). One potential reason for this difference is that the motif identified in our study could be a secondary motif for Efg1 binding. Additionally, we also see a lot of interactions of Efg1 along with other TFs like Rme1, Zcf8 and Aaf1 (Figure 2.5J), so there is a likely chance that there are cooperative binding events occurring under chlamydospore inducing conditions that may cause for alternative binding motif identification for Efg1. Similarly, also we note that one the motif generated for Nrg1 is similar to the reported binding motif for its homolog Nrg1 in *S. cerevisiae*. However, the other TF motifs identified in our study for Sfl1, Rme1, Cup9 and Zcf8 were not similar to the binding motif homologs reported for *S. cerevisiae*. For the remaining regulators Aaf1, Ume6 and Rfg1 we statistically determined significant motifs, but we were unable to verify them independently in comparison to *S. cerevisiae* as their orthology relationships are uncertain and their binding motifs have not been characterized.

2.4.3 Identifying functionally relevant targets of the chlamydospore regulatory network

To understand the connections between the nine core regulators and chlamydospore formation in *C. albicans*, we performed RNA-seq on the mutant TF regulators and ChIP-seq on the nine GFP tagged regulators under chlamydospore inducing conditions. It is important to note that chlamydospores are usually observed *in vitro* at the lateral or terminal ends of hyphae, and that Δ/Δ*ume6* mutant strain is yeast locked while the Δ/Δ*nrg1* mutant strain is hyper filamentous under hyphal inducing conditions, and as such the chlamydospore transcriptional network at least in part overlaps with the hyphal morphogenesis transcriptional network [13,68,72,73].

From these large datasets, we attempted to identify a set of target genes that might have important roles in chlamydospore formation in *C. albicans*. We grouped the genes based on connectivity and node degree denoting the number of core TFs binding in the upstream regulatory region of a target gene. With this analysis, we found 30 genes that bound by all nine core regulators in their upstream regulatory regions, however, not all ChIP-seq events can be corelated with a corresponding change in the differential gene expression from the RNA-seq dataset. So, out of 30 commonly bound target genes select genes which differentially regulated in varying combinations of the nine core TF mutant datasets and also in WT strain under chlamydospore inducing vs non-chlamydospore inducing conditions (threshold of $\log_2>0.58$ and $\log_2< -0.58$, padj value of ≤ 0.05) were identified. Additionally, five of these target genes were upregulated and three genes downregulated in reference WT strain under chlamydospore inducing conditions. Further, genes were selected and prioritized for further analyses as functionally relevant targets based on the differential gene expression datasets in TF mutants compared to WT strain under chlamydospore inducing conditions and also between WT strain chlamydospore inducing vs non-chlamydospore inducing conditions ($\log_2>1.5$ and $\log_2< -1.5$, padj value of ≤ 0.05). Additionally, even in the absence direct binding interaction, some highly differentially expressed target genes in TF mutants were prioritized for further study as functionally relevant targets of the chlamydospore network. A heat map showing the differential gene expression along with the number of core TF binding events detected in their upstream regulatory regions is shown in Figure 2.6A. Additionally, we also note that multiple transcription factors (~43 TFs) have been identified as downstream targets of the network and are regulated by multiple core regulators. From the TF mutant library genetic screen, these TF mutants belong to chlamydospore index CI-2. We also note ~11 kinases that are downstream targets of the network and are regulated by multiple core regulators. These downstream targets as TFs and kinases are listed in Table S2.1.

To determine whether the select downstream target genes identified by this analysis affect chlamydospore formation, we constructed homozygous deletion mutant strains for each of these target genes. We observed significant chlamydospore formation defects in the target gene mutants compared to the reference WT strain under chlamydospore inducing conditions (Figure 2.6C). orf19.4459 has been previously reported to be involved in chlamydospore pathway, five target genes are uncharacterized, and two target genes have been reported to be involved in cell wall synthesis. A majority of the select target gene deletion mutant strains formed less chlamydospores relative to the WT strain under chlamydospore inducing conditions (CI-2), however, two target gene deletion strains, Δ/Δ*orf19.2899* and Δ/Δ*mep2* formed higher number of chlamydospores relative to WT strain (Figure 2.6B). Additionally, reintroduction of the ectopic copy of wild-type allele back into each of the nine core TF regulator mutants and the eighteen candidate target genes reversed the chlamydospore formation defect (six core TF that mutants failed to form chlamydospores, three core TF mutants and two candidate target gene mutants that form higher number of chlamydospore relative to WT strain under chlamydospore inducing conditions and the varying degree of chlamydospore formation defects of the remainder of the candidate target genes) of each mutant (Figure S2.6).

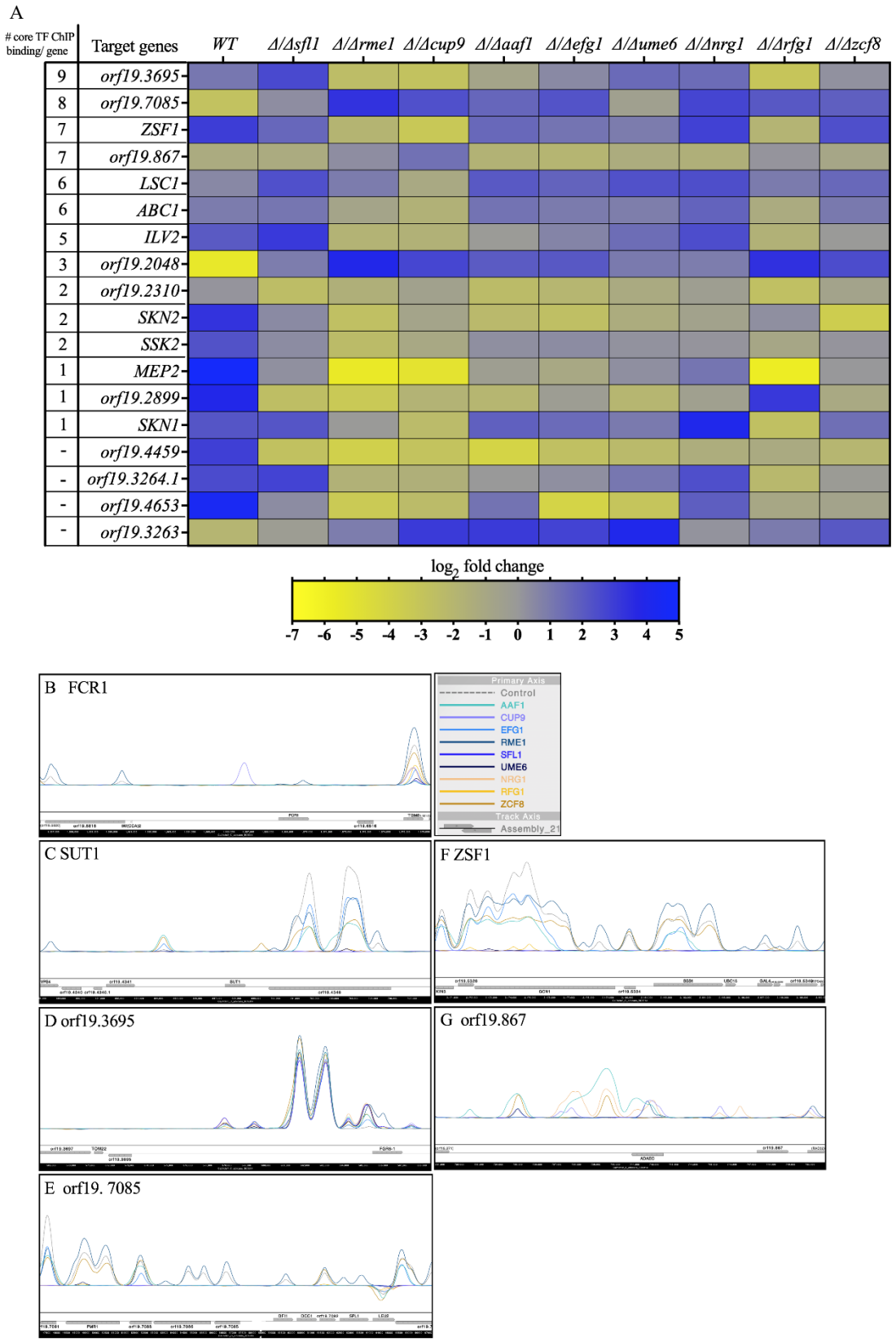
A
core TF ChIP binding/ gene
Target genes
WT
Δ/Δsfl1
Δ/Δrme1
Δ/Δcup9
Δ/Δaaf1
Δ/Δefg1
Δ/Δume6
Δ/Δnrg1
Δ/Δrfg1
Δ/Δzcf8
9 orf19.3695
8 orf19.7085
7 ZSF1
7 orf19.867
6 LSC1
6 ABC1
5 ILV2
3 orf19.2048
2 orf19.2310
2 SKN2
2 SSK2
1 MEP2
1 orf19.2899
1 SKN1
- orf19.4459
- orf19.3264.1
- orf19.4653
- orf19.3263
log2 fold change
-7 -6 -5 -4 -3 -2 -1 0 1 2 3 4 5
B FCR1
Primary Axis
Control
AAF1
CUP9
EFG1
RME1
SFL1
UME6
NRG1
RFG1
ZCF8
Track Axis
Assembly_21
C SUT1
F ZSF1
D orf19.3695
G orf19.867
E orf19. 7085

H

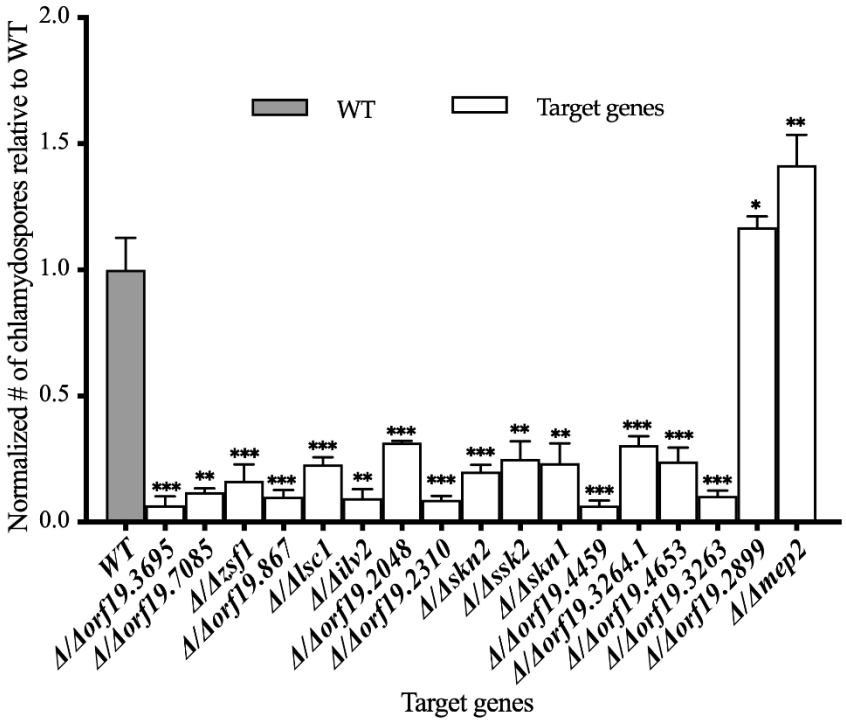

Figure 2.6 Functionally relevant target genes of the chlamydospore regulatory network.

(A) Using node connectivity analysis of our ChIP-seq and gene expression RNA-seq data, we identified a set of 18 candidate target genes (*orf19.3695, orf19.7085, ZSF1, orf19.867, LSC1, ILV2, orf19.2048, orf19.2310, SKN2, SSK2, , SKN1, orf19.4459, orf19.3264.1, orf19.4653, orf19.3263, , orf19.2899* and *MEP2*) that were differentially regulated (log_2>1.5 and log_2< -1.5) in combinations of each chlamydospore regulator mutant to the reference strain under chlamydospore inducing conditions. The left panel shows the number of core TF binding interactions detected in the upstream regulatory regions of the target genes as detected via ChIP-seq. (B) ChIP-seq enrichment data for the binding of nine chlamydospore core regulators in the upstream regulatory regions of select candiate target genes. IP binding for Sfl1-GFP (purple), Rme1-GFP (dark blue), Cup9-GFP (light purple), Aaf1-GFP (teal), Efg1-GFP (navy blue), Ume6-GFP (black), Nrg1-GFP (orange), Rfg1-GFP (yellow), Zcf8-GFP (brown) strains are shown. The select target gene ChIP-seq binding data was mapped and plotted onto the chromosomes containing (B) *FCR1*, (C) *SUT1*, (D) *orf19.3695*, (E) *orf19.7085*, (F) *ZSF1*, and (G) *orf19.867* using Mochiview [57] are shown. (H) Chlamydospore formation was measured for the eighteen target gene deletion mutants relative to WT strain. The average of the number of chlamydospores formed for each strain grown under chlamydospore inducing conditions was calculated from three biological replicates. For ease of interpretation, the WT strain chlamydospore formation value is set to 1 and normalized chlamydospore formation by of each selected deletion mutant relative WT strain under chlamydospore inducing conditions is shown. Statistical significance (*p* values) was calculated using Student's unpaired two-tailed t-tests assuming unequal variance for $p \leq 0.05$ (*), and $p \leq 0.01$ (**) and $p \leq 0.001$ (***).

2.5 Discussion and conclusion

Sporulation has been an important aspect of microbial life cycles and is known to produce dormant spores under unfavorable environmental conditions of extreme of temperature, desiccation and UV radiations. These spores remain dormant until the return of favorable conditions and germinate and produce viable cells [74,75]. The spores are metabolically quiescent, stress resistant and poised for germination. As a part of their life cycles, many fungal species produce chlamydospores; however, the functions of chlamydospores vary in different species. For example, in some soilborne *Fusarium* species, chlamydospores provide long term survival under unfavorable conditions and have the ability to germinate upon return of favorable conditions. The environmental cues needed for chlamydospore formation are also species-specific [76]. For *Candida* species, chlamydospores are enigmatic structures that form laterally or terminally to hyphae and pseudohyphae and are only known to be produced by two members of the *Candida* clade. *C. albicans* forms chlamydospores under stressful conditions and chlamydospores are part of *C. albicans* morphological transitions, however, their functions are still unknown. Given that two of the pathogenic *Candida* species produce chlamydospores, their formation and existence raise a possibility of an unidentified selective advantage provided by chlamydospores to these species. Additionally, little is known about how chlamydospore formation is regulated. In this study, we have comprehensively mapped the regulatory network controlling chlamydospore formation in *C. albicans* using forward genetics and genome wide approaches. We describe a master circuit of nine core regulators that form an elaborate, interwoven transcriptional network controlling chlamydospore formation in *C. albicans*. A subset of core regulators were found to control each other, and together the nine core regulators control ~3200 downstream target genes (~48% of *C. albicans* genome).

2.5.1 Core chlamydospore regulators

From the TF mutant library genetic screen, we identified nine regulators that were severely affected in their abilities to form chlamydospores. Of these nine regulators, when deleted six regulator mutant strains completely failed to form chlamydospores (Δ/Δ*sfl1*. Δ/Δ*rme1,* Δ/Δ*cup9,* Δ/Δ*aaf1,* Δ/Δ*efg1* and Δ/Δ*ume6*). Out of these six, two regulators mutant strains Δ/Δ*efg1* and Δ/Δ*rme1* have been previously implicated to play roles in chlamydospore formation. Sfl1 has been reported to be a negative regulator of flocculation and filamentation in *S. cerevisiae* and well as in *C. albicans* [77], Rme1 is known to regulate meiosis in *S. cerevisiae* [78], and Cup9 is a known repressor of filamentation [79]. Aaf1 is less studied in *C. albicans*. Efg1is known to act both as an activator as well as a repressor of filamentation depending on environmental cues [80]; under normoxic conditions, the Δ/Δ*efg1* mutant strain is defective in hyphal formation and Efg1 acts an activator of filamentation, however, under standard chlamydospore inducing oxygen limiting conditions, the Δ/Δ*efg1* mutant strain is hyperfilamentous [29]. Ume6 is known to be essential for hyphal extension and maintenance [80–82]. The Δ/Δ*ume6* mutant strain is yeast locked and did not form hyphae or pseudohyphae under the conditions tested, however it has been reported that some species, for e.g., *C. dubliniensis* form

chlamydospores and pseudohyphae, however, hyphae formation is less frequent, opens up a possibility of chlamydospore formation without hyphae [33]. Additionally, Δ/Δ*ume6* can be induced to form hyphae when incubated at 37°C in presence of YEPD + serum, and we have considered Ume6 as one of the core regulators [72].

From the TF mutant library genetic screen, three regulator mutants formed higher number of chlamydospores relative to reference strain (Δ/Δ*nrg1,* Δ/Δ*rfg1* and Δ/Δ*zcf8*). Nrg1 is a highly conserved TF and acts as a general repressor of transcription in *C. albicans* via Tup1-Ssn6 [80], and Δ/Δ*nrg1* mutant strains are known to be hyperfilamentous under non filament inducing conditions [68]. Only *C. dubliniensis* but not *C. albicans* can form chlamydospores when cells are grown on Staib agar, and this species specific difference has been mainly attributed to differential expression of *NRG1* between the two species, in which, *CdNRG1* is specifically downregulated to allow for formation of chlamydospores on Staib agar, and deletion of *CaNRG1* allows for chlamydospore formation on Staib agar [30]. Nrg1 is thought to repress hyphal genes by recruiting the corepressor Tup1-Ssn6 complex which repress hyphal genes [68]. Zcf8 is proposed to play a role in adhesion [83]. The Δ/Δ*rfg1* mutant strain is hyperfilamentous, and Rfg1 is a known repressor of filamentation [84], possibly via the same mechanism as Nrg1 (Tup1-Ssn6 dependent). It is know that there is interplay between the hyphal regulators Nrg1, Rfg1, Efg1 and Ume6 [82]; additionally, Nrg1 is also known to act in a Ubr1-Sok1 mediated pathway with Cup9 to regulate hyphal formation. Not surprisingly, there are multiple TFs regulating hyphal formation that overlap with the chlamydospore regulatory network identified here.

2.5.2 Interwoven chlamydospore regulatory network and circuit complexity

The *C. albicans* chlamydospore regulatory network is large, highly interwoven and complex. There are several examples of complex regulatory networks reported in *C. albicans*, for example, the biofilm regulatory network [51] and the white-opaque switch network [71]. There are also complete regulatory networks reported in other microorganisms, such as spore formation in *Bacillus subtilis* [85] and hematopoietic and embryonic stem cell differentiation in mammals [86,87]. These regulatory networks have similarities in that they have a group of core master regulators working together to control themselves and each other and a large set of downstream target genes.

Many observations can be made from the chlamydospore regulatory network and its corresponding regulatory circuit. First, autoregulation of only one core TF; Cup9 is an unexpected and interesting finding since in most *C. albicans* regulatory circuits studied to date, the core TFs typically bind their own upstream intergenic regions and autoregulate themselves [51,71,88]. Second, Rme1 controls a subset of downstream target genes on its own (~50% genes) without sharing them with any other core TF, indicating that Rme1 is the most independent regulator of the chlamydospore network. Third, Nrg1 possibly acts in the role of a central repressor for the pathway, repressing five core TFs and activating Rfg1, a known repressor of *C. albicans* morphogenesis [84]. Fourth, we note that Zcf8 has zero regulators binding in its upstream regulatory regions suggesting that in the sequence of events, Zcf8 may act upstream to all the core TFs. It is also important to note that Rme1 and Zcf8 share the most downstream target gene connections (198 genes). Fourth, we note that Sfl1 and Efg1 have no outgoing interactions, possibly indicating that these core TFs

act downstream of other core TFs. Lastly, it is also important to note that we identified ~43 additional transcription factors as downstream targets of various core regulators and performing genome wide binding and expression analyses for these regulators could be interesting in future studies. In particular, studying TFs like Czf1, Fcr1, Rob1, Tye7 and Sfu1, which are known to have various roles in filamentation, glycolysis, and response to iron utilization would be of importance. Additionally, we identified 11 kinases as downstream targets, such as Ssk2, which is a MAP kinase kinase kinase known to activate MAPK Hog1, and would be of interest since Hog1 is reported to be essential for chlamydospore formation [34].

Further, we note in a comparison between KEGG enrichment pathways for chlamydospore high-former strains and chlamydospore non-former strains, we see an enrichment primarily for two interesting categories, the peroxisome biogenesis/fatty acid degradation pathways and SNARE vesicular transport mechanisms. Lipids are a known component of chlamydospores, and this KEGG pathway enrichment suggests an intriguing possibility that lipids are actively produced and metabolized in chlamydospores, hinting that chlamydospores may function as nutrient storage structures [23,35]. The enrichment of the SNARE vesicular transport pathway suggests that cargo molecules could be actively transported in chlamydospores.

2.5.3 Conservation of the chlamydospore regulatory network

We preliminarily examined the evolutionary history of the chlamydospore network by performing orthologous pairwise comparisons of protein coding sequences of the nine core regulators and the 27 downstream target genes commonly bound by the core regulators. We considered the evolutionary occurrence of these select proteins in three fungal species that are known to form chlamydospores (*Cryptococcus neofomans, Paracoccidioides brasiliensis* and *Blastomyces dermitidis*) [76,89,90] and different members of the *Candida* genus (i.e., *C. dubliniensis, C. tropicalis, C. glabrata* and *C. parapsilosis*) as well as *S. cerevisiae*. We found that ~65% of the selected genes are conserved across a majority of distantly related fungal species (from *Paracoccidioides brasiliensis* to *C. albicans*; not including *C. neoformans*), and we refer to these as "old" genes (e.g., *CUP9*, *EFG1*, *NRG1*, *CHT1* and *RPL10*). We found that the remaining ~35% of these genes were newly evolved and are conserved only in the CTG clade species, and we refer to these as "young" genes (e.g., *AAF1*, *ZCF8*, *orf19.5775* and *orf19.6896*). Young genes can arise, for example, by horizontal gene transfer and de novo gene formation. Two interesting observations from these evolutionary analyses are that (1) *ALS5*, *ALS9* and *PTP3* were not conserved and possibly lost during evolution in *C. parapsilosis*; (2) *orf19.6898* is conserved in all species tested except *C. glabrata* and *S. cerevisiae* and was likely lost in the ancestor of these species. Future evolutionary analyses including all genes of the chlamydospore network will be important to get a complete understanding of the evolutionary history of this complex network.

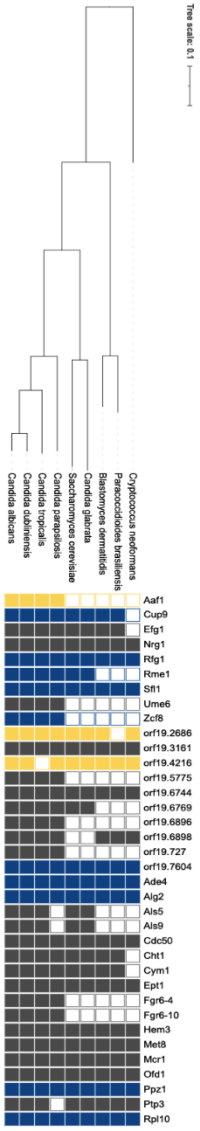

Figure 2.7 Conservation of chlamydospore regulatory network. The conservation of the 9 TFs and 27 commonly bound target genes were analyzed by identifying orthologs of these genes among *C. albicans* and non-*albicans* CTG clade *Candida* species*, S. cerevisiae, C. glabrata* and *Cryptococcus neofomans, Paracoccidioides brasiliensis* and *Blastomyces dermitidis* using OrthoFinder [59,60]. *orf19.5191*, *orf19.5735.3* and *orf19.4712* were excluded from this analysis due to ambiguous annotations for these genes. The ortholog of *EFG1* was not identified in *C. tropicalis* using this software as there is a gap in the assembly of the reference strain at this locus. Mancera et al., however, characterized and identified *EFG1* in *C. tropicalis* [91]. The color of the gene column indicates differential expression in chlamydospore formation in the *C. albicans* WT strain compared to the control. Gray denotes no differential expression (abs (log_2Fold-Change < 0.58), or FDR adjusted p-value > 0.05), blue denotes upregulation (log_2Fold-Change > 0.58 and FDR adjusted *p*-value < 0.05) and yellow denotes downregulation (log_2Fold-Change < -0.58 and FDR adjusted p-value < 0.05) in chlamydospore inducing conditions in the *C. albicans* WT strain. The filled squares indicate presence of an ortholog of this gene in the corresponding species, where orthology was assessed by comparing the protein sequence from *C. albicans* against the proteome of the corresponding species.

To summarize, the chlamydospore regulatory network of *C. albicans* is highly interwoven consisting of nine core regulators and over 3200 target genes, where every target gene is bound by at least one core regulator, and ~70% of target genes (~2,300) are differentially regulated under chlamydospore inducing conditions. The lipid degradation pathways and SNARE vesicular transport KEGG pathways were enriched in chlamydospore high former mutant strains of the core regulators. The downstream target genes belonged to multiple functional groups ranging from transcription factors, kinases, synthases, and stress regulator proteins, and a large subset of target genes are uncharacterized (~70%). Lastly, network conservation analyses based on orthologous relationships of proteins within the chlamydospore network revealed that the network is comprised largely of “old” genes (65%) interspersed with some relatively “young” genes (35%), indicative of the network being fairly well conserved.

2.6 Supplementary Materials

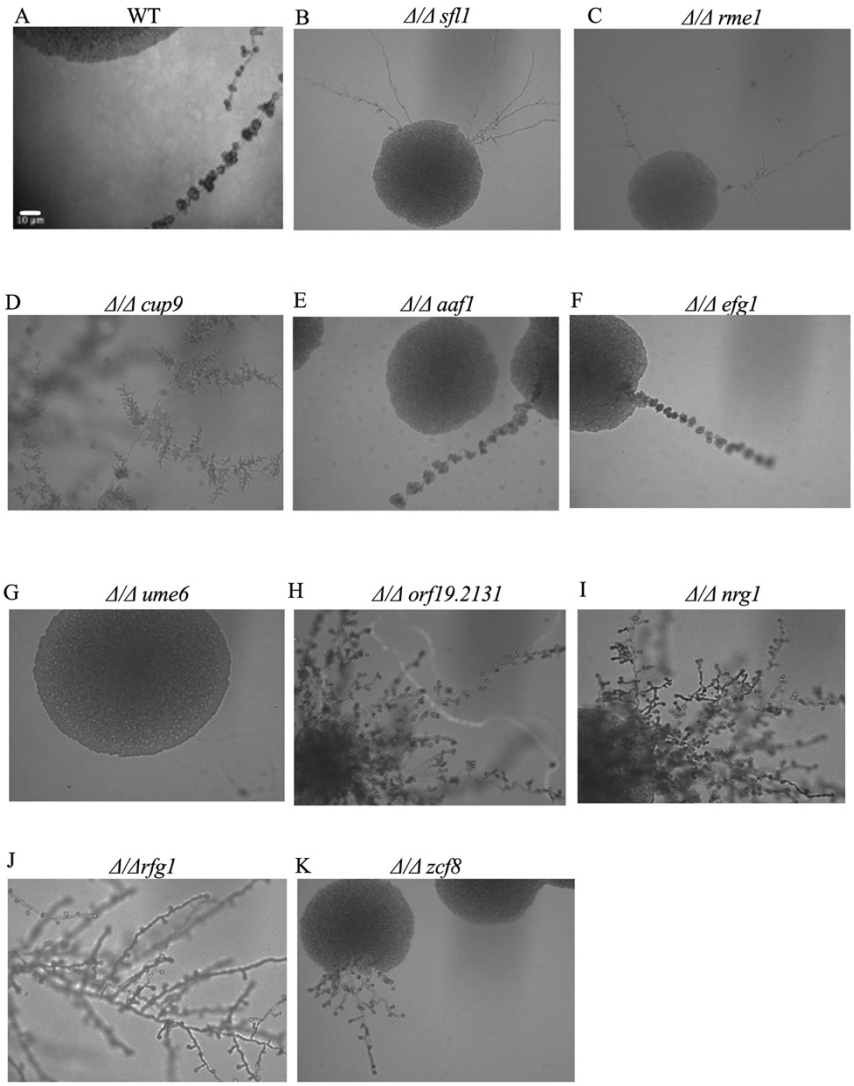

Figure S2.1 Colony and cellular phenotypes of core chlamydospore transcription factor mutant strains under on rice extract (RE) Tween 80 medium.
Chlamydospore formation was achieved under standard inducing conditions on rice extract Tween 80 in the dark at room temperature for 8 days following which the plates were observed at 20X objective with a brightfield microscopy. Representative images are shown for (A) WT, (B) TF001 Δ/Δ*sfl1*, (C) TF028 *Δ/Δrme1*, (D) TF061 Δ/Δ*cup9*, (E) TF128 Δ/Δ*aaf1*, (F) TF156 Δ/Δ*efg1*, (G) TF179 Δ/Δ*ume6*, (H) TF210 Δ/Δ*orf19.2131*, (I) TF125 Δ/Δ*nrg1*, (J) TF166 Δ/Δ*rfg1*, (K) TF141 Δ/Δ*zcf8*. Scale bar represents 10 μM.

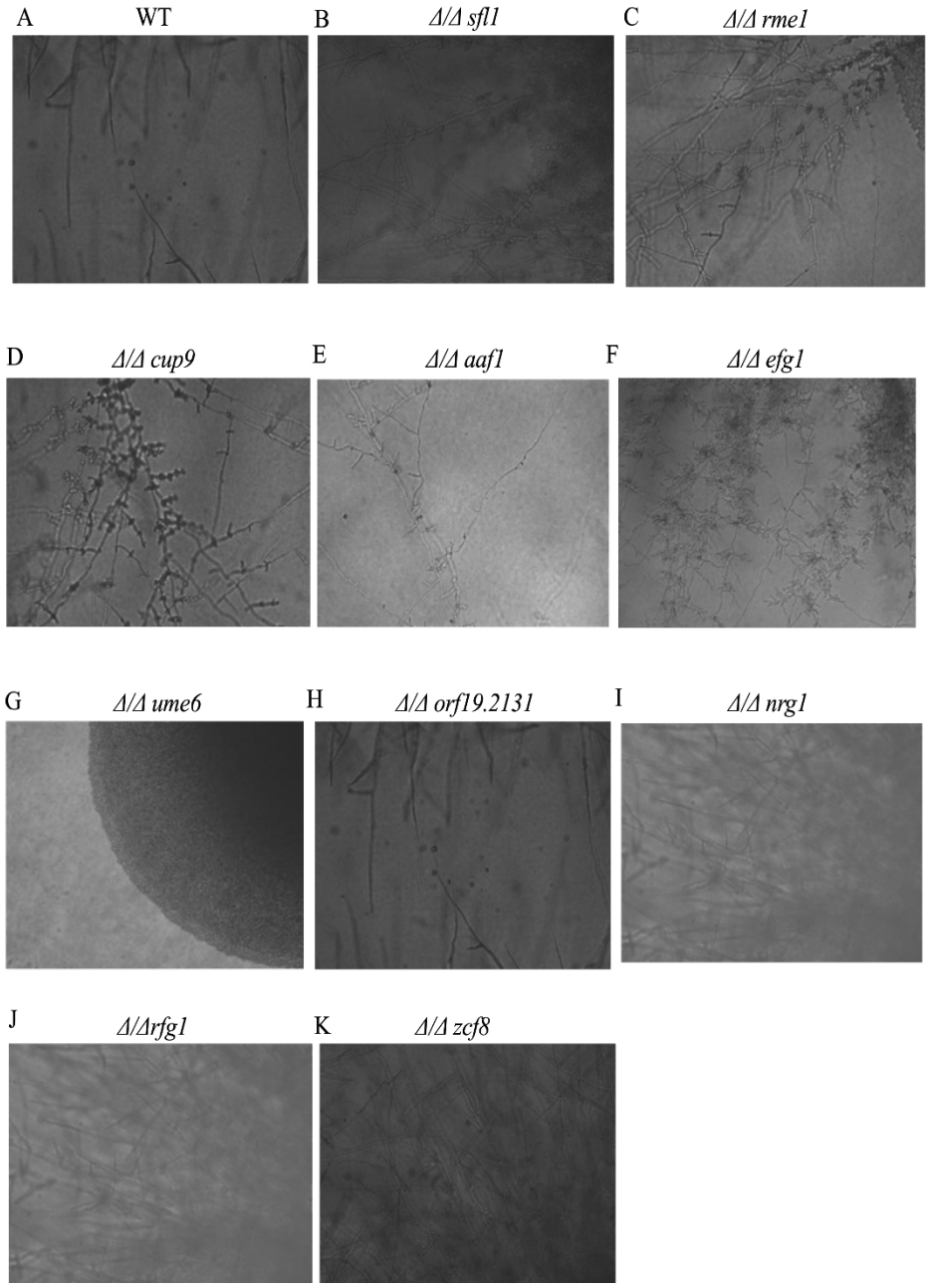

Figure S2.2 Colony and cellular phenotypes of core chlamydospore transcription factor mutant strains under on Potato Carrot Bile (PCB) agar medium. Chlamydospore formation was achieved under standard inducing conditions on potato carrot bile agar medium in the dark at room temperature under oxygen limiting conditions for 8 days following which the plates were observed at 20X objective with a brightfield microscopy. Representative images are shown for (A) WT, (B) TF001 Δ/Δ*sfl1*, (C) TF028 Δ/Δ*rme1*, (D) TF061 Δ/Δ*cup9*, (E) TF128 Δ/Δ*aaf1*, (F) TF156 Δ/Δ*efg1*, (G) TF179 Δ/Δ*ume6*, (H) TF210 Δ/Δ*orf19.2131*, (I) TF125 Δ/Δ*nrg1*(J) TF166 Δ/Δ*rfg1*, (K) TF141 Δ/Δ*zcf8*. Scale bar represents 10 μM.

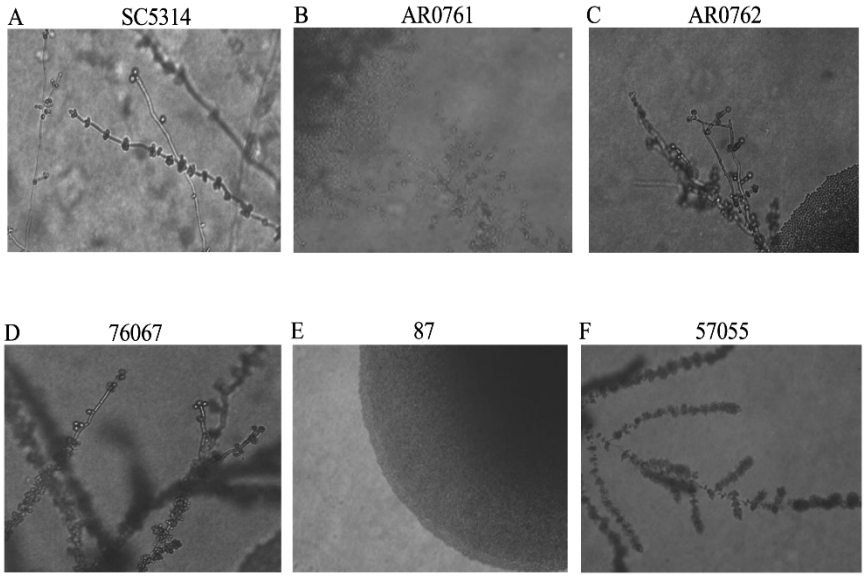

Figure S2.3 Colony morphology and cellular phenotypes for chlamydospore formation by *C. albicans* clinical isolates. Chlamydospore formation was achieved under standard inducing conditions on CMA Tween 80 medium in the dark at room temperature under oxygen limiting conditions for 8 days following which the plates were observed at 20X objective with a brightfield microscopy. Representative images are shown for (A) SC5314, (B) AR0761, (C) AR0762, (D) 76067, (E) 87 (F) 57055. Scale bar represents 10 μM.

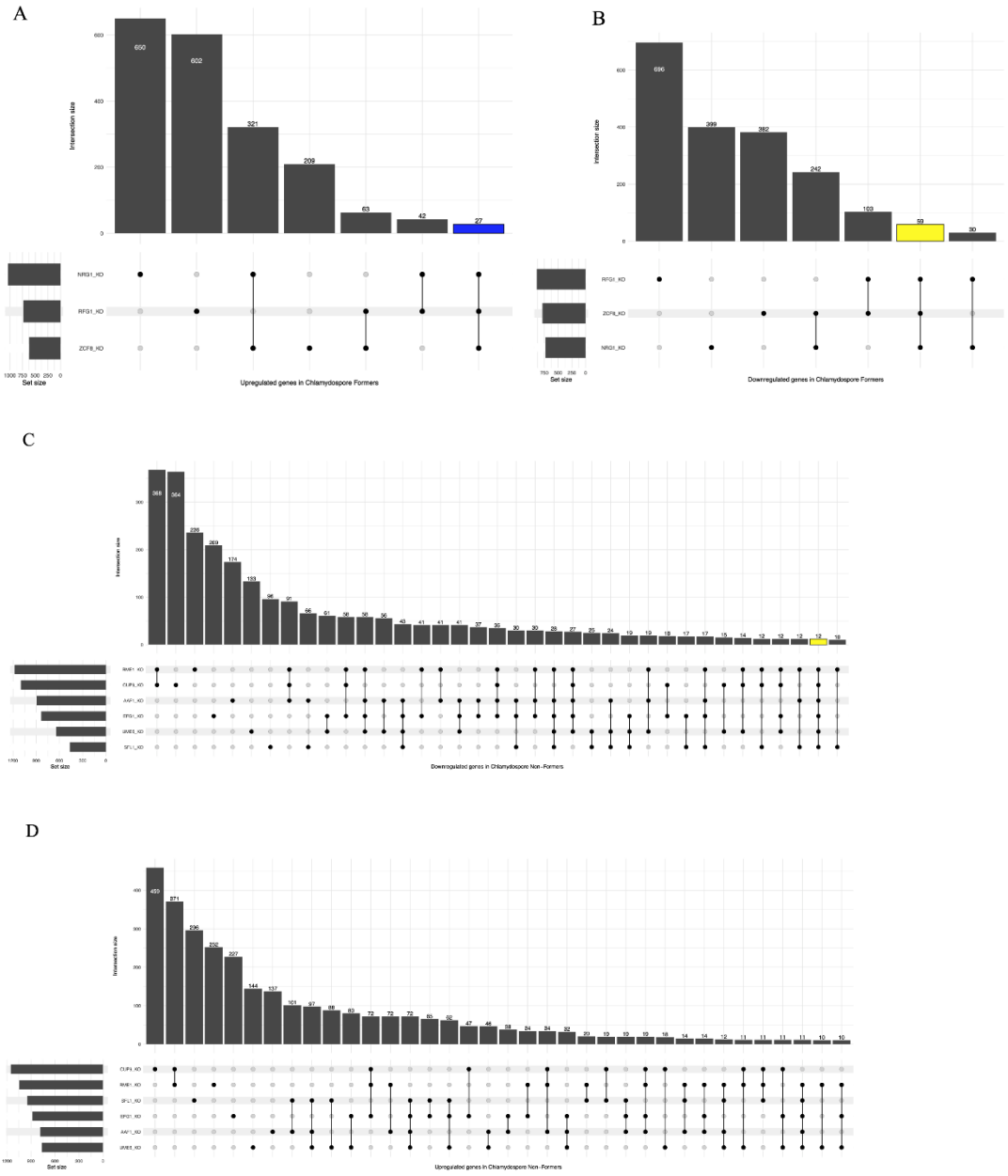

Figure S2.4 Upset plots showing the commonly upregulated and downregulated genes for chlamydospore high-formers and chlamydospore non-former strains (log_2-Fold Change < -0.58, adjusted p-value < 0.05**).** The three chlamydospore high-former strains (Δ/Δ*nrg1,* Δ/Δ*rfg1,* Δ/Δ*zcf8)* and six chlamydospore non-former strains *(*Δ/Δ*sfl1,* Δ/Δ*rme1,* Δ/Δ*cup9,* Δ/Δ*aaf1,* Δ/Δ*efg1,* Δ/Δ*ume6)* were grown under standard chlamydospore inducing conditions and RNA-seq was performed on the harvested cells. A) genes commonly upregulated in chlamydospore high-former strains, (B) genes commonly downregulated genes in chlamydospore high-former strains (C) genes commonly downregulated genes in chlamydospore non-former strains (D) commonly upregulated genes in chlamydospore non-former strains.

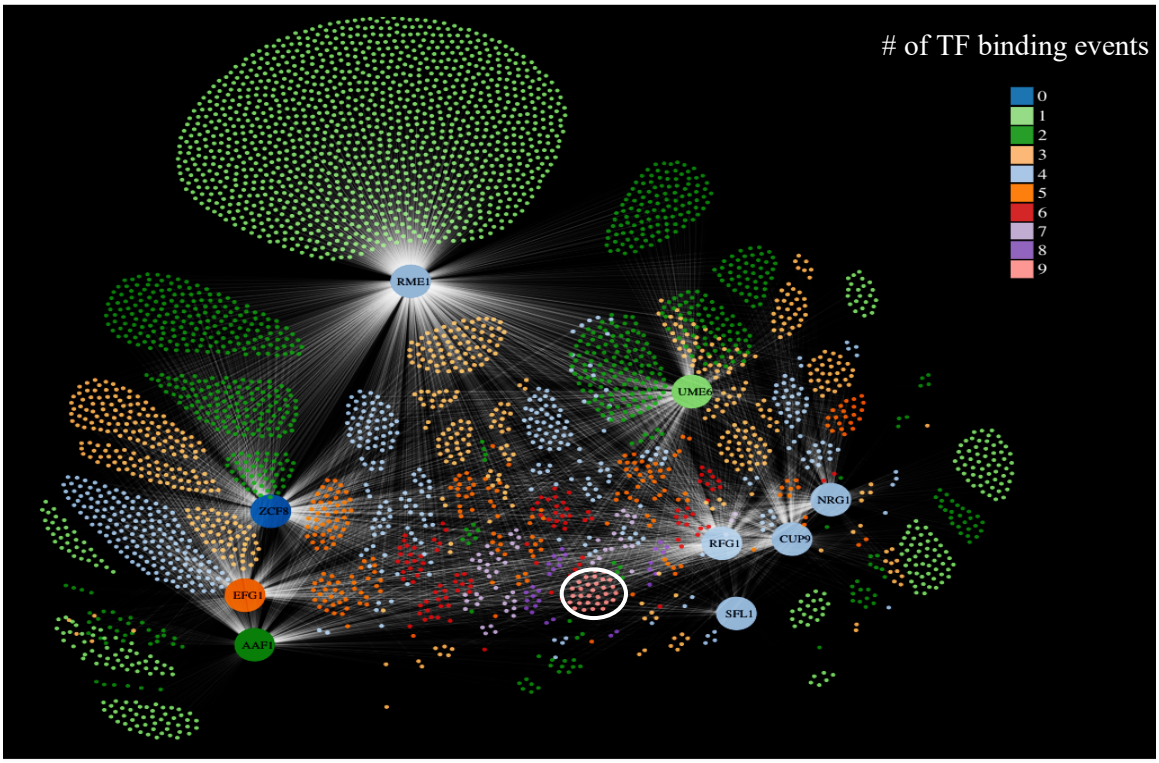

Figure S2.5 The *C. albicans* chlamydospore regulatory network with emphasis on number of ChIP binding events detected for each gene. The nine chlamydospore core regulators are represented by nine large circular hubs. Smaller circles represent target genes, which are connected by their respective regulators by lines, indicating a direct interaction as determined by genome wide ChIP-seq binding events under chlamydospore inducing conditions. A gene that is differentially expressed in WT strain under chlamydospore inducing conditions vs non-chlamydospore inducing conditions (RNA-seq based on a $\log_2$ fold change of 0.58) is a part of the network and the TF binding interactions by 9 core TF regulators are shown. A directed line is indicative of a ChIP binding event between source core TF regulator binding upstream regulatory of the target gene. The color of the nodes indicates the number of core TF regulator binding events detected in the upstream regulatory regions of the target gene, ranging from blue (0 core TF binding detected) to pink (all 9 core TFs bind upstream regulatory regions of the target gene).

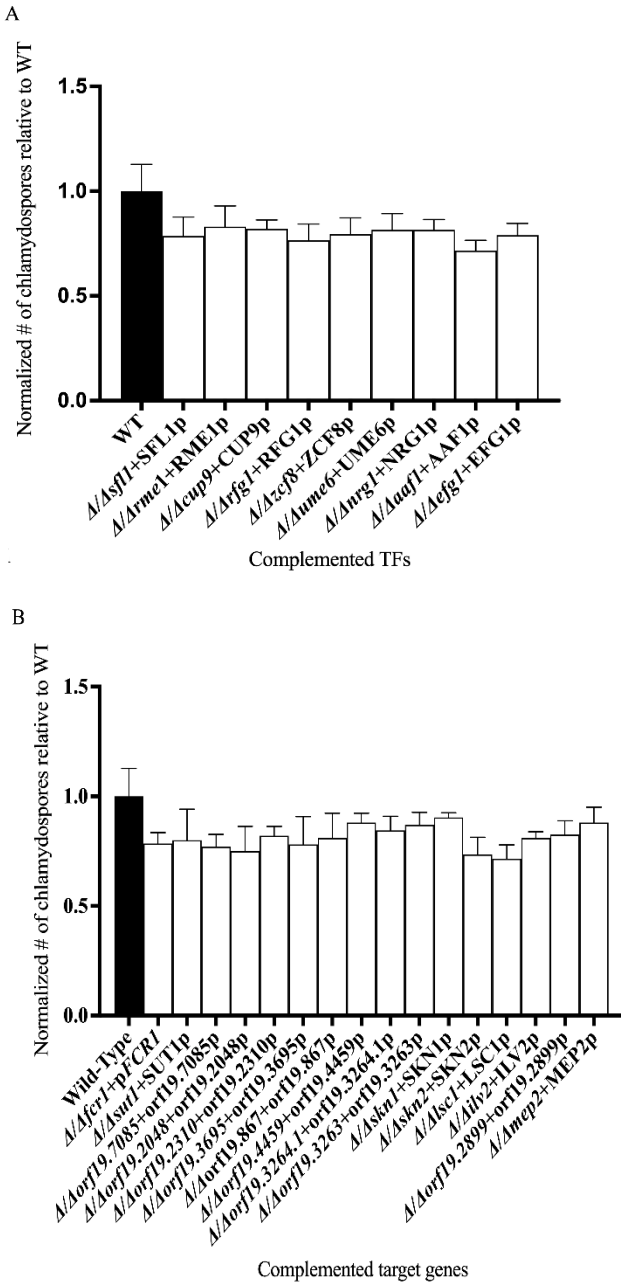

Figure S2.6 Chlamydospore formation by the complemented strains. The complemented strains were generated by adding the wild-type allele back into the (A) nine-core regulator mutant strains and (B) eighteen target gene candidates was assessed under standard chlamydospore inducing conditions. For ease of interpretation, the reference strain chlamydospore formation values are set at 1 and normalized chlamydospore formation by of each selected gene relative WT strain is shown.

Table S2.1 List of downstream target gene transcription factors and kinases of chlamydospore regulatory network as identified from RNA-seq and ChIP-seq datasets.

Orf #	Gene	WT strain differential regulation under inducing conditions	# TFs regulating	Regulated by
Transcription factors				
orf19.1035	War1	Upregulated	6	*ZCF8, EFG1, RFG1, UME6, AAF1, RME1*
orf19.3127	Czf1	Upregulated	5	*ZCF8, EFG1, CUP9, AAF1, RME1*
orf19.2287	Rpa12	Downregulated	5	*ZCF8, EFG1, UME6, AAF1, RME1*
orf19.6817	Fcr1	Upregulated	5	*NRG1, RFG1, UME6, CUP9, RME1*
orf19.3193	Fcr3	Downregulated	4	*EFG1, NRG1, CUP9, RME1*
orf19.4941	Tye7	Upregulated	4	*RFG1, UME6, CUP9, RME1*
orf19.5210	orf19.5210	Upregulated	4	*ZCF8, EFG1, UME6, RME1*
orf19.6680	Fgr27	Downregulated	4	*ZCF8, EFG1, AAF1, RME1*
orf19.4998	Rob1	Upregulated	4	*ZCF8, EFG1, AAF1, RME1*
orf19.4869	Sfu1	Upregulated	3	*ZCF8, AAF1, RME1*
orf19.2623	Ecm22	Downregulated	3	*ZCF8, UME6, RME1*
orf19.4342	Sut1	Non-DE	3	*ZCF8, EFG1, AAF1*
orf19.3753	Sef1	Downregulated	3	*NRG1, RFG1, RME1*
orf19.5992	Wor2	Downregulated	3	*NRG1, CUP9, AAF1*
orf19.2646	Zcf13	Upregulated	3	*RFG1, UME6, RME1*
orf19.3308	Stb5	Non-DE	2	*ZCF8, EFG1*
orf19.4524	Zcf24	Downregulated	2	*ZCF8, RME1*
orf19.3012	Aro80	Upregulated	2	*ZCF8, RME1*
orf19.801	Tbf1	Non-DE	2	*ZCF8, RME1*
orf19.7468	Vhr1	Downregulated	2	*ZCF8, RME1*
orf19.6124	Ace2	Downregulated	2	*EFG1, NRG1*
orf19.4752	Msn4	Upregulated	2	*NRG1, RME1*

orf19.1253	Pho4	Non-DE	1	*RME1*
orf19.1396	Age2	Non-DE	1	*RME1*
orf19.3722	orf19.3722	Non-DE	1	*AAF1*
orf19.7046	Met28	Non-DE	1	*NRG1*
orf19.971	Skn7	Downregulated	1	*RME1*
orf19.5338	Gal4	Non-DE	1	*ZCF8*
orf19.7381	Ahr1	Non-DE	1	*NRG1*
orf19.255	Zcf1	Non-DE	1	*NRG1*
orf19.1168	Zcf3	Downregulated	1	*CUP9*
orf19.1604	Rha1	Downregulated	1	*CUP9*
orf19.1926	Sef2	Upregulated	1	*RME1*
orf19.2842	Gzf3	Upregulated	1	*RME1*
orf19.4568	Zcf25	Downregulated	1	*RME1*
orf19.3190	Hal9	Non-DE	1	*RME1*
orf19.4776	Lys143	Upregulated	1	*RME1*
orf19.3405	Zcf18	Downregulated	1	*RME1*
orf19.3187	Znc1	Downregulated	1	*RME1*
orf19.3328	Hot1	Upregulated	1	*RME1*
orf19.431	Zcf2	Upregulated	1	*RME1*
orf19.7317	Uga33	Non-DE	1	*RME1*
orf19.3809	Bas1	Upregulated	1	*RME1*
Kinases				
orf19.3331	Abc1	Upregulated	6	*ZCF8, NRG1, RFG1, UME6, AAF1, RME1*
orf19.3669	Sha3	Downregulated	4	*ZCF8, UME6, RME1, CUP9*
orf19.5580	Tel1	Non-DE	3	*ZCF8, RME1, EFG1*
orf19.2290	Tor1	Downregulated	2	*ZCF8, RME1*
orf19.5325	Kin3	Downregulated	2	*EFG1, RME1*
orf19.3775	Ssk2	Upregulated	2	*AAF1, RME1*
orf19.147	Yak1	Non-DE	1	*EFG1*
orf19.7044	Rim15	Downregulated	1	*AAF1*
orf19.399	orf19.399	Upregulated	1	*RME1*
orf19.6243	Vps34	Downregulated	1	*RME1*
orf19.2320	orf19.2320	Downregulated	1	*RME1*

2.7 References

1. Stajich, J.E.; Berbee, M.L.; Blackwell, M.; Hibbett, D.S.; James, T.Y.; Spatafora, J.W.; Taylor, J.W. The Fungi. *Curr. Biol.* **2009**, *19*, 840–845.
2. Boyce, K.J.; Andrianopoulos, A. Fungal dimorphism: the switch from hyphae to yeast is a specialized morphogenetic adaptation allowing colonization of a host. *FEMS Microbiol. Rev.* **2015**, *035*, 797–811.
3. Sardinha Francisco, C.; Ma, X.; Zwyssig, M.M.; Mcdonald, B.A.; Palma-Guerrero, J. Morphological changes in response to environmental stresses in the fungal plant pathogen *Zymoseptoria tritici*. *Sci. Rep.* **2019**, *9*.
4. Li, Z.; Nielsen, K. Morphology Changes in Human Fungal Pathogens upon Interaction with the Host. *J. Fungi* **2017**, *3*.
5. Bensasson, D.; Dicks, J.; Ludwig, J.M.; Bond, C.J.; Elliston, A.; Roberts, I.N.; James, S.A. Diverse Lineages of*Candida albicans* Live on Old Oaks. *Genetics* **2019**, *211*, 277–288.
6. Nobile, C.J.; Johnson, A.D. *Candida albicans* biofilms and human disease. *Annu. Rev. Microbiol.* **2015**, *69*, 71–92.
7. Williams, R.B.; Lorenz, M.C.; Biology, H.; Williams, R.B.; Lorenz, M.C. Multiple Alternative Carbon Pathways Combine To Promote *Candida albicans* Stress Resistance, Immune Interactions, and Virulence. *MBio* **2020**, *11*, 1–18.
8. Ene, I. V; Cheng, S.-C.; Netea, M.G.; Brown, A.J.P. Growth of *Candida albicans* Cells on the Physiologically Relevant Carbon Source Lactate Affects Their Recognition and Phagocytosis by Immune Cells. *Infect. Immun.* **2013**, *81*, 238–248.
9. Ene, I. V.; Brunke, S.; Brown, A.J.P.; Hube, B. Metabolism in fungal pathogenesis. *Cold Spring Harb. Perspect. Med.* **2014**, *4*, 1–21.
10. Brown, A.J.P.; Budge, S.; Kaloriti, D.; Tillmann, A.; Jacobsen, M.D.; Yin, Z.; Ene, I. V; Bohovych, I.; Sandai, D.; Kastora, S.; et al. Stress adaptation in a pathogenic fungus. *J. Exp. Biol.* 2014, *217*, 144–155.
11. Odds, F.C.; Kerridge, D. Morphogenesis in *Candida albicans*. *Crit. Rev. Microbiol.* **1985**, *12*, 45–93.
12. Noble, S.M.; Gianetti, B.A.; Witchley, J.N. *Candida albicans* cell-type switching and functional plasticity in the mammalian host. *Nat. Rev. Microbiol.* **2017**, *15*, 96–108.
13. Villa, S.; Hamideh, M.; Weinstock, A.; Qasim, M.N.; Hazbun, T.R.; Sellam, A.; Hernday, A.D.; Thangamani, S. Transcriptional control of hyphal morphogenesis in *Candida albicans*. *FEMS Yeast Res.* 2020, *20*, 5.
14. Staib, P.; Morschhäuser, J. *Chlamydospore formation in* Candida albicans *and* Candida dubliniensis *– an enigmatic developmental programme*; 2007; Vol. 50, pp. 1–12;.
15. Palige, K.; Linde, J.; Martin, R.; Böttcher, B.; Citiulo, F.; Sullivan, D.J.; Weber, J.; Staib, C.; Rupp, S.; Hube, B.; et al. Global Transcriptome Sequencing Identifies Chlamydospore Specific Markers in *Candida albicans* and *Candida dublliniensis*. *PLoS One* **2013**, *8*.
16. Nobile, C.J.; Bruno, V.M.; Richard, M.L.; Davis, D.A.; Mitchell, A.P. Genetic control of chlamydospore formation in *Candida albicans*. *Microbiology* **2003**.

17. Whiteway, M.; Bachewich, C. Morphogenesis in Candida albicans. *Annu. Rev. Microbiol.* **2007**, *61*, 529–553.
18. Dujardin, L.; Walbaum, S.; Biguet, J. Chlamydosporulation in "*Candida albicans*". Course of the morphogenesis; influence of light and sowing density. *Ann. Microbiol. (Paris). 131A*, 141–149.
19. Cole, G.T.; Seshan, K.R.; Phaneuf, M.; Lynn, K.T. Chlamydospore-like cells of *Candida albicans* in the gastrointestinal tract of infected, immunocompromised mice. *Can. J. Microbiol.* **1991**, *37*, 637–646.
20. Chabasse, D.; Bouchara, J.P.; de Gentile, L.; Chennebault, J.M. Candida albicans chlamydospores observed in vivo in a patient with AIDS. *Ann. Biol. Clin. (Paris).* **1988**, *46*, 817–818.
21. Daróczy, J.; Galgóczy, J.; Simon, G. Scanning Electron Microscopy of *Candida albicans* Chlamydospores. *Mycoses* **1988**, *31*, 523–526.
22. Miller, S.E.; Spurlock, B.O.; Michaels, G.E. Electron microscopy of young *Candida albicans* chlamydospores. *J. Bacteriol.* **1974**, *119*, 992–999.
23. Jansons, V.K.; Nickerson, W.J. Chemical Composition of Chlamydospores of *Candida albicans*. *J. Bacteriol.* **1970**, *104*, 922–932.
24. Navarathna, D.H.M.L.P.; Pathirana, R.U.; Lionakis, M.S.; Nickerson, K.W.; Roberts, D.D. *Candida albicans* ISW2 Regulates Chlamydospore Suspensor Cell Formation and Virulence In Vivo in a Mouse Model of Disseminated Candidiasis. *PLoS One* **2016**, *11*, e0164449.
25. Vidotto, V.; Bruatto, M.; Accattatis, G.; Caramello, S.; Vidotto, V, Bruatto M, Accattatis G, C.S.; Vidotto, V.; Bruatto, M.; Accattatis, G.; Caramello, S. Observation on the nucleic acids in the chlamydospores of *Candida albicans*. *New Microbiol.* **1996**, *19*, 327–334.
26. Citiulo, F.; Moran, G.P.; Coleman, D.C.; Sullivan, D.J. Purification and germination of *Candida albicans* and *Candida dubliniensis* chlamydospores cultured in liquid media. *FEMS Yeast Res.* **2009**, *9*, 1051–1060.
27. Raudonis, B.M.; Smith, A.G. Germination of the chlamydospores of *Candida albicans*. *Mycopathologia* **1982**, *78*, 87–91.
28. Bakerspigel A, B.S. A possible function of the chlamydospores of *Candida albicans*. *Mycopathol Mycol Appl* **1974**, *54*, 147–52.
29. Sonneborn, A.; Bockmühl, D.P.; Ernst, J.F. Chlamydospore formation in *Candida albicans* requires the Efg1p morphogenetic regulator. *Infect. Immun.* **1999**, *67*, 5514–5517.
30. Staib, P.; Morschhäuser, J. Differential expression of the NRG1 repressor controls species-specific regulation of chlamydospore development in *Candida albicans* and *Candida dubliniensis*. *Mol. Microbiol.* **2005**, *55*, 637–652.
31. Hernández-Cervantes, A.; Znaidi, S.; van Wijlick, L.; Denega, I.; Basso, V.; Ropars, J.; Sertour, N.; Sullivan, D.; Moran, G.; Basmaciyan, L.; et al. A conserved regulator controls asexual sporulation in the fungal pathogen *Candida albicans*. *Nat. Commun.* **2020**, *11*, 6224.
32. Ghosh, A.K.; Wangsanut, T.; Fonzi, W.A.; Rolfes, R.J. The GRF10 homeobox gene regulates filamentous growth in the human fungal pathogen *Candida albicans* . *FEMS Yeast Res.* **2015**, *15*.

33. Bettina, B.; Pollath Christine , Peter Staib, B.H.S.B. *Candida* species rewired hyphae developmental programs for chlamydospore formation. *Front. Microbiol.* **2016**, *7*, 1–17.
34. Alonso-Monge, R.; Navarro-García, F.; Román, E.; Negredo, A.I.; Eisman, B.; Nombela, C.; Pla, J. The Hog1 Mitogen-Activated Protein Kinase Is Essential in the Oxidative Stress Response and Chlamydospore Formation in *Candida albicans*. *Eukaryot. Cell* **2003**, *2*, 351–361.
35. Krishnamurthy, S.; Plaine, A.; Albert, J.; Prasad, T.; Prasad, R.; Ernst, J.F. Dosage-dependent functions of fatty acid desaturase Ole1p in growth and morphogenesis of *Candida albicans*. *Microbiology* **2004**, *150*, 1991–2003.
36. Noble, S.M.; French, S.; Kohn, L.A.; Chen, V.; Johnson, A.D. Systematic screens of a *Candida albicans* homozygous deletion library decouple morphogenetic switching and pathogenicity. *Nat. Genet.* **2010**, *42*, 590–606.
37. Meyers, E.; Miraglia, G.J.; Smith, D.A.; Basch, H.; Pansy, F.E.; Trejo, W.H.; Donovick, R. Biological Characterization of Prasinomycin, a Phosphorus-containing Antibiotic. *Appl. Microbiol.* **1968**, *16*, 603–608.
38. Homann, O.R.; Dea, J.; Noble, S.M.; Johnson, A.D. A phenotypic profile of the *Candida albicans* regulatory network. *PLoS Genet.* **2009**, *5*.
39. Fox, E.P.; Bui, C.K.; Nett, J.E.; Hartooni, N.; Mui, M.C.; Andes, D.R.; Nobile, C.J.; Johnson, A.D. An expanded regulatory network temporally controls *Candida albicans* biofilm formation. *Mol. Microbiol.* **2015**, *96*, 1226–1239.
40. Huangid, M.Y.; Woolfordid, C.A.; May, G.; Mcmanusid, C.J.; Mitchellid, A.P. Circuit diversification in a biofilm regulatory network. *PLoS Pathog.* **2019**, *15*.
41. Kurtzman, C.P.; Fell, J.W.; Boekhout, T.; Robert, V. Methods for isolation, phenotypic characterization and maintenance of yeasts. *The Yeasts* **2011**, *1*, 87–110.
42. Ingle, S.; Kodgire, S.; Shiradhone, A.; Patil, R.; Zore, G. Chlamydospore specific proteins of *Candida albicans*. *Data* **2017**, *2*, doi:10.3390.
43. Nguyen, N.; Quail, M.M.F.; Hernday, A.D. An Efficient, Rapid, and Recyclable System for CRISPR-Mediated Genome Editing in *Candida albicans*. *mSphere* **2017**, *2*, e00149–17.
44. Moll, P.; Ante, M.; Seitz, A.; Reda, T. QuantSeq 3′ mRNA sequencing for RNA quantification. *Nat. Methods* **2014**, *11*, i–iii.
45. Dobin, A.; Davis, C.A.; Schlesinger, F.; Drenkow, J.; Zaleski, C.; Jha, S.; Batut, P.; Chaisson, M.; Gingeras, T.R. Sequence analysis STAR: ultrafast universal RNA-seq aligner. **2013**, *29*, 15–21.
46. Conway, J.R.; Lex, A.; Gehlenborg, N. UpSetR: An R package for the visualization of intersecting sets and their properties. *Bioinformatics* **2017**, *33*, 2938–2940.
47. Lex, A.; Gehlenborg, N.; Strobelt, H.; Vuillemot, R.; Pfister, H. UpSet: Visualization of intersecting sets. *IEEE Trans. Vis. Comput. Graph.* **2014**, *20*, 1983–1992.
48. Kuleshov, M. V; Jones, M.R.; Rouillard, A.D.; Fernandez, N.F.; Duan, Q.; Wang, Z.; Koplev, S.; Jenkins, S.L.; Jagodnik, K.M.; Lachmann, A.; et al. Enrichr: a comprehensive gene set enrichment analysis web server 2016 update. *Nucleic*

Acids Res. **2016**, *44*.
49. Luo, W.; Pant, G.; Bhavnasi, Y.K.; Blanchard, S.G.; Brouwer, C. Pathview Web: user friendly pathway visualization and data integration. *Nucleic Acids Res.* **2017**, *45*, 501–508.
50. Lohse, M.B.; Johnson, A.D. Identification and Characterization of Wor4, a New Transcriptional Regulator of White-Opaque Switching. *Genes, Genomes, Genet.* **2016**, *6*, 721–729.
51. Nobile, C.J.; Fox, E.P.; Nett, J.E.; Sorrells, T.R.; Mitrovich, Q.M.; Hernday, A.D.; Tuch, B.B.; Andes, D.R.; Johnson, A.D. A recently evolved transcriptional network controls biofilm development in *Candida albicans*. *Cell* **2012**, *148*, 126–138.
52. Babraham Bioinformatics - FastQC A Quality Control tool for High Throughput Sequence Data Available online: https://www.bioinformatics.babraham.ac.uk/projects/fastqc/ (accessed on Jan 2, 2021).
53. Bolger, A.M.; Lohse, M.; Usadel, B. Trimmomatic: A flexible trimmer for Illumina sequence data. *Bioinformatics* **2014**, *30*, 2114–2120.
54. Skrzypek, M.S.; Binkley, J.; Binkley, G.; Miyasato, S.R.; Simison, M.; Sherlock, G. The *Candida* Genome Database (CGD): Incorporation of Assembly 22, systematic identifiers and visualization of high throughput sequencing data. *Nucleic Acids Res.* **2017**, *45*, D592–D596.
55. Langmead, B.; Salzberg, S.L. Fast gapped-read alignment with Bowtie 2. *Nat. Methods* **2012**, *9*, 357–359.
56. Gaspar, J.M. Improved peak-calling with MACS2. *bioRxiv* 2018, 496521.
57. Homann, O.R.; Johnson, A.D. MochiView: Versatile software for genome browsing and DNA motif analysis. *BMC Biol.* **2010**, *8*, 49.
58. Li, H.; Handsaker, B.; Wysoker, A.; Fennell, T.; Ruan, J.; Homer, N.; Marth, G.; Abecasis, G.; Durbin, R. The Sequence Alignment/Map format and SAMtools. *Bioinformatics* **2009**, *25*, 2078–2079.
59. Emms, D.M.; Kelly, S. OrthoFinder: solving fundamental biases in whole genome comparisons dramatically improves orthogroup inference accuracy. *Genome Biol.* **2015**, *16*, 1–14.
60. Emms, D.M.; Kelly, S. OrthoFinder: Phylogenetic orthology inference for comparative genomics. *Genome Biol.* **2019**, *20*, 1–14.
61. Emms, D.M.; Kelly, S. STRIDE: Species tree root inference from gene duplication events. *Mol. Biol. Evol.* **2017**, *34*, 3267–3278.
62. Emms, D.M.; Kelly, S. STAG: Species Tree Inference from All Genes. *doi https//doi.org/10.1101/267914* 2018, 267914.
63. Letunic, I.; Bork, P. Interactive Tree of Life (iTOL) v4: Recent updates and new developments. *Nucleic Acids Res.* **2019**, *47*.
64. Turner, S.A.; Butler, G. The *Candida* Pathogenic Species Complex. *Cold Spring Harb. Perspect Med 2014* **2014**, 4:a019778.
65. Santos, M.A.S.; Gomes, A.C.; Santos, M.C.; Carreto, L.C.; Moura, G.R. The genetic code of the fungal CTG clade. *Comptes Rendus - Biol.* **2011**, *334*, 607–611.

66. Noble, S.M.; Johnson, A.D. Strains and strategies for large-scale gene deletion studies of the diploid human fungal pathogen *Candida albicans*. *Eukaryot. Cell* **2005**, *4*, 298–309.
67. Rosenthal, S.A.; And, D.; Furnari, B.A. Chlamysdospore production by*Candida albicans*: Comparison of dehydrated rice extract agar with other media. *J. Invest. Dermatol.* **1958**, *32*, 115–116.
68. Braun, B.R.; Kadosh, D.; Johnson, A.D. NRG1, a repressor of filamentous growth in *Candida albicans* , is down-regulated during filament induction. *EMBO J.* **2001**, *20*, 4753–4761.
69. Lohman, B.K.; Weber, J.N.; Bolnick, D.I. Evaluation of TagSeq, a reliable low-cost alternative for RNAseq. *Mol. Ecol. Resour.* **2016**.
70. Zhang, Y.; Liu, T.; Meyer, C.A.; Eeckhoute, J.; Johnson, D.S.; Bernstein, B.E.; Nussbaum, C.; Myers, R.M.; Brown, M.; Li, W.; et al. Model-based analysis of ChIP-Seq (MACS). *Genome Biol.* **2008**, *9*, R137.
71. Hernday, A.D.; Lohse, M.B.; Fordyce, P.M.; Nobile, C.J.; DeRisi, J.L.; Johnson, A.D. Structure of the transcriptional network controlling white-opaque switching in *Candida albicans*. *Mol. Microbiol.* **2013**, *90*, 22–35.
72. Banerjee, M.; Thompson, D.S.; Lazzell, A.; Carlisle, P.L.; Pierce, C.; Monteagudo, C.; López-Ribot, J.L.; Kadosh, D. UME6, a novel filament-specific regulator of *Candida albicans* hyphal extension and virulence. *Mol. Biol. Cell* **2008**, *19*, 1354–1365.
73. Volker R.Stoldt, Anja Sonneborn, C.E.L. and J.F.E.; Stoldt, V.R.; Sonneborn, A.; Leuker, C.E.; Ernst, J.F. Efg1p, an essential regulator of morphogenesis of the human pathogen *Candida albicans*, is a member of a conserved class of bHLH proteins regulating morphogenetic processes in fungi. *EMBO J* **1997**, *16*, 1982–1991.
74. Sephton-Clark, P.C.S.; Voelz, K. Spore Germination of Pathogenic Filamentous Fungi. In *Advances in Applied Microbiology*; Academic Press Inc., 2018; Vol. 102, pp. 117–157 ISBN 9780128151846.
75. Feofilova, E.P.; Ivashechkin, A.A.; Alekhin, A.I.; Sergeeva, Y.E. Fungal spores: Dormancy, germination, chemical composition, and role in biotechnology (review). *Appl. Biochem. Microbiol.* **2012**, *48*, 1–11.
76. Lin, X.; Heitman, J. Chlamydospore Formation during Hyphal Growth in *Cryptococcus neoformans*. *Eukaryot. Cell* **2005**, *4*, 1746–1754.
77. Bauer, J.; Wendland, J. *Candida albicans* Sfl1 suppresses flocculation and filamentation. *Eukaryot. Cell* **2007**, *6*, 1736–1744.
78. Covitz, P.A.; Mitchell, A.P. Repression by the yeast meiotic inhibitor RME1. *Genes Dev.* **1993**, *7*, 1598–1608.
79. Lu, Y.; Su, C.; Unoje, O.; Liu, H. Quorum sensing controls hyphal initiation in *Candida albicans* through Ubr1-mediated protein degradation. *Proc. Natl. Acad. Sci. U. S. A.* **2014**, *111*, 1975–1980.
80. Basso, V.; Znaidi, S.; Bachellier-Bassi, S.; D'Enfert, C.; Znaidi, S.; Bachellier-Bassi, S. From Genes to Networks: The Regulatory Circuitry Controlling *Candida albicans* Morphogenesis. *Curr. Top. Microbiol. Immunol.* **2019**, *422*, 61–69.
81. Childers, D.S.; Kadosh, D. Filament Condition-Specific Response Elements

Control the Expression of NRG1 and UME6, Key Transcriptional Regulators of Morphology and Virulence in *Candida albicans*. *PLoS One* **2015**, *10*, e0122775.
82. Zeidler, U.; Lettner, T.; Lassnig, C.; Muller, M.M.¨; Lajko, R.; Hintner, H.; Breitenbach, M.; Bito, A. UME6 is a crucial downstream target of other transcriptional regulators of true hyphal development in *Candida albicans*. *FEMS Yeast Res.* **2009**, *9*, 126–142.
83. Finkel, J.S.; Xu, W.; Huang, D.; Hill, E.M.; Desai, J. V; Woolford, C.A.; Nett, J.E.; Taff, H.; Norice, C.T.; Andes, D.R.; et al. Portrait of *Candida albicans* Adherence Regulators. *PLoS Pathog* **2012**, *8*, 1002525.
84. Khalaf, R.A.; Zitomer, R.S. The DNA Binding Protein Rfg1 Is a Repressor of Filamentation in *Candida albicans*. *Genetics* **2001**, *157*, 1503–1512.
85. Süel, G.M.; Garcia-Ojalvo, J.; Liberman, L.M.; Elowitz, M.B. An excitable gene regulatory circuit induces transient cellular differentiation. *Nature* **2006**, *440*, 545–550.
86. Wilson, N.K.; Foster, S.D.; Wang, X.; Knezevic, K.; Schütte, J.; Kaimakis, P.; Chilarska, P.M.; Kinston, S.; Ouwehand, W.H.; Dzierzak, E.; et al. Combinatorial transcriptional control in blood stem/progenitor cells: Genome-wide analysis of ten major transcriptional regulators. *Cell Stem Cell* **2010**, *7*, 532–544.
87. Young, R.A. Control of the embryonic stem cell state. *Cell* 2011, *144*, 940–954.
88. Rodriguez, D.L.; Quail, M.M.; Hernday, A.D.; Nobile, C.J. Transcriptional Circuits Regulating Developmental Processes in *Candida albicans*. *Front. Cell. Infect. Microbiol.* **2020**, *10*.
89. Miyaji, M.; Sano, A.; Sharmin, S.; Kamei, K.; Nishimura, K. The Role of Chlamydospores of *Paracoccidioides brasiliensis*. *Jpn. J. Med. Mycol* **2003**, *44*, 133–138.
90. DeLamater, E.D. The Nuclear Cytology of *Blastomyces dermatitidis*. *Mycologia* **1948**, *40*, 430–444.
91. Mancera, E.; Porman, A.M.; Cuomo, C.A.; Bennett, R.J.; Johnson, A.D. Finding a missing gene: EFG1 regulates morphogenesis in *Candida tropicalis*. *Genes, Genomes, Genet.* **2015**, *5*, 849–856.

CHAPTER 3

Visible Lights Combined with Photosensitizing Compounds Are effective against *Candida albicans* Biofilms, *Microorganisms*, 500, 9

microorganisms MDPI

Article

Visible Lights Combined with Photosensitizing Compounds Are Effective against *Candida albicans* Biofilms

Priyanka Bapat [1,2], Gurbinder Singh [1] and Clarissa J. Nobile [1,3,*]

3.1 Abstract

Fungal infections are increasing in prevalence worldwide, especially in immunocompromised individuals. Given the emergence of drug-resistant fungi and the fact that there are only three major classes of antifungal drugs available to treat invasive fungal infections, there is a need to develop alternative therapeutic strategies effective against fungal infections. *Candida albicans* is a commensal of the human microbiota that is also one of the most common fungal pathogens isolated from clinical settings. *C. albicans* possesses several virulence traits that contribute to its pathogenicity, including the ability to form drug resistant biofilms, which can make *C. albicans* infections particularly challenging to treat. Here, we explored red, green, and blue visible lights alone and in combination with common photosensitizing compounds for their efficacies at inhibiting and disrupting *C. albicans* biofilms. We found that blue light inhibited biofilm formation and disrupted mature biofilms on its own and that the addition of photosensitizing compounds improved its antibiofilm potential. Red and green lights, however, inhibited biofilm formation only in combination with photosensitizing compounds but had no effects on disrupting mature biofilms. Taken together, these results suggest that photodynamic therapy may be an effective non-drug treatment for fungal biofilm infections that is worthy of further exploration.

3.2. Introduction

Fungi cause a wide range of diseases in humans ranging from superficial skin to life-threatening disseminated infections, especially in immunocompromised and critically ill individuals [1]. C*andida albicans* is a common fungus that typically resides as a benign commensal member of the human microbiota, colonizing the skin and mucosal surfaces of healthy humans [2]. It is also an opportunistic pathogen that can cause both superficial skin and mucosal infections as well as severe systemic infections under permissive host environmental conditions [3,4]. *C. albicans* has multiple virulence mechanisms that contribute to its pathogenicity, including the ability to form physically recalcitrant and drug resistant biofilms, that can make *C. albicans* infections particularly challenging to treat [5].

Biofilms are communities of adherent microbial cells encased in extracellular matrices that are often resistant and/or tolerant to antimicrobial agents and the host immune response [6–8]. The *C. albicans* biofilm life cycle occurs in four sequential stages: adherence, initiation, maturation, and dispersal (Figure 1A). In the adherence stage, planktonic (free-floating) yeast-form cells adhere to biotic surfaces (e.g., mucosal layers and epithelial cell layers) or abiotic surfaces (e.g., catheters, heart valves, and dentures) [9]. In the initiation stage, the yeast-form cells proliferate to form an anchoring basal cell layer and begin to differentiate into hyphal and pseudohyphal cells. In the maturation stage, the hyphal cells elongate and a protective extracellular matrix that is composed of proteins, carbohydrates, nucleic acids, and lipids, surrounds the cells within the biofilm. In the dispersal stage, which completes the *C. albicans* biofilm life cycle, yeast-form cells are released from the biofilm, where they can repeat the biofilm life cycle by forming biofilm at secondary sites in the host or can enter the bloodstream to cause life-threatening systemic infections [3,4,8].

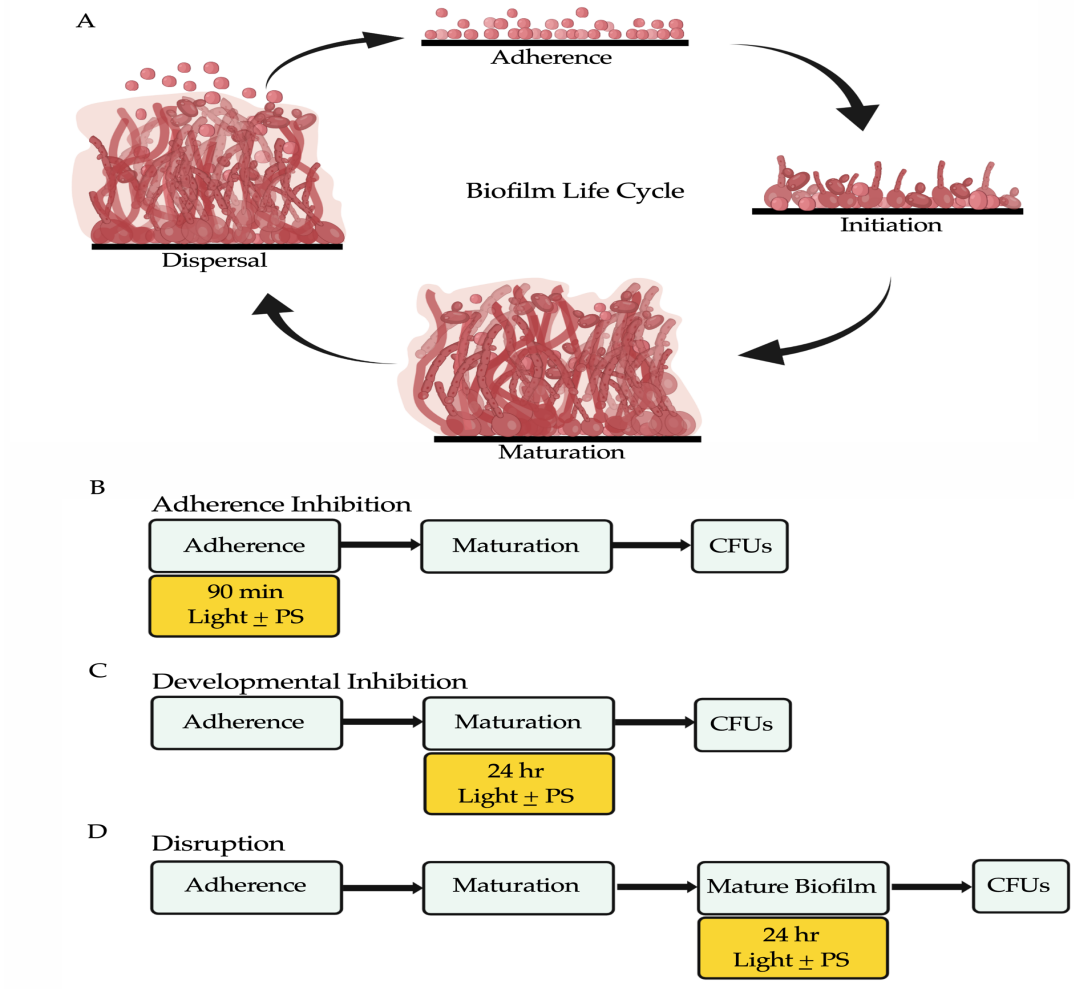

Figure 3.1. The *C. albicans* biofilm life cycle and the biofilm assays used in this study to assess the antibiofilm properties of visible lights and photosensitizing compounds.

(A) The *C. albicans* biofilm life cycle occurs in four sequential stages: adherence, initiation, maturation and dispersal. In the adherence stage, planktonic yeast-form cells adhere to a surface. In the initiation stage, the yeast-form cells proliferate forming an anchoring basal cell layer and begin to differentiate into hyphal and pseudohyphal cells. In the maturation stage, the hyphal cells elongate, and a protective extracellular matrix surrounds the cells. In the dispersal stage, yeast-form cells are released from the biofilm and the life cycle repeats. (B) Overview of the adherence inhibition biofilm assay, where the visible light of interest with (+) or without (-) the photosensitizing compound (PS) of interest were present during the 90-min adherence stage of biofilm formation. (C) Overview of the developmental inhibition biofilm assay, where the visible light of interest with (+) or without (-) the PS of interest were present during the 24-h maturation stage of biofilm formation. (D) Overview of the disruption biofilm assay, where the visible light of interest with (+) or without (-) the PS of interest were present for an additional 24 h on a mature (24-h) biofilm. Colony forming units (CFUs) were measured to determine viable cell counts at the end of each biofilm assay. This figure was creating using BioRender.com.

Antifungal drugs are the most commonly used therapeutic agents for treating fungal infections [10]. Only three major classes of antifungal drugs (the polyenes, azoles, and echinocandins) are currently used to treat invasive fungal infections in humans, and it has been a challenge to develop new and effective antifungal drugs, especially with efficacy against biofilms [11–14]. Existing antifungal drugs often have significant side effects in humans, causing toxicity to the liver, kidneys, and central nervous system [15,16]. Additionally, some *Candida* clinical isolates are naturally resistant and/or tolerant to antifungal drugs or can develop resistance over time, further reducing treatment efficacy [17,18]. The paucity of effective antifungal drugs with low toxicity to humans, combined with an increase in antifungal drug resistance in *Candida* clinical isolates, has prompted the search for alternative non-drug therapeutic strategies to treat fungal infections [19].

Photodynamic therapy has been used over the last 40 years to treat oncologic skin conditions, such as basal cell carcinoma and actinic keratosis [20,21], and more recently to treat benign skin conditions, such as acne vulgaris and viral warts [22]. Currently, and in light of the emergence of drug resistant infections in the clinic, photodynamic therapy as a non-drug antimicrobial strategy has been gaining considerable scientific interest [23–26]. Photodynamic therapy relies on a light source, a non-toxic photosensitizing compound that can absorb and transfer electrons after light absorption, and molecular oxygen that acts as an electron acceptor [23]. The typical output of photodynamic therapy is reactive oxygen species (ROS) (e.g., singlet oxygen, hydroxyl radicals, and superoxide anions) that are produced when the photosensitizing compound is excited by light; these ROS can then have cytotoxic effects on the targeted cells, such as cancer cells and microbial cells [27,28]. Unlike traditional antimicrobial drugs, photodynamic therapy as an antimicrobial strategy would affect multiple non-specific microbial targets simultaneously, making it unlikely for resistance to be developed. Based on its fundamental mechanisms of action, photodynamic therapy could be a clinically useful non-drug antimicrobial therapeutic strategy that is worthy of further exploration.

The visible light spectrum can be broadly divided into red (620-700 nm), green (500-560 nm), and blue (400-490 nm) wavelengths [23,24,29,30], where several discreet

wavelengths within each spectrum have been shown to display antimicrobial properties [29,31–33]. To date, of the visible lights, blue light has been the most studied for its antimicrobial properties, where it has been shown to effectively kill pathogenic bacteria and fungi *in vitro*, including drug-resistant bacteria in both planktonic and biofilm forms [34–47]. Comparatively, the antimicrobial properties of red and green lights have been much less studied to date [29,48–51].

Although the use of lights in the visible spectrum can have antimicrobial effects on targeted microbial cells on their own, likely by generating ROS through the photoexcitation of naturally occurring photosensitizing compounds (e.g., flavoproteins and porphyrins) [28,40], the combined antimicrobial effects of visible lights with exogenous synthetic photosensitizing compounds have been shown to significantly increase the generation of ROS *in vitro* [26,42,52,53]. There are many non-toxic synthetic photosensitizing compounds that have been developed to date [54–57], but in this study we focus on the classic and commonly used photosensitizing compounds new methylene blue, toluidine blue O, and rose bengal (Figure S1). New methylene blue and toluidine blue O are structurally similar phenothiazinium salts absorbing between 600-660 nm, while rose bengal is a xanthene salt absorbing between 500-550 nm [42,47,52,58,59].

Prior work on *C. albicans* has shown that the combination of blue light with rose bengal reduced *C. albicans* cell viability in both planktonic and biofilm forms [59]. Additionally, a combination of blue light with toluidine blue O inhibited *C. albicans* biofilm formation [47]. For red light, in combination with new methylene blue, *C. albicans* cell viability in the planktonic form was reduced [60]. Finally, for green light in combination with rose bengal, *C.albicans* cell viability in both planktonic and biofilm forms was reduced [61]. To our knowledge, no studies to date have compared different visible lights alone or in combination with photosensitizing compounds to assess their efficacies at inhibiting and disrupting *C. albicans* biofilms at different stages of biofilm formation. Our study assesses the effects of these lights at the adherence stage of biofilm formation, throughout the course of biofilm formation, and on mature biofilms. In addition, our study includes *C. albicans* strains of different genetic backgrounds, which is important for understanding the real-world utility of antimicrobial photodynamic therapy in clinical settings.

In this study, we examined and compared the effects of red, green, and blue visible lights alone and in combination with the classic and commonly used photosensitizing compounds new methylene blue, toluidine blue O, and rose bengal to assess their efficacies at inhibiting *C. albicans* biofilm formation and at disrupting mature *C. albicans* biofilms. We found that blue light inhibited biofilm formation and disrupted mature biofilms on its own and that the addition of photosensitizing compounds improved its antibiofilm potential. Red and green lights, however, inhibited biofilm formation only in combination with photosensitizing compounds, but had no effects on disrupting mature biofilms.

3.3 Materials and Methods

3.3.1 Strains and media

All experiments were performed using the wildtype *C. albicans* strain SN250 [62]. Results using SN250 were validated using the *C. albicans* clinical isolates SC5314 [63] and Strain #0761 (AR0761) (Centers for Disease Control and Prevention (CDC) AR Isolate Bank, Drug Resistance *Candida* species panel; https://wwwn.cdc.gov/ARIsolateBank/). *C. albicans* cells were recovered from -80°C glycerol stocks for two days at 30°C on yeast extract peptone dextrose (YPD) agar plates (1% yeast extract (Thermo Fisher Scientific, Catalog #211929), 2% Bacto peptone (Gibco, Catalog #211677), 2% dextrose (Fisher Scientific, Catalog #D16-3), and 2% agar (Criterion, Catalog #89405-066)). Overnight cultures were grown for ~15 h at 30°C, shaking at 225 rpm in YPD liquid medium (1% yeast extract (Thermo Fisher Scientific, Catalog #211929), 2% Bacto peptone (Gibco, Catalog #211677), and 2% dextrose (Fisher Scientific, Catalog #D16-3)). All biofilm assays were performed using Spider medium (10 g/L nutrient broth (VWR, Catalog #89405-794), 10 g/L mannitol (Alfa Aesar, Catalog #A14030), 4 g/L K_2PO_4 (Fisher Scientific, Catalog #P290-212)), at pH 7.2.

3.3.2 Light sources and photosensitizing compounds

A red light-emitting diode (LED) light source (ABI LED lighting, Catalog #GR-PAR38-26W-RED, 26-Watt 620-630 nm, outputting 176 J/cm^2), a green LED light source (ABI LED lighting, Catalog #GR-PAR38-24W-520NM, 24-Watt 520-530 nm, outputting 204 J/cm^2), and a blue LED light source (ABI LED lighting, Catalog #GR-PAR38-24W-BLU, 24-Watt 450 nm, outputting 240 J/cm^2) were placed 8 inches from the biofilm wells and used as indicated in the biofilm assays. Average LED light intensity measurements for each light source at a distance of 8 inches away from the biofilm assay plates were 6500 lux for red light, 6700 lux for green light, and 5900 lux for blue light.

The photosensitizing compounds new methylene blue (Sigma Aldrich, Catalog #B-4631), toluidine blue O (Sigma Aldrich, Catalog #T3260) and rose bengal (Sigma Aldrich, Catalog #198250) were used as indicated in the biofilm assays. The photosensitizing compounds were dissolved in phosphate buffered saline (PBS) (HyClone, Catalog #16777-252) at a stock concentration of 10 mM and diluted to a working concentration of 400 µM in Spider medium, which was used to grow the biofilms. Stocks of the photosensitizing compounds were prepared fresh every two weeks, filter sterilized, and stored at 4^{0}C in the dark.

3.3.3 Biofilm assays

The adherence inhibition, developmental inhibition, and disruption biofilm assays were performed as described previously [64,65] except that instead of taking optical density readings at the end of the biofilm assays, we measured colony forming units (CFUs) to assess the efficacies of the visible lights with or without photosensitizing compounds at reducing *C. albicans* viable cell counts from the biofilms. This modification was made because the photosensitizing compounds on their own elevated optical density readings by absorbing light, and as such optical density readings did not accurately reflect biofilm growth or thickness.

In brief, biofilms were grown in triplicate on the bottoms of sterile flat-bottomed 12-well non-tissue culture treated polystyrene plates (Corning, Catalog #351143). The 12-well plates were seeded at a final OD_{600} of 0.5 in a final volume of 2 mL Spider medium and grown for 90 min at 37°C with shaking at 250 rpm in an ELMI shaker (M2 Scientifics, Catalog #ELMI-TRMS04). After the initial 90-min adherence period, the wells were gently washed with PBS and fresh Spider medium was added to each well. The plates were sealed with breathable sealing membranes (Sigma Aldrich, Catalog #Z380059) and grown at 37°C with shaking at 250 rpm in an ELMI shaker for 24 h. For the adherence inhibition biofilm assay, the biofilms were exposed to red, green, or blue visible lights with or without a photosensitizing compound during the 90-min adherence stage of biofilm formation (Figure 1B). For the developmental inhibition biofilm assay, the biofilms were exposed to red, green, or blue visible lights with or without a photosensitizing compound throughout the first 24 h of biofilm growth, but not during the initial 90-min adherence stage (Figure 1C). For the disruption biofilm assay, medium was removed from each well containing a mature 24-h biofilm, fresh Spider medium was added to each well, the plates were re-sealed, and the mature biofilms were exposed to red, green, or blue visible lights with or without a photosensitizing compound for an additional 24 h (Figure 1D). The 12-well plates were divided such that half of one plate was exposed to the light of interest and the other half was covered with foil and served as a no light control.

3.3.4 Determination of colony forming units (CFUs) from biofilms

CFU determinations from biofilms were performed as previously described [64,65]. Briefly, biofilms were scraped from the bottoms of each well of a 12-well plate using a sterile spatula, vigorously vortexed, serially diluted in PBS, and plated onto YPD agar plates. The plates were incubated at room temperature for 3 days and colonies were counted to determine CFUs/mL. Statistical significance was determined using a student's unpaired two-tailed t-test assuming unequal variance.

We note that we do not recommend measuring metabolic reduction of the tetrazolium salt reagent 2,3-bis-(2-methoxy-4-nitro-5-sulfophenyl)-2H-tetrazolium-5-carboxanilide (XTT) as a method to assess metabolic activity in the presence of photosensitizing compounds because the photosensitizing compounds on their own (as is the case with the photosensitizing compounds used in our study) can elevate optical density readings by absorbing light in this colorimetric assay, and as such the XTT assay would not accurately reflect metabolic activity after treatment.

3.3.5 Viability staining of biofilm cells

Viability staining was performed on cells resuspended from biofilms and directly on biofilms under each light and photosensitizing compound treatment condition using the LIVE/DEAD *Bac*Light viability kit (Invitrogen, Catalog #L7012) as described in [66] for use on *C. albicans* biofilms, and according to the manufacturer's protocol. Briefly, the samples were incubated with 3 µL SYTO9 and 3 µL of propidium iodide in the dark at 30°C for 20 min. Following incubation, the samples were imaged by fluorescence microscopy at 20X magnification with a green laser (GFP/green channel; 470 nm excitation wavelength) and a red laser (Texas Red/red channel; 585 nm excitation

wavelength) using an EVOS Cell Imaging System (Life Technologies, Catalog #EVOS FL Cell Imaging System).

We note that due to an artifact of using this LIVE/DEAD stain when combined with certain photosensitizing compounds directly on biofilms, where the dead cells on the top of the biofilms appeared black (rather than red) likely due to their faster uptake of the photosensitizing compound over the LIVE/DEAD stain, we were unable to acquire valid images for certain treatment combinations when this stain was performed directly on biofilms. This artifact was not as readily apparent when using this LIVE/DEAD stain on cells resuspended from biofilms, and thus we were able to obtain valid images for all treatment combinations when this stain was performed on cells resuspended from biofilms.

3.3.6 Assessment of cellular morphologies of biofilm cells

Cells resuspended from biofilms under each light and photosensitizing compound treatment condition were imaged by brightfield microscopy at 20X magnification using an EVOS Cell Imaging System (Life Technologies, Catalog #EVOS FL Cell Imaging System) and the presence of hyphae, pseudohyphae, and yeast-form cells was qualitatively assessed.

3.4 Results

3.4.1 Effects of red, green, and blue visible lights on *C. albicans* biofilms

To determine the effects of red, green, and blue visible lights alone (i.e., without the addition of exogenous photosensitizing compounds), we first performed the three biofilm assays in the presence individually of red, green, and blue light treatments. We found that, compared to the untreated control, red and green lights alone had no effects on biofilm formation in any of the three biofilm assays (Figure 2A-B), and that blue light alone had no effect at inhibiting biofilm formation in the adherence inhibition assay (Figure 2C). Blue light alone, however, was highly effective at inhibiting *C. albicans* biofilm formation by ~65% in the developmental inhibition biofilm assay (p = 0.0005) and at disrupting mature biofilms by ~60% in the disruption biofilm assay (p = 0.0006) compared to the untreated control (Figure 2C).

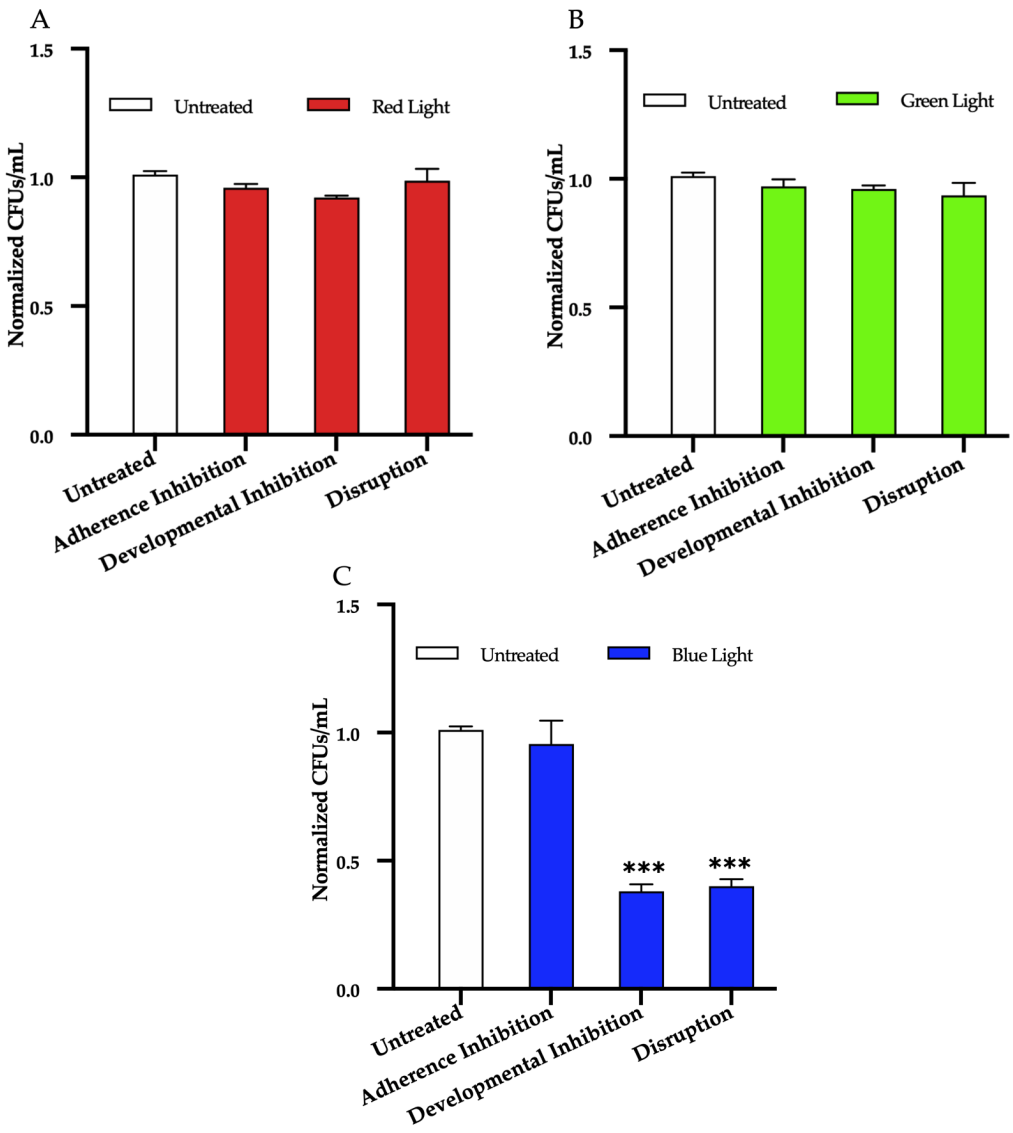

Figure 3.2. Effects of red, green and blue visible lights on *C. albicans* biofilms. *C. albicans* biofilms were exposed individually to red, green, and blue lights in the adherence inhibition, developmental inhibition, and disruption biofilm assays. Colony forming units per 1mL (CFUs/mL) were measured to determine viable cell counts from the biofilms at the end of each biofilm assay. Effects of (A) red light, (B) green light, and (C) blue light in the three different biofilm assays are shown. Standard deviations are shown for each sample (n=3). The average CFUs/mL of the untreated control samples for each assay were normalized to 1. Significance comparisons are relative to the untreated control and were determined using student's unpaired two-tailed t-tests assuming unequal variance for $p \leq 0.001$ (***).

3.4.2 Effects of red, green, and blue visible lights in combination with exogenous photosensitizing compounds on *C. albicans* biofilms

We next assessed the effects of red, green, and blue visible lights in combination with the commonly used exogenous photosensitizing compounds new methylene blue, toluidine blue O, and rose bengal on *C. albicans* biofilms. We found that, compared to the untreated control, red light alone, and each photosensitizing compound alone, red light in combination with any of the three photosensitizing compounds had no effects on biofilm formation in the adherence inhibition biofilm assay (Figure 3A). Red light when combined with any of the three photosensitizing compounds in the developmental inhibition biofilm assay, however, was moderately effective at inhibiting *C. albicans* biofilm formation by ~30% when combined with new methylene blue ($p = 0.03$), ~40% when combined with toluidine blue O ($p = 0.03$), and ~45% when combined with rose bengal ($p = 0.005$) relative to the average of the untreated control, red light alone, and each photosensitizing compound alone (Figure 3B). We also assessed the effects of red light in combination with the three photosensitizing compounds on mature *C. albicans* biofilms in the disruption biofilm assay. We found that, compared to the untreated control, red light alone, and each photosensitizing compound alone, red light in combination with any of the three photosensitizing compounds had no effects on biofilm formation in the disruption biofilm assay (Figure 3C). Similar results were observed for red light in combination with these photosensitizing compounds on biofilm formation of two different *C. albicans* clinical isolates (see Figure S2 for results of the developmental inhibition biofilm assay on additional *C. albicans* strains).

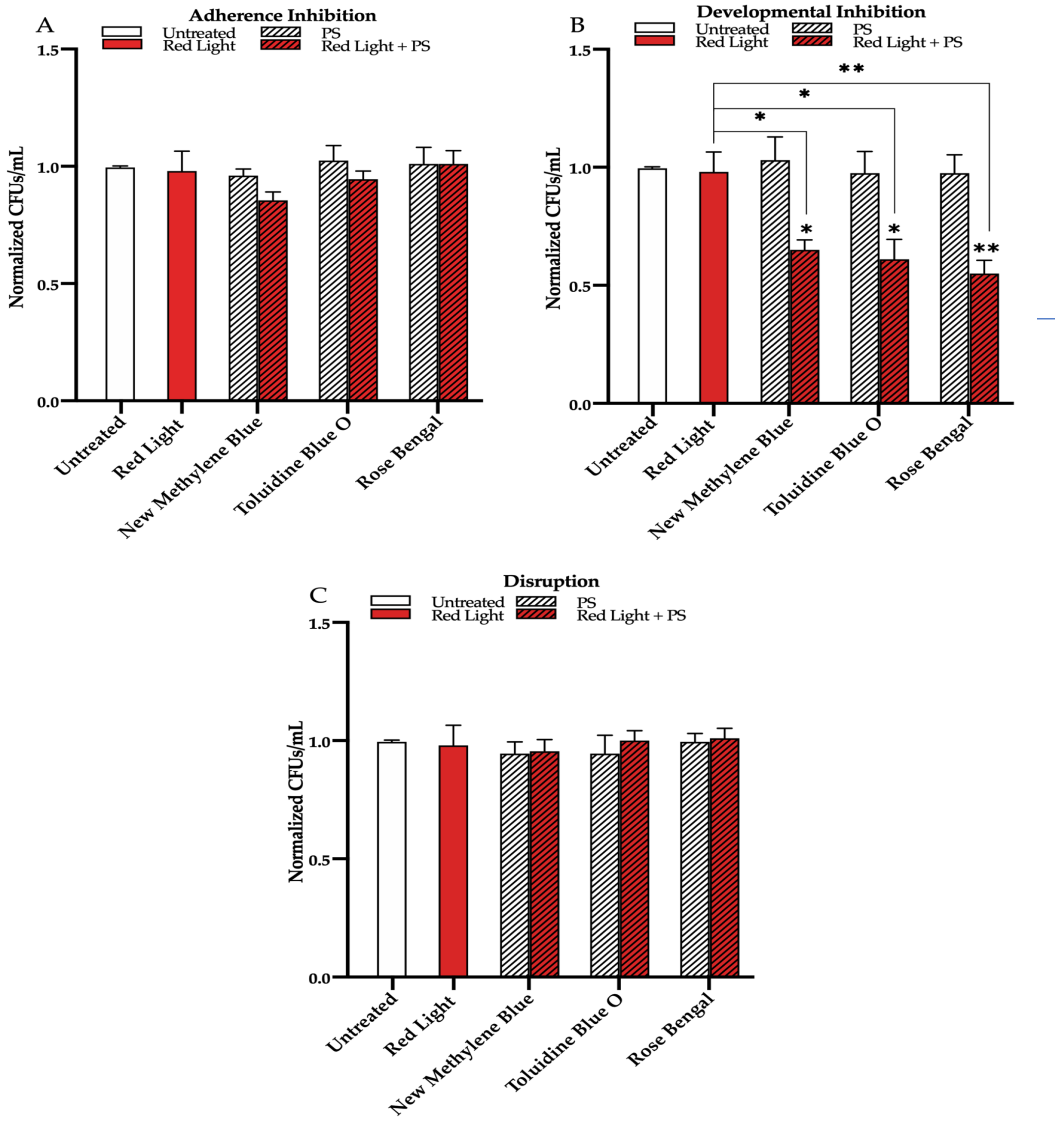

Figure 3.3. Effects of red visible light in combination with the photosensitizing compounds new methylene blue, toluidine blue O, and rose bengal on *C. albicans* biofilms. Effects of red light in combination with the photosensitizing compounds in the (A) adherence inhibition, (B) developmental inhibition, and (C) disruption biofilm assays. Untreated control (Untreated), red light alone (Red Light), photosensitizing compound alone (PS), and red light in combination with the photosensitizing compound (Red Light + PS) are shown. Colony forming units per 1mL (CFUs/mL) were measured to determine viable cell counts from the biofilms at the end of each biofilm assay. Standard deviations are shown for each sample (n=3). The average CFUs/mL of the untreated control samples for each assay were normalized to 1. Significance comparisons are relative to the untreated control unless otherwise noted with significance bars and were determined using student's unpaired two-tailed t-tests assuming unequal variance for $p \leq 0.05$ (*), and $p \leq 0.01$ (**).

Next, we found that compared to the untreated control, green light alone, and each photosensitizing compound alone, green light in combination with any of the three photosensitizing compounds had no effects on biofilm formation in the adherence inhibition biofilm assay (Figure 4A). Green light when combined with any of the three photosensitizing compounds in the developmental inhibition biofilm assay, however, was moderately effective at inhibiting *C. albicans* biofilm formation by ~45% when combined with new methylene blue ($p = 0.004$), ~25% when combined with toluidine blue O ($p = 0.02$), and ~30% when combined with rose bengal ($p = 0.03$) relative to the average of the untreated control, green light alone, and each photosensitizing compound alone (Figure 4B). We also assessed the effects of green light in combination with the three photosensitizing compounds on mature *C. albicans* biofilms in the disruption biofilm assay. We found that, compared to the untreated control, green light alone, and each photosensitizing compound alone, green light in combination with any of the three photosensitizing compounds had no effects on biofilm formation in the disruption biofilm assay (Figure 4C). Similar results were observed for green light in combination with these photosensitizing compounds on biofilm formation of two different *C. albicans* clinical isolates (see Figure S3 for results of the developmental inhibition biofilm assay on additional *C. albicans* strains).

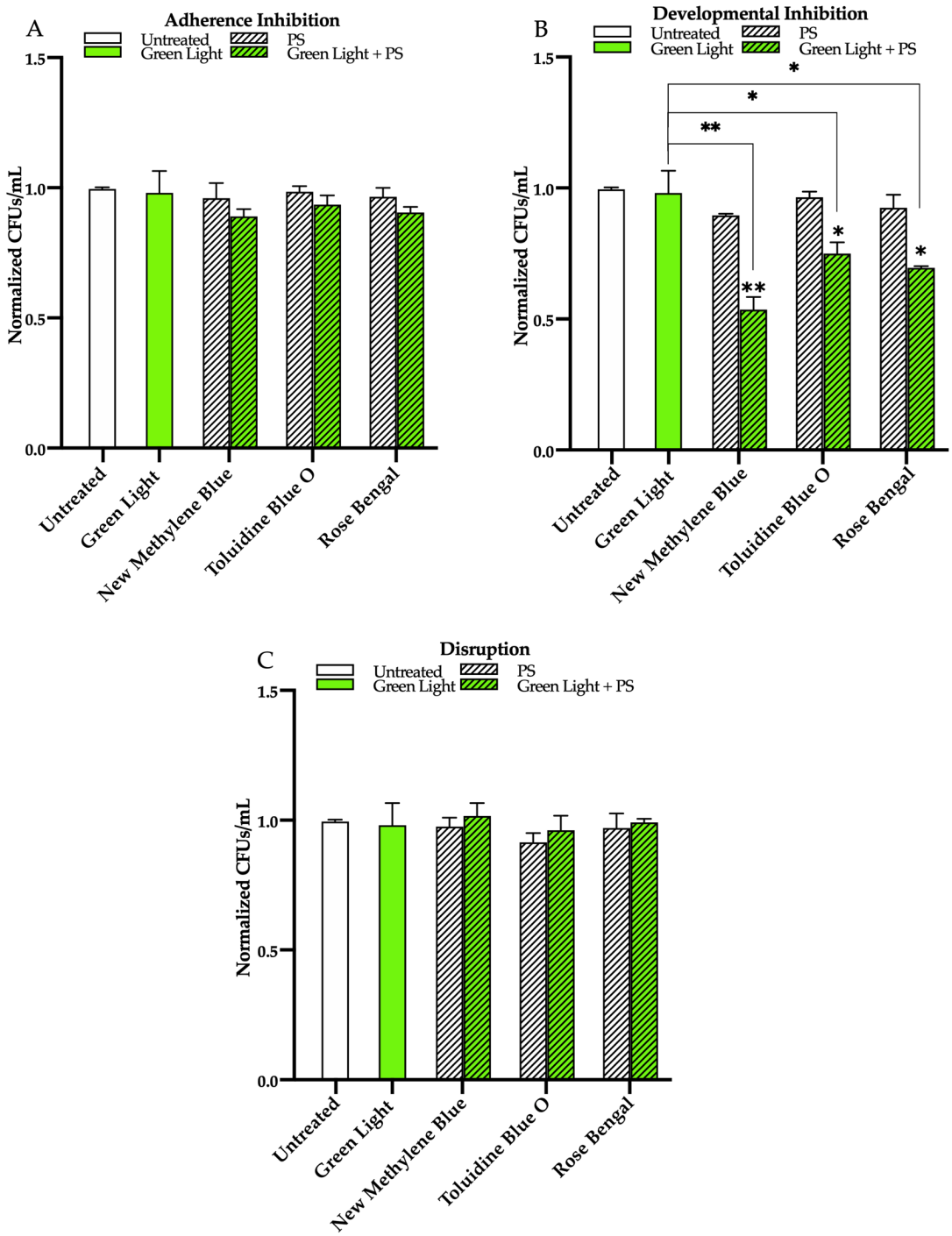

Figure 3.4. Effects of green visible light in combination with the photosensitizing compounds new methylene blue, toluidine blue O, and rose bengal on *C. albicans* biofilms. Effects of green light in combination with the photosensitizing compounds in the (A) adherence inhibition, (B) developmental inhibition, and (C) disruption biofilm assays. Untreated control (Untreated), green light alone (Green Light), photosensitizing compound

alone (PS), and green light in combination with the photosensitizing compound (Green Light + PS) are shown. Colony forming units per 1mL (CFUs/mL) were measured to determine viable cell counts from the biofilms at the end of each biofilm assay. Standard deviations are shown for each sample (n=3). The average CFUs/mL of the untreated control samples for each assay were normalized to 1. Significance comparisons are relative to the untreated control unless otherwise noted with significance bars and were determined using student's unpaired two-tailed t-tests assuming unequal variance for $p \leq 0.05$ (*), and $p \leq 0.01$ (**).

We found that compared to the untreated control, blue light alone, and each photosensitizing compound alone, blue light in combination with any of the three photosensitizing compounds had no effects on biofilm formation in the adherence inhibition biofilm assay (Figure 5A). Blue light when combined with any of the three photosensitizing compounds in the developmental inhibition biofilm assay, however, was highly effective at inhibiting *C. albicans* biofilm formation by ~80% when combined with new methylene blue ($p = 0.0005$), ~80% when combined with toluidine blue O ($p = 0.0006$), and ~70% when combined with rose bengal ($p = 0.0008$) relative to the average of the untreated control, and each photosensitizing compound alone (Figure 5B). Compared to the biofilm inhibitory effects of blue light alone, the combination of blue light with any of the three photosensitizing compounds in the developmental inhibition biofilm assay had an additive biofilm inhibitory effect of an additional 17% for new methylene blue ($p = 0.01$), 15% for toluidine blue O ($p = 0.01$), and 10% for rose bengal ($p = 0.04$) (Figure 5B). Similar results were observed for blue light in combination with these photosensitizing compounds on biofilm formation of two different *C. albicans* clinical isolates (see Figure S4A-B for results of the developmental inhibition biofilm assay on additional *C. albicans* strains).

Finally, we assessed the effects of blue light in combination with the three photosensitizing compounds on mature *C. albicans* biofilms in the disruption biofilm assay. We found that, compared to the untreated control, and each photosensitizing compound alone, blue light was effective at disrupting mature biofilms by ~75% when combined with new methylene blue ($p = 0.0001$), ~70% when combined with toluidine blue O ($p = 0.0009$), and ~60% when combined with rose bengal ($p = 0.0009$) (Figure 5C). Compared to the biofilm disruption effects of blue light alone, the combination of blue light with the photosensitizing compounds in the disruption biofilm assay had an additive biofilm disruption effect of an additional 14% for new methylene blue ($p = 0.01$) and 12% for toluidine blue O ($p = 0.03$) (Figure 5C). Compared to the biofilm disruption effect of blue light alone, no additive biofilm disruption effects were observed when blue light was combined with rose bengal (Figure 5C). Similar results were observed for blue light in combination with these photosensitizing compounds on biofilm formation of two different *C. albicans* clinical isolates, with the exception that for one of the clinical isolates (AR0761), an additive effect was also observed when blue light was combined with rose bengal in the disruption biofilm assay (see Figure S4C-D for results of the disruption biofilm assay on additional *C. albicans* strains).

As an independent assay for cell viability, we also performed LIVE/DEAD staining under the same conditions that we performed CFU determinations. We performed the

LIVE/DEAD staining assay both on cells resuspended from biofilms and directly on biofilms under the different light and photosensitizing compound treatment conditions. Our cell viability staining results were consistent with our CFU determinations for all treatment conditions (see Figures S5-S8 for representative images from the LIVE/DEAD staining assay performed on cells resuspended from biofilms and Figures S9-S12 for representative images from the LIVE/DEAD staining assay preformed directly on biofilms). Lastly, we note that there were no qualitative differences in cellular morphologies (i.e., in the presence of hyphae, pseudohyphae, and yeast-form cells) between the untreated biofilms and biofilms treated with each of the three lights with or without the photosensitizing compounds (see Figure S13 for representative cellular morphology images for the treatment conditions with the largest antibiofilm effects for each light).

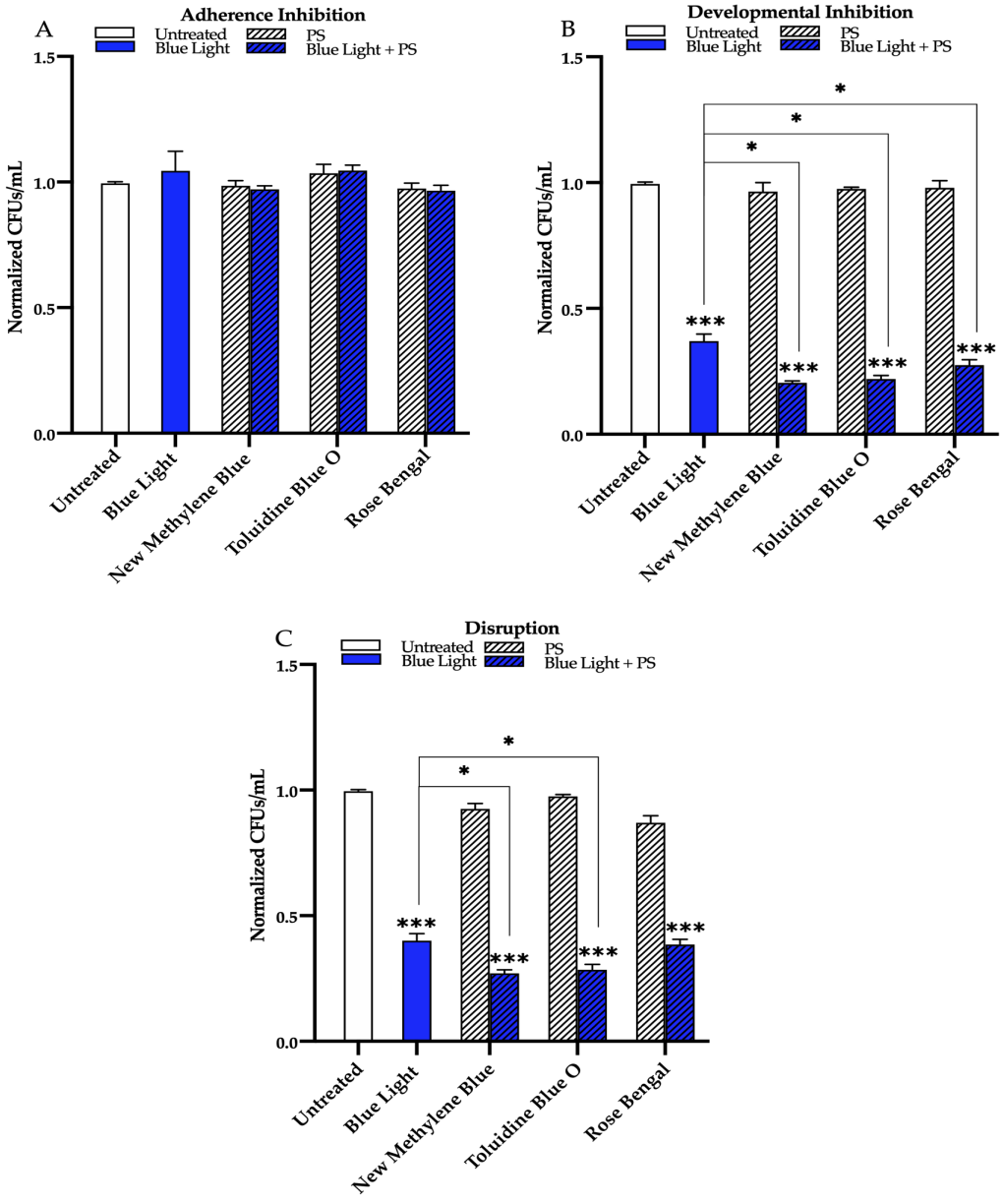

Figure 3.5. Effects of blue visible light in combination with the photosensitizing compounds new methylene blue, toluidine blue O, and rose bengal on *C. albicans* biofilms. Effects of blue light in combination with the photosensitizing compounds in the (A) adherence inhibition, (B) developmental inhibition, and (C) disruption biofilm assays. Untreated control (Untreated), blue light alone (Blue Light), photosensitizing compound alone (PS), and blue light in combination with the photosensitizing compound (Blue Light + PS) are shown. Colony forming units per 1mL (CFUs/mL) were measured to determine viable cell counts from the biofilms at the end of each biofilm assay. Standard deviations are shown for each sample (n=3). The average CFUs/mL of the untreated control samples for each assay were normalized to 1. Significance comparisons are relative to the untreated control unless otherwise noted with significance bars and were determined using student's unpaired two-tailed t-tests assuming unequal variance for $p \leq 0.05$ (*), and $p \leq 0.001$ (***).

3.5 Discussion

Photodynamic therapy has been used to treat skin conditions for decades; however, its potential use as an antimicrobial strategy is only beginning to be recognized. Photodynamic therapy is thought to rely on the localized production of ROS that can have cytotoxic effects on the targeted cells. To comprehensively assess the potential utility of photodynamic therapy against *C. albicans* biofilms, we examined and compared the effects of red, green, and blue visible lights alone and in combination with the classic and commonly used photosensitizing compounds new methylene blue, toluidine blue O, and rose bengal. We note that the light intensities for each light we used in this study were similar, with red light at 6500 lux, green light at 6700 lux, and blue light at 5900 lux. Thus, the marginal differences in light intensities between the three lights did not seem to affect the results, especially given that blue light had the lowest light intensity but was the most effective against *C. albicans* biofilms. In fact, blue light alone was the only visible light tested that had antibiofilm properties on its own, where it markedly prevented biofilm formation when it was applied for 24 h throughout biofilm development, as well as markedly disrupted mature biofilms when it was applied for 24 h on a mature biofilm. Interestingly, when blue light alone was applied for just 90 min during the initial adherence stage of biofilm formation, it had no effects on inhibiting biofilm formation, indicating that prolonged exposure to blue light (i.e., longer than 90 min) is necessary for its antibiofilm potential. The combination of the photosensitizing compounds with red and green lights had moderate effects on preventing biofilm formation but had no effects on the initial 90-min adherence stage of biofilm formation or at disrupting mature biofilms. The fact that none of the light and photosensitizing compound combination treatments were effective at inhibiting biofilm formation during the 90-min adherence stage of biofilm formation was surprising. These findings indicate that exposure time to the light and photosensitizing compound treatments is an important factor in the antibiofilm efficacy of photodynamic therapy that may be related to the levels of ROS produced during the treatments. One hypothesis that could be tested in future studies is whether there is a direct relationship between light exposure time and ROS production.

Our findings indicate that the photosensitizing compounds were successful at sensitizing the biofilms to red and green lights when applied throughout biofilm

development (i.e., for 24 h). The combination of the photosensitizing compounds with blue light had the most striking antibiofilm properties, where significant additive antibiofilm effects were observed in preventing biofilm formation and disrupting mature biofilms, significantly above those of blue light alone. Generally, these additive effects were especially noticeable when blue light was combined with new methylene blue and toluidine blue O, the two phenothiazinium salt photosensitizing compounds assessed. Overall, these findings indicate that photosensitizing compounds are effective at sensitizing the biofilm cells to light exposure, likely enhancing the production of ROS, and increasing cytotoxicity of the biofilm cells, with blue light plus new methylene blue, followed closely by blue light plus toluidine blue O, as the most effective treatment combinations against *C. albicans* biofilms.

Although the mechanism of action of blue light on microorganisms is not fully understood, a common hypothesis in the field is that exposure to blue light induces photoexcitation of naturally occurring endogenous photosensitizing compounds inside the microbial cells, such as flavoproteins and porphyrins, ultimately leading to ROS production and microbial cell death [40,44,45,67,68]. Indeed, one study has shown a clear correlation between porphyrin levels and microbial cell cytotoxicity upon exposure to blue light [69]. Consistent with this hypothesis, our work demonstrates that blue light alone induces *C. albicans* cell death within a biofilm, and that this effect is enhanced by the addition of photosensitizing compounds that lead to a further increase in the production of ROS.

In the context of biofilm infections, there are a number of drawbacks of traditional antifungal drug therapies that are overcome by the use of photodynamic antimicrobial therapies. First, the development of antifungal drug resistance after exposure to antifungal drugs can render traditional antifungal drug treatments virtually ineffective against biofilm infections. Given that photodynamic therapy generates ROS that affect multiple non-specific microbial targets simultaneously (e.g., causing lipid peroxidation, nucleic acid oxidation, and protein oxidation), it is unlikely that antimicrobial resistance to photodynamic therapy could be developed, and antimicrobial resistance to photodynamic therapy has not been reported to date [70–72]. Second, antifungal drugs, especially the polyenes (e.g., amphotericin B), have significant toxicities to human cells and are typically administered systemwide (e.g., intravenously) [11]. Photodynamic therapy utilizes non-toxic photosensitizing compounds combined with visible lights that pose little toxicity concerns to humans [23,25]. In addition, photodynamic therapy can be spatially confined to the infection area, thus limiting exposure of human cells to the treatment, and eliminating the toxicities associated with antifungal drugs administered systemwide. Third, antifungal drugs fail to penetrate into the lower levels of mature biofilms due to high microbial cell densities and the presence of the extracellular matrix, which has been shown to sequester antifungal drugs [73–75]. When photodynamic therapy is applied directly to the biofilm and ROS are produced, the small sizes of the ROS molecules should allow them to be easily transported into the lower levels of the biofilm via simple and/or facilitated diffusion, and ROS should be less likely to be sequestered by the extracellular matrix [12,76]. We note, however, that the physiological effects of photodynamic therapy on the extracellular matrix of biofilms has not been directly studied to date and is an area of interest for future studies in the field. Fourth, in order to effectively treat a biofilm infection, understanding the microbial composition of the biofilm is important in administering effective

antimicrobial drug treatments. The majority of biofilm infections are not caused by a single microbial species, but are rather polymicrobial in nature, even containing microbial species that span different phylogenetic kingdoms, such as bacteria and fungi [4,77,78]. Studies have shown that polymicrobial biofilms are often much more resistant to antimicrobial drugs than single species biofilms and are thus extremely challenging to treat [79]. Photodynamic therapy bypasses the need to know what microbial species are present in a polymicrobial biofilm infection because it has broad-spectrum antimicrobial efficacy, and has been shown to be effective against bacteria and fungi, even within polymicrobial biofilms [34,40,80–85]. Lastly, the mechanisms of action of almost all existing antimicrobial drugs (e.g. antibiotics and antifungals) target microbial metabolic processes, and thus require that the microbial cells are metabolically active in order to be effective [86–90]. This requirement poses significant inconsistencies in antimicrobial drug effectiveness in biofilms, where heterogeneous cell populations are located throughout the biofilm architecture with different levels of metabolic activity [74,91,92]. In addition, metabolically dormant phenotypic microbial cell variants within mature biofilms, called persister cells, are particularly difficult to eradicate with traditional antimicrobial drugs [74,88,93–95]. Photodynamic therapy, which uses ROS to kill microbial cells, does not require that the microbial cells are metabolically active, and there is some evidence to suggest that photodynamic therapy is effective against bacterial persister cells [25,96].

Given that there are only three major classes of antifungal drugs that are currently used to treat invasive fungal infections in humans, and that it has been a challenge to develop new and effective antifungal drugs, especially with efficacy against biofilms, there is a significant unmet medical need for new antifungal therapeutic strategies. Our work adds to the existing body of literature demonstrating that photodynamic therapy has the potential to be a clinically useful non-drug therapeutic strategy that is highly effective against *C. albicans* biofilms that could dramatically change the way we treat infectious diseases. Based on the present study as well as others in the field, photodynamic therapy shows excellent potential as a treatment approach for biofilm and other chronic infections. To date, most discussed clinical applications of photodynamic therapy for the treatment of infections are largely in the dermatology field, where photodynamic therapy could be applied to local infections on the skin using topical photosensitizing compounds and localized light exposure [97]. However, there are many other applications for photodynamic therapy that also show potential, such as its use in dentistry to treat persistent endodontic infections, such as periodontitis, peri-implantitis, and lesions from caries [98–100]. Despite its clear potential, the clinical use of photodynamic therapy to treat infections is still in its early stages and has not advanced as rapidly as other antimicrobial therapies. This is largely due to certain major limitations of its use, such as the fact that it needs to be applied locally and to areas of the body that can be accessed by light; thus its use against systemic infections is less likely to be feasible [97]. Another major limitation is that photodynamic therapy has not yet been standardized with clear and well-defined clinical parameters for the treatment of patients with infections. For example, we do not yet have defined effective dosages of photosensitizing compounds and we do not yet have standardized defined parameters for the duration of light exposure to be used in the treatment of specific types of infections [97]. Nonetheless, we believe that photodynamic therapy has great potential for clinical use in the treatment of localized infections, and its

limitations in regard to standardizations should be overcome in the future with the development of defined clinical protocols.

3.6 Supplementary Materials

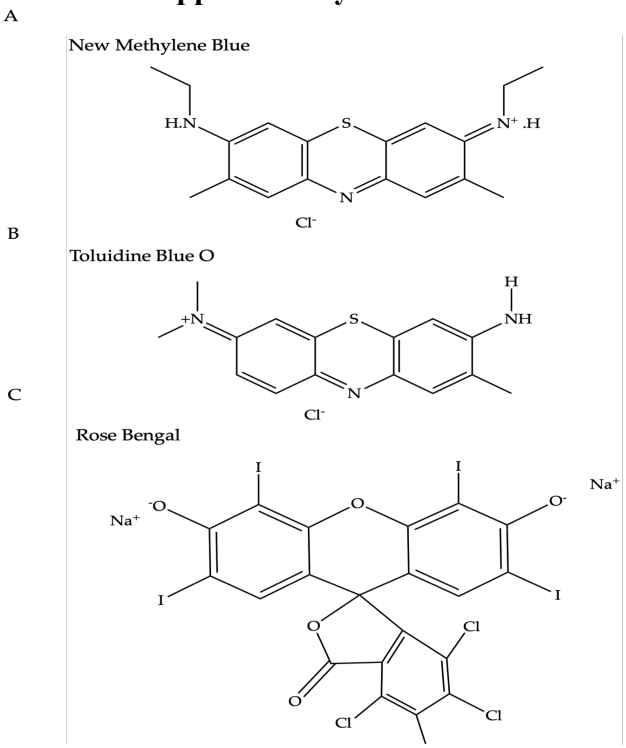

Figure S3.1. Chemical structures of the photosensitizing compounds used in these studies. (A) New methylene blue, (B) toluidine blue O, and (C) rose bengal are shown.

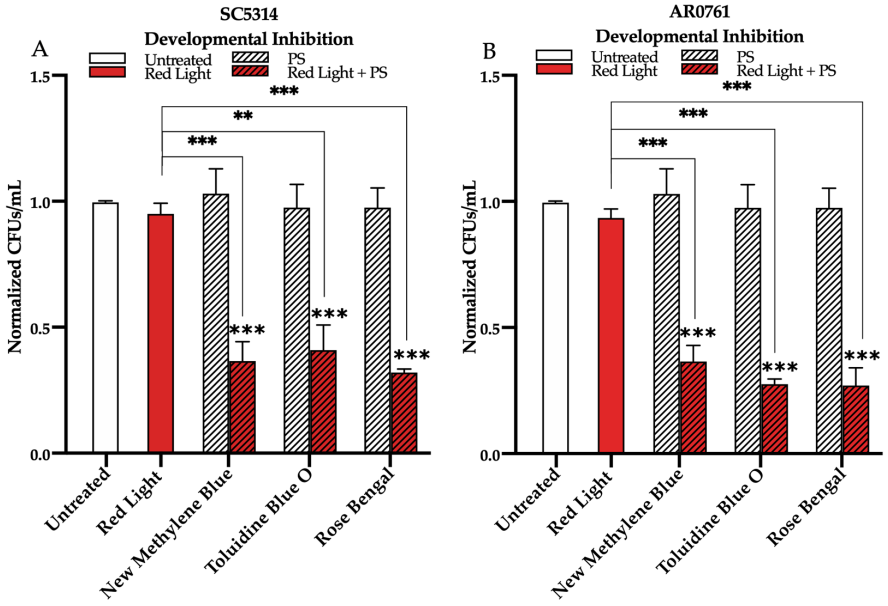

Figure S3.2. Effects of red visible light in combination with the photosensitizing compounds new methylene blue, toluidine blue O, and rose bengal on biofilms formed by additional *C. albicans* strains. Effects of red light in combination with the photosensitizing compounds on the clinical isolates (A) SC5314 and (B) AR0761 in the developmental inhibition biofilm assay. Untreated control (Untreated), red light alone (Red Light), photosensitizing compound alone (PS), and red light in combination with the photosensitizing compound (Red Light + PS) are shown. Colony forming units per 1mL (CFUs/mL) were measured to determine viable cell counts from the biofilms at the end of each biofilm assay. Standard deviations are shown for each sample (n=3). The average CFUs/mL of the untreated control for each assay were normalized to 1. Significance comparisons are relative to an untreated control unless otherwise noted with significance bars and were determined using student's unpaired two-tailed t-tests assuming unequal variance for $p \leq 0.01$ (**), and $p \leq 0.001$ (***).

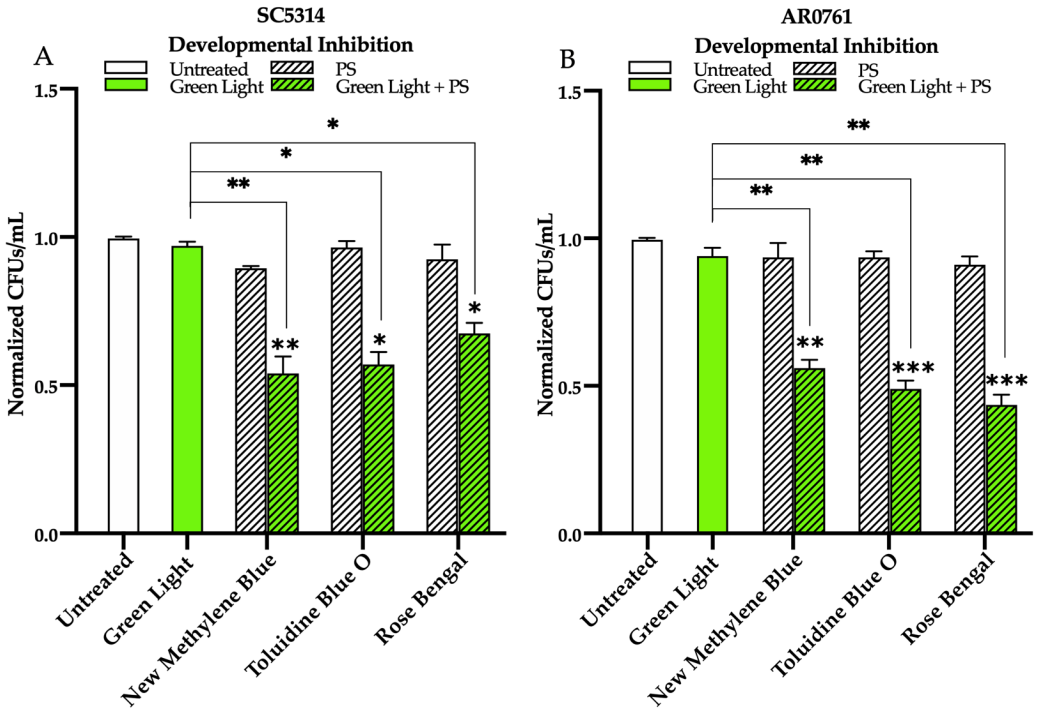

Figure S3.3. Effects of green visible light in combination with the photosensitizing compounds new methylene blue, toluidine blue O, and rose bengal on biofilms formed by additional *C. albicans* strains. Effects of green light in combination with the photosensitizing compounds on the clinical isolates (A) SC5314 and (B) AR0761. Untreated control (Untreated), green light alone (Green Light), photosensitizing compound alone (PS), and green light in combination with the photosensitizing compound (Green Light + PS) are shown. Colony forming units per 1mL (CFUs/mL) were measured to determine viable cell counts from the biofilms at the end of each biofilm assay. Standard deviations are shown for each sample (n=3). The average CFUs/mL of the untreated control for each assay were normalized to 1. Significance comparisons are relative to an untreated

control unless otherwise noted with significance bars and were determined using student's unpaired two-tailed t-tests assuming unequal variance for $p \leq 0.05$ (*), $p \leq 0.01$ (**), and $p \leq 0.001$ (***).

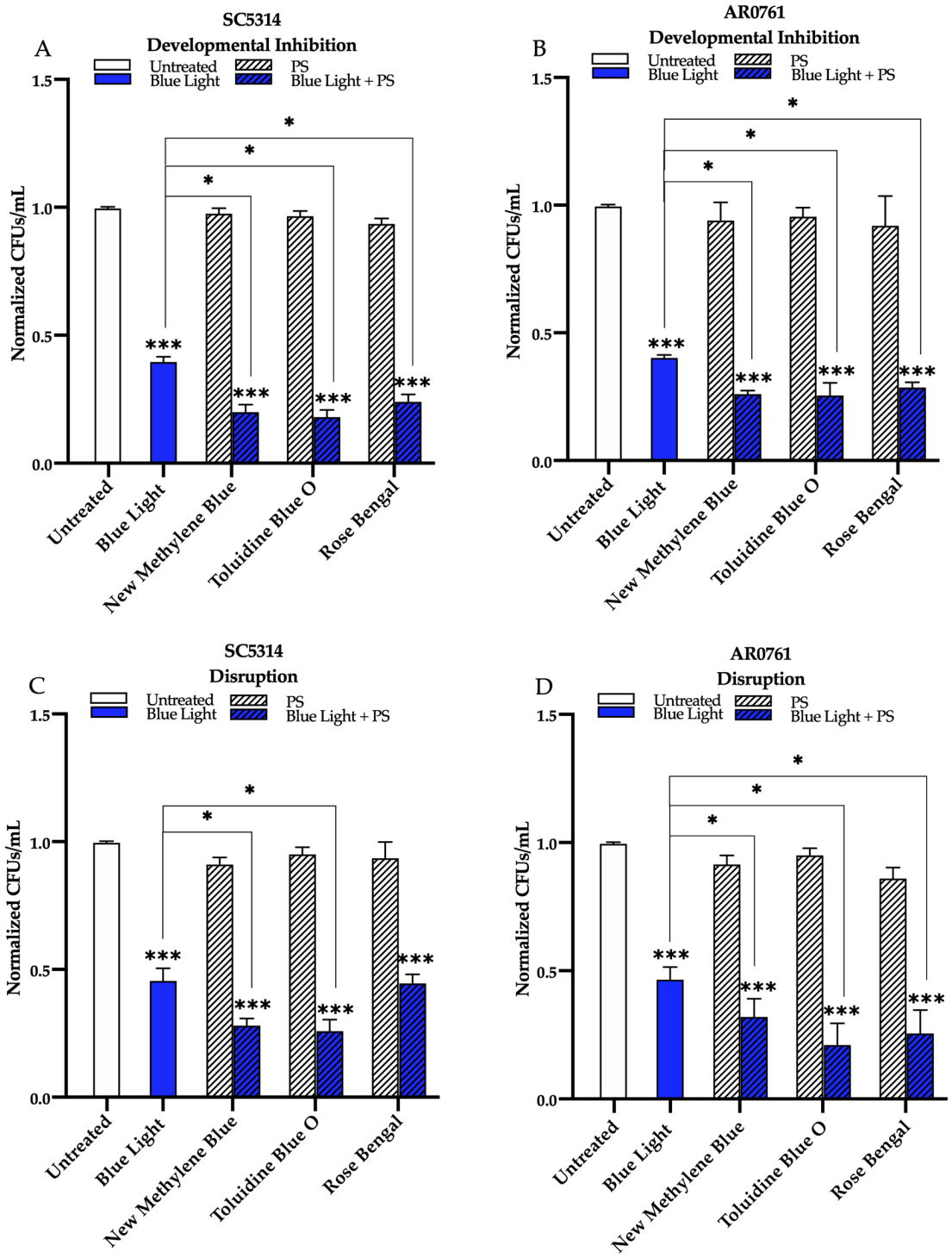

Figure S3.4. Effects of blue visible light in combination with the photosensitizing compounds new methylene blue, toluidine blue O, and rose bengal on biofilms formed by additional *C. albicans* strains. Effects of blue light in combination with the photosensitizing compounds on the clinical isolates (A) SC5314 and (B) AR0761 in the developmental inhibition biofilm assay. Effects of blue light in combination with the photosensitizing compounds on the clinical isolates (C) SC5314 and (D) AR0761 in the disruption biofilm assay. Untreated control (Untreated), blue light alone (Blue Light), photosensitizing compound alone (PS), and blue light in combination with the photosensitizing compound (Blue Light + PS) are shown. Colony forming units per 1mL (CFUs/mL) were measured to determine viable cell counts from the biofilms at the end of each biofilm assay. Standard deviations are shown for each sample (n=3). The average CFUs/mL of the untreated control for each assay were normalized to 1. Significance comparisons are relative to an untreated control unless otherwise noted with significance bars and were determined using student's unpaired two-tailed t-tests assuming unequal variance for $p \leq 0.05$ (*), and $p \leq 0.001$ (***).

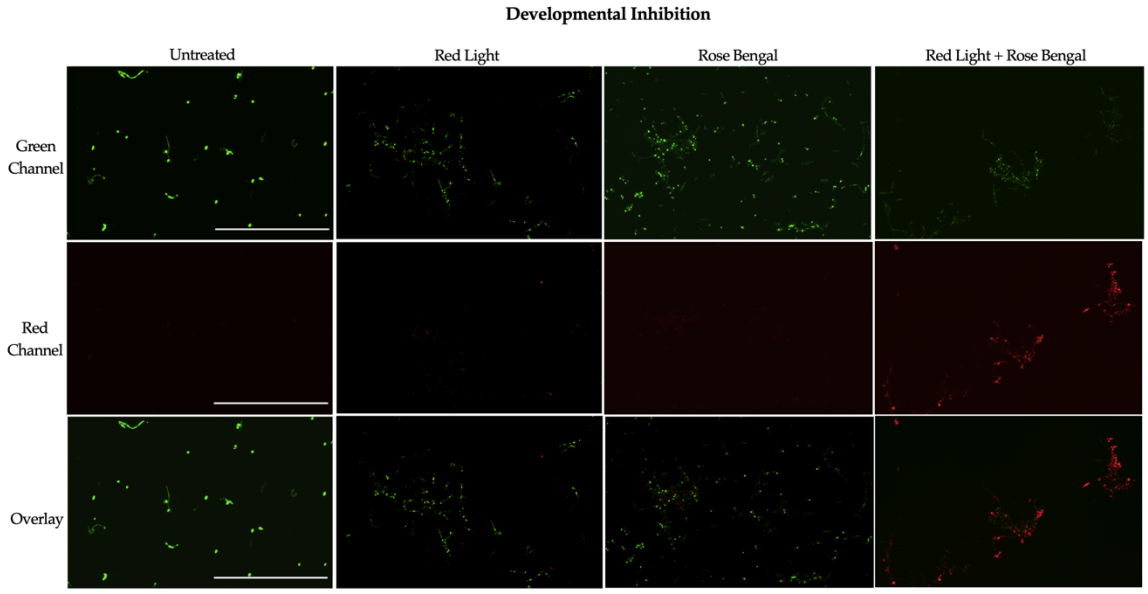

Figure S3.5. Effects of red visible light in combination with the photosensitizing compound rose bengal on cell viability of cells resuspended from biofilms in the developmental inhibition biofilm assay. The viability of cells resuspended from biofilms was assessed using the LIVE/DEAD *Bac*Light viability kit, where green fluorescence indicates live cells and red fluorescence indicates dead cells. The samples were imaged by fluorescence microscopy at 20X magnification with a green laser (GFP/green channel) shown in the top panel, a red laser (Texas Red/red channel) shown in the middle panel, and overlayed shown in the bottom panel. Representative images are shown for the untreated control (Untreated), red light alone (Red Light), rose bengal photosensitizing compound alone (Rose Bengal), and red light in combination with rose bengal photosensitizing compound (Red Light + Rose Bengal). Scale bars represent 200 μm.

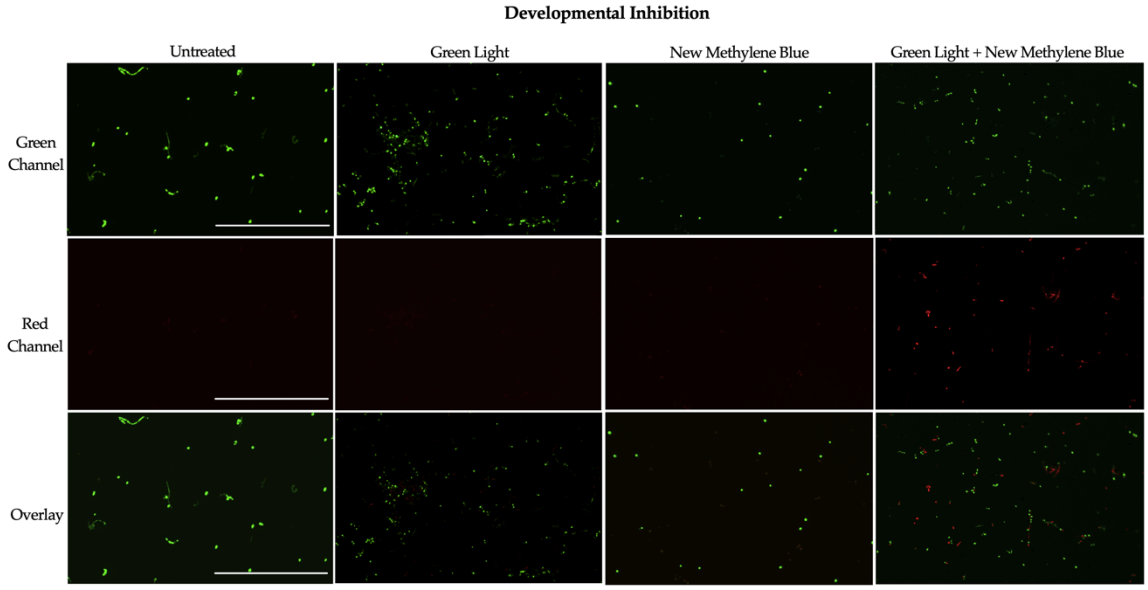

Figure S3.6. Effects of green visible light in combination with the photosensitizing compound new methylene blue on cell viability of cells resuspended from biofilms in the developmental inhibition biofilm assay. The viability of cells resuspended from biofilms was assessed using the LIVE/DEAD *Bac*Light viability kit, where green fluorescence indicates live cells and red fluorescence indicates dead cells. The samples were imaged by fluorescence microscopy at 20X magnification with a green laser (GFP/green channel) shown in the top panel, a red laser (Texas Red/red channel) shown in the middle panel, and overlayed shown in the bottom panel. Representative images are shown for the untreated control (Untreated), green light alone (Green Light), new methylene blue photosensitizing compound alone (New Methylene Blue), and green light in combination with new methylene blue photosensitizing compound (Green Light + New Methylene Blue). Scale bars represent 200 µm.

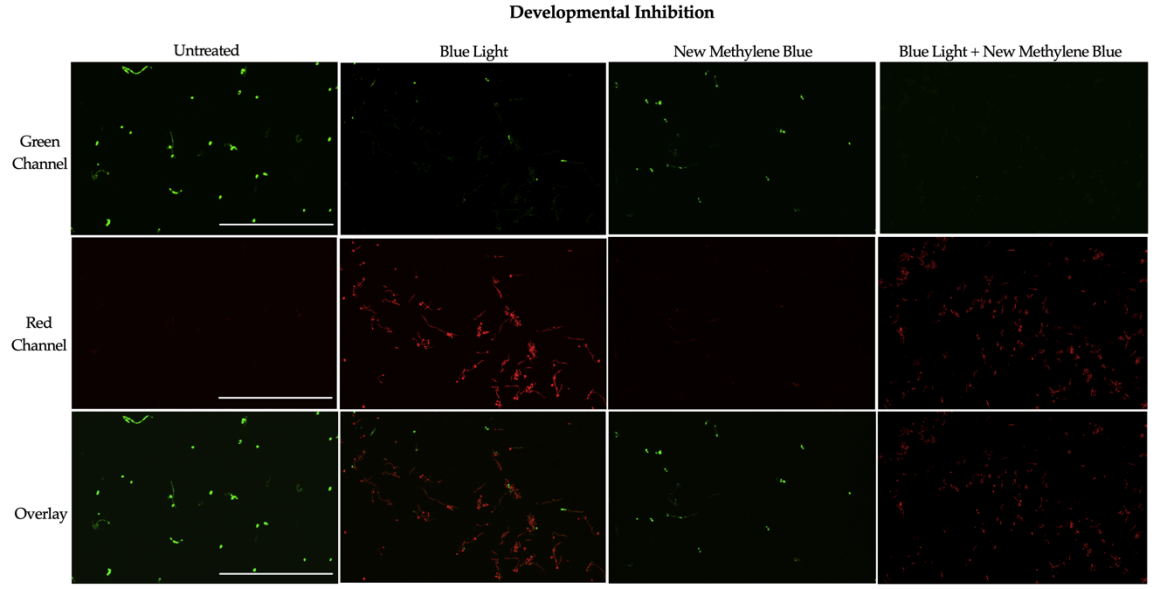

Figure S3.7. Effects of blue visible light in combination with the photosensitizing compound new methylene blue on cell viability of cells resuspended from biofilms in the developmental inhibition biofilm assay. The viability of cells resuspended from biofilms was assessed using the LIVE/DEAD *Bac*Light viability kit, where green fluorescence indicates live cells and red fluorescence indicates dead cells. The samples were imaged by fluorescence microscopy at 20X magnification with a green laser (GFP/green channel) shown in the top panel, a red laser (Texas Red/red channel) shown in the middle panel, and overlayed shown in the bottom panel. Representative images are shown for the untreated control (Untreated), blue light alone (Blue Light), new methylene blue photosensitizing compound alone (New Methylene Blue), and blue light in combination with new methylene blue photosensitizing compound (Blue Light + New Methylene Blue). Scale bars represent 200 μm.

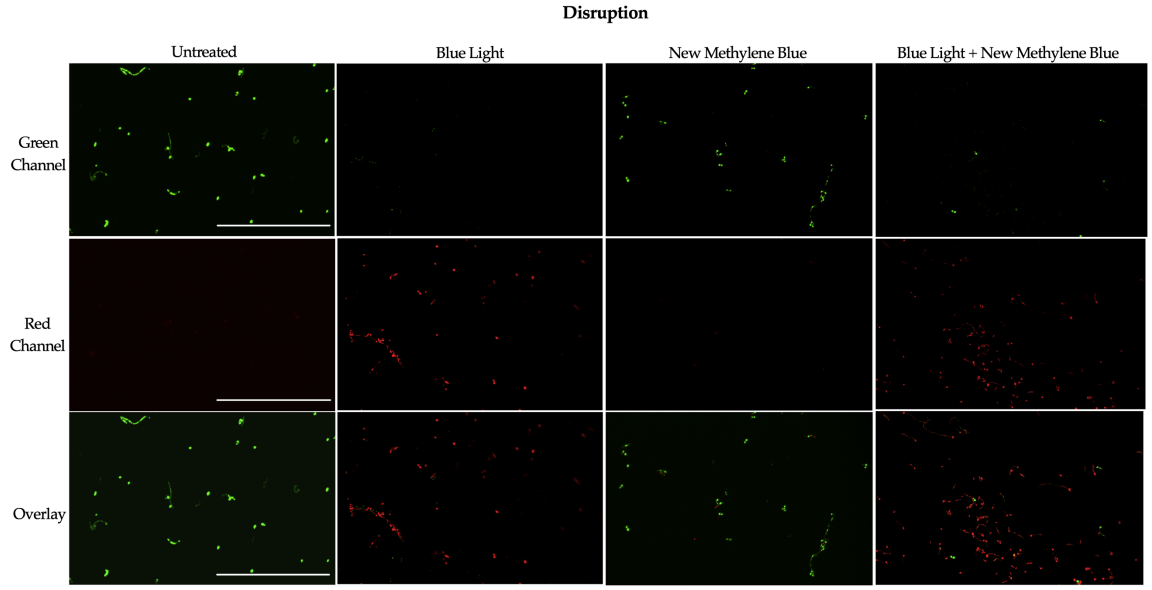

Figure S3.8. Effects of blue visible light in combination with the photosensitizing compound new methylene blue on cell viability of cells resuspended from biofilms in the disruption biofilm assay. The viability of cells resuspended from biofilms was assessed using the LIVE/DEAD *Bac*Light viability kit, where green fluorescence indicates live cells and red fluorescence indicates dead cells. The samples were imaged by fluorescence microscopy at 20X magnification with a green laser (GFP/green channel) shown in the top panel, a red laser (Texas Red/red channel) shown in the middle panel, and overlayed shown in the bottom panel. Representative images are shown for the untreated control (Untreated), blue light alone (Blue Light), new methylene blue photosensitizing compound alone (New Methylene Blue), and blue light in combination with new methylene blue photosensitizing compound (Blue Light + New Methylene Blue). Scale bars represent 200 μm.

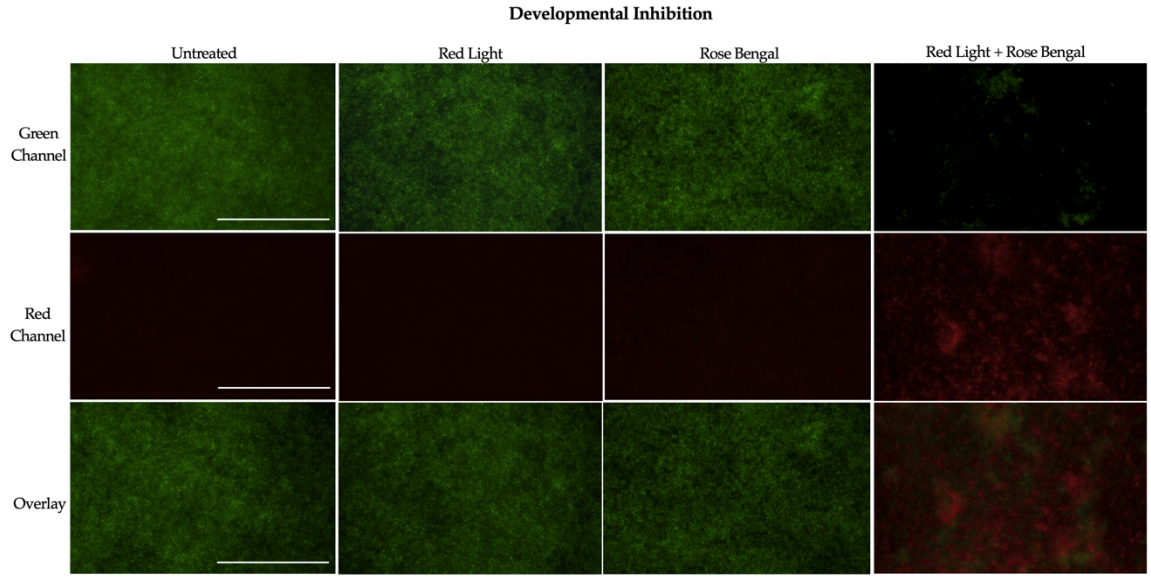

Figure S3.9. Effects of red visible light in combination with the photosensitizing compound rose bengal on cell viability of biofilms in the developmental inhibition biofilm assay. The viability of biofilms was assessed using the LIVE/DEAD *Bac*Light viability kit, where green fluorescence indicates live cells and red fluorescence indicates dead cells. The samples were imaged by fluorescence microscopy at 20X magnification with a green laser (GFP/green channel) shown in the top panel, a red laser (Texas Red/red channel) shown in the middle panel, and overlayed shown in the bottom panel. Representative images are shown for the untreated control (Untreated), red light alone (Red Light), rose bengal photosensitizing compound alone (Rose Bengal), and red light in combination with rose bengal photosensitizing compound (Red Light + Rose Bengal). Scale bars represent 200 μm.

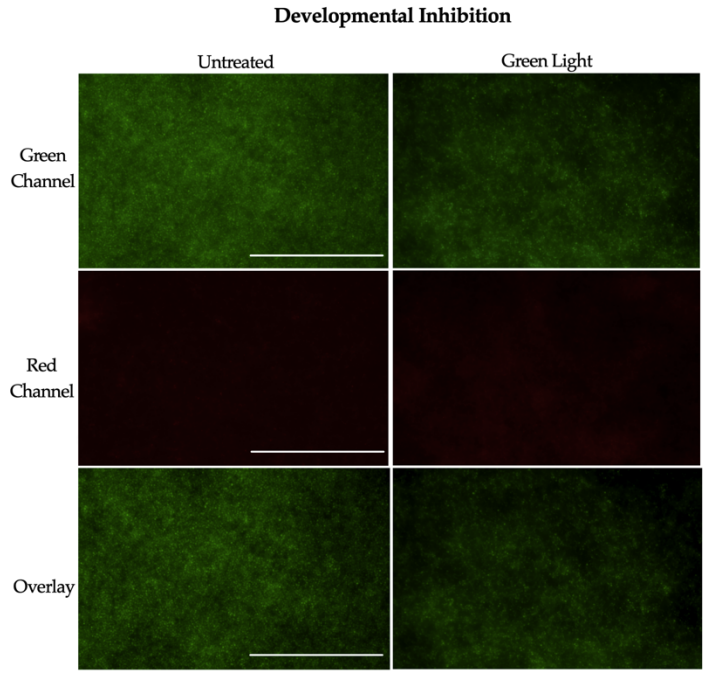

Figure S3.10. Effects of green visible light on cell viability of biofilms in the developmental inhibition biofilm assay. The viability of biofilms was assessed using the LIVE/DEAD *Bac*Light viability kit, where green fluorescence indicates live cells and red fluorescence indicates dead cells. The samples were imaged by fluorescence microscopy at 20X magnification with a green laser (GFP/green channel) shown in the top

panel, a red laser (Texas Red/red channel) shown in the middle panel, and overlayed shown in the bottom panel. Representative images are shown for the untreated control (Untreated), and green light alone (Green Light). Scale bars represent 200 μm.

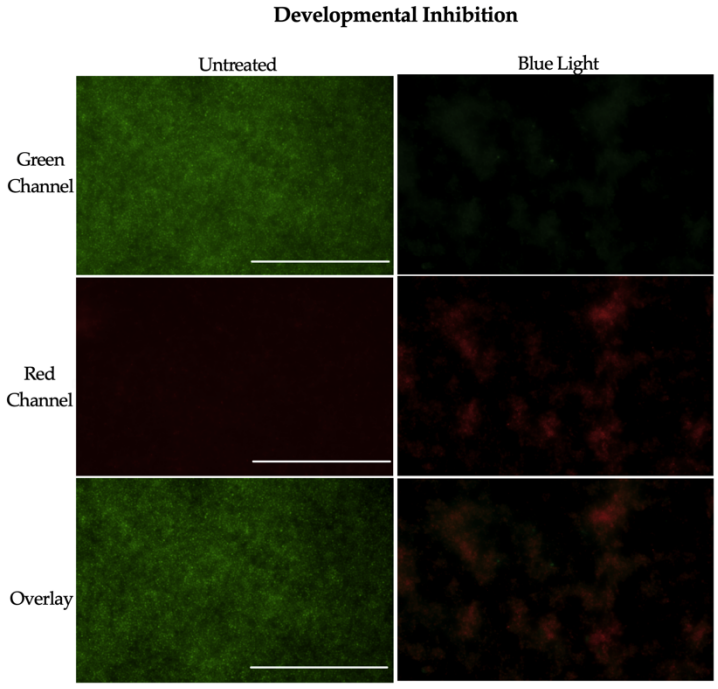

Figure S3.11. Effects of blue visible light on cell viability of biofilms in the developmental inhibition biofilm assay. The viability of biofilms was assessed using the LIVE/DEAD *Bac*Light viability kit, where green fluorescence indicates live cells and red fluorescence indicates dead cells. The samples were imaged by fluorescence microscopy at 20X magnification with a green laser (GFP/green channel) shown in the top panel, a red laser (Texas Red/red channel) shown in the middle panel, and overlayed shown in the bottom panel. Representative images are shown for the untreated control (Untreated), and blue light alone (Blue Light). Scale bars represent 200 μm.

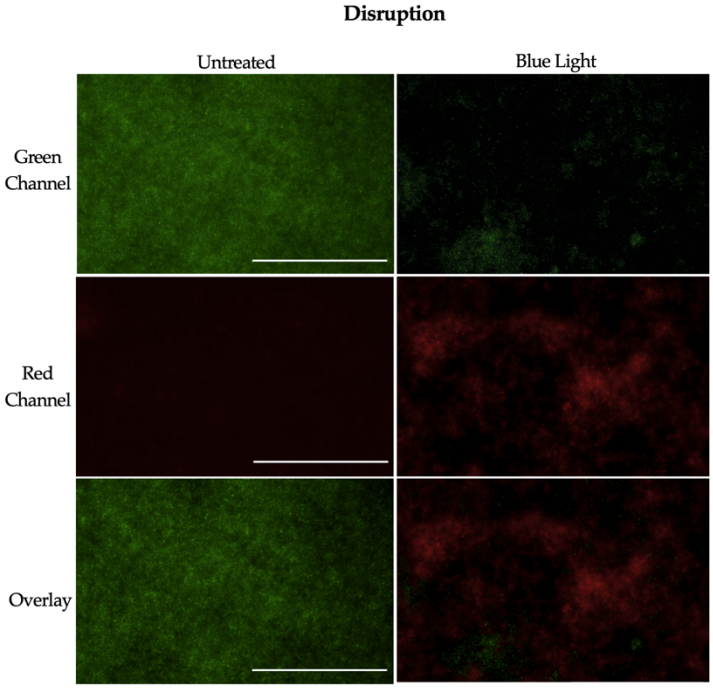

Figure S3.12. Effects of blue visible light on cell viability of biofilms in the disruption biofilm assay. The viability of biofilms was assessed using the LIVE/DEAD *Bac*Light viability kit, where green fluorescence indicates live cells and red fluorescence indicates dead cells. The samples were imaged by fluorescence microscopy at 20X magnification with a green laser (GFP/green channel) shown in the top panel, a red laser (Texas Red/red channel) shown in the middle panel, and overlayed shown in the

bottom panel. Representative images are shown for the untreated control (Untreated), and blue light alone (Blue Light). Scale bars represent 200 μm.

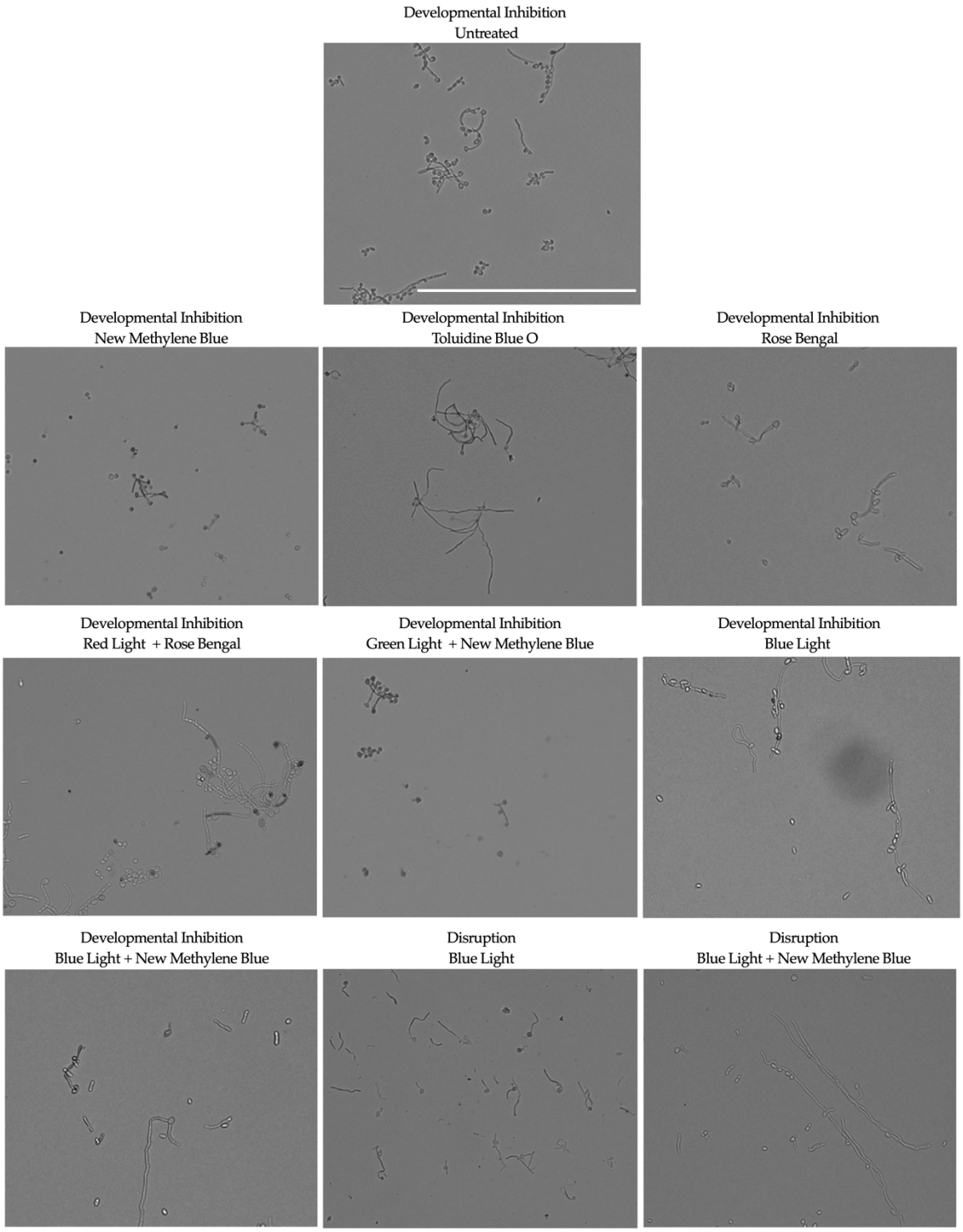

Figure S3.13. Assessment of cellular morphology of biofilm cells. Cells resuspended from biofilms were imaged by brightfield microscopy at 20X magnification. Biofilm cell

morphologies consisting of hyphae, pseudohyphae and yeast-form cells were observed. Representative images are shown for the untreated control in the developmental inhibition biofilm assay (Developmental Inhibition Untreated), new methylene blue photosensitizing compound alone in the developmental inhibition biofilm assay (Developmental Inhibition New Methylene Blue), toluidine blue O photosensitizing compound alone in the developmental inhibition biofilm assay (Developmental Inhibition Toluidine Blue O), rose bengal photosensitizing compound alone in the developmental inhibition biofilm assay (Developmental Inhibition Rose Bengal), red light in combination with rose bengal photosensitizing compound in the developmental inhibition biofilm assay (Developmental Inhibition Red Light + Rose Bengal), green light in combination with new methylene blue photosensitizing compound in the developmental inhibition biofilm assay (Developmental Inhibition Green Light + New Methylene Blue), blue light in the developmental inhibition biofilm assay (Developmental Inhibition Blue Light), blue light in combination with new methylene blue photosensitizing compound in the developmental inhibition biofilm assay (Developmental Inhibition Blue Light + New Methylene Blue), blue light in the disruption biofilm assay (Disruption Blue Light), and blue light in combination with new methylene blue photosensitizing compound in the disruption biofilm assay (Disruption Blue Light + New Methylene Blue). Scale bar represents 200 μm.

3.7 References

1. Brown, G.D.; Denning, D.W.; Gow, N.A.; Levitz, S.M.; Netea, M.G.; White, T.C. Hidden killers: Human fungal infections. *Sci. Transl. Med.* **2012**, *4*(165), 165rv13-165rv13.
2. Romo, J.A.; Kumamoto, C.A. On commensalism of *Candida*. *J. Fungi (Basel)* **2020**, *6*(1), 16.
3. Nobile, C.J.; Johnson, A.D. *Candida albicans* biofilms and human disease. *Annu. Rev. Microbiol.* **2015**, *69*, 71–92.
4. Gulati, M.; Nobile, C.J. *Candida albicans* biofilms: development, regulation, and molecular mechanisms. *Microbes Infect.* **2016**, *18*(5), 310–321.
5. Mayer, F.L.; Wilson, D.; Hube, B. *Candida albicans* pathogenicity mechanisms. *Virulence* **2013**, *4*(2), 119–128.
6. Kolter, R.; Greenberg, E.P. Microbial sciences:The superficial life of microbes. *Nature* **2006**, *441*(7091), 300–302.
7. LóPez, D.; Vlamakis, H.; Kolter, R. Biofilms. *Cold Spring Harb. Perspect. Biol.* **2010**, *2*(7):a000398.
8. Uppuluri, P.; Chaturvedi, A.K.; Srinivasan, A.; Banerjee, M.; Ramasubramaniam, A.K.; Köhler, J.R.; Kadosh, D.; Lopez-Ribot, J.L. Dispersion as an important step in the *Candida albicans* biofilm developmental cycle. *PLoS Pathog.* **2010**, *6*(3):e1000828.
9. Francolini, I.; Donelli, G. Prevention and control of biofilm-based medical-device-related infections. *FEMS Immunol. Med. Microbiol.* **2010**, *59*, 227–238.
10. Odds, F.C.; Brown, A.J.; Gow, N.A. Antifungal agents: Mechanisms of action. *Trends Microbiol.* **2003**, *11*, 272–279.
11. Roemer, T.; Krysan, D.J. Antifungal drug development: Challenges, unmet clinical

needs, and new approaches. *Cold Spring Harb. Perspect. Med.* **2014**, *4*, 1–15.
12. Prasad, R.; Shah, A.H.; Rawal, M.K. Mechanism of action and drug resistance. *Adv in Exp Med and Biol*; **2016**, *892*, 327-349.
13. Nobile, C.J.; Ennis, C.L.; Hartooni, N.; Johnson, A.D.; Lohse, M.B. A selective serotonin reuptake inhibitor, a proton pump inhibitor, and two calcium channel blockers inhibit *Candida albicans* biofilms. *Microorganisms* **2020**, *8*(5): 756.
14. Lohse, M.B.; Gulati, M.; Craik, C.S.; Johnson, A.D.; Nobile, C.J. Combination of antifungal drugs and protease inhibitors prevent *Candida albicans* biofilm formation and disrupt mature biofilms. *Front. Microbiol.* **2020**, *11*:1027.
15. Williams, D.W.; Kuriyama, T.; Silva, S.; Malic, S.; Lewis, M.A. *Candida* biofilms and oral candidosis: Treatment and prevention. *Periodontol. 2000* **2011**, *55*(1), 250–265.
16. Benitez, L.L.; Carver, P.L. Adverse effects associated with long-term administration of azole antifungal agents. *Drugs* **2019**, *79*, 833–853.
17. Dixon, D.M.; Walsh, T.J. Antifungal Agents. In: *Medical Microbiology*; 4th ed.; Editor Baron S.; Galveston (TX): University of Texas Medical Branch at Galveston, USA; **1996**; Chapter 76.
18. Liu, X.; Wang, D.; Yu, C.; Li, T.; Liu, J.; Sun, S. Potential antifungal targets against a *Candida* biofilm based on an enzyme in the arachidonic acid cascade-a review. *Front. Microbiol.* **2016**, *7*, 1–9.
19. Sardi, J.C.O.; Scorzoni, L.; Bernardi, T.; Fusco-Almeida, A.M.; Mendes Giannini, M.J.S. *Candida* species: current epidemiology, pathogenicity, biofilm formation, natural antifungal products and new therapeutic options. *J. Med. Microbiol.* **2013**, *62*, 10–24.
20. Cohen, D.K.; Lee, P.K. Photodynamic Therapy for Non-Melanoma Skin Cancers. *Cancers (Basel).* **2016**, *8*(10): 90.
21. Agostinis, P.; Berg, K.; Cengel, K.A.; Foster, T.H.; Girotti, A.W.; Gollnick, S.O.; Hahn, S.M.; Hamblin, M.R.; Juzeniene, A.; Kessel, D.; Korbelik, M; Moan, J; Mroz, P; Nowis, D; Piette, J; Wilson, BC; Golab, J. Photodynamic therapy of cancer: An update. *CA Cancer J. Clin.* **2011**, *61*, 250–281.
22. Kim, M.; Jung, Y.; Park, H.J. Topical PDT in the treatment of benign skin diseases: Principles and new applications. *Int. J. Mol. Sci.* **2015**, *16*(10), 23259–23278.
23. Wainwright, M.; Maisch, T.; Nonell, S.; Plaetzer, K.; Almeida, A.; Tegos, G.P.; Hamblin, M.R. Photoantimicrobials—are we afraid of the light? *Lancet Infect. Dis.* **2017**, *17*(2), e49–e55.
24. Cieplik, F.; Deng, D.; Crielaard, W.; Buchalla, W.; Hellwig, E.; Al-Ahmad, A.; Maisch, T. Antimicrobial photodynamic therapy – what we know and what we don't. *Crit. Rev. Microbiol.* **2018**, *44*(5), 571–589.
25. Hamblin, M.R.; Hasan, T. Photodynamic therapy: A new antimicrobial approach to infectious disease? *Photochem. Photobio.l Sci.* **2004**, *3*(5), 436–450.
26. Wainwright, M.; Phoenix, D.; Laycock, S.L; Wareing, D.R.; Wright, P.A. Photobactericidal activity of phenothiazinium dyes against methicillin-resistant strains of *Staphylococcus aureus*. *FEMS Microbiol. Lett.* **1998**, *160*(2), 177–181.
27. Lyon, J.P.; Moreira, L.M.; de Moraes, P.C.; dos Santos, F.V.; de Resende, M.A.

Photodynamic therapy for pathogenic fungi. *Mycoses* **2011**, *54*(5), e265–e271.
28. Vatansever, F.; de Melo, W.C.; Avci, P.; Vecchio, D.; Sadasivam, M.; Gupta, A.; Chandran, R.; Karimi, M.; Parizotto, N.A.; Yin, R.; Tegos, G.P.; Hamblin, M.R. Antimicrobial strategies centered around reactive oxygen species - bactericidal antibiotics, photodynamic therapy, and beyond. *FEMS Microbiol. Rev.* **2013**, *37*(6), 955–989.
29. Gwynne, P.J.; Gallagher, M.P. Light as a Broad-Spectrum Antimicrobial. *Antimicrob. Front Microbiol* **2018**, *9:*119.
30. Bruno, T.J.; Svoronos, P.D.N. CRC Handbook of Fundamental Spectroscopic Correlation Charts; 1st ed.; CRC Press, Boca Raton, USA, **2005**.
31. St. Denis, T. G.; Dai, T.; Izikson, L.; Astrakas, C.; Anderson, R. R.; Hamblin, M. R.; Tegos, G.P. All you need is light: antimicrobial photoinactivation as an evolving and emerging discovery strategy against infectious disease. *Virulence* **2011**, *2*(6), 509–520.
32. Kumar, A.; Ghate, V.; Kim, M.J.; Zhou, W.; Khoo, G.H.; Yuk, H.G. Antibacterial efficacy of 405, 460 and 520 nm light emitting diodes on *Lactobacillus plantarum*, *Staphylococcus aureus* and *Vibrio parahaemolyticus*. *J. Appl. Microbiol.* **2016**, *120*(1), 49–56.
33. Kim, S.; Kim, J.; Lim, W.; Jeon, S.; Kim, O.; Koh, J.T.; Kim, C.S.; Choi, H.; Kim, O. *In vitro* bactericidal effects of 625, 525, and 425nm wavelength (red, green, and blue) light-emitting diode irradiation. *Photomed. Laser Surg.* **2013**, *31*(11), 554–562.
34. Dai, T.; Gupta, A.; Huang, Y.Y.; Sherwood, M.E.; Murray, C.K.; Vrahas, M.S.; Kielian, T.; Hamblin, M.R. Blue light eliminates community-acquired methicillin-resistant *Staphylococcus aureus* in infected mouse skin abrasions. *Photomed. Laser Surg.* **2013**, *31*(11), 531–538.
35. Ferrer-Espada, R.; Wang, Y.; Goh, X.S.; Dai, T. Antimicrobial blue light inactivation of microbial isolates in biofilms. *Lasers Surg. Med.* **2020**, *52*(5), 472–478.
36. Moorhead, S.; Maclean, M.; Macgregor, S.J.; Anderson, J.G. Comparative sensitivity of *Trichophyton* and *Aspergillus* conidia to inactivation by violet-blue light exposure. *Photomed. Laser Surg.* **2016**, *34*(1), 36–41.
37. Guffey, J.S.; Payne, W.; Buchanan, B.; Daugherty, J.; Meurer;, L.; Hensley, P. Susceptibility of *Trichophyton mentagrophytes* to visible light wavelengths. *Adv. Skin Wound Care* **2017**, *30*(5), 218–222.
38. Murdoch, L.E.; McKenzie, K.; Maclean, M.; MacGregor, S.J.; Anderson, J.G. Lethal effects of high-intensity violet 405-nm light on *Saccharomyces cerevisiae, Candida albicans*, and on dormant and germinating spores of *Aspergillus niger*. *Fungal Biol.* **2013**, *117*(7-8), 519–527.
39. Trzaska, W.J.; Wrigley, H.E.; Thwaite, J.E.; May, R.C. Species-specific antifungal activity of blue light. *Sci. Rep.* **2017**, *7* (1), 4605.
40. Wang, Y.; Wang, Y.; Wang, Y.; Murray, C.K.; Hamblin, M.R.; Hooper, D.C.; Dai, T. Antimicrobial blue light inactivation of pathogenic microbes: State of the art. *Drug Resist. Updat.* **2017**, *33–35*,1–22.
41. Halstead, F.D.; Thwaite, J.E.; Burt, R.; Laws, T.R.; Raguse, M.; Moeller, R.;

Webber, M.A.; Oppenheim, B.A. Antibacterial activity of blue light against nosocomial wound pathogens growing planktonically and as mature biofilms. *Appl. Environ. Microbiol.* **2016**, *82*(13), 4006–4016.

42. Cieplik, F.; Tabenski, L.; Buchalla, W.; Maisch, T. Antimicrobial photodynamic therapy for inactivation of biofilms formed by oral key pathogens. *Front. Microbiol.* **2014**, *5*:405
43. de Sousa, N.T.; Santos, M.F.; Gomes, R.C.; Brandino, H.E.; Martinez, R.; de Jesus Guirro, R.R. Blue laser inhibits bacterial growth of *Staphylococcus aureus, Escherichia coli,* and *Pseudomonas aeruginosa*. *Photomed. Laser Surg.* **2015**, *33*(5), 278–282.
44. Zhang, Y.; Zhu, Y.; Chen, J.; Wang, Y.; Sherwood, M.E.; Murray, C.K.; Vrahas, M.S.; Hooper, D.C.; Hamblin, M.R.; Dai, T. Antimicrobial blue light inactivation of *Candida albicans* : *In vitro* and *in vivo* studies. *Virulence* **2016**, *7*(5), 536–545.
45. Wang, C.; Yang, Z.; Peng, Y.; Guo, Y.; Yao, M.; Dong, J. Application of 460 nm visible light for the elimination of *Candida albicans in vitro* and *in vivo*. *Mol. Med. Rep.* **2018**, *18*(2), 2017–2026.
46. Dai, T. The antimicrobial effect of blue light: What are behind? *Virulence* **2017**, *8 (6)*, 649–652.
47. Pinto, A.P.; Rosseti, I.B.; Carvalho, M.L.; da Silva, B.G.M.; Alberto-Silva, C.; Costa, M.S. Photodynamic Antimicrobial Chemotherapy (PACT), using Toluidine blue O inhibits the viability of biofilm produced by *Candida albicans* at different stages of development. *Photodiagnosis Photodyn. Ther.* **2018**, *21*, 182–189.
48. Panariello, B.H.D.; Garcia, B.A.; Duarte, S. Daily phototherapy with red light to regulate *Candida albicans* biofilm growth. *J. Vis. Exp.* **2019**, (146), e59326.
49. Huh, S.Y.; Na, J.I.; Huh, C.H.; Park, K.C. The effect of photodynamic therapy using indole-3-acetic acid and green light on acne vulgaris. *Ann. Dermatol.* **2012**, *24*(1), 56–60.
50. Boral, H.; Metin, B.; Döğen, A.; Seyedmousavi, S.; Ilkit, M. Overview of selected virulence attributes in *Aspergillus fumigatus, Candida albicans, Cryptococcus neoformans, Trichophyton rubrum*, and *Exophiala dermatitidis*. *Fungal Genet. Biol.* **2018**, *111*, 92–107.
51. Vural, E.; Winfield, H.L.; Shingleton, A.W.; Horn, T.D.; Shafirstein, G. The effects of laser irradiation on *Trichophyton rubrum* growth. *Lasers Med. Sci.* **2008**, *23*(4), 349–353.
52. Carvalho, G.G.; Felipe, M.P.; Costa, M.S. The photodynamic effect of methylene blue and toluidine blue on *Candida albicans* is dependent on medium conditions. *J. Microbiol.* **2009**, *47*(5), 619–623.
53. Romano, R.A.; Pratavieira, S.; Silva, A.P.D.; Kurachi, C.; Guimarães, F.E.G. Light-driven photosensitizer uptake increases *Candida albicans* photodynamic inactivation. *J. Biophotonics* **2017**, *10*(11), 1538–1546.
54. Abrahamse, H.; Hamblin, M.R. New photosensitizers for photodynamic therapy. *Biochem. J* **2016**, *473*(4), 347–364.
55. Wainwright, M.; Crossley, K.B. Methylene Blue-a Therapeutic Dye for All Seasons? *J. Chemother.* **2002**, *14*, 431–443.
56. Jajarm, H.H.; Falaki, F.; Sanatkhani, M.; Ahmadzadeh, M.; Ahrari, F.; Shafaee, H.

A comparative study of toluidine blue-mediated photodynamic therapy versus topical corticosteroids in the treatment of erosive-atrophic oral lichen planus: a randomized clinical controlled trial. *Lasers Med Sci* **2015**, *30*(5), 1475–1480.

57. Ali, M.F. Topical delivery and photodynamic evaluation of a multivesicular liposomal rose bengal. *Lasers Med. Sci.* **2011**, *26*(2), 267–275.
58. Wiench, R.; Skaba, D.; Stefanik, N.; Kępa, M.; Gilowski, Ł.; Cieślar, G.; Kawczyk-Krupka, A. Assessment of sensitivity of selected *Candida* strains on antimicrobial photodynamic therapy using diode laser 635 nm and toluidine blue – *in vitro* research. *Photodiagnosis Photodyn. Ther.* **2019**, *27*, 241–247.
59. Costa, A.C.; Rasteiro, V.M.; Pereira, C.A.; Rossoni, R.D.; Junqueira, J.C.; Jorge, A.O. The effects of rose bengal- and erythrosine-mediated photodynamic therapy on *Candida albicans*. *Mycoses* **2012**, *55*(1), 56–63.
60. Dai, T.; Bil de Arce, V.J.; Tegos, G.P.; Hamblin, M.R. Blue dye and red light, a dynamic combination for prophylaxis and treatment of cutaneous *Candida albicans* infections in mice. *Antimicrob. Agents Chemother.* **2011**, *55*(12), 5710–5717.
61. Freire, F.; Costa, A.C.; Pereira, C.A.; Beltrame Junior, M.; Junqueira, J.C.; Jorge, A.O. Comparison of the effect of rose bengal-and eosin Y-mediated photodynamic inactivation on planktonic cells and biofilms of *Candida albicans*. *Lasers Surg. Med.* **2014**, *29*(3), 949–955.
62. Noble, S.M.; French, S.; Kohn, L.A.; Chen, V.; Johnson, A.D. Systematic screens of a *Candida albicans* homozygous deletion library decouple morphogenetic switching and pathogenicity. *Nat. Genet.* **2010**, *42*(7), 590–598.
63. Meyers, E.; Miraglia, G.J.; Smith, D.A.; Basch, H.I.; Pansy, F.E.; Trejo, W.H.; Donovick, R. Biological characterization of prasinomycin, a phosphorus-containing antibiotic. *Appl. Microbiol.* **1968**, *16*(4), 603–608.
64. Gulati, M.; Lohse, M.B.; Ennis, C.L.; Gonzalez, R.E.; Perry, A.M.; Bapat, P.; Arevalo, A.V.; Rodriguez, D.L.; Nobile, C.J. *In vitro* culturing and screening of *Candida albicans* biofilms. *Curr. Protoc. Microbiol.* **2018**, *50*(1), e60.
65. Lohse, M.B.; Gulati, M.; Valle Arevalo, A.; Fishburn, A.; Johnson, A.D.; Nobile, C.J. Assessment and optimizations of *Candida albicans in vitro* biofilm assays. *Antimicrob. Agents Chemother.* **2017**, *61*(5), e02749-16.
66. Jin, Y.; Zhang, T.; Samaranayake, Y.H.; Fang, H.H.; Yip, H.K.; Samaranayake, L.P. The use of new probes and stains for improved assessment of cell viability and extracellular polymeric substances in *Candida albicans* biofilms. *Mycopathologia* **2005**, *159*(3), 353–360.
67. Durantini, E.N. New insights into the antimicrobial blue light inactivation of *Candida albicans*. *Virulence* **2016**, *7*(5), 493–494.
68. Dai, T.; Gupta, A.; Murray, C.K.; Vrahas, M.S.; Tegos, G.P.; Hamblin, M.R. Blue light for infectious diseases: *Propionibacterium acnes, Helicobacter pylori* , and beyond? *Drug Resist. Updat.* **2012**, *15*(4), 223–236.
69. Hamblin, M.R.; Viveiros, J.; Yang, C.; Ahmadi, A.; Ganz, R.A.; Tolkoff, M.J. *Helicobacter pylori* accumulates photoactive porphyrins and is killed by visible light. *Antimicrob. Agents Chemother.* **2005**, *49*(7), 2822–2827.
70. Winckler, K.D. Special section: focus on anti-microbial photodynamic therapy

(PDT). *J. Photochem. Photobiol. B Biol.* **2007**, *86*(1), 43–44.
71. Rajesh, S.; Koshi, E.; Philip, K.; Mohan, A. Antimicrobial photodynamic therapy: An overview. *J. Indian Soc. Periodontol.* **2011**, *15*(4), 323–327.
72. Maisch, T. Resistance in antimicrobial photodynamic inactivation of bacteria. *Photochem. Photobiol. Sci.* **2015**, *14*(8), 1518–1526.
73. Al-Fattani, M.A.; Douglas, L.J. Penetration of *Candida* biofilms by antifungal agents. *Antimicrob. Agents Chemother.* **2004**, *48*(9), 3291–3297.
74. Taff, H.T.; Mitchell, K.F.; Edward, J.A.; Andes, D.R. Mechanisms of *Candida* biofilm drug resistance. *Future Microbiol.* **2013**, *8*(10), 1325–1337.
75. Al-Fattani, M.A.; Douglas, L.J. Biofilm matrix of *Candida albicans* and *Candida tropicalis*: chemical composition and role in drug resistance. *J. Med. Microbiol.* **2006**, *55*(pt 8), 999–1008.
76. Möller, M.N.; Cuevasanta, E.; Orrico, F.; Lopez, A.C.; Thomson, L.; Denicola, A. Diffusion and transport of reactive species across cell membranes. *Adv Exp Med Biol* **2019**, *1127*, 3–19.
77. Wolcott, R.; Costerton, J.W.; Raoult, D.; Cutler, S.J. The polymicrobial nature of biofilm infection. *Clin. Microbiol. Infect.* **2013**, *19*(2), 107–112.
78. Lohse, M.B.; Gulati, M.; Johnson, A.D.; Nobile, C.J. Development and regulation of single-and multi-species *Candida albicans* biofilms. *Nat Rev Microbiol.* **2018**, *16*(1), 19–31.
79. Orazi, G.; O'Toole, G.A. "It takes a village": Mechanisms underlying antimicrobial recalcitrance of polymicrobial biofilms. *J. Bacteriol.* **2019**, *202*(1), e00530-19.
80. Hu, X.; Huang, Y.Y.; Wang, Y.; Wang, X.; Hamblin, M.R. Antimicrobial photodynamic therapy to control clinically relevant biofilm infections. *Front. Microbiol.* **2018**, *9*:1299.
81. Briggs, T.; Blunn, G.; Hislop, S.; Ramalhete, R.; Bagley, C.; Mckenna, D.; Coathup, M. Antimicrobial photodynamic therapy-a promising treatment for prosthetic joint infections. *Lasers Med. Sci.* **2018**, *33*(3), 523–532.
82. Shany-Kdoshim, S.; Polak, D.; Houri-Haddad, Y.; Feuerstein, O. Killing mechanism of bacteria within multi-species biofilm by blue light. *J. Oral Microbiol.* **2019**, *11*(1), 1628577.
83. Dai, T.; Hamblin, M.R. Visible Blue Light is Capable of Inactivating *Candida albicans* and Other Fungal Species. *Photomed. Laser Surg.* **2017**, *35*, 345–346.
84. Ferrer-Espada, R.; Liu, X.; Goh, X.S.; Dai, T. Antimicrobial blue light inactivation of polymicrobial biofilms. *Front. Microbiol.* **2019**, *10*, 721.
85. Diogo, P.; Mota, M.; Fernandes, C.; Sequeira, D.; Palma, P.; Caramelo, F.; Neves, M.G.P.M.S.; Faustino, M.A.F.; Gonçalves, T.; Santos, J.M. Is the chlorophyll derivative Zn(II)e6Me a good photosensitizer to be used in root canal disinfection? *Photodiagnosis Photodyn. Ther.* **2018**, *22*, 205–211.
86. Stokes, J.M.; Lopatkin, A.J.; Lobritz, M.A.; Collins, J.J. Bacterial metabolism and antibiotic efficacy. *Cell Metab.* **2019**, *30*(2), 251–259.
87. Bojsen, R.; Regenberg, B.; Folkesson, A. *Saccharomyces cerevisiae* biofilm tolerance towards systemic antifungals depends on growth phase. *BMC Microbiol.* **2014**, *14*, 305.

88. Lafleur, M.D.; Kumamoto, C.A.; Lewis, K. *Candida albicans* biofilms produce antifungal-tolerant persister cells. *Antimicrob. Agents Chemother.* **2006**, *50*(11), 3839–3846.
89. Kuhn, D.M.; George, T.; Chandra, J.; Mukherjee, P.K.; Ghannoum, M.A. Antifungal susceptibility of *Candida* biofilms: unique efficacy of amphotericin B lipid formulations and echinocandins. *Antimicrob. Agents Chemother.* **2002**, *46*(6) 1773–1780.
90. Hurdle, J.G.; O' Neill, A.J.; Chopra, I.; Lee, R.E. Targeting bacterial membrane function: an underexploited mechanism for treating persistent infections. *Nat. Rev. Microbiol.* **2011**, *9*(1), 62–75.
91. Wimpenny, J.; Manz, W.; Szewzyk, U. Heterogeneity in biofilms. *FEMS Microbiol. Rev.* **2000**, *24*(5), 661–671.
92. Mah, T.F.; O'Toole, G.A. Mechanisms of biofilm resistance to antimicrobial agents. *Trends Microbiol.* **2001**, *9*(1), 34–39.
93. Lewis, K. Persister Cells. *Annu. Rev. Microbiol.* **2010**, *64*, 357–372.
94. Stewart, P.S. Mechanisms of antibiotic resistance in bacterial biofilms. *Int. J. Med. Microbiol* **2002**, *292*(2), 107–113.
95. Fox, E.P.; Singh-Babak, S.D.; Hartooni, N.; Nobile, C.J. Biofilms and antifungal resistance. In *Antifungals: From genomics to resistance and the development of novel agents*; Caister Academic Press, UK, **2015**; pp. 71–90.
96. Oppezzo, O.J.; Forte Giacobone, A.F. Lethal effect of photodynamic treatment on persister bacteria. *Photochem. Photobiol.* **2018**, *94*(1), 186–189.
97. Kharkwal, G.B.; Sharma, S.K.; Huang, Y.Y.; Dai, T.; Hamblin, M.R. Photodynamic therapy for infections: clinical applications. *Lasers Surg. Med.* **2011**, *43*(7), 755–767.
98. Dai, T.; Huang, Y.Y.; Hamblin, M.R. Photodynamic therapy for localized infections-state of the art. *Photodiagnosis Photodyn. Ther.* **2009**, *6*(3-4), 170–188.
99. Diogo, P.; Faustino M.A.F.; Neves, M.Graca.P.M.S.; Palma, P.J.; Baptista, I.P.; Gonçalves, T.; Santos, J.M. An insight into advanced approaches for photosensitizer optimization in endodontics—A critical review. *J. Funct. Biomater.* **2019**, *10*(4), 44.
100. Diogo, P.; Gonçalves, T.; Palma, P.J.; Santos, J.M.; Jefferies, S. Photodynamic antimicrobial chemotherapy for root canal system asepsis: A narrative literature review. *Int. J. Dent.* **2015**, *2015*, 269205.

CHAPTER 4

Photodynamic therapy is effective against *Candida auris* biofilms

Submitted to *Frontiers in Cellular and Infection Microbiology*; Authors: Bapat Priyanka S, Nobile Clarissa J.

4.1 Abstract

Fungal infections are increasing in prevalence worldwide. The paucity of available antifungal drug classes, combined with the increased occurrence of multidrug resistance in fungi, has led to new clinical challenges in the treatment of fungal infections. *Candida auris* is a recently emerged multidrug resistant human fungal pathogen that has become a worldwide public health threat. *C. auris* clinical isolates are often resistant to one or more antifungal drug classes, and thus, there is a high unmet medical need for the development of new therapeutic strategies effective against *C. auris*. Additionally, *C. auris* possesses several virulence traits, including the ability to form biofilms, further contributing to its drug resistance, and complicating the treatment of *C. auris* infections. Here we assessed red, green, and blue visible lights alone and in combination with photosensitizing compounds for their efficacies against *C. auris* biofilms. We found that (1) blue light inhibited and disrupted *C. auris* biofilms on its own and that the addition of photosensitizing compounds improved its antibiofilm potential; (2) red light inhibited and disrupted *C. auris* biofilms, but only in combination with photosensitizing compounds; and (3) green light inhibited *C. auris* biofilms in combination with photosensitizing compounds, but had no effects on disrupting *C. auris* biofilms. Taken together, these results suggest that photodynamic therapy could be an effective non-drug therapeutic strategy against multidrug resistant *C. auris* biofilm infections.

4.2 Introduction

Fungi cause a wide range of infections in humans, ranging from superficial skin to life-threatening disseminated infections [1]. Antifungal drugs are the most commonly used therapeutic agents for treating fungal infections, with only three major classes of antifungal drugs (the polyenes, azoles, and echinocandins) available to treat invasive fungal infections in humans [2,3]. The azoles and polyenes target the fungal cell membrane, while echinocandins target the fungal cell wall; thus, there is a need for new antifungal strategies with distinct mechanisms of action [2,3].

Candida auris is a recently emerged human fungal pathogen belonging to the *Candida/Clavispora* clade that was first isolated from the ear canal of a patient in Japan in 2009, and has since been identified in over 35 countries [4,5]. *C. auris* is highly transmissible through surface contact, and has been isolated from the surfaces of windows, floors, curtains, bedrails, monitors, and other surfaces in healthcare settings [6–8]. In infected patients, *C. auris* is typically isolated from the skin, nares, wounds, axilla, and urinary tracts, as well as the bloodstream, bones, and cerebrospinal fluids of patients with severe invasive infections [7,9–11]. Once *C. auris* infections become systemic, they are

associated with high mortality rates, ranging from 30-72%, with the highest mortality rates reported in patients with histories of extended hospital stays, implanted medical devices, or patients who have previously been treated with antifungal drugs [12–17].

Since its emergence in 2009, *C. auris* clinical isolates have been reported to be resistant to one or more of the three major classes of antifungal drugs used to treat invasive fungal infections, with 90% resistant to at least one antifungal drug class, 30% resistant to at least two antifungal drug classes, and a handful displaying pan-resistance to all three major antifungal drug classes [15,18–21]. *C. auris* resistance mechanisms are multifactorial, and have been reported to include the overexpression of the major facilitator superfamily (MFS) and ATP-binding cassette (ABC) drug efflux pumps, mutations in the ergosterol biosynthesis pathway, such as in the *ERG11* gene, and mutations in the *FKS1* gene, encoding a glucan synthase [12,22–25]. Given its heightened drug resistance and transmissibility, *C. auris* has become a serious global health threat [21,23,26].

In the current coronavirus disease 2019 (COVID-19) pandemic, coinfections of *C. auris* with severe acute respiratory syndrome coronavirus 2 (SARS-CoV-2), have been increasingly reported, with high mortality rates (~60%), especially for critically ill patients who remain in the hospital for extended periods of time (>20 days) and in patients with implanted medical devices (e.g., catheters and ventilators) [27–30]. Additionally, high mortality rates (50-60%), have also been reported for *C. auris*-SARS-CoV-2 coinfections in patients with underlying chronic conditions, such as diabetes mellitus and kidney disease [28,31–35]. The increased spread of *C. auris* infections during the COVID-19 pandemic is likely facilitated, at least in part, by the transformation of intensive care units and other hospital facilities into dedicated COVID-19 units, which foster ideal conditions for *C. auris* outbreaks [27,36].

C. auris possesses multiple virulence traits that contribute to its pathogenicity, including the formation of biofilms [15,18]. Biofilms are defined as communities of adherent microbial cells encased in a protective extracellular matrix [37,38]. *C. auris* biofilms are composed primarily of yeast-form cells interspersed with pseudohyphal cells that are encased in a mannan and glucan extracellular matrix [24,39,40]. Although planktonic *C. auris* cells display antifungal drug resistance on their own, *C. auris* cells isolated from biofilms are even more resistant to antifungal drugs than their free-floating counterparts [7,12,39,41]. *C. auris* biofilm formation is thought to occur in four sequential stages: adherence, initiation, maturation, and dispersal [22,24] (Figure 1A). In the adherence stage, planktonic *C. auris* yeast-form cells adhere to biotic surfaces (e.g., skin, and mucosal layers) or abiotic surfaces (e.g., catheters, and prosthetic joints). In the initiation stage, the adhered *C. auris* yeast-form cells begin to proliferate, and some pseudohyphal cells develop. In the maturation stage, the cells within the *C. auris* biofilm continue to proliferate and an extracellular matrix that encases the biofilm cells is formed. Finally, in the dispersal stage, *C. auris* yeast-form cells leave the biofilm to adhere to and form biofilms on new surfaces or enter the bloodstream to cause systemic infections.

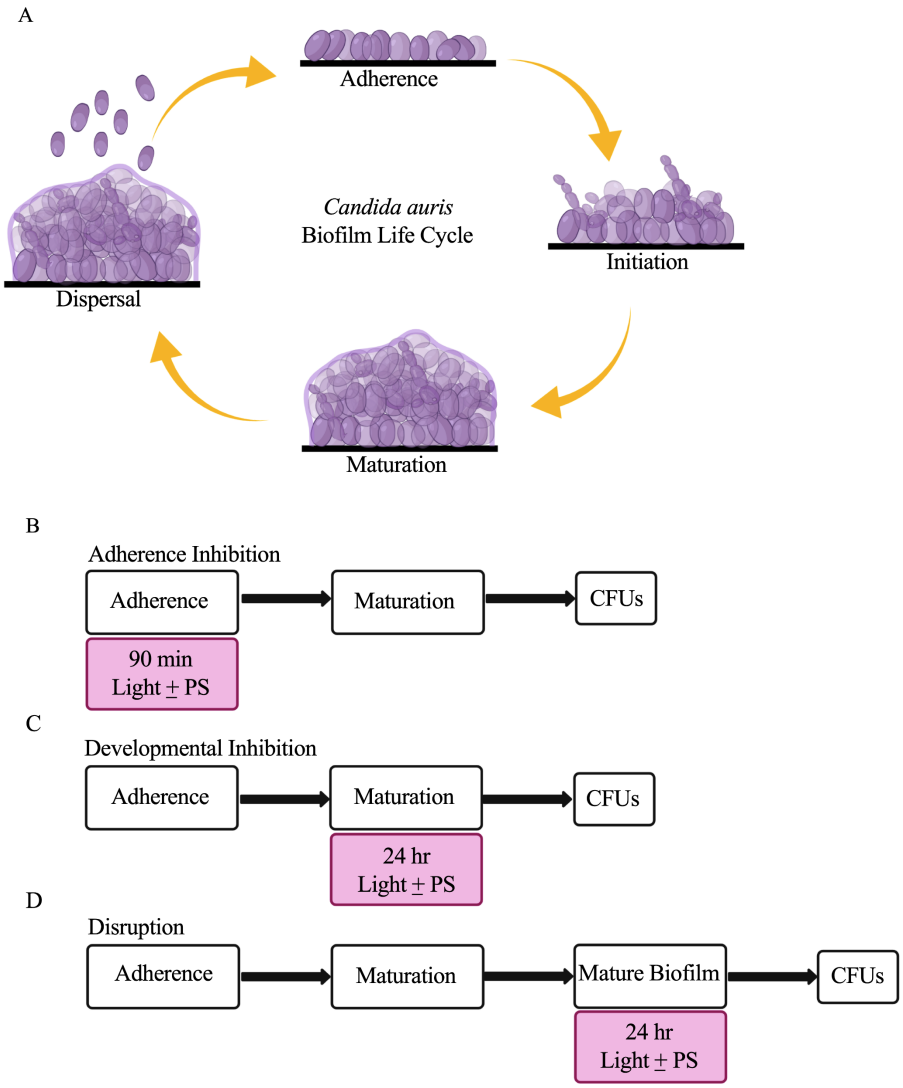

Figure 4.1. The *C. auris* biofilm life cycle and the three biofilm assays used in this study to assess the antibiofilm properties of visible lights with and without photosensitizing compounds. (A) The *C. auris* biofilm life cycle occurs in four sequential stages: adherence, initiation, maturation, and dispersal. In the adherence stage, planktonic *C. auris* yeast-form cells adhere to a surface. In the initiation stage, the adhered cells begin to proliferate, and some pseudohyphal cells are formed. In the maturation stage, the cells continue to proliferate and an extracellular matrix composed of glucans and mannans encases the biofilm cells. Finally, in the dispersal stage, yeast-form cells leave the biofilm to adhere to and form biofilms on new surfaces, or enter the bloodstream to cause systemic infections. (B) Overview of the adherence inhibition biofilm assay, where the visible light of interest with (+) and without (-) the photosensitizing compound (PS) were present during the 90-min adherence stage of biofilm formation. (C) Overview of the developmental inhibition biofilm assay, where the visible light of interest with (+) and without (-) the PS

of interest were present during the 24-h maturation stage of biofilm formation. (D) Overview of the disruption biofilm assay, where the visible light of interest with (+) and without (-) the PS of interest were present for an additional 24 h on a mature (24-h) biofilm. CFUs were measured to determine viable cell counts at the end of each biofilm assay. This figure was creating using BioRender.com.

Given that *C. auris* clinical isolates are often resistant to one or more antifungal drug classes, there is a high unmet medical need for the development of new therapeutic strategies effective against *C. auris*. Photodynamic therapy has been used for the past 40 years to treat oncologic skin conditions, and more recently to treat benign inflammatory skin conditions, such as acne vulgaris and viral warts [42–44]. It has also been gaining scientific interest as a non-drug therapeutic strategy to treat a variety of infections [45]. Photodynamic therapy relies on a light source, a non-toxic photosensitizing compound, and molecular oxygen [46–48]. Following light exposure and absorption, the photosensitizing compound transfers electrons to molecular oxygen, which acts as an electron acceptor, ultimately leading to the production of cytotoxic reactive oxygen species (ROS), such as singlet oxygen, hydroxyl radicals, and superoxide anions (Wainwright *et al*. 2017; St. Denis *et al*. 2011; Lyon *et al*. 2011; Vatansever *et al*. 2013). Unlike traditional antimicrobial drugs, photodynamic therapy affects multiple non-specific microbial targets simultaneously, making it unlikely for resistance to develop. Based on its fundamental mechanisms of action, photodynamic therapy could be a clinically useful therapeutic strategy effective against infections, including those caused by multidrug resistant *C. auris*.

Broadly, the visible light spectrum can be divided into red (620-700 nm), green (500-560 nm), and blue (400-490 nm) wavelengths, of which certain discreet wavelengths have been reported to display antimicrobial properties [45,46,49,52,53]. Blue light has been the most studied for its antimicrobial properties, where it has been shown to effectively kill several different species of pathogenic bacteria and fungi, including methicillin resistant *Staphylococcus aureus*, carbapenem resistant *Klebsiella pneumoniae*, and ß-lactam resistant *Escherichia coli* [54–67]. Comparatively, the antimicrobial properties of red and green lights have been much less studied to date [52,68–70].

Although visible lights can have antimicrobial effects on targeted microbial cells on their own, likely by generating ROS through the photoexcitation of naturally occurring photosensitizing compounds (e.g., flavoproteins and porphyrins), the combined antimicrobial effects of visible lights with exogenous synthetic photosensitizing compounds have been shown to significantly increase the generation of ROS [48,62,71,72]. Recently, the antimicrobial effects of red, green, and blue visible lights alone and in combination with the classic photosensitizing compounds new methylene blue, toluidine blue O, and rose bengal, were comprehensively assessed against *Candida albicans* biofilms [73]. In this study, blue light was found to inhibit and disrupt *C. albicans* biofilms on its own and the addition of photosensitizing compounds improved its antibiofilm potential, while red and green lights were found to inhibit *C. albicans* biofilm formation only in combination with photosensitizing compounds, but were unable to disrupt biofilms. In terms of *C. auris*, to our knowledge, only one study to date has assessed the effects of photodynamic therapy on *C. auris* biofilms. In this study, red light combined with the

photosensitizing compound methylene blue was found to be highly effective at reducing viable cell counts from *C. auris* biofilms [74].

To better understand the utility of photodynamic therapy against *C. auris* infections, here we comprehensively assessed the efficacies of red, green, and blue visible lights alone and in combination with the classic photosensitizing compounds new methylene blue, toluidine blue O, and rose bengal, against *C. auris* biofilms. We found that blue light inhibited and disrupted *C. auris* biofilms on its own, and that the addition of photosensitizing compounds improved its antibiofilm potential. We found that red light inhibited and disrupted *C. auris* biofilms, but only in combination with photosensitizing compounds. Finally, we found that green light inhibited *C. auris* biofilms in combination with photosensitizing compounds, but had no effects on disrupting *C. auris* biofilms. In general, the effects we observed on *C. auris* biofilms were similar across biofilms formed by different *C. auris* clinical isolates from distinct genetic clades that display different antifungal drug susceptibilities.

4.3 Materials and Methods

4.3.1 Strains and media

Given that the effects of visible lights on *C. albicans* biofilms have been comprehensively assessed (Bapat et.al 2021), we used the *C. albicans* clinical isolate SC5314 [75] as a reference strain in this study. We used the following *C. auris* clinical isolates: Strain #0383 (AR0383; South African clade), Strain #0389 (AR0389; South Asian clade), and Strain #0390 (AR0390; South Asian clade) (Centers for Disease Control and Prevention AR Isolate Bank, Drug Resistance *Candida* species panel; https://wwwn.cdc.gov/ARIsolateBank/; accessed on 02/20/2021). The minimum inhibitory concentrations (MICs) for representative drugs from the three major antifungal drug classes used to treat invasive fungal infections for each *C. auris* isolate used in this study have been reported previously (Lockhart *et al*., 2017; https://www.cdc.gov/fungal/candida-auris/c-auris-antifungal.html/; accessed on 05/07/2021), and can be found in Table S1. *C. auris* and *C. albicans* cells were recovered from -80˚C glycerol stocks for two days at 30˚C on yeast extract peptone dextrose (YPD) agar plates (1% yeast extract (Thermo Fisher Scientific, Catalog #211929), 2% Bacto peptone (Gibco, Catalog #211677), 2% dextrose (Fisher Scientific Catalog #D16-3), and 2% agar (Criterion, Catalog #89405-066)). Overnight cultures were grown for ~15 h at 30˚C, shaking at 225 rpm in YPD liquid medium (1% yeast extract (Thermo Fisher Scientific, Catalog #211929), 2% Bacto peptone (Gibco, Catalog #211677), and 2% dextrose (Fisher Scientific Catalog #D16-3)). All biofilm assays were performed using RPMI-1640 medium with L-glutamine and without sodium bicarbonate (Sigma Aldrich, Catalog #R6504-10X1L), supplemented with 34.5 g/L MOPS (Sigma Aldrich, Catalog #M3183), adjusted to pH 7.2 with sodium hydroxide (Fisher Scientific, Catalog #S318-100), and filter sterilized using a 0.22 µm filter (Corning, Catalog #431098).

4.3.2 Light sources and photosensitizing compounds

A red LED light source (ABI LED lighting, Catalog #GR-PAR38-26W-RED, 26-Watt 620-630 nm, outputting 176 J/cm^2), a green LED light source (ABI LED lighting,

#GR-PAR38-24W-520nm, 24-Watt 520-530 nm, outputting 204 J/cm^2), and a blue LED light source (ABI LED lighting, GR-PAR38-24W-BLU, 24-Watt 450 nm, outputting 240 J/cm^2) were placed at a distance of 8 inches from the biofilm wells and were used as indicated in the biofilm assays. Average LED light intensity measurements for each light source at this distance were 6500 lux for red light, 6700 lux for green light, and 5900 lux for blue light.

The photosensitizing compounds new methylene blue (Sigma Aldrich, Catalog #B-4631), toluidine blue O (Sigma Aldrich, Catalog #T3260), and rose bengal (Sigma Aldrich, Catalog #198250) were added alone and in combination with the red, green, and blue visible lights in the biofilm assays. The photosensitizing compounds were dissolved in PBS (HyClone, Catalog #16777-252) at a stock concentration of 10 mM and diluted to a working concentration of 400 μM in RPMI-1640 medium, which was used to grow the biofilms. Stocks of the photosensitizing compounds were prepared fresh every two weeks, filter sterilized using a 0.22 μm filter, and stored at 4°C in the dark.

4.3.3 Biofilm assays

The adherence inhibition, developmental inhibition, and disruption biofilm assays were performed as described previously [73], where colony forming units (CFUs) were measured at the end of the assays to assess the efficacies of the visible lights with or without photosensitizing compounds at reducing *C. auris* and *C. albicans* viable cell counts from the biofilms.

In brief, biofilms were grown in triplicate on the bottoms of sterile flat-bottomed 12-well non-tissue culture treated polystyrene plates (Corning, Catalog #351143). The 12-well plates were seeded with *Candida* cells at a final OD_{600} of 0.5 in a final volume of 2 mL of RPMI-1640 medium and grown for 90 min at 37°C, with shaking at 250 rpm in an ELMI shaker (M2 Scientifics, Catalog #ELMI-TRMS 04). After the 90-min adherence stage, the wells were washed gently with PBS and fresh RPMI-1640 medium was added to each well. The plates were sealed with breathable sealing membranes (Sigma Aldrich, Catalog #Z380059) and grown for 24 h at 37°C, with shaking at 250 rpm in an ELMI shaker. For the adherence inhibition biofilm assay, the biofilms were exposed to red, green, or blue visible lights with or without a photosensitizing compound during the 90-min adherence stage of biofilm formation (Figure 1B). For the developmental inhibition biofilm assay, the biofilms were exposed to red, green, or blue visible lights with or without a photosensitizing compound throughout the first 24 h of biofilm growth, but not during the initial 90-min adherence stage (Figure 1C). For the disruption biofilm assay, biofilms were grown, medium was removed from each well containing mature 24-h biofilms, fresh RPMI-1640 medium was added to each well, the plates were re-sealed, and the mature biofilms were exposed to red, green, or blue visible lights with or without a photosensitizing compound for an additional 24 h (Figure 1D). The 12-well plates were divided such that half of one plate was exposed to the light of interest and the other half was covered with foil and served as a no light control.

4.3.4 Determination of colony forming units (CFUs) from *Candida* biofilms

CFU determinations from biofilms were performed as previously described (Gulati *et al*. 2018; Lohse *et al*. 2017; Bapat et.al 2021). Briefly, biofilms were scraped from the

bottoms of the each well of a 12-well plate using a sterile spatula, vigorously vortexed, serially diluted in PBS, and plated onto YPD agar plates. The plates were incubated at 30˚C for 2 days and colonies were counted to determine CFUs/mL. Statistical significance was determined using Student's unpaired two-tailed t-tests assuming unequal variance.

4.3.5 Viability staining of *C. auris* biofilms

To assess the viability of *C. auris* biofilm cells, viability staining was performed both on *C. auris* biofilms directly and on *C. auris* cells resuspended from biofilms under each light and photosensitizing compound treatment condition using the LIVE/DEAD *Bac*Light viability kit (Invitrogen, Catalog #L7012) as described previously for use on *C. albicans* biofilms [73,79], and according to the manufacturer's protocol. Briefly, the samples were incubated with 3 μL of SYTO9 and 3 μL of propidium iodide in the dark at 30˚C for 20 min. Following incubation, the samples were imaged by fluorescence microscopy at 20X magnification with a green laser (GFP/green channel; 470 nm excitation wavelength) and a red laser (Texas Red/red channel; 585 nm excitation wavelength) using an EVOS Cell Imaging System (Life Technologies, Catalog #EVOS FL Cell Imaging System).

4.4 Results

4.4.1 Blue visible light alone is effective against *C. auris* biofilms

To determine whether red, green, and blue visible lights on their own can affect *C. auris* biofilm development, we first performed the three biofilm assays in the presence of each of these visible light treatments. We used three *C. auris* clinical isolates encompassing two different genetic clades (AR0383 from the South African clade, AR0389 from the South Asian clade, and AR0390 from the South Asian clade). We found that red and green visible lights on their own had no effects on *C. auris* biofilms in any of the three biofilm assays compared to the untreated control (Figure 2A-B; Figure S1A-B). We also found that blue light on its own had no effect at inhibiting *C. auris* biofilm formation in the adherence inhibition biofilm assay compared to the untreated control (Figure 2C; Figure S1C). However, blue light on its own was effective at inhibiting *C. auris* biofilm formation by 77% (averaging all three *C. auris* strains) in the developmental inhibition biofilm assay (p=0.0001) (Figure 2C; Figure S1C). We also found that blue light on its own was effective at disrupting *C. auris* biofilms by 57% (averaging all three *C. auris* strains) in the disruption biofilm assay (p=0.0004) (Figure 2C; Figure S1C).

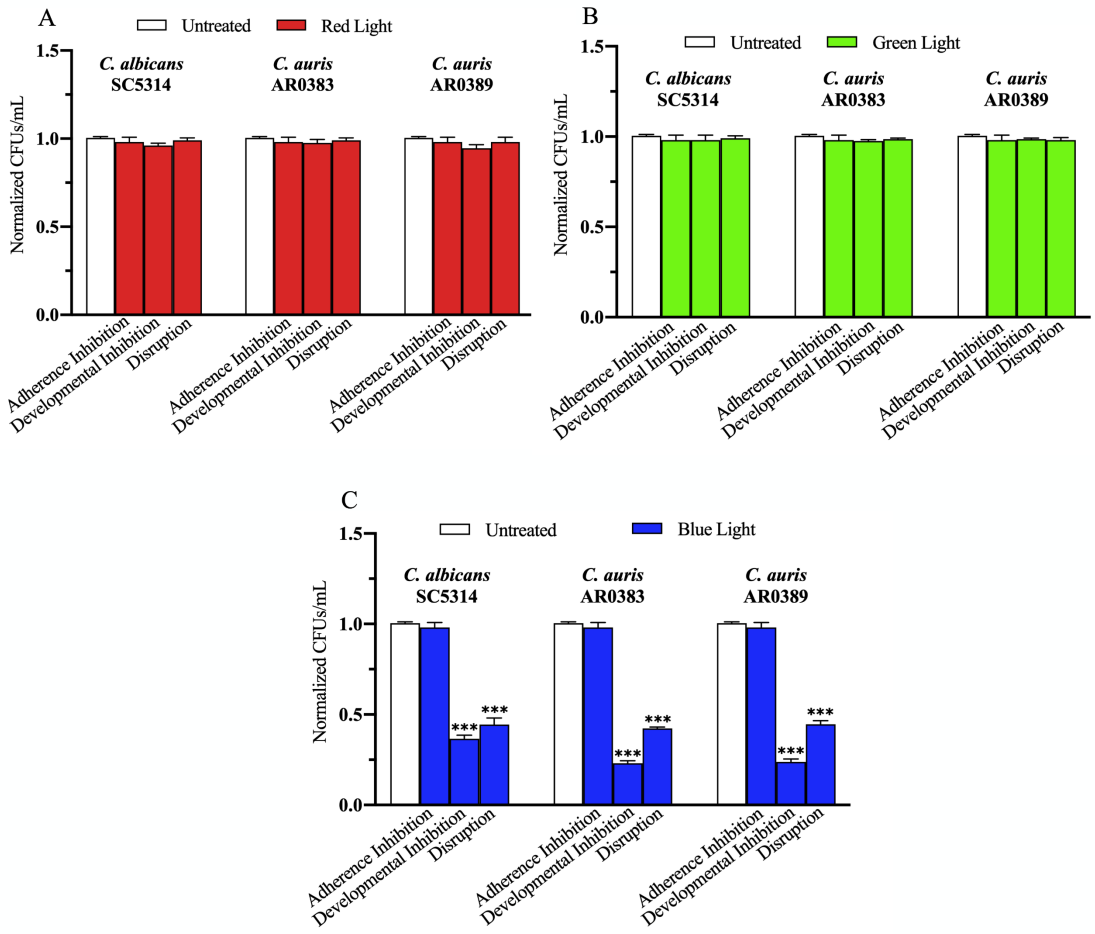

Figure 4.2. Blue visible light alone is effective against *C. auris* biofilms. *C albicans* (SC5314) and *C. auris* (AR0383 and AR0389) biofilms were exposed to red, green, and blue visible lights individually in the adherence inhibition, developmental inhibition, and disruption biofilm assays. CFUs/mL were counted to determine viable cell counts at the end of each of the biofilm assays. Effects of (A) red light alone (Red Light), (B) green light alone (Green Light), and (C) blue light alone (Blue Light) in the three different biofilm assays compared to an untreated control (Untreated). Standard deviations are shown for each sample (n=3). The average CFUs/mL of the untreated control samples for each assay were normalized to 1. Significance comparisons are relative to the untreated control and were determined using student's unpaired two-tailed t-tests assuming unequal variance for $p \leq 0.001$ (***).

4.4.2 Red, green, and blue visible lights in combination with photosensitizing compounds are effective against *C. auris* biofilms

To determine whether red, green, and blue visible lights combined with classic exogenous photosensitizing compounds can affect *C. auris* biofilm development, we performed the three biofilm assays in the presence of each of these visible light treatments

plus new methylene blue, toluidine blue O, and rose bengal, and assessed the effects of this treatment on *C. auris* biofilms formed by AR0383, AR0389, and AR0390. Compared to the average of the untreated control, red light on its own, and each photosensitizing compound on its own (i.e., the three negative controls), we found that red light plus any of the photosensitizing compounds had no effect on *C. auris* biofilm formation in the adherence inhibition biofilm assay (Figure 3A; Figure S2A). Compared to the average of the three negative controls, we found that red light plus any of the photosensitizing compounds was effective at inhibiting *C. auris* biofilm formation by 58% when combined with new methylene blue (p=0.0001), 58% when combined with toluidine blue O (p=0.0002), and 55% when combined with rose bengal (p=0.0001) (averaging all three *C. auris* strains) in the developmental inhibition biofilm assay (Figure 3B; Figure S2B). Compared to the average of the three negative controls, we found that red light plus any of the photosensitizing compounds was effective at disrupting mature *C. auris* biofilms by 71% when combined with new methylene blue (p=0.0005), 76% when combined with toluidine blue O (p=0.0004), and 32% when combined with rose bengal (p=0.009) (averaging all three *C. auris* strains) in the disruption biofilm assay (Figure 3C; Figure S2C).

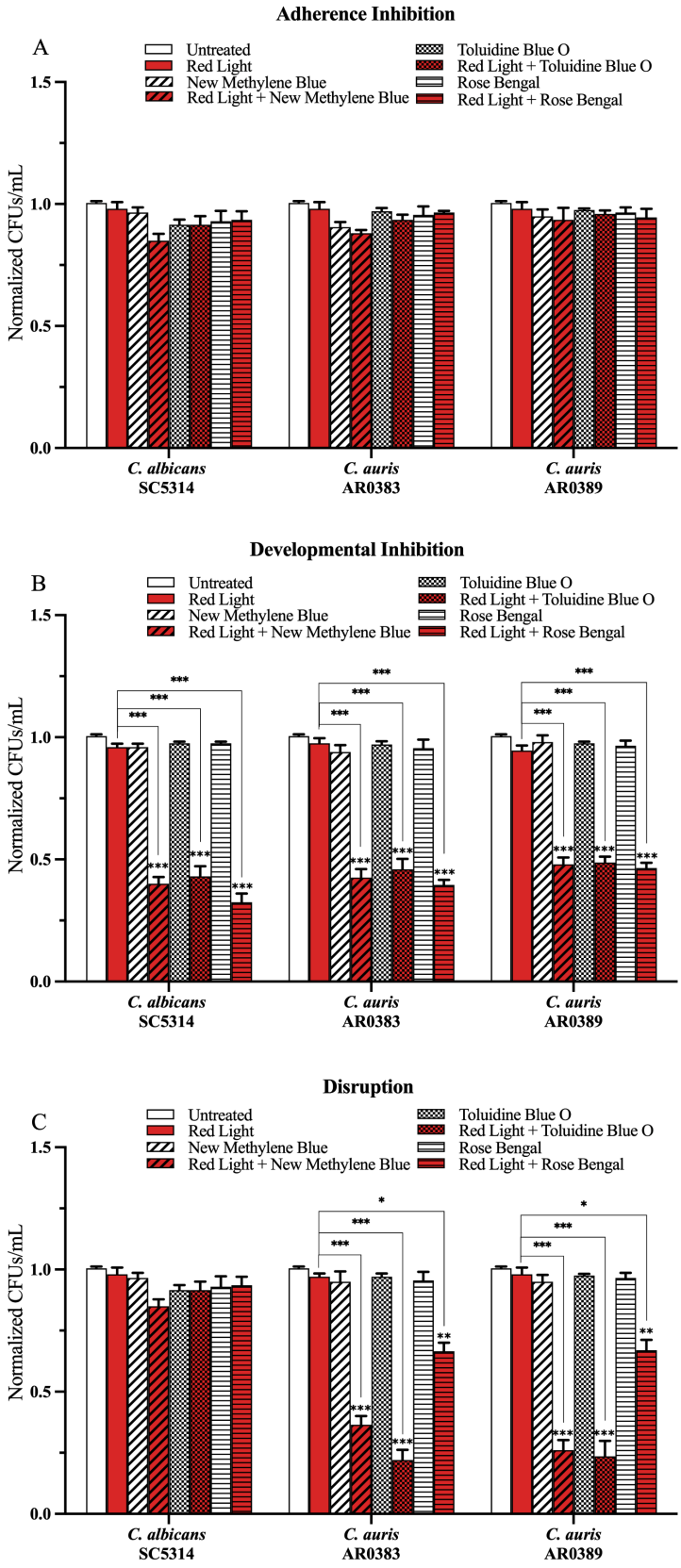
Adherence Inhibition
A
Untreated
Red Light
New Methylene Blue
Red Light + New Methylene Blue
Toluidine Blue O
Red Light + Toluidine Blue O
Rose Bengal
Red Light + Rose Bengal
Normalized CFUs/mL
1.5
1.0
0.5
0.0
C. albicans SC5314
C. auris AR0383
C. auris AR0389
Developmental Inhibition
B
Untreated
Red Light
New Methylene Blue
Red Light + New Methylene Blue
Toluidine Blue O
Red Light + Toluidine Blue O
Rose Bengal
Red Light + Rose Bengal
Normalized CFUs/mL
***
C. albicans SC5314
C. auris AR0383
C. auris AR0389
Disruption
C
Untreated
Red Light
New Methylene Blue
Red Light + New Methylene Blue
Toluidine Blue O
Red Light + Toluidine Blue O
Rose Bengal
Red Light + Rose Bengal
Normalized CFUs/mL
*
**
***
C. albicans SC5314
C. auris AR0383
C. auris AR0389

Figure 4.3. Red visible light in combination with photosensitizing compounds is effective against *C. auris* biofilms. *C albicans* (SC5314) and *C. auris* (AR0383 and AR0389) biofilms were exposed to red visible light with and without the photosensitizing compound indicated in the (A) adherence inhibition, (B) developmental inhibition, and (C) disruption biofilm assays. Untreated control (Untreated), red light alone (Red Light), photosensitizing compound alone (New Methylene Blue, Toluidine Blue O, and Rose Bengal), and red light in combination with the photosensitizing compound (Red Light + New Methylene Blue, Red Light + Toluidine Blue O, and Red Light + Rose Bengal) are shown. CFUs/mL were measured to determine viable cell counts from the biofilms at the end of each biofilm assay. Standard deviations are shown for each sample (n=3). The average CFUs/mL of the untreated control samples for each assay were normalized to 1. Significance comparisons are relative to the untreated control unless otherwise noted with significance bars and were determined using student's unpaired two-tailed t-tests assuming unequal variance for $p \leq 0.05$ (*), $p \leq 0.01$ (**), and $p \leq 0.001$ (***).

Compared to the average of the untreated control, green light on its own, and each photosensitizing compound on its own (i.e., the three negative controls), we found that green light plus any of the photosensitizing compounds had no effect on *C. auris* biofilm formation in the adherence inhibition biofilm assay (Figure 4A; Figure S3A). Compared to the average of the three negative controls, we found that green light plus any of the photosensitizing compounds was effective at inhibiting *C. auris* biofilm formation by 62% when combined with new methylene blue (p=0.004), 76% when combined with toluidine blue O (p=0.0007), and 74% when combined with rose bengal (p=0.0004) (averaging all three *C. auris* strains) in the developmental inhibition biofilm assay (Figure 4B; Figure S3B). Compared to the average of the three negative controls, we found that green light plus any of the photosensitizing compounds was not effective at disrupting mature *C. auris* biofilms (averaging all three *C. auris* strains) in the disruption biofilm assay (Figure 4C; Figure S3C).

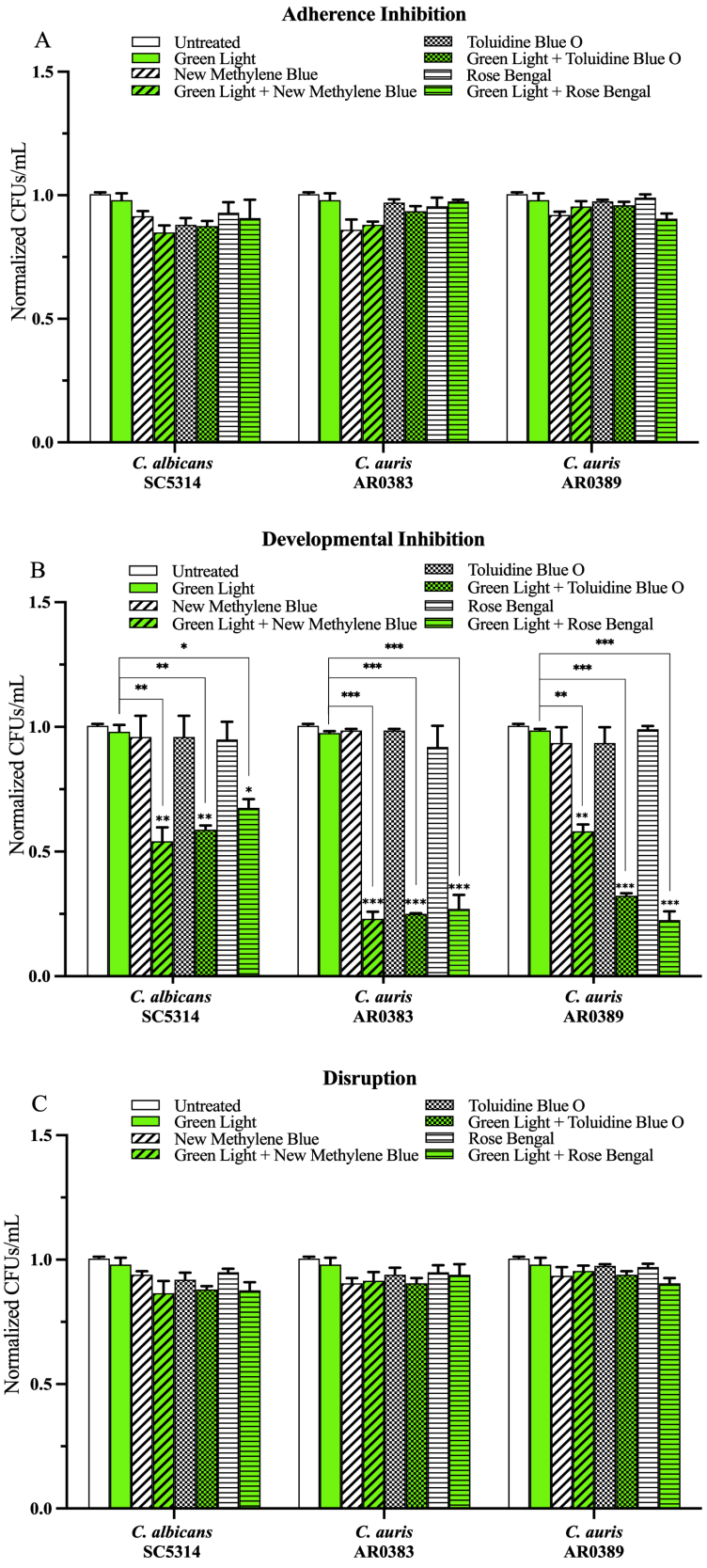
Adherence Inhibition
A
Untreated
Green Light
New Methylene Blue
Green Light + New Methylene Blue
Toluidine Blue O
Green Light + Toluidine Blue O
Rose Bengal
Green Light + Rose Bengal
Normalized CFUs/mL
1.5
1.0
0.5
0.0
C. albicans SC5314
C. auris AR0383
C. auris AR0389
Developmental Inhibition
B
Untreated
Green Light
New Methylene Blue
Green Light + New Methylene Blue
Toluidine Blue O
Green Light + Toluidine Blue O
Rose Bengal
Green Light + Rose Bengal
Normalized CFUs/mL
1.5
1.0
0.5
0.0
*
**
***
C. albicans SC5314
C. auris AR0383
C. auris AR0389
Disruption
C
Untreated
Green Light
New Methylene Blue
Green Light + New Methylene Blue
Toluidine Blue O
Green Light + Toluidine Blue O
Rose Bengal
Green Light + Rose Bengal
Normalized CFUs/mL
1.5
1.0
0.5
0.0
C. albicans SC5314
C. auris AR0383
C. auris AR0389

Figure 4.4. Green visible light in combination with photosensitizing compounds is effective against *C. auris* biofilms. *C albicans* (SC5314) and *C. auris* (AR0383 and AR0389) biofilms were exposed to green visible light with and without the photosensitizing compound indicated in the (A) adherence inhibition, (B) developmental inhibition, and (C) disruption biofilm assays. Untreated control (Untreated), green light alone (Green Light), photosensitizing compound alone (New Methylene Blue, Toluidine Blue O, and Rose Bengal), and green light in combination with the photosensitizing compound (Green Light + New Methylene Blue, Green Light + Toluidine Blue O, and Green Light + Rose Bengal) are shown. CFUs/mL were counted to determine viable cell counts at the end of each of the biofilm assays. Standard deviations are shown for each sample (n=3). The average CFUs/mL of the untreated control samples for each assay were normalized to 1. Significance comparisons are relative to the untreated control unless otherwise noted with significance bars and were determined using student's unpaired two-tailed t-tests assuming unequal variance for $p \leq 0.05$ (*), and $p \leq 0.01$ (**) and $p \leq 0.001$ (***).

Compared to the average of the untreated control, blue light on its own, and each photosensitizing compound on its own, we found that blue light plus any of the three photosensitizing compounds had no effect on *C. auris* biofilm formation in the adherence inhibition biofilm assay (Figure 5A; Figure S4A). Since blue light on its own was effective at inhibiting and disrupting *C. auris* biofilms in the developmental inhibition biofilm assay and the disruption biofilm assay, respectively (Figure 2C; Figure S1C), we compared the effects of blue light plus the three photosensitizing compounds to the average of the untreated control and each photosensitizing compound on its own (i.e., the two negative controls) for these biofilm assays. Compared to the average of the two negative controls, we found that blue light plus any of the photosensitizing compounds was effective at inhibiting *C. auris* biofilm formation by 84% when combined with new methylene blue (p=0.00001), 85% when combined with toluidine blue O (p=0.00001), and 78% when combined with rose bengal (p=0.0001) (averaging all three *C. auris* strains) in the developmental inhibition biofilm assay (Figure 5B; Figure S4B). Compared to the biofilm inhibitory effects of blue light on its own, we found that blue light plus new methylene blue had an additive inhibitory effect of 7% (p=0.01), and blue light plus toluidine blue O had an additive inhibitory effect of 8% (p=0.01) (averaging all three *C. auris* strains) in the developmental inhibition biofilm assay (Figure 5B; Figure S4B). We did not observe an additive inhibitory effect of blue light plus rose bengal against *C. auris* biofilms in the developmental inhibition biofilm assay (Figure 5B; Figure S4B). Compared to the average of the two negative controls, we found that blue light plus any of the photosensitizing compounds was effective at disrupting mature *C. auris* biofilms by 79% when combined with new methylene blue (p=0.0003), 79% when combined with toluidine blue O (p=0.0002), and 66% when combined with rose bengal (p=0.007) (averaging all three *C. auris* strains) in the disruption biofilm assay (Figure 5C; Figure S4C). Compared to the biofilm disruption effects of blue light on its own, the combination of blue light plus new methylene blue had an additive biofilm disruption effect of 22% (p=0.002), blue light plus toluidine blue O had an additive effect of 22% (p=0.002), and blue light plus rose bengal had an additive effect of 9% (p=0.01) (averaging all three *C. auris* strains) in the disruption biofilm assay (Figure 5C; Figure S4C).

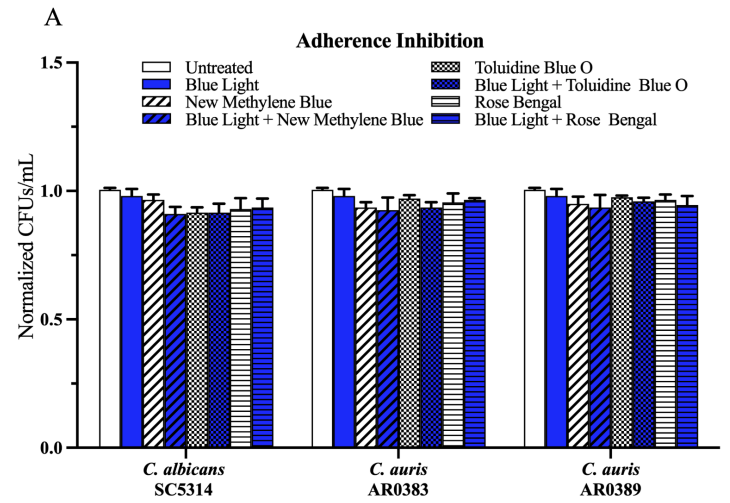
A
Adherence Inhibition
Untreated
Blue Light
New Methylene Blue
Blue Light + New Methylene Blue
Toluidine Blue O
Blue Light + Toluidine Blue O
Rose Bengal
Blue Light + Rose Bengal
Normalized CFUs/mL
1.5
1.0
0.5
0.0
C. albicans SC5314
C. auris AR0383
C. auris AR0389

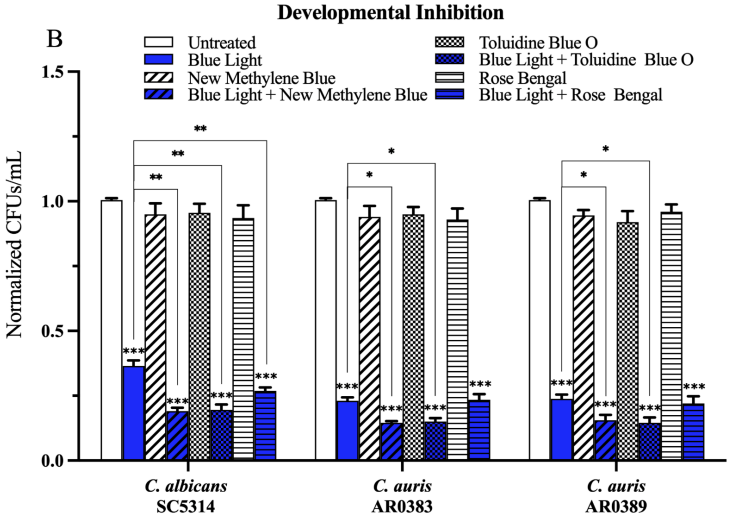
Developmental Inhibition
B
Untreated
Blue Light
New Methylene Blue
Blue Light + New Methylene Blue
Toluidine Blue O
Blue Light + Toluidine Blue O
Rose Bengal
Blue Light + Rose Bengal
Normalized CFUs/mL
1.5
1.0
0.5
0.0
C. albicans SC5314
C. auris AR0383
C. auris AR0389

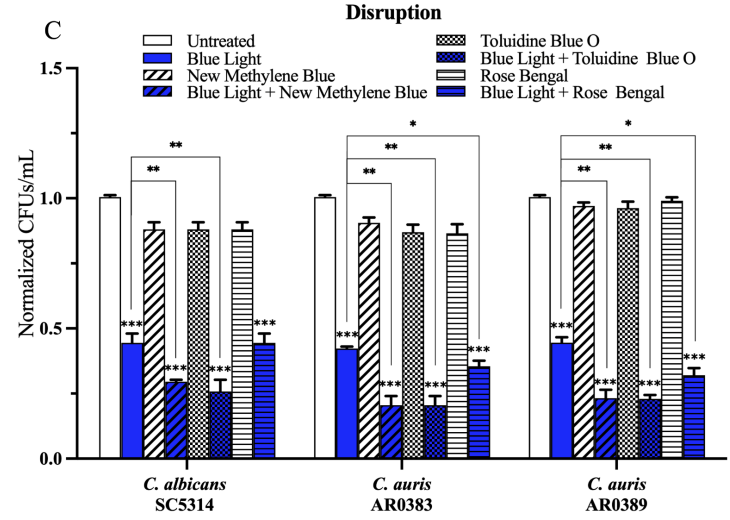
Disruption
C
Untreated
Blue Light
New Methylene Blue
Blue Light + New Methylene Blue
Toluidine Blue O
Blue Light + Toluidine Blue O
Rose Bengal
Blue Light + Rose Bengal
Normalized CFUs/mL
1.5
1.0
0.5
0.0
C. albicans SC5314
C. auris AR0383
C. auris AR0389

Figure 4.5. Blue visible light in combination with photosensitizing compounds is effective against *C. auris* biofilms. *C albicans* (SC5314) and *C. auris* (AR0383 and AR0389) biofilms were exposed to blue visible light with and without the photosensitizing compound indicated in the (A) adherence inhibition, (B) developmental inhibition, and (C) disruption biofilm assays. Untreated control (Untreated), blue light alone (Blue Light), photosensitizing compound alone (New Methylene Blue, Toluidine Blue O, and Rose Bengal), and blue light in combination with the photosensitizing compounds (Blue Light + New Methylene Blue, Blue Light + Toluidine Blue O, and Blue Light + Rose Bengal) are shown. CFUs/mL were counted to determine viable cell counts at the end of each of the biofilm assays. Standard deviations are shown for each sample (n=3). The average CFUs/mL of the untreated control samples for each assay were normalized to 1. Significance comparisons are relative to the untreated control unless otherwise noted with significance bars and were determined using student's unpaired two-tailed t-tests assuming unequal variance for $p \leq 0.05$ (*), $p \leq 0.01$ (**), and $p \leq 0.001$ (***).

Finally, as an independent assay for biofilm cell viability, we performed LIVE/DEAD staining assays on both *C. auris* biofilms directly and on *C. auris* cells resuspended from biofilms under the different visible light and photosensitizing compound treatment conditions. Our cell viability staining results were consistent with our CFU determinations for all treatment conditions (see Figures S5-S9 for representative images from the LIVE/DEAD staining assays performed directly on *C. auris* biofilms formed by AR0383 and Figures S10-S14 for representative images from the LIVE/DEAD staining assays performed on *C. auris* cells resuspended from biofilms formed by AR0383).

4.5 Discussion

Photodynamic therapy is used today to treat oncological and inflammatory skin conditions; however, its potential use as an antimicrobial strategy is only beginning to be recognized. Photodynamic therapy relies on the localized production of ROS that can have cytotoxic effects on targeted cells. To determine the utility of photodynamic therapy for use against *C. auris* infections, we assessed the antibiofilm effects of red, green, and blue visible lights alone and in combination with the classic photosensitizing compounds new methylene blue, toluidine blue O, and rose bengal on *C. auris* biofilms. We found that, of the visible lights tested, blue light was the only visible light that had antibiofilm properties on its own against *C. auris* biofilms, where it markedly prevented biofilm formation when it was applied throughout biofilm development, as well as markedly disrupted biofilms when it was applied on a mature biofilm. Overall, we found that red, green, and blue visible lights when combined with photosensitizing compounds, prevented *C. auris* biofilm formation when applied throughout biofilm development; however, only red and blue lights in combination with photosensitizing compounds disrupted mature *C. auris* biofilms. Interestingly, none of the visible lights and photosensitizing compound combination treatments were effective at inhibiting *C. auris* biofilms during the 90-min adherence stage of biofilm formation, highlighting the importance of exposure time in the antibiofilm efficacy of photodynamic therapy.

Our findings on *C. auris* biofilms indicate that photosensitizing compounds can sensitize *C. auris* biofilms to visible lights when applied throughout biofilm development (i.e., over the course of a 24-hr period). We found that the combination treatments of red

and blue lights with the photosensitizing compounds had the most striking antibiofilm effects, where these treatments both prevented *C. auris* biofilm formation as well as disrupted mature *C. auris* biofilms, significantly above red and blue light treatments alone. These effects were especially notable when red and blue lights were combined with new methylene blue and toluidine blue O, which are both phenothiazinium salt photosensitizing compounds. Although the detailed mechanisms of how photosensitizing compounds sensitize *C. auris* biofilms to light exposure are not understood, photosensitizing compounds are generally known to enhance the production of ROS [45,62,80], which likely leads to cytotoxicity of *C. auris* biofilm cells. Overall, our findings demonstrate that blue light plus toluidine blue O, followed closely by blue light plus new methylene blue, red light plus toluidine blue O, and then red light plus new methylene blue, are the most effective photodynamic therapy treatment combinations against *C. auris* biofilms.

In general, the majority of our findings on the effects of visible lights in combination with photosensitizing compounds on *C. auris* biofilms are consistent with the effects of these treatments on *C. albicans* biofilms [73]; however, there are two notable species-specific differences that we would like to point out. First, we found that red light in combination with photosensitizing compounds was effective at disrupting mature *C. auris* biofilms by 60% on average, while this treatment had no effect on *C. albicans* biofilms. Second, we found that green light in combination with toluidine blue O, and green light in combination with rose bengal, were on average more effective at preventing *C. auris* biofilm formation by 32% and 42%, respectively, than they were at preventing *C. albicans* biofilm formation. These observed species-specific differences in treatment efficacies suggest that photodynamic therapy may be overall more effective against *C. auris* biofilms than against *C. albicans* biofilms, which may, in part, be due to structural differences between *C. auris* and *C. albicans* biofilms. For example, *C. auris* biofilms are generally thinner than *C. albicans* biofilms, and are composed of yeast-form cells with occasional pseudohyphal cells that are encased in a glucan and mannan extracellular matrix [24,39,40]. *C. albicans* biofilms, on the other hand, are generally thicker than *C. auris* biofilms, and are composed of yeast-form cells, pseudohyphal cells, and hyphal cells, encased in an extracellular matrix composed of proteins, lipids, carbohydrates, and nucleic acids [81–84]. These structural differences between *C. auris* and *C. albicans* biofilms could influence the efficacies of photodynamic therapy by affecting the uptake of photosensitizing compounds and the traversal of visible lights throughout the biofilm architecture [41]. In addition, differences in cell wall composition between *C. auris* and *C. albicans* cells could also impact how visible lights and photosensitizing compounds interact with the cell wall and thus impact the antibiofilm effectiveness of photodynamic therapy. The *C. auris* cell wall, for example, contains distinct cell surface mannans that are absent from the *C. albicans* cell wall as well as elevated chitin levels relative to the *C. albicans* cell wall [85–87].

Since antimicrobial photodynamic therapy relies on the localized production of ROS to cause oxidation of microbial lipids, proteins, and carbohydrates, it is likely to have broad-spectrum antimicrobial activity against many different microorganisms [47,88–90]. Indeed, there is evidence to suggest that photodynamic therapy is effective at killing of a wide range of microorganisms, including pathogenic gram-positive and gram-negative bacteria, protozoa, fungi, and even viruses [50,63,91–95]. In fact, in the current COVID-

19 pandemic, antimicrobial photodynamic therapy has been suggested as a potential therapeutic strategy to use against COVID-19 infections [96–98]. Consistent with this idea, one recent study demonstrated that red light in combination with photosensitizing compounds was effective at inhibiting SARS-CoV-2 viral replication within mammalian Vero E6 cells [99]. Given that the prevalence of *C. auris*-SARS-CoV-2 coinfections have been increasing throughout the COVID-19 pandemic and that there is evidence to suggest that photodynamic therapy could be effective against *C. auris* and SARS-CoV-2 infections individually, photodynamic therapy could be a promising therapeutic strategy to consider for these as well as other coinfections in the clinic.

Recently, pan-resistant clinical isolates of *C. auris* that are resistant to all three of the major classes of antifungal drugs available to treat invasive fungal infections in humans have been reported in several countries, including the United States [100]. Despite the emergence of these pan-resistant isolates, antifungal drugs remain the most commonly used treatment for *C. auris* infections [12,13]. Based on our findings as well as numerous findings in the literature on the effectiveness of antimicrobial photodynamic therapies against a multitude of pathogenic microorganisms across phylogenetic kingdoms, we believe that photodynamic therapy could be a valuable therapeutic strategy that should be explored further for use against *C. auris* infections. In the context of *C. auris* infections, there are at least three major drawbacks of traditional antifungal drug therapies that are overcome by the use of photodynamic therapy. First, the development of antifungal drug resistance after exposure to antifungal drugs can render traditional antifungal drug treatments virtually ineffective against fungal infections. This is frequently observed in the context of *C. auris* infections, and in fact, the majority of *C. auris* clinical isolates are resistant to at least one antifungal drug class [12,18,21]. Given that photodynamic therapy generates ROS that affect multiple non-specific microbial targets simultaneously, it is unlikely that *C. auris* resistance to photodynamic therapy could be developed, and antimicrobial resistance to photodynamic therapy, in general, has not been reported to date. Second, antifungal drugs, especially the polyenes, are known to cause significant toxicities to human cells and are typically administered systemwide (e.g., intravenously) [101]. Photodynamic therapy uses non-toxic photosensitizing compounds combined with visible lights that pose little toxicity concerns to humans [46,47]. In addition, photodynamic therapy can be spatially confined to an area of interest, thus limiting unnecessary exposure of human cells to the treatment. Third, the mechanisms of action of almost all existing antimicrobial drugs target microbial metabolic processes, and thus require that the microbial cells are metabolically active in order to be effective [102–104]. This requirement poses significant inconsistencies in antimicrobial drug effectiveness within heterogeneous microbial cell populations. This is especially true in the context of biofilms, where heterogeneous cell populations are present throughout the biofilm architecture with varying levels of metabolic activity [105–107]. In addition, metabolically dormant phenotypic cell variants within mature biofilms, called persister cells, are markedly difficult to eradicate with traditional antimicrobial drugs [105,108–110]. *C. auris* biofilms, in particular, are notorious for displaying low susceptibilities to existing antifungal drugs, including caspofungin and amphotericin B, which is likely the result of, at least in part, cell heterogeneity within *C. auris* biofilms [22,39]. Photodynamic therapy does not require that

microbial cells are metabolically active, and there is some evidence to suggest that photodynamic therapy is effective against persister cells in bacteria [47,111].

In summary, our results suggest that photodynamic therapy is highly effective at inhibiting *C. auris* biofilm formation and at disrupting mature *C. auris* biofilms *in vitro.* Given that there are only three classes of antifungal drugs used to treat invasive fungal infections and that pan-resistant *C. auris* isolates have been emerging that have rendered the use of these antifungal drugs ineffective, new therapeutic strategies effective against *C. auris* are urgently needed. Our work suggests that photodynamic therapy could be a clinically viable option in combating *C. auris* infections that should be explored further.

4.6 Supplementary Materials

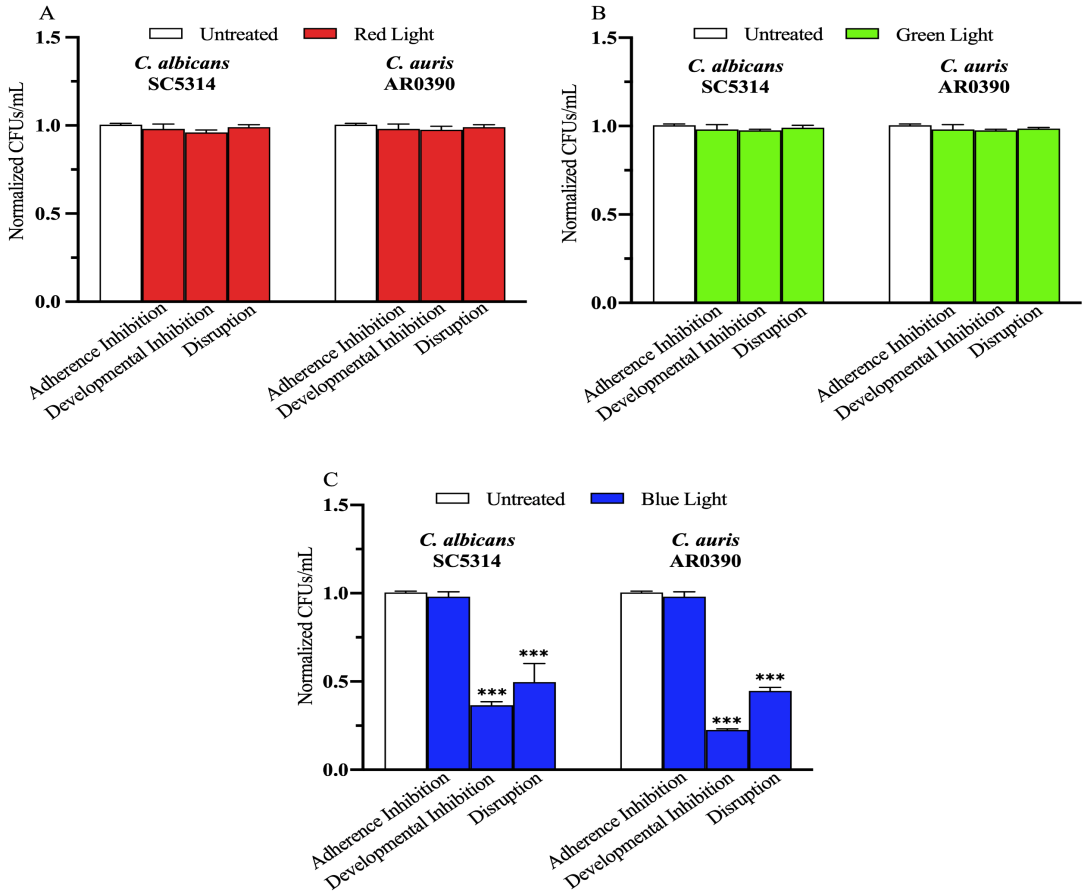

Figure S4.1. Blue visible light alone is effective against biofilms formed by an additional *C. auris* clinical isolate. *C. albicans* (SC5314) and *C. auris* (AR0390) biofilms were exposed to red, green, and blue visible lights individually in the adherence inhibition, developmental inhibition, and disruption biofilm assays. CFUs/mL were counted to determine viable cell counts at the end of each of the biofilm assays. Effects of (A) red light alone (Red Light), (B) green light alone (Green Light), and (C) blue light alone (Blue Light) in the three different biofilm assays compared to an untreated control (Untreated). Standard deviations are shown for each sample (n=3). The average CFUs/mL of the

untreated control samples for each assay were normalized to 1. Significance comparisons are relative to the untreated control and were determined using student's unpaired two-tailed t-tests assuming unequal variance for $=p \leq 0.001$ (***).

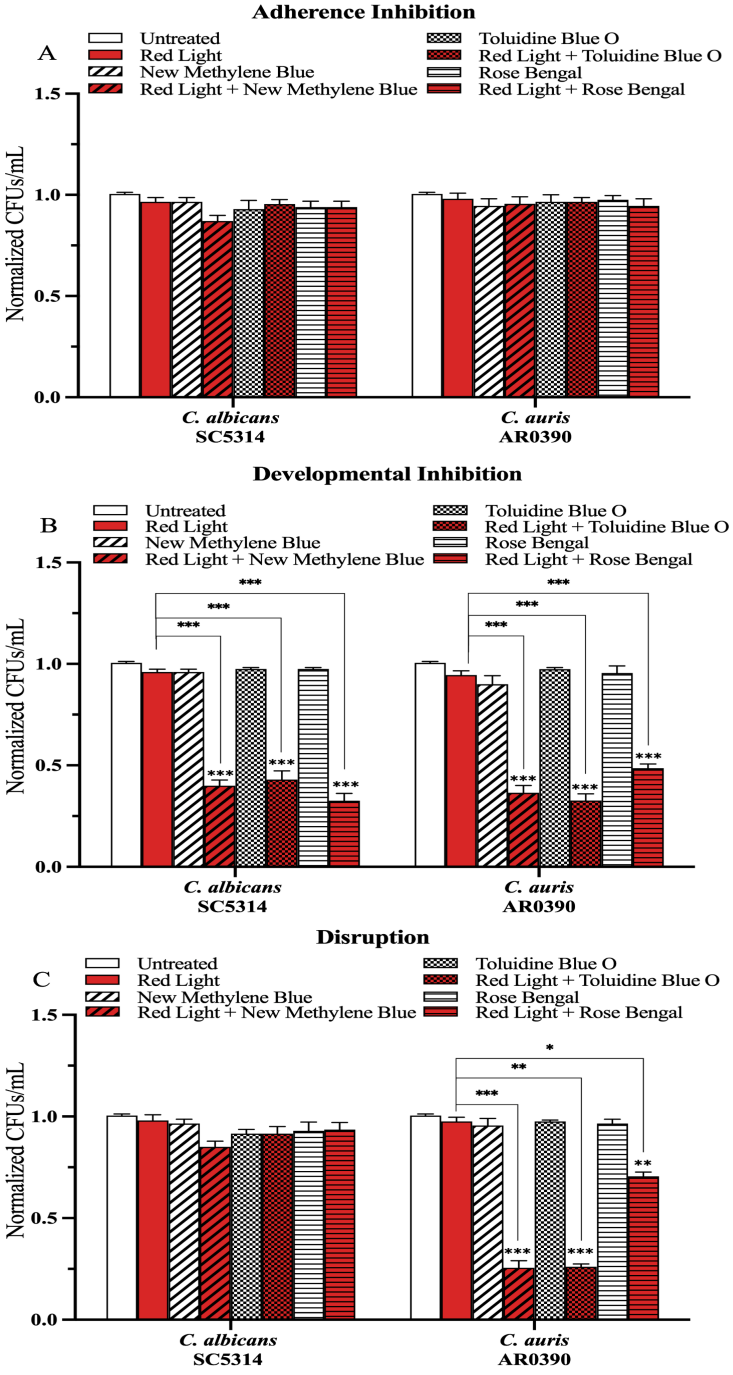

Figure S4.2. Red visible light in combination with photosensitizing compounds is effective against biofilms formed by an additional *C. auris* clinical isolate. *C albicans*

(SC5314) and *C. auris* (AR0390) biofilms were exposed to red visible light with and without the photosensitizing compound indicated in the (A) adherence inhibition, (B) developmental inhibition, and (C) disruption biofilm assays. Untreated control (Untreated), red light alone (Red Light), photosensitizing compound alone (New Methylene Blue, Toluidine Blue O, and Rose Bengal), and red light in combination with the photosensitizing compound (Red Light + New Methylene Blue, Red Light + Toluidine Blue O, and Red Light + Rose Bengal) are shown. CFUs/mL were measured to determine viable cell counts from the biofilms at the end of each biofilm assay. Standard deviations are shown for each sample (n=3). The average CFUs/mL of the untreated control samples for each assay were normalized to 1. Significance comparisons are relative to the untreated control unless otherwise noted with significance bars and were determined using student's unpaired two-tailed t-tests assuming unequal variance for $p \leq 0.05$ (*), $p \leq 0.01$ (**), and $p \leq 0.001$ (***).

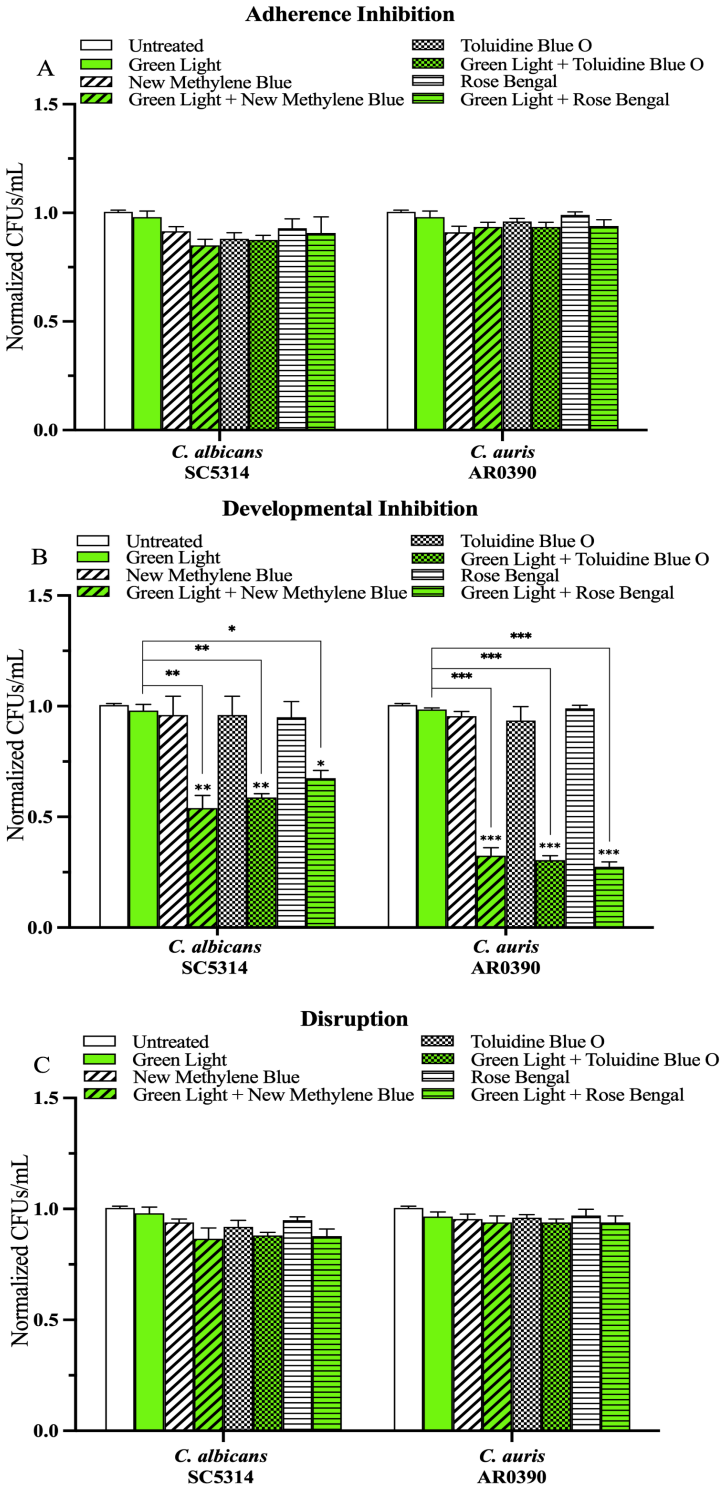

Figure S4.3. Green visible light in combination with photosensitizing compounds is effective against biofilms formed by an additional *C. auris* clinical isolate. *C albicans* (SC5314) and *C. auris* (AR0390) biofilms were exposed to green visible light with and

without the photosensitizing compound indicated in the (A) adherence inhibition, (B) developmental inhibition, and (C) disruption biofilm assays. Untreated control (Untreated), green light alone (Green Light), photosensitizing compound alone (New Methylene Blue, Toluidine Blue O, and Rose Bengal), and green light in combination with the photosensitizing compound (Green Light + New Methylene Blue, Green Light + Toluidine Blue O, and Green Light + Rose Bengal) are shown. CFUs/mL were counted to determine viable cell counts at the end of each of the biofilm assays. Standard deviations are shown for each sample (n=3). The average CFUs/mL of the untreated control samples for each assay were normalized to 1. Significance comparisons are relative to the untreated control unless otherwise noted with significance bars and were determined using student's unpaired two-tailed t-tests assuming unequal variance for $p \leq 0.05$ (*), and $p \leq 0.01$ (**) and $p \leq 0.001$ (***).

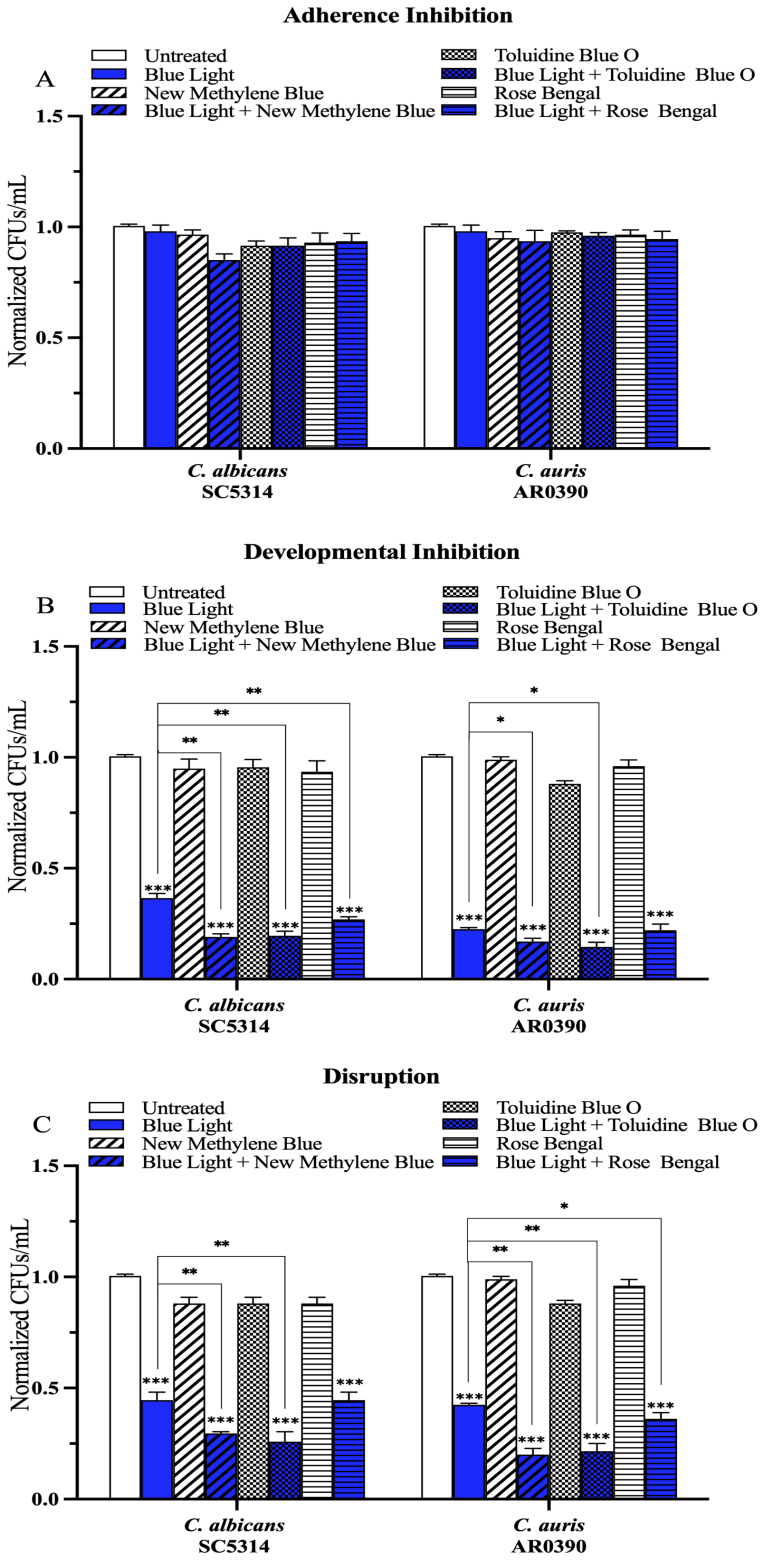

Figure S4.4 Blue visible light in combination with photosensitizing compounds is effective against biofilms formed by an additional *C. auris* clinical isolate. *C albicans*

(SC5314) and *C. auris* (AR0390) biofilms were exposed to blue visible light with and without the photosensitizing compound indicated in the (A) adherence inhibition, (B) developmental inhibition, and (C) disruption biofilm assays. Untreated control (Untreated), blue light alone (Blue Light), photosensitizing compound alone (New Methylene Blue, Toluidine Blue O, and Rose Bengal), and blue light in combination with the photosensitizing compounds (Blue Light + New Methylene Blue, Blue Light + Toluidine Blue O, and Blue Light + Rose Bengal) are shown. CFUs/mL were counted to determine viable cell counts at the end of each of the biofilm assays. Standard deviations are shown for each sample (n=3). The average CFUs/mL of the untreated control samples for each assay were normalized to 1. Significance comparisons are relative to the untreated control unless otherwise noted with significance bars and were determined using student's unpaired two-tailed t-tests assuming unequal variance for $p \leq 0.05$ (*), $p \leq 0.01$ (**), and $p \leq 0.001$ (***)

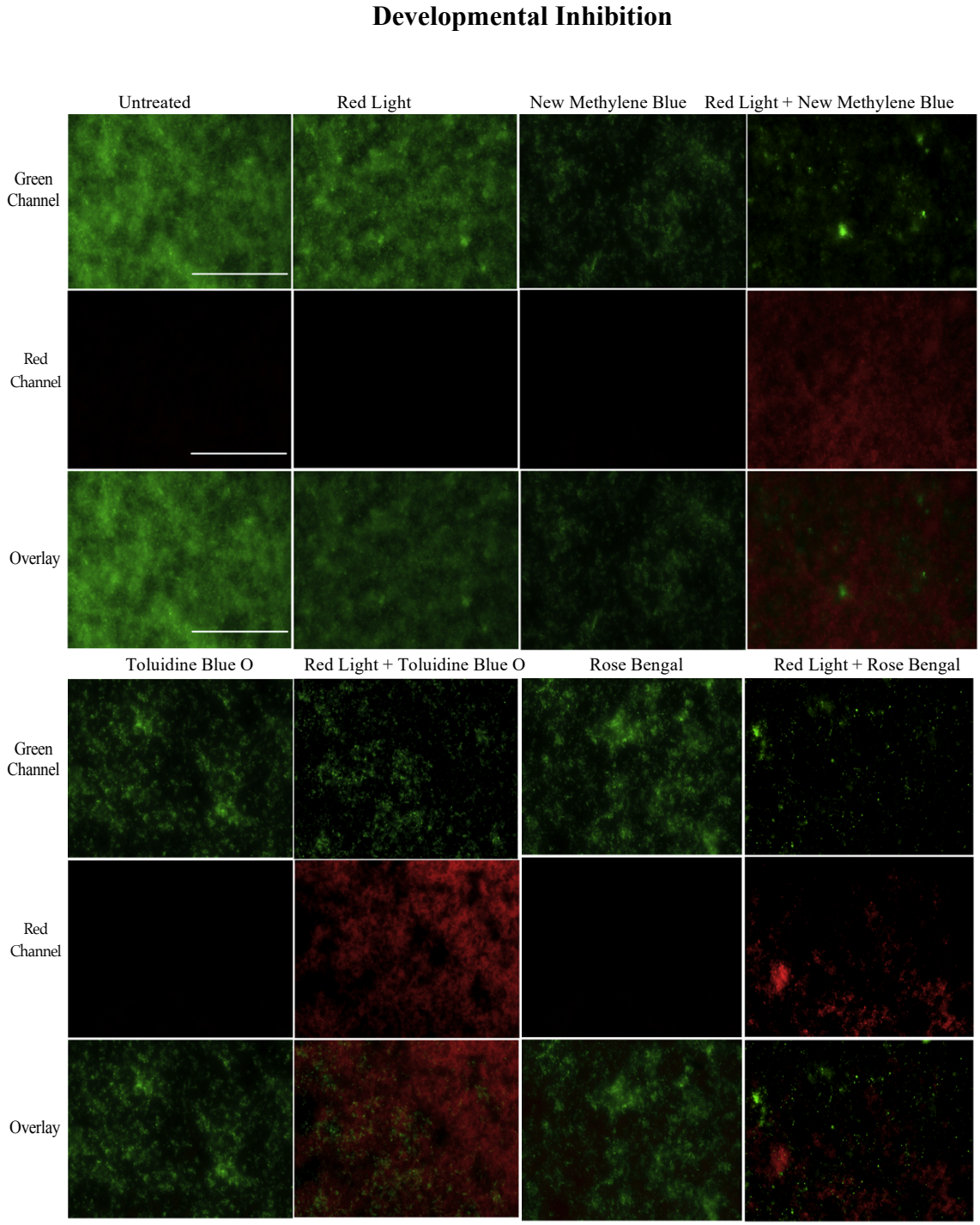

Figure S4.5. Red visible light in combination with photosensitizing compounds is effective at reducing the cell viability of *C. auris* biofilms in the developmental inhibition biofilm assay. The viability of *C. auris* (AR0383) biofilms was assessed using the LIVE/DEAD *Bac*Light viability kit, where green fluorescence indicates live cells, and red fluorescence indicates dead cells. The samples were imaged by fluorescence microscopy at 20X magnification with a green laser (GFP/green channel) shown in the top

panels, a red laser (Texas Red/red channel) shown in the middle panels, and overlayed shown in the bottom panels for each set of images. Representative images are shown for the untreated control (Untreated), red light alone (Red Light), new methylene blue photosensitizing compound alone (New Methylene Blue), red light in combination with new methylene blue photosensitizing compound (Red Light + New Methylene Blue), toluidine blue O photosensitizing compound alone (Toluidine Blue O), red light in combination with toluidine blue O photosensitizing compound (Red Light + Toluidine Blue O), rose bengal photosensitizing compound alone (Rose Bengal) and red light in combination with rose bengal photosensitizing compound (Red Light + Rose Bengal). Scale bars represent 200μm.

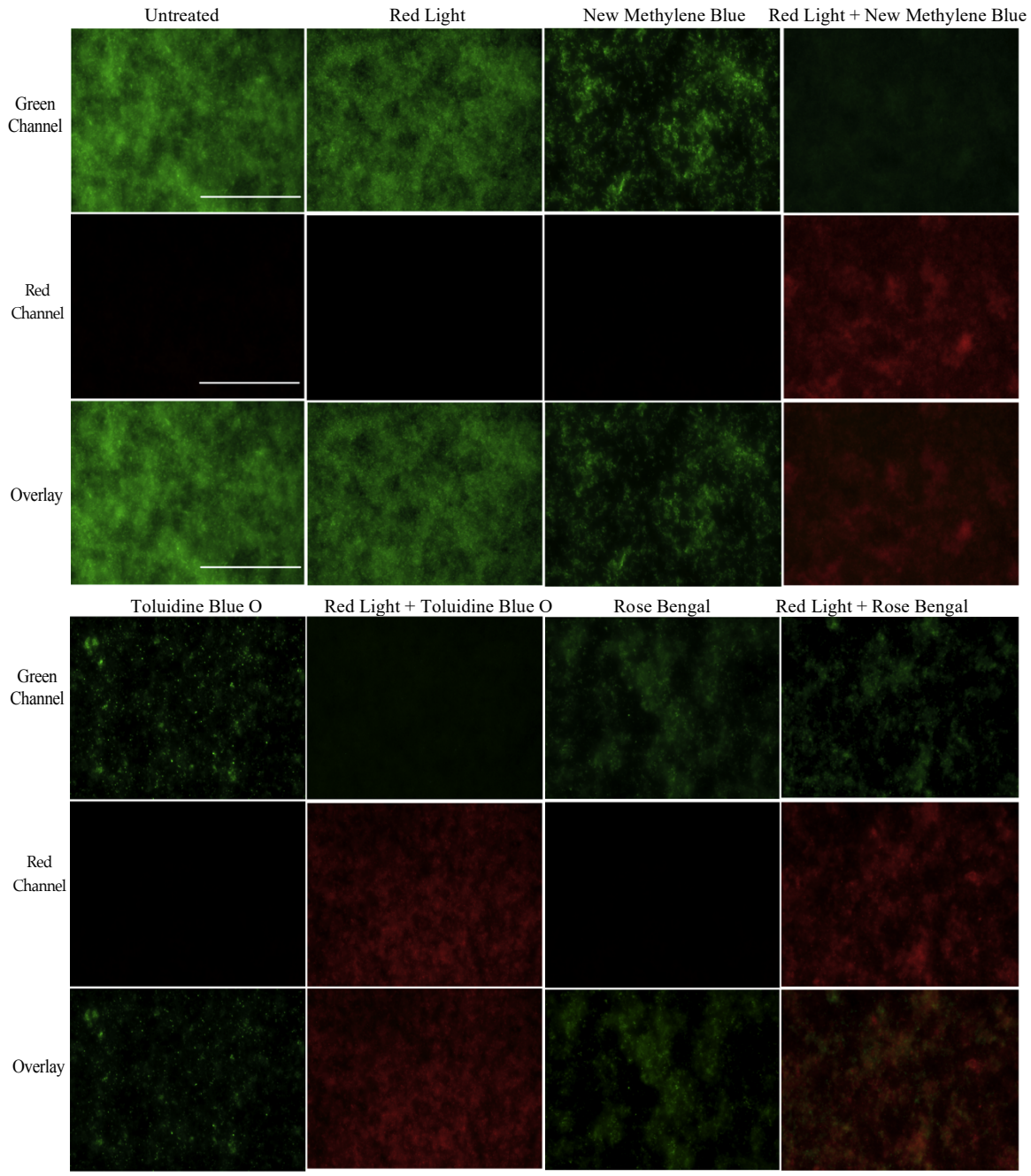

Figure S4.6. Red visible light in combination with photosensitizing compounds is effective at reducing the cell viability of *C. auris* biofilms disruption biofilm assay. The viability of *C. auris* (AR0383) biofilms was assessed using the LIVE/DEAD *Bac*Light viability kit, where green fluorescence indicates live cells, and red fluorescence indicates dead cells. The samples were imaged by fluorescence microscopy at 20X magnification with a green laser (GFP/green channel) shown in the top panels, a red laser (Texas Red/red

channel) shown in the middle panels, and overlayed shown in the bottom panels for each set of images. Representative images are shown for the untreated control (Untreated), red light alone (Red Light), new methylene blue photosensitizing compound alone (New Methylene Blue), red light in combination with new methylene blue photosensitizing compound (Red Light + New Methylene Blue), toluidine blue O photosensitizing compound alone (Toluidine Blue O), red light in combination with toluidine blue O photosensitizing compound (Red Light + Toluidine Blue O), rose bengal photosensitizing compound alone (Rose Bengal) and red light in combination with rose bengal photosensitizing compound (Red Light + Rose Bengal). Scale bars represent 200μm.

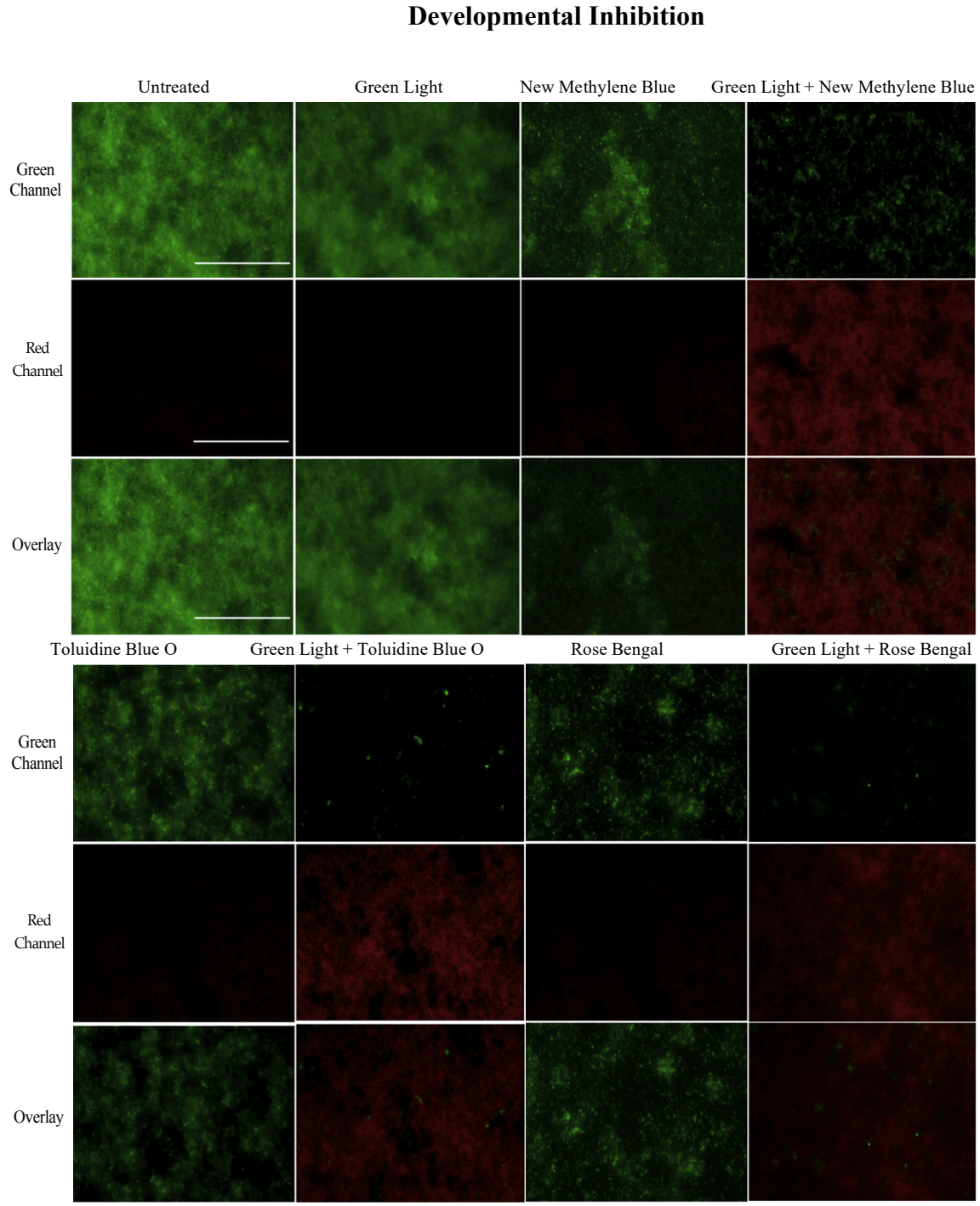

Figure S4.7. Green visible light visible light in combination with photosensitizing compounds is effective at reducing the cell viability of *C. auris* biofilms in the developmental inhibition biofilm assay. The viability of *C. auris* (AR0383) biofilms was assessed using the LIVE/DEAD *Bac*Light viability kit, where green fluorescence indicates live cells, and red fluorescence indicates dead cells. The samples were imaged by fluorescence microscopy at 20X magnification with a green laser (GFP/green channel)

shown in the top panels, a red laser (Texas Red/red channel) shown in the middle panels, and overlayed shown in the bottom panels for each set of images. Representative images are shown for the untreated control (Untreated), green light alone (Green Light), new methylene blue photosensitizing compound alone (New Methylene Blue), green light in combination with new methylene blue photosensitizing compound (Green Light + New Methylene Blue), toluidine blue O photosensitizing compound alone (Toluidine Blue O), green light in combination with toluidine blue O photosensitizing compound (Green Light + Toluidine Blue O), rose bengal photosensitizing compound alone (Rose Bengal) and green light in combination with rose bengal photosensitizing compound (Green Light + Rose Bengal). Scale bars represent 200μm.

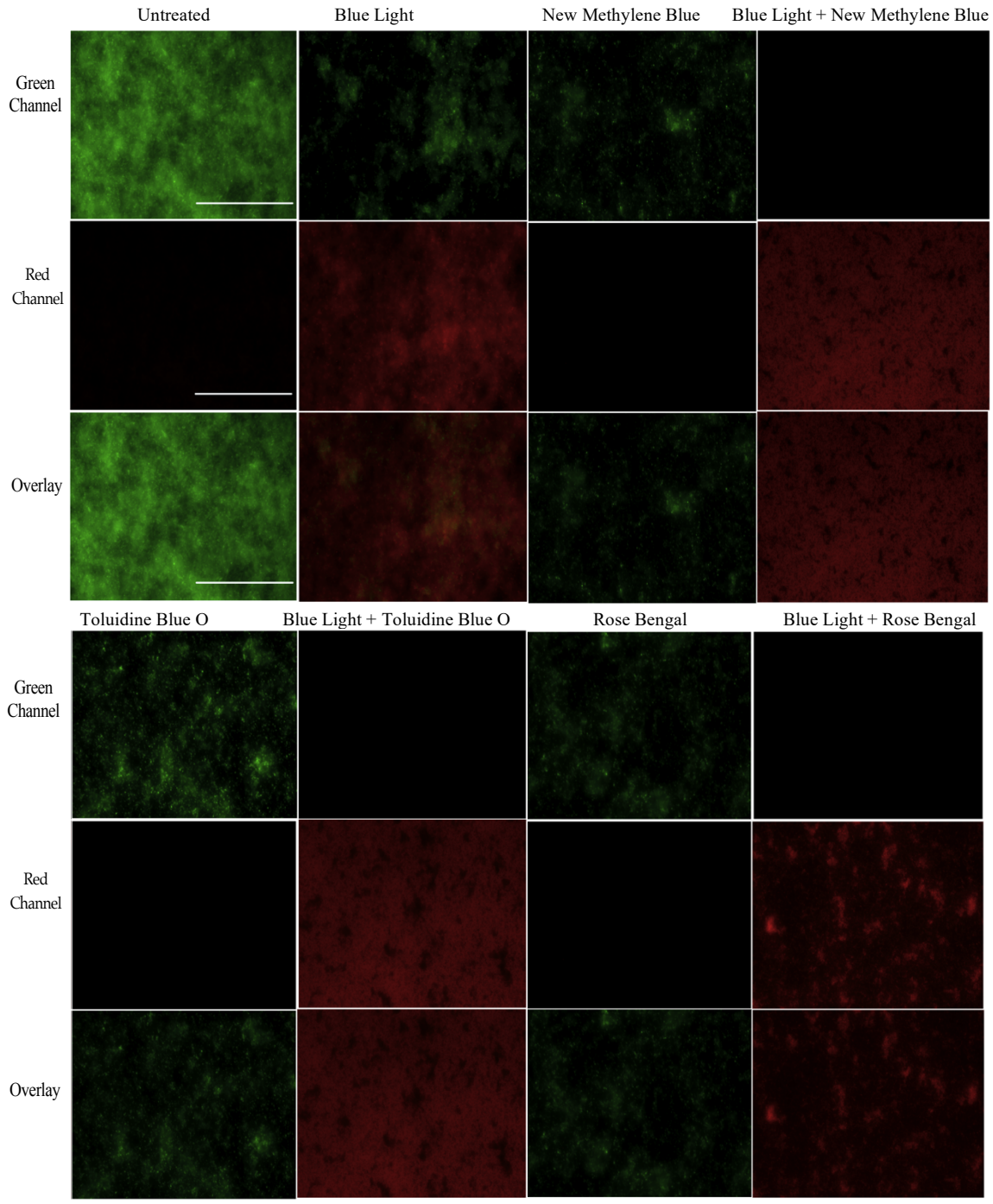

Figure S4.8. Blue visible light in combination with photosensitizing compounds is effective at reducing the cell viability of *C. auris* biofilms in the developmental inhibition biofilm assay. The viability of *C. auris* (AR0383) biofilms was assessed using

the LIVE/DEAD *Bac*Light viability kit, where green fluorescence indicates live cells, and red fluorescence indicates dead cells. The samples were imaged by fluorescence microscopy at 20X magnification with a green laser (GFP/green channel) shown in the top panels, a red laser (Texas Red/red channel) shown in the middle panels, and overlayed shown in the bottom panels for each set of images. Representative images are shown for the untreated control (Untreated), blue light alone (Blue Light), new methylene blue photosensitizing compound alone (New Methylene Blue), blue light in combination with new methylene blue photosensitizing compound (Blue Light + New Methylene Blue), toluidine blue O photosensitizing compound alone (Toluidine Blue O), blue light in combination with toluidine blue O photosensitizing compound (Blue Light + Toluidine Blue O), rose bengal photosensitizing compound alone (Rose Bengal) and blue light in combination with rose bengal photosensitizing compound (Blue Light + Rose Bengal). Scale bars represent 200μm.

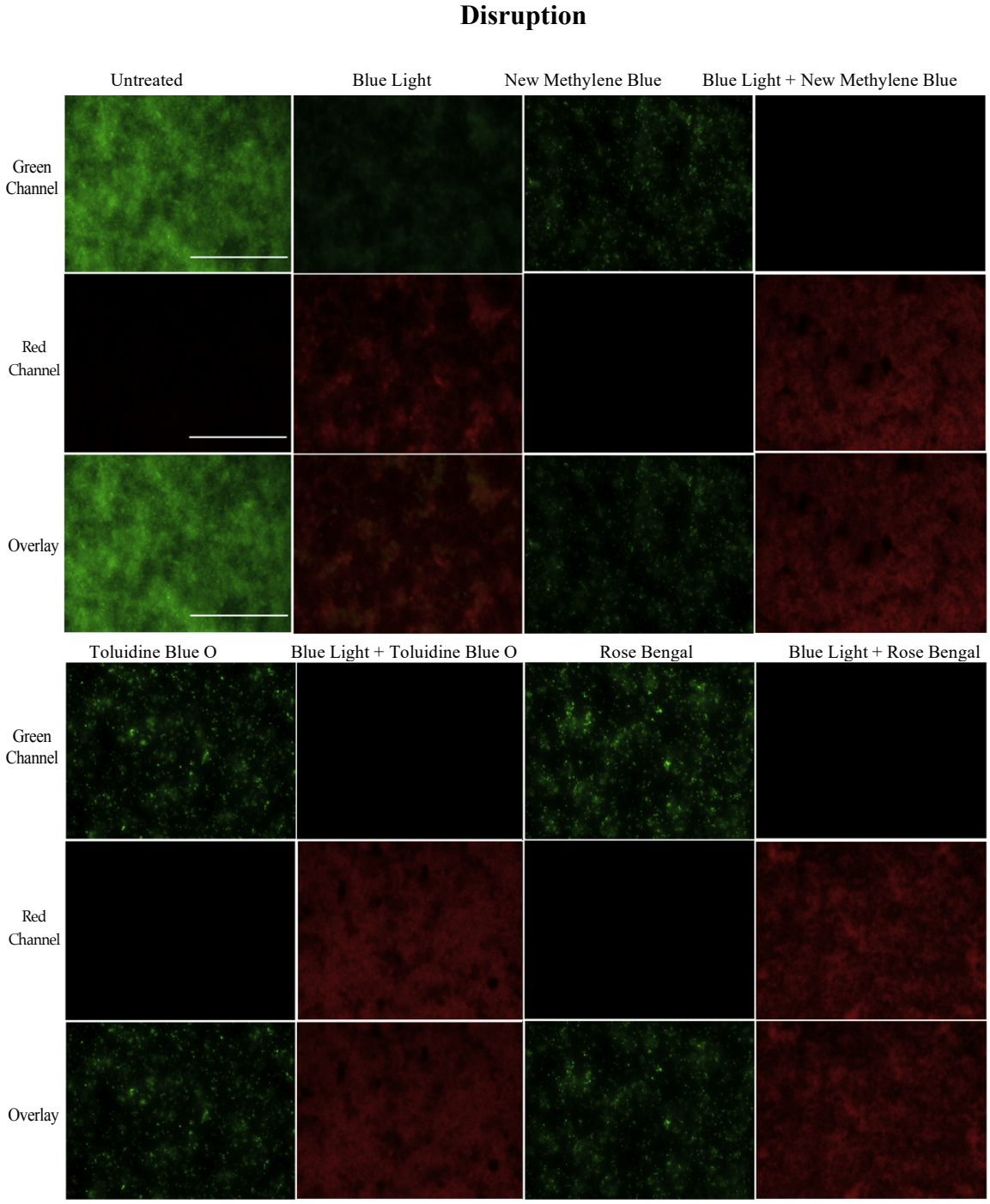

Figure S4.9. Blue visible light in combination with photosensitizing compounds is effective at reducing the cell viability of *C. auris* biofilms disruption biofilm assay. The viability of *C. auris* (AR0383) biofilms was assessed using the LIVE/DEAD *Bac*Light viability kit, where green fluorescence indicates live cells, and red fluorescence indicates dead cells. The samples were imaged by fluorescence microscopy at 20X magnification with a green laser (GFP/green channel) shown in the top panels, a red laser (Texas Red/red

channel) shown in the middle panels, and overlayed shown in the bottom panels for each set of images. Representative images are shown for the untreated control (Untreated), blue light alone (Blue Light), new methylene blue photosensitizing compound alone (New Methylene Blue), blue light in combination with new methylene blue photosensitizing compound (Blue Light + New Methylene Blue), toluidine blue O photosensitizing compound alone (Toluidine Blue O), blue light in combination with toluidine blue O photosensitizing compound (Blue Light + Toluidine Blue O), rose bengal photosensitizing compound alone (Rose Bengal) and blue light in combination with rose bengal photosensitizing compound (Blue Light + Rose Bengal). Scale bars represent 200μm.

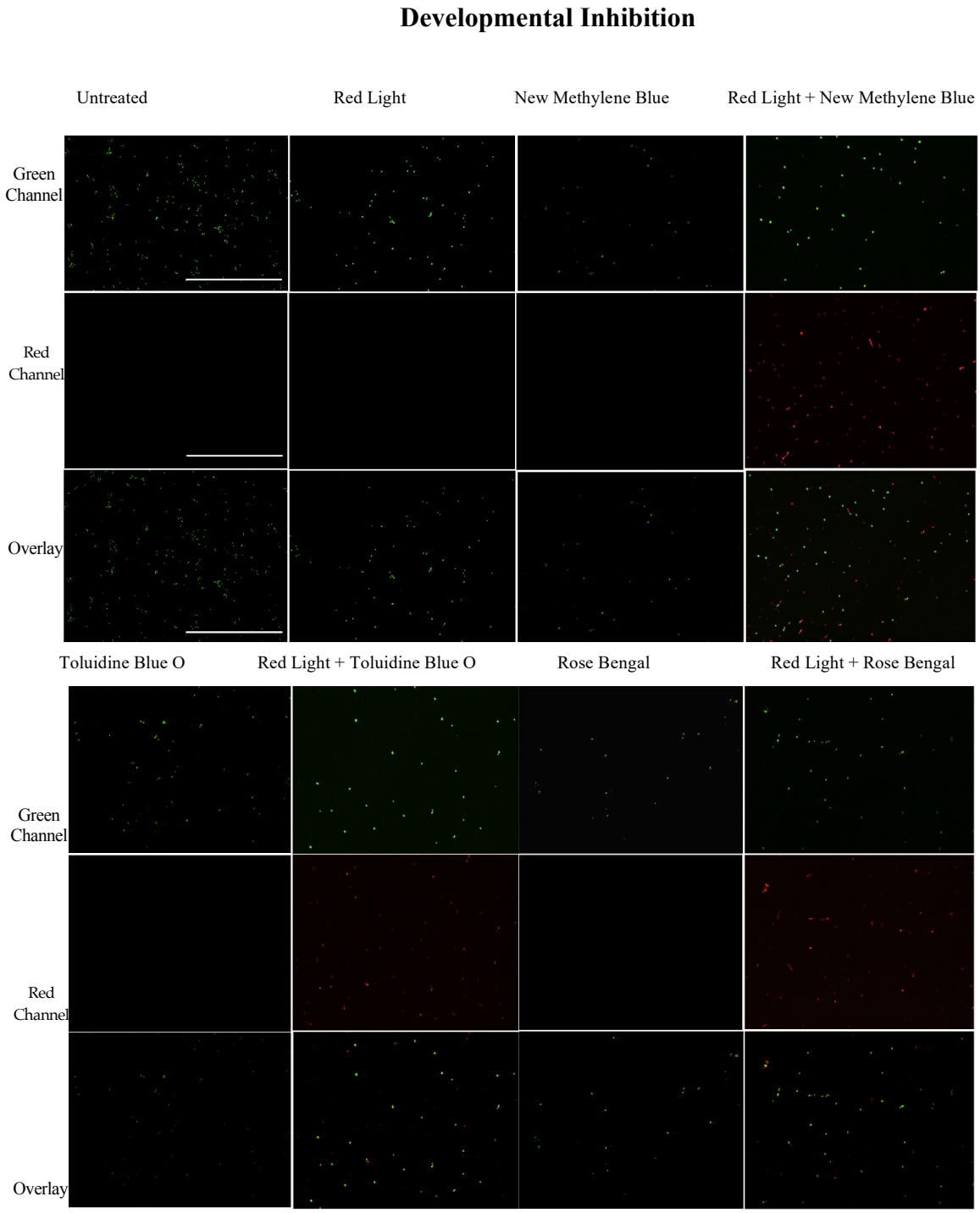

Figure S4.10. Red visible light in combination with photosensitizing compounds is effective at reducing the cell viability of cells resuspended from C. *auris* biofilms in the developmental inhibition biofilm assay. The viability of *C. auris* (AR0383) cells resuspended from biofilms was assessed using the LIVE/DEAD *Bac*Light viability kit, where green fluorescence indicates live cells, and red fluorescence indicates dead cells. The samples were imaged by fluorescence microscopy at 20X magnification with a green

laser (GFP/green channel) shown in the top panels, a red laser (Texas Red/red channel) shown in the middle panels, and overlayed shown in the bottom panels for each set of images. Representative images are shown for the untreated control (Untreated), red light alone (Red Light), new methylene blue photosensitizing compound alone (New Methylene Blue), red light in combination with new methylene blue photosensitizing compound (Red Light + New Methylene Blue), toluidine blue O photosensitizing compound alone (Toluidine Blue O), red light in combination with toluidine blue O photosensitizing compound (Red Light + Toluidine Blue O), rose bengal photosensitizing compound alone (Rose Bengal) and red light in combination with rose bengal photosensitizing compound (Red Light + Rose Bengal). Scale bars represent 200μm.

Disruption

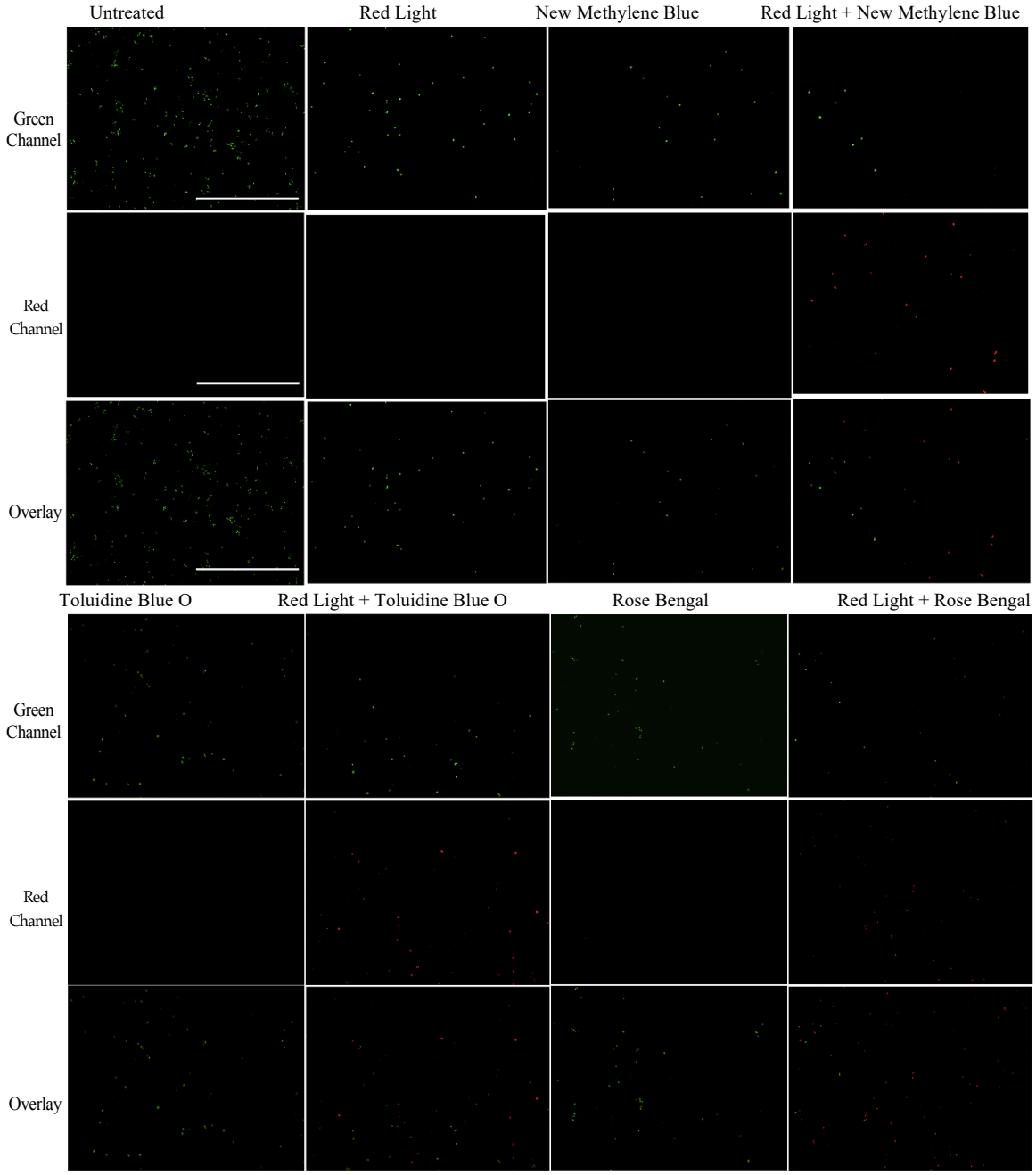

Figure S4.11. Red visible light in combination with photosensitizing compounds is effective at reducing the cell viability of cells resuspended from C. *auris* biofilms in the disruption biofilm assay. The viability of *C. auris* (AR0383) cells resuspended from biofilms was assessed using the LIVE/DEAD *Bac*Light viability kit, where green fluorescence indicates live cells, and red fluorescence indicates dead cells. The samples were imaged by fluorescence microscopy at 20X magnification with a green laser

(GFP/green channel) shown in the top panels, a red laser (Texas Red/red channel) shown in the middle panels, and overlayed shown in the bottom panels for each set of images. Representative images are shown for the untreated control (Untreated), red light alone (Red Light), new methylene blue photosensitizing compound alone (New Methylene Blue), red light in combination with new methylene blue photosensitizing compound (Red Light + New Methylene Blue), toluidine blue O photosensitizing compound alone (Toluidine Blue O), red light in combination with toluidine blue O photosensitizing compound (Red Light + Toluidine Blue O), rose bengal photosensitizing compound alone (Rose Bengal) and red light in combination with rose bengal photosensitizing compound (Red Light + Rose Bengal). Scale bars represent 200μm.

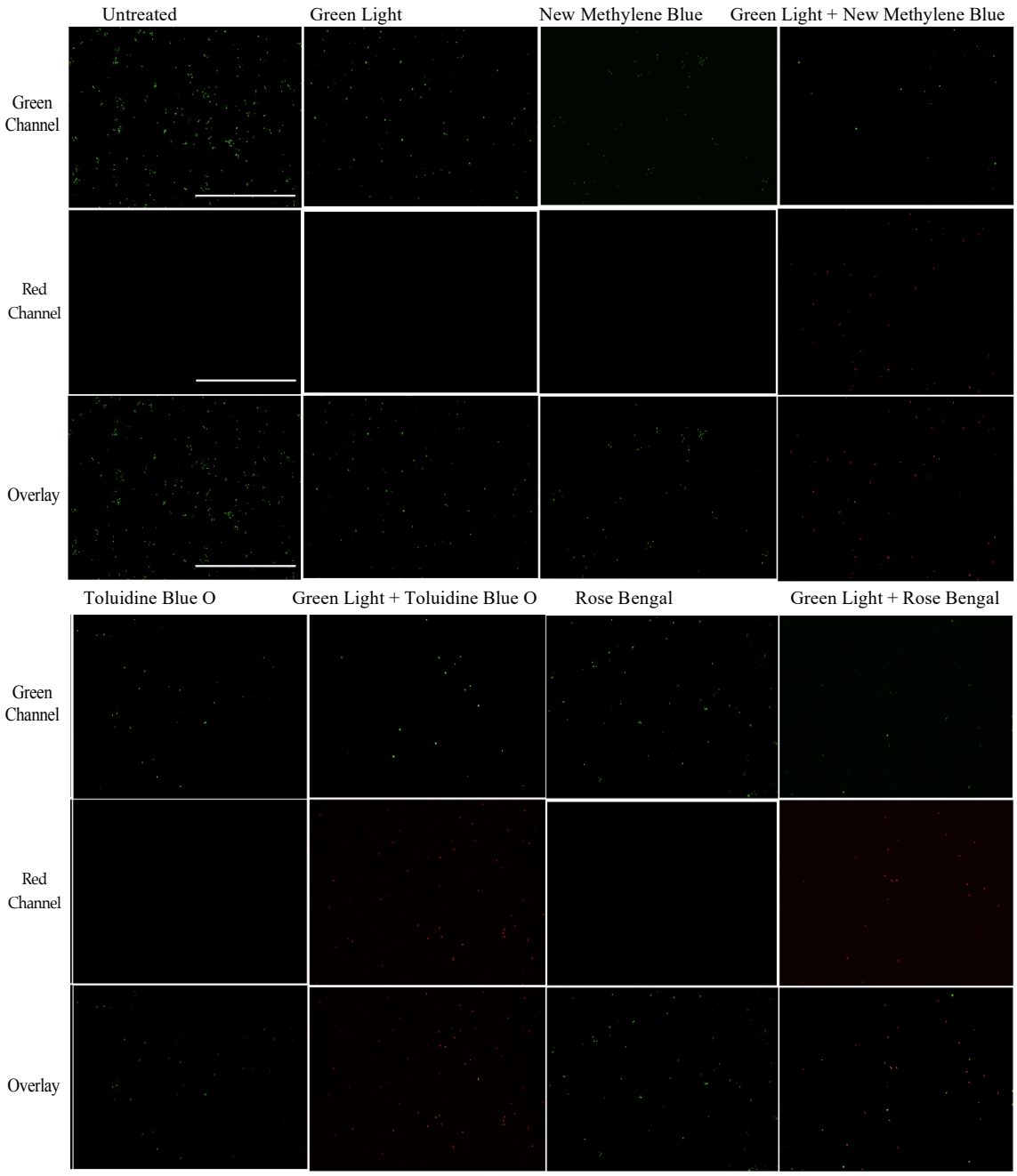

Figure S4.12. Green visible light in combination with photosensitizing compounds is effective at reducing the cell viability of cells resuspended from C. *auris* biofilms in the developmental inhibition biofilm assay. The viability of *C. auris* (AR0383) cells resuspended from biofilms was assessed using LIVE/DEAD *Bac*Light viability kit, where

green fluorescence indicates live cells, and red fluorescence indicates dead cells. The samples were imaged by fluorescence microscopy at 20X magnification with a green laser (GFP/green channel) shown in the top panels, a red laser (Texas Red/red channel) shown in the middle panels, and overlayed shown in the bottom panels for each set of images. Representative images are shown for the untreated control (Untreated), green light alone (Green Light), new methylene blue photosensitizing compound alone (New Methylene Blue), green light in combination with new methylene blue photosensitizing compound (Green Light + New Methylene Blue), toluidine blue O photosensitizing compound alone (Toluidine Blue O), green light in combination with toluidine blue O photosensitizing compound (Green Light + Toluidine Blue O), rose bengal photosensitizing compound alone (Rose Bengal) and green light in combination with rose bengal photosensitizing compound (Green Light + Rose Bengal). Scale bars represent 200μm.

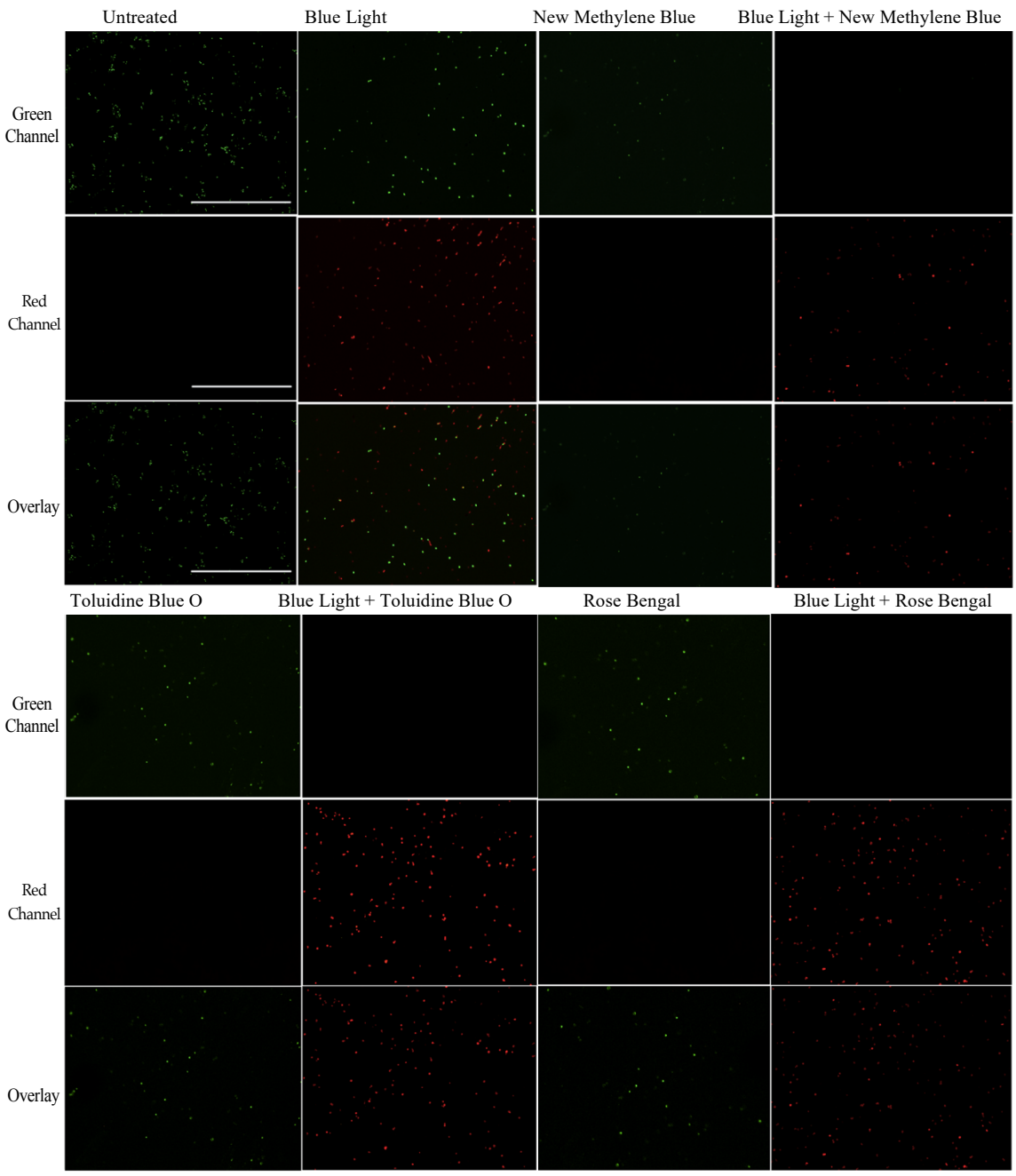

Figure S4.13. Blue visible light in combination with photosensitizing compounds is effective at reducing the cell viability of cells resuspended from C. *auris* biofilms in the developmental inhibition biofilm assay. The viability of *C. auris* (AR0383) cells resuspended from biofilms was assessed using the LIVE/DEAD *Bac*Light viability kit, where green fluorescence indicates live cells, and red fluorescence indicates dead cells. The samples were imaged by fluorescence microscopy at 20X magnification with a green

laser (GFP/green channel) shown in the top panels, a red laser (Texas Red/red channel) shown in the middle panels, and overlayed shown in the bottom panels. Representative images are shown for the untreated control (Untreated), blue light alone (Blue Light), new methylene blue photosensitizing compound alone (New Methylene Blue), blue light in combination with new methylene blue photosensitizing compound (Blue Light + New Methylene Blue), toluidine blue O photosensitizing compound alone (Toluidine Blue O), blue light in combination with toluidine blue O photosensitizing compound (Blue Light + Toluidine Blue O), rose bengal photosensitizing compound alone (Rose Bengal) and blue light in combination with rose bengal photosensitizing compound (Blue Light + Rose Bengal). Scale bars represent 200μm.

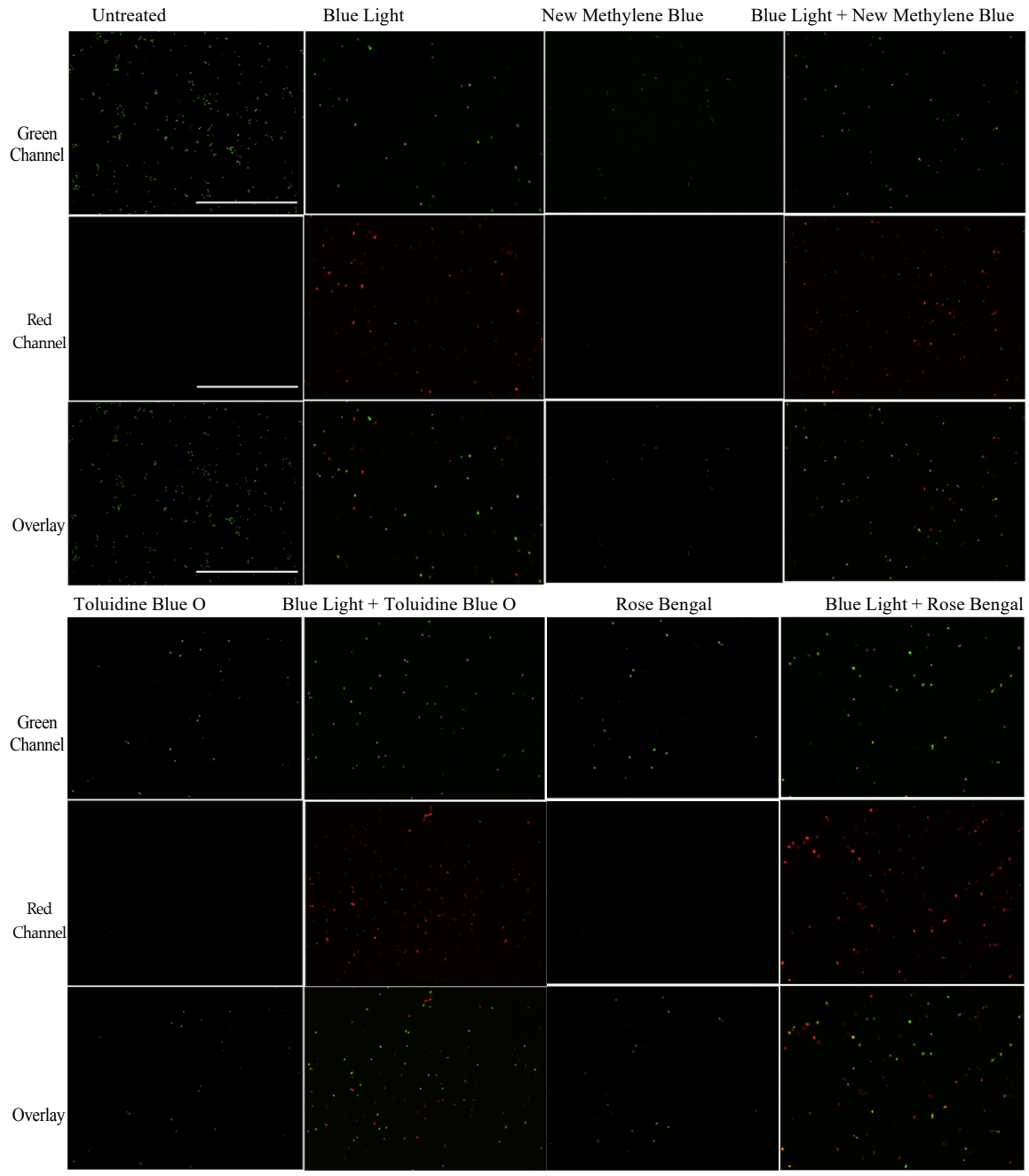

Figure S4.14. Blue visible light in combination with photosensitizing compounds is effective at reducing the cell viability of cells resuspended from C. *auris* biofilms in the disrutpion biofilm assay. The viability of *C. auris* (AR0383) cells resuspended from biofilms was assessed using the LIVE/DEAD *Bac*Light viability kit, where green fluorescence indicates live cells, and red fluorescence indicates dead cells. The samples

were imaged by fluorescence microscopy at 20X magnification with a green laser (GFP/green channel) shown in the top panels, a red laser (Texas Red/red channel) shown in the middle panels, and overlayed shown in the bottom panels for each set of images. Representative images are shown for the untreated control (Untreated), blue light alone (Blue Light), new methylene blue photosensitizing compound alone (New Methylene Blue), blue light in combination with new methylene blue photosensitizing compound (Blue Light + New Methylene Blue), toluidine blue O photosensitizing compound alone (Toluidine Blue O), blue light in combination with toluidine blue O photosensitizing compound (Blue Light + Toluidine Blue O), rose bengal photosensitizing compound alone (Rose Bengal) and blue light in combination with rose bengal photosensitizing compound (Blue Light + Rose Bengal). Scale bars represent 200μm.

Table S4.1: **Reported MICs for the *C. auris* strains used in this study.**

	AR Bank Isolate, Clade, and MICs (μg/mL) [#]		
Antifungal drugs	AR0383 (South Africa)	AR0389 (South Asia)	AR0390 (South Asia)
Amphotericin B	0.38	4	4
Fluconazole	128	256	>256
Caspofungin	0.25	0.5	0.5

[#]MICs were reported in Lockhart *et al*., 2017; and https://www.cdc.gov/fungal/candida-auris/c-auris-antifungal.html/; accessed on 05/07/2021.

4.7 References

1. Brown, G.D.; Denning, D.W.; Gow, N.A.R.; Levitz, S.M.; Netea, M.G.; White, T.C. Hidden killers: Human fungal infections. *Sci. Transl. Med.* 2012, *4*, 165rv13-165rv13.

2. Odds, F.C.; Brown, A.J.P.; Gow, N.A.R. Antifungal agents: Mechanisms of action. *Trends Microbiol.* **2003**, *11*, 272–279.

3. Prasad, R.; Shah, A.H.; Rawal, M.K.; Prasad, R.; Shah, A.H.; Rawal, M.K. Mechanism of Action and Drug Resistance. In *Yeast Membrane Transport. Advances in Experimental Medicine and Biology*; 2016; Vol. 892.

4. Satoh, K.; Makimura, K.; Hasumi, Y.; Nishiyama, Y.; Uchida, K.; Yamaguchi, H. *Candida auris* sp. nov., a novel ascomycetous yeast isolated from the external ear canal of an inpatient in a Japanese hospital. *Microbiol. Immunol.* **2009**, *53*, 41–44.

5. Saris, K.; Meis, J.F.; Voss, A. *Candida auris*. *Curr. Opin. Infect. Dis.* **2018**, *31*, 334–340.

6. Welsh, R.M.; Bentz, M.L.; Shams, A.; Houston, H.; Lyons, A.; Rose, L.J.; Litvintseva, A.P. Survival, Persistence, and Isolation of the Emerging Multidrug-Resistant Pathogenic Yeast *Candida auris* on a Plastic Health Care Surface. *J.*

Clin. Microbiol. **2017**, *55*, 2996–3005.

7. Horton, M. V; Nett, J.E. *Candida auris* infection and biofilm formation: Going beyond the surface. *Curr. Clin. Microbiol. Reports* **2020**, *7*, 51–56.

8. Adams, E.; Quinn, M.; Tsay, S.; Poirot, E.; Chaturvedi, S.; Southwick, K.; Greenko, J.; Fernandez, R.; Kallen, A.; Vallabhaneni, S.; et al. *Candida auris* in healthcare facilities, New York, USA, 2013–2017. *Emerg. Infect. Dis.* **2018**, *24*, 1816–1824.

9. Calvo, B.; Melo, A.S.A.; Perozo-Mena, A.; Hernandez, M.; Francisco, E.C.; Hagen, F.; Meis, J.F.; Colombo, A.L. First report of *Candida auris* in America: Clinical and microbiological aspects of 18 episodes of candidemia. *J. Infect.* **2016**, *73*, 369–374.

10. Borman, A.M.; Szekely, A.; Johnson, E.M. Comparative pathogenicity of United Kingdom isolates of the emerging pathogen *Candida auris* and other key pathogenic *Candida* Species. *mSphere* **2016**, *1*.

11. Morales-López, S.E.; Parra-Giraldo, C.M.; Ceballos-Garzón, A.; Martínez, H.P.; Rodríguez, G.J.; Álvarez-Moreno, C.A.; Rodríguez, J.Y. Invasive infections with multidrug-resistant yeast *Candida auris*, Colombia. *Emerg. Infect. Dis.* 2017, *23*, 162–164.

12. Cortegiani, A.; Misseri, G.; Fasciana, T.; Giammanco, A.; Giarratano, A.; Chowdhary, A. Epidemiology, clinical characteristics, resistance, and treatment of infections by *Candida auris*. *J. Intensive Care* 2018, *6*.

13. Spivak, E.S.; Hanson, K.E. *Candida auris*: an emerging fungal pathogen. *J. Clin. Microbiol.* **2018**, *56*, e01588-17.

14. Osei Sekyere, J. *Candida auris*: A systematic review and meta-analysis of current updates on an emerging multidrug-resistant pathogen. *Microbiologyopen* **2018**, *7*.

15. Chakrabarti, A.; Singh, S. Multidrug-resistant *Candida auris*: an epidemiological review. *Expert Rev. Anti-infective Ther.* **2020**, *18*, 551–562.

16. Shastri, P.S.; Shankarnarayan, S.A.; Oberoi, J.; Rudramurthy, S.M.; Wattal, C.; Chakrabarti, A. *Candida auris* candidaemia in an intensive care unit – Prospective observational study to evaluate epidemiology, risk factors, and outcome. *J. Crit. Care* **2020**, *57*, 42–48.

17. Garcia-Bustos, V.; Salavert, M.; Ruiz-Gaitán, A.C.; Cabañero-Navalon, M.D.; Sigona-Giangreco, I.A.; Pemán, J. A clinical predictive model of candidaemia by *Candida auris* in previously colonized critically ill patients. *Clin. Microbiol. Infect.* **2020**, *26*, 1507–1513.

18. Forsberg, K.; Woodworth, K.; Walters, M.; Berkow, E.L.; Jackson, B.; Chiller, T.;

Vallabhaneni, S. *Candida auris*: The recent emergence of a multidrug-resistant fungal pathogen. *Med. Mycol.* **2019**, *57*, 1–12.

19. Cortegiani, A.; Misseri, G.; Giarratano, A.; Bassetti, M.; Eyre, D. The global challenge of *Candida auris* in the intensive care unit. *Crit. Care* **2019**, *23*, 4–6.

20. Eyre, D.W.; Sheppard, A.E.; Madder, H.; Moir, I.; Moroney, R.; Quan, T.P.; Griffiths, D.; George, S.; Butcher, L.; Morgan, M.; et al. A *Candida auris* Outbreak and Its Control in an Intensive Care Setting. *N. Engl. J. Med.* **2018**, *379*, 1322–1331.

21. Lockhart, S.R.; Etienne, K.A.; Vallabhaneni, S.; Farooqi, J.; Chowdhary, A.; Govender, N.P.; Colombo, A.L.; Calvo, B.; Cuomo, C.A.; Desjardins, C.A.; et al. Simultaneous emergence of multidrug-resistant *Candida auris* on 3 continents confirmed by whole-genome sequencing and epidemiological analyses. *Clin. Infect. Dis.* **2017**, *64*, 134–140.

22. Kean, R.; Delaney, C.; Sherry, L.; Borman, A.; Johnson, E.M.; Richardson, M.D.; Rautemaa-Richardson, R.; Williams, C.; Ramage, G. Transcriptome Assembly and Profiling of *Candida auris* Reveals Novel Insights into Biofilm-Mediated Resistance. *mSphere* **2018**, *3*.

23. Chaabane, F.; Graf, A.; Jequier, L. Review on antifungal resistance mechanisms in the emerging pathogen *Candida auris*. *Front. Microbiol.* **2019**, *10*, 1–8.

24. Dominguez, E.G.; Zarnowski, R.; Choy, H.L.; Zhao, M.; Sanchez, H.; Nett, J.E.; Andes, D.R. Conserved role for biofilm matrix polysaccharides in *Candida auris* drug resistance. *mSphere* **2019**, *4:e00680–1*, e00680-18.

25. Bravo Ruiz, G.; Lorenz, A. What do we know about the biology of the emerging fungal pathogen of humans *Candida auris* ? *Microbiol. Res.* **2021**, *242*, 126621.

26. Piedrahita, C.T.; Cadnum, J.L.; Jencson, A.L.; Shaikh, A.A.; Ghannoum, M.A.; Donskey, C.J. Environmental surfaces in healthcare facilities are a potential source for transmission of *Candida auris* and other *Candida* species. *Infect. Control Hosp. Epidemiol.* **2017**, *38*, 1107–1109.

27. Villanueva-Lozano, H.; Treviño-Rangel, R. de J.; González, G.M.; Ramírez-Elizondo, M.T.; Lara-Medrano, R.; Aleman-Bocanegra, M.C.; Guajardo-Lara, C.E.; Gaona-Chávez, N.; Castilleja-Leal, F.; Torre-Amione, G.; et al. Outbreak of *Candida auris* infection in a COVID-19 hospital in Mexico. *Clin. Microbiol. Infect.* 2021.

28. Chowdhary, A.; Tarai, B.; Singh, A.; Sharma Amit Multidrug-resistant *Candida auris* infections in critically ill Coronavirus disease patients, India, April-July 2020. *Emerg. Infect. Dis.* **2020**, *26*.

29. Steele, E.J.; Gorczynski, R.M.; Lindley, R.A.; Tokoro, G.; Temple, R.; Chandra

Wickramasinghe, N.; O'connor, C.Y. Origin of new emergent Coronavirus and *Candida* fungal diseases-Terrestrial or cosmic? In *Advances in Genetics*; 2020; Vol. 106, pp. 75–100.

30. Zuo, T.; Zhan, H.; Zhang, F.; Liu, Q.; Tso, E.Y.K.; Lui, G.C.Y.; Chen, N.; Li, A.; Lu, W.; Chan, F.K.L.; et al. Alterations in fecal fungal microbiome of patients With COVID-19 during time of hospitalization until discharge. *Gastroenterology* **2020**, *159*, 1302–1310.

31. Allaw, F.; Kara Zahreddine, N.; Ibrahim, A.; Tannous, J.; Taleb, H.; Rahman Bizri, A.; Dbaibo, G.; Kanj, S.S. First *Candida auris* outbreak during a COVID-19 pandemic in a tertiary-care center in Lebanon. *Pathogens* **2021**, *10*.

32. De Almeida, J.N.; Francisco, E.C.; Hagen, F.; Brandão, I.B.; Pereira, F.M.; Dias, P.H.P.; De Miranda Costa, M.M.; De Souza Jordão, R.T.; De Groot, T.; Colombo, A.L.; et al. Emergence of *Candida auris* in Brazil in a COVID-19 Intensive Care Unit. *J. Fungi* **2021**, *7*.

33. Rodriguez, J.Y.; Le Pape, P.; Lopez, O.; Esquea, K.; Labiosa, A.L.; Moreno-Alvarez, C. *Candida auris*: A latent threat to critically III patients with Coronavirus disease 2019. *Clin. Infect. Dis. Corresp.* **2020**.

34. Magnasco, L.; Mikulska, M.; Giacobbe, D.R.; Taramasso, L.; Vena, A.; Dentone, C.; Dettori, S.; Tutino, S.; Labate, L.; Di Pilato, V.; et al. Spread of carbapenem-resistant gram-negatives and *Candida auris* during the covid-19 pandemic in critically ill patients: One step back in antimicrobial stewardship? *Microorganisms* **2021**, *9*, 1–10.

35. Prestel, C.; Anderson, E.; Forsberg, K.; Lyman, M.; de Perio, M.A.; Kuhar, D.; Edwards, K.; Rivera, M.; Shugart, A.; Walters, M.; et al. *Candida auris* Outbreak in a COVID-19 Specialty Care Unit — Florida, July–August 2020. *MMWR. Morb. Mortal. Wkly. Rep.* **2021**, *70*, 56–57.

36. Chowdhary, A.; Sharma, A. The lurking scourge of multidrug resistant *Candida auris* in times of COVID-19 pandemic. *J. Glob. Antimicrob. Resist.* **2020**, *22*, 175–176.

37. Kolter, R.; Greenberg, E.P. The superficial life of microbes. *Nature* **2006**, *441*, 300–302.

38. López, D.; Vlamakis, H.; Kolter, R. Biofilms. *Cold Spring Harb. Perspect. Biol.* **2010**, *2*.

39. Sherry, L.; Ramage, G.; Kean, R.; Borman, A.; Johnson, E.M.; Richardson, M.D.; Rautemaa-Richardson, R. Biofilm-forming capability of highly virulent, multidrug-resistant *Candida auris*. *Emerg. Infect. Dis.* **2017**, *23*, 328–331.

40. Romera, D.; Aguilera-Correa, J.J.; Gadea, I.; Viñuela-Sandoval, L.; García-

Rodríguez, J.; Esteban, J. *Candida auris* : a comparison between planktonic and biofilm susceptibility to antifungal drugs. *J. Med. Microbiol.* **2019**, *68*, 1353–1358.

41. Larkin, E.; Hager, C.; Chandra, J.; Mukherjee, P.K.; Retuerto, M.; Salem, I.; Long, L.; Isham, N.; Kovanda, L.; Borroto-Esoda, K.; et al. The emerging pathogen *Candida auris*: Growth phenotype, virulence factors, activity of antifungals, and effect of SCY-078, a novel glucan synthesis inhibitor, on growth morphology and biofilm formation. *Antimicrob. Agents Chemother.* **2017**, *61*.

42. Kim, M.; Jung, Y.; Park, H.J. Topical PDT in the treatment of benign skin diseases: Principles and new applications. *Int. J. Mol. Sci.* **2015**, *16*, 23259–23278.

43. Cohen, D.K.; Lee, P.K.; Hamblin, M.R. Photodynamic therapy for non-melanoma skin cancers. *Cancers (Basel).* **2016**, *88*.

44. Agostinis, P.; Berg, K.; Cengel, K.A.; Foster, T.H.; Girotti, A.W.; Gollnick, S.O.; Hahn, S.M.; Hamblin, M.R.; Juzeniene, A.; Kessel, D.; et al. Photodynamic therapy of cancer: An update. *CA. Cancer J. Clin.* **2011**, *61*, 250–281.

45. Cieplik, F.; Deng, D.; Crielaard, W.; Buchalla, W.; Hellwig, E.; Al-Ahmad, A.; Maisch, T. Antimicrobial photodynamic therapy – what we know and what we don't. *Crit. Rev. Microbiol.* **2018**, *44*, 571–589.

46. Wainwright, M.; Maisch, T.; Nonell, S.; Plaetzer, K.; Almeida, A.; Tegos, G.P.; Hamblin, M.R. Photoantimicrobials—are we afraid of the light? *Lancet Infect. Dis.* 2017, *17*, e49–e55.

47. Hamblin, M.R.; Hasan, T. Photodynamic therapy: A new antimicrobial approach to infectious disease? *Photochem. Photobiol. Sci.* **2004**, *3*, 436–450.

48. Wainwright, M.; Phoenix, D.; Laycock, S.; Wareing, D.; Wright, P. Photobactericidal activity of phenothiazinium dyes against methicillin-resistant strains of *Staphylococcus aureus*. *FEMS Microbiol. Lett.* **1998**, *160*, 177–181.

49. Denis, T.G. St.; Dai, T.; Izikson, L.; Astrakas, C.; Anderson, R.R.; Hamblin, M.R.; Tegos, G.P. All you need is light. *Virulence* **2011**, *2*, 509–520.

50. Lyon, J.P.; Moreira, L.M.; de Moraes, P.C.G.; dos Santos, F.V.; de Resende, M.A. Photodynamic therapy for pathogenic fungi. *Mycoses* **2011**, *54*.

51. Vatansever, F.; de Melo, W.C.M.A.; Avci, P.; Vecchio, D.; Sadasivam, M.; Gupta, A.; Chandran, R.; Karimi, M.; Parizotto, N.A.; Yin, R.; et al. Antimicrobial strategies centered around reactive oxygen species - bactericidal antibiotics, photodynamic therapy, and beyond. *FEMS Microbiol. Rev.* 2013, *37*, 955–989.

52. Gwynne, P.J.; Gallagher, M.P. Light as a broad-spectrum antimicrobial. *Antimicrob. Front Microbiol* **2018**, *9*.

53. Bruno, J.T.; Svoronos, P. *CRC Handbook of Fundamental Spectroscopic Correlation Charts*; 2006;

54. Dai, T.; Gupta, A.; Huang, Y.-Y.; Sherwood, M.E.; Murray, C.K.; Vrahas, M.S.; Kielian, T.; Hamblin, M.R. Blue light eliminates community-acquired Methicillin-Resistant *Staphylococcus aureus* in infected mouse skin abrasions. *Photomed. Laser Surg.* **2013**, *31*, 531–538.

55. Ferrer-Espada, R.; Wang, Y.; Goh, X.S.; Dai, T. Antimicrobial blue light Inactivation of microbial isolates in biofilms. *Lasers Surg. Med.* **2019**, *52*, 472–478.

56. Moorhead, S.; Hons, B.; Maclean, M.; Macgregor, S.J.; Anderson, J.G. Comparative sensitivity of *Trichophyton* and *Aspergillus* conidia to inactivation by violet-blue light exposure. *Photomed. Laser Surg.* **2016**, *34*, 36–41.

57. Guffey, J.S.; Payne, W.; Buchanan, B.; Daugherty, J.; Meurer;, L.; Hensley, P. Susceptibility of *Trichophyton mentagrophytes* to visible light wavelengths. *Adv. Skin Wound Care* **2017**, *30*, 218–222.

58. Murdoch, L.E.; McKenzie, K.; Maclean, M.; MacGregor, S.J.; Anderson, J.G. Lethal effects of high-intensity violet 405-nm light on *Saccharomyces cerevisiae, Candida albicans*, and on dormant and germinating spores of *Aspergillus niger*. *Fungal Biol.* **2013**, *117*, 519–527.

59. Trzaska, W.J.; Wrigley, H.E.; Thwaite, J.E.; May, R.C. Species-specific antifungal activity of blue light. *Sci. Rep.* **2017**, *7*, 1–7.

60. Wang, Y.; Wang, Y.; Wang, Y.; Murray, C.K.; Hamblin, M.R.; Hooper, D.C.; Dai, T. Antimicrobial blue light inactivation of pathogenic microbes: State of the art. *Drug Resist. Updat.* **2017**, *33–35*, 1–22.

61. Halstead, F.D.; Thwaite, J.E.; Burt, R.; Laws, T.R.; Raguse, M.; Moeller, R.; Webber, M.A.; Oppenheim, B.A. Antibacterial activity of blue light against nosocomial wound pathogens growing planktonically and as mature biofilms. *Appl. Environ. Microbiol.* **2016**, *82*, 4006–4016.

62. Cieplik, F.; Tabenski, L.; Buchalla, W.; Maisch, T. Antimicrobial photodynamic therapy for inactivation of biofilms formed by oral key pathogens. *Front. Microbiol.* **2014**, *5*, 1–17.

63. Teixeira, N.; De Sousa, A.; Santos, M.F.; Gomes, R.C.; Brandino, H.E.; Martinez, R.; Roberto, R.; Guirro, J. Blue Laser Inhibits Bacterial Growth of *Staphylococcus aureus, Escherichia coli,* and *Pseudomonas aeruginosa*. *Photomed. Laser Ther.* **2015**, *33*, 278–282.

64. Zhang, Y.; Zhu, Y.; Chen, J.; Wang, Y.; Sherwood, M.E.; Murray, C.K.; Vrahas, M.S.; Hooper, D.C.; Hamblin, M.R.; Dai, T. Antimicrobial blue light inactivation

of *Candida albicans* : *In vitro* and *in vivo* studies. *Virulence* **2016**, *7*, 536–545.

65. Wang, C.; Yang, Z.; Peng, Y.; Guo, Y.; Yao, M.; Dong, J. Application of 460 nm visible light for the elimination of *Candida albicans in vitro* and *in vivo*. *Mol. Med. Rep.* **2018**, *18*, 2017–2026.

66. Dai, T. The antimicrobial effect of blue light: What are behind? *Virulence* **2017**, *8 (6)*, 649–652.

67. Pinto, A.P.; Rosseti, I.B.; Carvalho, M.L.; da Silva, B.G.M.; Alberto-Silva, C.; Costa, M.S.; Bueno Rosseti, I.; Lopes Carvalho, M.; Marques Da Silva, B.G.; Alberto-Silva, C.; et al. Photodynamic Antimicrobial Chemotherapy (PACT), using Toluidine blue O inhibits the viability of biofilm produced by *Candida albicans* at different stages of development. *Photodiagnosis Photodyn. Ther.* **2018**, *21*, 182–189.

68. Panariello, B.H.D.; Garcia, B.A.; Duarte, S. Daily phototherapy with red light to regulate *Candida albicans* biofilm growth. *J. Vis. Exp.* **2019**, e59326.

69. Huh, S.Y.; Na, J.I.; Huh, C.H.; Park, K.C. The effect of photodynamic therapy using indole-3-acetic acid and green light on *Acne vulgaris*. *Ann. Dermatol.* **2012**, *24*, 56–60.

70. Vural, E.; Winfield, H.L.; Shingleton, A.W.; Horn, T.D.; Shafirstein, G. The effects of laser irradiation on *Trichophyton rubrum* growth. *Lasers Med. Sci.* **2008**, *23*, 349–353.

71. Carvalho, G.G.; Felipe, M.P.; Costa, M.S. The photodynamic effect of methylene blue and toluidine blue on *Candida albicans* is dependent on medium conditions. *J. Microbiol.* **2009**, *47*, 619–623.

72. Romano, R.A.; Pratavieira, S.; Silva, A.P. d.; Kurachi, C.; Guimarães, F. Light-driven photosensitizer uptake increases *Candida albicans* photodynamic inactivation. *J. Biophotonics* **2017**, *10*, 1538–1546.

73. Bapat, P.; Singh, G.; Nobile, C.J. Visible lights combined with photosensitizing compounds are effective against *Candida albicans* biofilms. *Microorganisms* **2021**, *9*, 500.

74. Tan, J.; Liu, Z.; Sun, Y.; Yang, L.; Gao, L. Inhibitory effects of photodynamic Inactivation on planktonic cells and biofilms of *Candida auris*. *Mycopathologia* **2019**, *184*, 525–531.

75. Meyers, E.; Miraglia, G.J.; Smith, D.A.; Basch, H.; Pansy, F.E.; Trejo, W.H.; Donovick, R. Biological Characterization of Prasinomycin, a Phosphorus-containing Antibiotic. *Appl. Microbiol.* **1968**, *16*, 603–608.

76. Https://www.cdc.gov/fungal/candida-auris/c-auris-antifungal.html Antifungal

Susceptibility Testing and Interpretation | Candida auris | Fungal Diseases | CDC Available online: https://www.cdc.gov/fungal/candida-auris/c-auris-antifungal.html (accessed on Feb 5, 2021).

77. Gulati, M.; Lohse, M.B.; Ennis, C.L.; Gonzalez, R.E.; Perry, A.M.; Bapat, P.; Arevalo, A.V.; Rodriguez, D.L.; Nobile, C.J. In Vitro culturing and screening of *Candida albicans* biofilms. *Curr. Protoc. Microbiol.* **2018**, *50*.

78. Lohse, M.B.; Gulati, M.; Valle Arevalo, A.; Fishburn, A.; Johnson, A.D.; Nobile, C.J. Assessment and optimizations of *Candida albicans In Vitro* biofilm assays. *Antimicrob. Agents Chemother.* **2017**, *61*, e02749-16.

79. Jin, Y.; Zhang, T.; Samaranayake, Y.H.; Fang, H.H.P.; Yip, H.K.; Samaranayake, L.P. The use of new probes and stains for improved assessment of cell viability and extracellular polymeric substances in *Candida albicans* biofilms. *Mycopathologia* **2005**, *159*, 353–360.

80. Abrahamse, H.; Hamblin, M.R. New photosensitizers for photodynamic therapy. *Biochem. J* **2016**, *473*, 347–364.

81. Gulati, M.; Nobile, C.J. *Candida albicans* biofilms: development, regulation, and molecular mechanisms. *Microbes Infect.* **2016**, *18*, 310–321.

82. Zarnowski, R.; Westler, W.M.; Lacmbouh, G.A.; Marita, J.M.; Bothe, J.R.; Bernhardt, J.; Sahraoui, A.L.H.; Fontainei, J.; Sanchez, H.; Hatfeld, R.D.; et al. Novel entries in a fungal biofilm matrix encyclopedia. *MBio* **2014**, *5*, 1–13.

83. Mukherjee, P.K.; Chandra, J. *Candida* biofilms: development, architecture, and resistance. *Microbiol. Spectr.* **2015**, *3*, 1–24.

84. Nobile, C.J.; Johnson, A.D. *Candida albicans* biofilms and human disease. *Annu. Rev. Microbiol.* **2015**, *69*, 71–92.

85. Yan, L.; Xia, K.; Yu, Y.; Miliakos, A.; Chaturvedi, S.; Zhang, F.; Chen, S.; Chaturvedi, V.; Linhardt, R.J. Unique cell surface mannan of yeast pathogen *Candida auris* with selective binding to IgG. *ACS Infect. Dis* **2020**, *6*, 1018–1031.

86. Navarro-arias, M.J.; Hernández-chávez, M.J.; García-carnero, L.; Amezcua-hernández, D.; Lozoya-Pérez, N.; Estrada-Mata, E.; Martínez-Duncker, I.; Franco, B.; Mora-Montes, héctor M. Differential recognition of *Candida tropicalis*, *Candida guilliermondii*, *Candida krusei*, and *Candida auris* by human innate immune cells. *Infect. Drug Resist.* **2019**, *12*, 783–794.

87. Zamith-Miranda, D.; Heyman, H.M.; Cleare, L.G.; Couvillion, S.P.; Clair, G.C.; Bredeweg, E.L.; Gacser, A.; Nimrichter, L.; Nakayasu, E.S.; Nosanchuk, J.D. Multi-omics signature of *Candida auris* , an emerging and multidrug-resistant pathogen. *mSystems* **2019**, *4*.

88. Maisch, T. Resistance in antimicrobial photodynamic inactivation of bacteria. *Photochem. Photobiol. Sci.* **2015**, *14*, 1518–1526.

89. Jockusch, S.; Leet, D.; Turro, N.J.; Leonardt, E.F. *Photo-induced inactivation of viruses: Adsorption of methylene blue, thionine, and thiopyronine on QB bacteriophage bacteriophage*; 1996; Vol. 93;.

90. Carrera, E.T.; Dias, H.B.; Corbi, S.C.T.; Marcantonio, R.A.C.; Bernardi, A.C.A.; Bagnato, V.S.; Hamblin, M.R.; Rastelli, A.N.S. The application of antimicrobial photodynamic therapy (aPDT) in dentistry: A critical review. *Laser Phys.* **2016**, *26*.

91. De Lucca, A.J.; Carter-Wientjes, C.; Williams, K.A.; Bhatnagar, D. Blue light (470 nm) effectively inhibits bacterial and fungal growth. *Lett. Appl. Microbiol.* **2012**, *55*, 460–466.

92. Gardlo, K.; Horska, Z.; Enk, C.D.; Rauch, L.; Megahed, M.; Ruzicka, T.; Fritsch, C. Treatment of cutaneous leishmaniasis by photodynamic therapy. *J. Am. Acad. Dermatol.* **2003**, *48*, 893–896.

93. Kharkwal, G.B.; Sharma, S.K.; Huang, Y.Y.; Dai, T.; Hamblin, M.R. Photodynamic therapy for infections: Clinical applications. *Lasers Surg. Med.* **2011**, *43*, 755–767.

94. Wainwright, M. Photoinactivation of viruses. *Photochem Photobiol Sci* **2004**, *3*, 406–411.

95. Marotti, J.; Aranha, A.C.C.; Eduardo, C.D.P.; Ribeiro, M.S. Photodynamic therapy can be effective as a treatment for herpes simplex labialis. *Photomed. Laser Surg.* **2009**, *27*, 357–363.

96. Wiehe, A.; O'brien, J.M.; Senge, M.O. Trends and targets in antiviral phototherapy. *Photochem. Photobiol. Sci* **2019**, *18*, 2565.

97. Dias, L.D.; Bagnato, V.S. An update on clinical photodynamic therapy for fighting respiratory tract infections: A promising tool against COVID-19 and its co-infections. *Laser Phys. Lett.* **2020**, *17*.

98. Almeida, A.; Faustino, M.A.F.; Neves, M.G.P.M.S. Antimicrobial photodynamic therapy in the control of COVID-19. *Antibiotics* **2020**, *9*, 1–10.

99. Svyatchenko, V.A.; Nikonov, S.D.; Mayorov, A.P.; Gelfond, M.L.; Loktev, V.B. Antiviral photodynamic therapy: Inactivation and inhibition of SARS-CoV-2 *in vitro* using methylene blue and Radachlorin. *Photodiagnosis Photodyn. Ther.* **2021**, *33*.

100. Ostrowsky, B.; Greenko, J.; Adams, E.; Quinn, M.; O'Brien, B.; Chaturvedi, V.; Berkow, E.; Vallabhaneni, S.; Forsberg, K.; Chaturvedi, S.; et al. *Candida auris*

isolates resistant to three classes of antifungal medications — New York, 2019. *Morb. Mortal. Wkly. Rep.* **2020**, *69*, 6–9.

101. Roemer, T.; Krysan, D.J. Antifungal drug development: Challenges, unmet clinical needs, and new approaches. *Cold Spring Harb. Perspect. Med.* **2014**, *4*, 1–15.

102. Stokes, J.M.; Lopatkin, A.J.; Lobritz, M.A.; Collins, J.J. Bacterial Metabolism and Antibiotic Efficacy. *Cell Metab.* **2019**, *30*, 251–259.

103. Bojsen, R.; Regenberg, B.; Folkesson, A. *Saccharomyces cerevisiae* biofilm tolerance towards systemic antifungals depends on growth phase. *BMC Microbiol.* **2014**, *14*, 305.

104. Kuhn, D.M.; George, T.; Chandra, J.; Mukherjee, P.K.; Ghannoum, M.A. Antifungal Susceptibility of *Candida* Biofilms: Unique Efficacy of Amphotericin B Lipid Formulations and Echinocandins. *Antimicrob. Agents Chemother.* **2002**, *46*, 1773–1780.

105. Taff, H.T.; Mitchell, K.F.; Edward, J.A.; Andes, D.R. Mechanisms of *Candida albicans* biofilm drug resistance. *Future Microbiol.* 2013, *8*, 1325–1337.

106. Wimpenny, J.; Manz, W.; Szewzyk, U. Heterogeneity in biofilms. *FEMS Microbiol. Rev.* **2000**, *24*, 661–671.

107. Mah, T.-F.C.; O'Toole, G.A. Mechanisms of biofilm resistance to antimicrobial agents. *TRENDS Microbiol.* **2001**, *9*, 34–39.

108. Lewis, K. Persister Cells. *Annu. Rev. Microbiol.* **2010**, *64*, 357–372.

109. Stewart, P.S. Mechanisms of antibiotic resistance in bacterial biofilms. *Int. J. Med. Microbiol* **2002**, *292*, 107–113.

110. Fox, E.P.; Singh-Babak, S.D.; Hartooni, N.; Nobile, C.J. Biofilms and Antifungal Resistance. In *Antifungals: From Genomics to Resistance and the Development of Novel Agents*; Caister Academic Press, 2015; pp. 71–90.

111. Oppezzo, O.J.; Forte Giacobone, A.F. Lethal effect of photodynamic treatment on persister bacteria. *Photochem. Photobiol.* **2018**, *94*, 186–189.

THE END